Democratic and Popular Republic of Algeria

Ministry of Higher Education and Scientific Research

University Mohamed Khider of Biskra
Faculty of Exact Sciences and Science of Nature and Life

Department of Mater Science

Thesis Presented to obtain the degree of **Doctorate**
Speciality: Physics
Entitled:

Elaboration and characterization of undoped and doped indium oxide thin layers elaborated by sol gel process for photonic and photovoltaic applications

Presented by:

Rahima Nouadji

Publicly defended on: 10/11/2022

To the Jury composed by:

Mr. Mostapha Moumni	Professor	University of Batna 1	President
Mr. Abdallah Attaf	Professor	University of Biskra	Supervisor
Mr. Adel Bouhdjer	Lecturer ''A''	University of Batna 2	Co-Supervisor
Mrs. Hanane Saidi	Professor	University of Biskra	Examiner
Mrs. Malika Nouadji	Lecturer ''A''	University of Biskra	Examiner

Academic year: 2021-2022

DEDICATION

I dedicate my dissertation work to my family and many friends.

A special feeling of gratitude to my loving parents whose words of encouragement and push for tenacity ring in my ears.

My sisters and my brother have never left my side and are very special.

I also dedicate this dissertation to my many friends who have supported me throughout the process.

I dedicate this work and give special thanks to my fiance Elhoussine ATIKI for being there for me throughout the entire doctorate program.

You have been my best cheerleaders.

ACKNOWLEDGEMENT

First, I would like to thank ALLAH who gave me the health, the courage and the patience to carry out this work.

I particularly thank my supervisor, Mr. Attaf Abdallah, Professor in the Department of Matter Sciences Section of Physics Mohamed Khider University of Biskra, for agreeing to direct this work with great availability and efficiency, for sharing his experience with me, for the advice and encouragement throughout this work.

I would also like to thank my Co-supervisor Dr. Bouhdjer Adel for sharing their experience with me, for the advice and assistance throughout this work.

I would like to thanks Pr. Saidi Hanane, Dr. Nouadji Malika from University of Biskra and Pr. Moumni Mostapha from University of Batna for their interest in this work by accepting to be examiners and jury members.

I would also like to thank Pr. M. Saleh Aida, and Dr. Derbali Amar for sharing their experience with me, for the advice and assistance throughout this work.

I would like to thanks my friend Zeribi Fatma for their support.

Many thanks to all the teachers of the Department of Matter Sciences Section of Physics Mohamed Khider University of Biskra, my colleagues and all my friends.

Finally, I thank everyone who contributed directly or indirectly to the realization of this work.

ABSTRACT

Undoped indium oxide thin films have been deposited by sol-gel spin coating technique using indium (III) nitrate hydrate, absolute ethanol and acetyl acetone as precursor solution, solvent and stabilizer, respectively. The effects of the film thickness, pH solution and molar concentration precursors (indium III acetate anhydrous and indium III chloride anhydrous as precursor and acetyl acetone as solvent) on the structural, morphological, optical and electrical properties of In_2O_3 films have been studied. Doped indium oxide thin films have been deposited by sol-gel spin coating technique using indium (III) chloride anhydrous, absolute acetyl acetone as precursor solution and solvent, respectively. The effects of Sb doping and Ba doping on the structural, morphological, optical and electrical properties of In_2O_3 films have been studied. All films have been characterized by multiple techniques such as X-ray diffraction (XRD),UV-Visible spectroscopy, scanning electron microscope (SEM), and four probe method to investigate the physical properties of indium oxide films. X-ray diffraction analysis showed that the films are polycrystalline in nature having cubic crystal structure with preferred growth orientation along (222) plane. The growth of the films changed the direction from [111] to [100]. SEM images show that the films are homogenous, uniform and dense without any pin holes and cracks. The transmittance of In_2O_3 films was high up to 90%and it is probably related to the good crystalline quality of the films. The optical gap was found to vary between 2.95 and 3.23 eV. The electrical measurements revealed the resistivity have values about1.5×10^{-4}– 1.7×10^{-2}(Ω.cm) which made these films suitable for optoelectronic applications.

Keywords: Thin film, indium oxide, sol-gel, spin coating technique, doping, optical properties, electrical properties.

الملخص

تم ترسيب الشرائح الرقيقة لأكسيد الإنديوم الغير مطعم بواسطة تقنية الطرد المركزي سائل – هلام باستخدام نترات الإنديوم الثلاثي المميه، الإيثانول وأسيتيل الأسيتون كمصدر، مذيب ومثبت على التوالي. وقد تم دراسة تأثير كل من السمك، ، محلول الأس الهيدروجيني(pH) والتركيز المولي لمختلف مصادر الأنديوم (اسيتات الأنديوم الثلاثي و كلوريد الأنديوم الثلاثي) على الخصائص البنيوية، المورفولوجية، الضوئية والكهربائية لشرائح أكسيد الإنديوم الرقيقة. تم ترسيب الشرائح الرقيقة لأكسيد الأنديوم المطعم بواسطة تقنية الطرد المركزي سائل – هلام باستخدام كلوريد الأنديوم وأسيتيل الأسيتون كمصدر و مذيب على التوالي وقد تم دراسة تأثير تطعيم الأنتيمون و الباريوم على الخصائص البنيوية، المورفولوجية، الضوئية والكهربائية لشرائح أكسيد الإنديوم الرقيقة. تم توصيف كل الشرائح باستعمال عدة طرق مثل انعراج الأشعة السينية، ، المجهر الإلكتروني الماسح، مطيافية التألق الضوئي.أظهرت تحاليل انعراج الأشعة السينية أن الشرائح ذات طبيعة متعددة التبلور ببنية مكعبية الشكل مع اتجاه مفضل للنمو وفق المستوي (222)وتغير اتجاه نمو الشرائح من [111]إلى[100]. كما بينت صور المجهر الالكتروني الماسح أن الشرائح ذات سطح متجانس، متماثل وكثيف دون وجود أي مسامات أو شقوق. إضافة إلى ذلك كانت نفاذية شرائح أكسيد الإنديوم عالية بحيث وصلت إلى النسبة ،90%وقد يعود ذلك للتبلور الجيدة لهذه الشرائح.كما تتراوح قيم فجوة النطاق الممنوع ما بين2.95 و 3.23إلكترون فولط. فضلا عن ذلك، أظهرت القياسات الكهربائية أن مقاومية شرائح أكسيد الإنديوم تتراوح ما بين 1.7×10^{-2} –1.5×10^{-4}أوم.سم مما يجعلها صالحة للاستعمال في التطبيقات الكهروضوئية.

.

الكلمات المفتاحية :الشرائح الرقيقة، أكسيد الإنديوم، سائل – هلام، تقنية الطرد المركزي، تطعيم، خصائص ضوئية، خصائص كهربائية.

RÉSUME

Les couches minces d'oxyde d'indium ont été déposées par la technique de sol-gel spin coating en utilisant du nitrate hydraté d'indium (III), l'éthanol absolu et l'acétylacétone comme précurseur, solvant et stabilisant, respectivement. Les effets de l'épaisseur, concentration molaire des précurseurs et pH de solution sur les propriétés structurelles, morphologiques, optiques et électriques des films d'In_2O_3 ont été étudiés. Doper des couches minces d'oxyde d'indium ont été déposées par la technique de sol-gel spin coating en utilisant du indium III chlorure et l'acétylacétone comme précurseur et solvant, respectivement. Les effets d'antimoine et barium dopé les couches minces d'oxyde indium. Tous les films ont été caractérisés par de nombreuses techniques telles que la diffraction desrayons X (DRX), la spectroscopie UV-Visible, le microscope électronique à balayage (MEB), et la méthode de quatre points pour étudier les propriétés physiques des films d'oxyde d'indium. L'analyse par diffraction des rayons X a montré que les films sont de nature polycristalline et présentent une structure cristalline cubique avec une orientation de croissance préférée selon le plan (222). La croissance changé la direction de [111] à [100]. Les images de MEB montrent que les films sont des surfaces homogènes, uniformes et denses, sans aucune de porosité et fissures. La transmittance des couches d'In_2O_3 était élevée jusqu'à 90% et est probablement liée à la bonne qualité cristalline des films. Le gap optique variait entre 2.95 et 3.23 eV. Les mesures électriques ont révélé que la résistivité des couches préparées changées de 1.5×10^{-4}à 1.7×10^{-2}(Ω.cm),ce qui rend ces films adaptés aux applications optoélectroniques.

Mots-clés: couche mince, oxyde d'indium, sol-gel, technique de spin coating, dopage, propriétés optique, propriétés électrique.

CONTENTS TABLE

DEDICATION i

ACKNOWLEDGEMENT ii

ABSTRACT iii

الملخص iv

RÉSUME v

CONTENTS TABLE vi

LIST OF FIGURES ix

LIST OF TABLES xiii

GENERAL INTRODUCTION 1

CHAPTER 1 3

Review of indium oxide thin films 3

Introduction: 4

1.1 The types of precursor (In_2O_3): 4

1.2 Methods of In_2O_3thin films deposition: 5

1.2.1 Spin coating: 5

1.2.2 Spray pyrolysis: 6

1.2.3 Thermal evaporation: 7

1.2.4 Pulsed laser deposition PLD: 8

1.2.5 Electron beam evaporation: 9

1.2.6 Sputtering: 10

1.3 The properties of indium oxide thin films: 11

1.3.1 The structural properties of In2O3 thin films: 12

1.3.2 The optical properties: 17

1.3.3 Electrical properties: 23

1.4 Applications of In_2O_3 thin films: 27

1.4.1 Optoelectronic devices, including solar cells: 27

1.4.2 Gas sensors: 27

1.4.3 Electronic Displays: 27

1.4.4 Humidity sensors: 28
Conclusion: 28
CHAPTER 2 29
Spin coating deposition and characterization methods for in_2o_3 thin films 29
Introduction 30
2.1 Processing steps of preparation In_2O_3thin films using spin coating technique: 30
2.2 Influence of films thickness: 31
2.2.1 Preparation of solution: 31
2.2.2 Preparation of the films: 32
2.3 Influence of pH solution: 2.3.1 Preparation of solution: 33
2.3.2 Preparation of the films: 34
2.4 Influence of precursor source: 35
2.4.1 Preparation of solution: 35
2.4.2 Preparation of thin films: 35
2.5 Influence of doping In_2O_3 thin films: 36
2.5.1 Preparation of solution: 36
2.5.2 Preparation of thin films: 37
2.6 The adhesion test: 37
2.7 Film thickness: 37
2.8 Film characterization technique: 38
2.8.1 Scanning electron microscopy (SEM): 38
2.8.2 Energy dispersive X-ray spectroscopy (EDS or EDX) 39
2.8.3 X-ray diffraction (XRD): 40
2.8.4 UV-Visible spectroscopy: 44
2.8.4.1 Optical band gap: 45
2.8.4.2 Energy Urbach : 46
2.8.5 Electrical properties: 47
CHAPTER 03 49
EFFECT OF FILM THICKNESS AND pH SOLUTION 49
Introduction: 50
3.1The influence of film thickness: 50

3.1.1 Structural properties: 50
3.1.2 Morphological properties: 55
3.1.3 Compositional properties: 56
3.1.4 Optical properties: 57
3.1.5 Electrical properties: 59
3.2 The influence of pH solution: 60
3.2.1 Structural properties: 60
3.2.2 Optical properties: 63
3.2.3 Morphological properties: 66
3.2.4 The compositional properties: 66
3.2.5 Electrical properties: 67
Conclusion: 68
CHAPTER 4: 70
Effect of molar concentration precursors 70
Introduction: 71
4.1 Precursor In_2Cl_3: 71
4.1.1 Film thickness: 71
4.1.2 The structural properties: 72
4.1.3 Morphological properties: 75
4.1.4 Compositional properties: 76
4.1.5 Optical properties: 78
4.1.6 Electrical properties: 81
4.2 Acetate Indium precursor: 82
4.2.1 Film thickness: 82
4.2.2 Structural properties: 83
4.2.3 Morphological properties: 85
4.2.4 Compositional properties: 86
4.2.5 Optical properties: 88
4.2.6 Electrical properties: 91
4.3 Comparison: 92
Conclusion: 93

CHAPTER 05 94
Sb and Ba doped indium oxide thin films 94
Introduction: 95
5.1 Influence of Sb-doping In_2O_3: 95
5.1.1 Structural properties: 95
5.1.2 Morphological properties: 99
5.1.3 Compositional properties: 99
5.1.4 Optical properties: 100
5.1.5 Electrical properties: 103
5.2 Influence of Ba-doped In_2O_3 thin films: 105
5.2.1 Structural properties: 105
5.2.2 Morphological properties: 108
5.2.3 Compositional properties: 108
5.2.4 Optical properties: 109
5.2.5 Electrical properties: 112
Conclusion: 113
GENERAL CONCLUSION AND PERSPECTIVES 114
1. General conclusion 115
2. Perspectives 117
REFERANCES 118

LIST OF FIGURES

Fig1.1: Stages of spin coating on substrate. 6
Fig1.2: Schema of a spray pyrolysis system. 7
Figure 1.3:The phenomenon of thermal evaporation in a schematic[41]. 8
Fig1.4:Technical details of PLD deposition [49]. 9
Fig1.5: Electron beam deposition process in schematic[41]. 10
Fig1.6:A schematic representation showing the standard sputtering technique[57]. 11
Fig1.7: Crystallographic structure , cubic bixbyte structure of indium oxide(1/16 of the units) and one unit cell of In_2O_3[43, 54]. 13
Fig1.8: XRD diffraction pattern of In_2O_3 thin films deposited on glass, single crystalline Si (400) and KCl single crystal substrates [76]. 14

Fig1.9 :θ−2θ X-ray diffraction patterns recorded for In2O3 films grown on c-cut sapphire substrates at 200, 300, 400 and 500 °C[77]. 15

Fig1.10 : The typical XRD patterns and SEM micrographs(as the insets) for the as-deposited In_2O_3 thin films and for the In2O3 thin films of thickness 600 nm annealed at 400 °C 16

Fig 1.11:X-ray diffraction patterns of In_2O_3 thin films. 17

Fig 1.12: Optical spectra of transmittance and reflectance for non-irradiated and irradiated In_2O_3: Fe thin films at gamma doses: 1, 5, 10 and 100 kGy.....18

Fig 1.14: Spectral behavior of absorption coefficient (α) with wavelength of non- irradiated and irradiated In_2O_3:Fe at different gamma doses: 1, 5, 10 and 100 kGy. 19

Fig 1.14: Plots of $(\alpha h\nu)^{1/2}$ versus hν for non-irradiated and irradiated In_2O_3:Fe at various gamma doses: 1, 5, 10 and 100 kGy. 20

Fig 1.15: Variation of energy band gap values and Urbach energy for non-irra- diated and irradiated In_2O_3: Fe at gamma doses: 1, 5, 10 and 100 kGy.....21

Fig1.16: Optical transmittance spectra of In_2O_3 films formed at different annealing temperatures.22

Fig 1.17: Transmission spectra of In_2O_3 analyzed samples (inside are presented reflec- tions spectra for the same samples).....23

Fig 1.18: Optical transmittance of In_2O_3 films annealed at different temperatures.....23

Fig 1.19: Effect of substrate temperature on resistivity, carrier concentration and mobility of ICeO films deposited without any oxygen gas in the chamber. 24

Fig 1.20: Effect of oxygen content on resistivity, carrier concentration and mobility of ICeO films deposited at 160 ◦C.....25

Fig 1.22: The variation of resistivity, carrier concentration and mobility for ITO thin films a function annealing temperature. 26

Fig 2.1: Holmarc spin coater.....31

Fig2.2: the sol gel synthesis procedure of prepared In2O3 thin films.....31

Fig 2.3: Cut glass substrates using a sharp pen. 32

Fig 2.4: The cleaning of glass substrate and films deposition. 33

Fig 2.5: Flow chart showing the schematic diagram for In_2O_3 thin films preparation. 33

Fig 2.6: Experimental procedure for the pH adjustment in the In_2O_3 solution.....34

Fig 2.7: The sol gel synthesis procedure of prepared In2O3 thin films. 36

Fig2.8: Variety of interaction products evolved due to interaction of a primary electron beam and specimen (sample).....39

Fig 2.9:Energy dispersive X-ray spectroscopy[91].....40

Fig 2.10: Schematic of X-ray diffraction According to Bragg.....41

Fig 2.11: Schematic diagram of thin-film grazing incidence X-ray diffraction (a) using diffractometer circle Q is the scattering vector and S is the surface normal which is not parallel for each other. (b) Experimental setup of GIXRD. 41

Fig 2.12: Determination of β from stranger orientation [74]. 43

Fig 2.13: Schematic representation of the UV-Visible spectrophotometer[105] 45

Fig 2.14 :Plot of $(ahv)^2$ vs. hv for the vacuum-evaporated CdS film[109]. 46

Fig 2.14: Function of distribution of the energy states in the bands[75].....46

Fig 2.15: Determined the Urbach energy for ZnO:Al [112]. 47

Fig 2.16: four-points method. 47

Fig 3.1: Direct thickness measurement of the film of In_2O_3 from the cross sectional SEM images. 51

Fig 3.2: Variation of the film thickness with the number of layers. 51

Fig3.3: XRD patterns of nano-crystalline In2O3 thin films for different film thickness.Fig 3.4:Variation of peak (222) position of In_2O_3 thin films at different film thickness. 52

Fig 3.5: The texture coefficient of In2O3 thin films as function of film thickness along (222), (400) and (440) directions.....53

Fig 3.6: The evolution of grain sizeand strainof In_2O_3 thin filmsat different film thickness 54

Fig 3.7: SEM micrographs of the In2O3 thin films at different film thickness: (a) 175 nm, (b) 330 nm, (c) 520 nm, (d) 690 nm and (e) 910 nm. 55

Fig 3.8: EDX spectrum ofthe In_2O_3 thin films at different film thickness:(a) 175nm, (b) 330nm, (c) 520nm, (d) 690nm and (e) 910nm. 56

Fig 3.9: The transmittance spectra of In_2O_3 thin films prepared with various film thickness. 57

Fig 3.11: The plot of (h*v*) 2 against h*v* of In_2O_3 thin films and inset shows the variation of optical band gap (Eg) as a function of film thickness. 58

Fig 3.12: The variation of film thickness for In_2O_3thin films at various pH solution. 60

Fig 3.13: The XRD results of In_2O_3 thin films with various of pH solution. 60

Fig 3.14: the variation of crystallite size, strain and dislocation density against the pH solution.62

Fig 3.15: The transmittance of In_2O_3 thin films with different pH solution. 63

Fig3.16: The tauc plot of $(\alpha hv)^2$ as function hv at different pH solution. 64

Fig 3.17: The plot ln(α) as function photon energy (hv) at different pH solution. 64

Fig 3.18: The variation of band gap Eg and Urbach energy Eu at different pH solution. 65

Fig 3.19: The SEM images of indium oxide thin films at lower pH (0.84) and higher pH (9.58).65

Fig 3.20 : The energy dispersive of lower pH and higher pH solution for indium oxide thin films.66

Fig3.21: The variation of resistivity as function pH solution for indium oxide thin films.....67

Fig 4.1: The variation of film thickness when the molarity increases.....71

Fig 4.2: The XRD patterns of In_2O_3 thin films at different molar concentration. 72

Fig 4.3: The variation of crystallite size D, strain and dislocation density as function molar concentration precursor. 73

Fig 4.4: The texture coefficient TC(hkl) of In_2O_3 thin films at different molar concentration precursor. 74

Fig 4.5: The SEM images of In_2O_3 thin films deposited at various molar concentration precursor (0.05M, 0.1M, 0.15M, 0.2M, and 0.25M).....75

Fig 4.6: The EDS of indium oxide films deposited at different molar concentration precursor (0.15M, 0.2M and 0.2M).Table 4.2: The weight percentage of In and O for In_2O_3 films deposited at different molar concentration precursor. 76

Fig 4.7: The transmittance spectra of In_2O_3 thin films deposited at different molar concentration precursor. 78

Fig 4.8: The plot $(\alpha h\nu)^2$ as function $(h\nu)$ for In_2O_3 films deposited at different molar concentration precursor (0.1M, 0.15M, 0.2M and 0.25M). 78

Fig 4.9: The plot $\ln(\alpha)$ as function $(h\nu)$ for In_2O_3 films deposited at different molar concentration precursor (0.1M, 0.15M, 0.2M and 0.25M). 79

Fig 4.10: The variation of band gap energy and Urbach energy with different molar concentration precursor. 80

Fig 4.11: The variation of resistivity for In_2O_3 films deposited at various molar concentration precursor. 81

Fig 4.12: The variation of film thickness as function molar concentration precursor. 82

Fig 4.13: The XRD patterns of In_2O_3 thin films deposited at different molar concentration precursor. 83

Fig 4.14: The variation of crystallite size, strain and dislocation density with several values of molar concentration precursor. 84

Fig 4.15: The SEM images of In_2O_3 thin films deposited at various molar concentration precursor (0.05M, 0.1M, 0.15M, 0.2M and 0.25M) for indium acetate. 85

Fig 4.16: The EDX spectra of indium oxide thin films prepared at various molar concentration precursors. 87

Fig 4.17: The transmittance spectra of In_2O_3 thin films prepared at different molar concentration precursor. 88

Fig 4.18: The plot $(\alpha h\nu)^2$ versus photon energy $(h\nu)$ of In_2O_3 thin films prepared at different molar concentration precursor (0.1M, 0.15M, 0.2M and 0.25M).....89

Fig 4.19: The plot of $\ln(\alpha)$ as function molar concentration precursor (indium acetate). 89

Fig 4.20: The variation of band gap energy Eg and Urbach energy Eu as function molar concentration precursors. 90

Fig 4.21: The variation of electrical resistivity at various molar concentration precursors (indium acetate). 91

Fig 5.1: The XRD patterns of undoped and Sb-doped indium oxide thin films.....95

Fig 5.2: The variation of crystallite size D, strain ε and dislocation density with Sb doping concentration. 96

Fig 5.3: The texture coefficient TC(hkl) for Sb doped indium oxide thin films. 97

Fig 5.4: The SEM results of Sb-doped In_2O_3 films deposited at various Sb doping concentration.98

Fig 5.5: EDX spectra of undoped and Sb-doped In_2O_3 films. 99

Fig 5.6: Optical transmittance spectra of Sb doped In_2O_3 thin films.....100

Fig 5.7: plot of (αhν)2 as function (hν) for different concentration of Sb doping In_2O_3thin films.101

Fig 5.8: The plot of ln(α) as function hν for Sb-doping In_2O_3 thin films. 102

Fig 5.9: The variation of band gap energy Eg and Urbach energy Eu as function of Sb doping concentration for Sb-doping In_2O_3 thin films.....102

Fig 5.10: The variation of electrical resistivity and conductivity as function Sb doping concentration. 103

Fig 5.11: The XRD patterns of Ba-doped In_2O_3 thin films at different Ba concentration.....105

Fig 5.12: The texture coefficient TC(hkl) of Ba doped indium oxide thin films. 107

Fig 5.13: The SEM image of undoped and Ba doped In_2O_3 films at 9mol%. 107

Fig 5.14: The EDX spectra of undoped and Ba doped In_2O_3 films at 9mol%.....108

Fig 5.15: The transmittance of undoped and Ba doped In_2O_3 film at various Ba doping concentration. 109

Fig 5.16: The plot $(\alpha h\nu)^2$against the photon energy incident (hν) of undoped and Ba doped In_2O_3 thin films.....109

Fig 5.17: The plot Ln(α) as function photon energy incident (hν) for undoped and Ba doped indium oxide thin films. 110

Fig 5.18: The variation of optical band gap energy Eg and Urbach energy Eu at various Ba doped concentration. 111

Fig 5.19: The variation of electrical resistivity and electrical conductivity of undoped and Ba doped indium oxide films..... 111

LIST OF TABLES

Table 1.1: The different precursor of indium metals.....4

Table 1.2: The theoretical properties of indium oxide. 12

Table 1.3:The structural parameters of indium oxide thin films of thickness 600nm annealed at 400°C. 16

Table 1.4: The FWHM, average crystallite size of various molarities of indium oxide thin films.17

Table 1.5: Mobility (l), electrical resistivity (q), and volume carrier concentration (Nv)of In_2O_3 material before and after gamma irradiation. 26

Table2.1: The parameters of chemical products.....32

Table2.2: The parameters of chemical products.....34

Table2. 3: The parameters of chemical products.....35

Table2.4: The parameters of chemical products.....37

Table3.1: Crystallite sizes, dislocation density and strain values of In_2O_3 thin films extracted from XRD analysis. 54

Table3.2: Structural parameters information ofprepared In_2O_3thin films for different films thickness. 54

Table 3.3: Electrical resistivity, carrier concentration and carrier mobility values of In_2O_3 thin films deposited using sol-gel spin coating method.....58

Table 3.4: Structural parameters information of prepared In_2O_3thin films for different pH. 60

Table 3.5: The crystallite size D, FWHM, strain and dislocation density for In2O3 thin films prepared at different pH solution. 61

Table 3.6: The atomic and weight percentage of oxygen and indium.....66

Table4.1: The lattice parameters of In_2O_3 thin films with variation of molar concentration precursor. 73

Table4.3: The lattice parameters of In_2O_3 thin films with variation of molar concentration precursor. 84

Table 4.4: The atomic and weight percentage of In and O for In_2O_3 thin films at different molar concentration. 86

Table 5.1: Structural parameters information of prepared Sb-doped In_2O_3thin films for different concentration of Sb.....96

Table 5.2: Results of quantitative elemental analysis of Sb-doped In_2O_3 thin films.....99

Table 5.3: The variation of electrical measurement as function of Sb doping InO thin films. ..103

Table 5.4: The XRD parameters of Ba-doped In_2O_3 films.....105

Table 5.5: The variation of calculated parameters from XRD patterns of undoped and Ba doped In_2O_3 film at different Ba concentration. 106

Table 5.6: The weight and atomic percentage of element for undoped and Ba doped In_2O_3 films at 9mol%. 108

GENERAL INTRODUCTION

GENERAL INTRODUCTION

A. Research background:

In the last few years, a human life is independent to semiconducting thin films which play important role in all fields especially field of optoelectronic, microelectronic and communication technologies [1]. Among them, the transparent conductive oxides (TCO) such as SnO_2, CdO, ZnO, In_2O_3, TiO_2 etc[2,3]have been extensively studied, because of their unique physical and chemical properties and having large number of applications, such as photovoltaic solar cells[4], sensordevices [5], light-emitting diode devices [6] and flat panel displays[7]. Among these oxides,In_2O_3 is an important one of the best suited materials for many electronic applications due to its fascinating properties. It is an *n*-type semiconductor with a wide band gap (E_g ~3.65eV) [8], high optical transmittance (in the visible region) and good electrical c onductivity [9]. This is making it suitable to use as photovoltaic devices, solar cell, transparent windows, liquid crystal displays, light emitting diode (LED) and gas sensors[10,11].

There are a lot of researchers have studied the effect of several parameters on the structural, optical and electrical properties of Indium(III) oxide (In_2O_3) in order to improve their properties[12,13], using different method. As well known, the films thickness is one of the most important fact, so this leading to investigating the effect this fact on physical properties of our samples. By the way, several deposition techniques have been widely used to produce In_2O_3 thin films including RF magnetron sputtering [14], chemical vapor deposition (CVD)[15], spray ultrasonic , thermal evaporation[16], spray pyrolysis [17], pulsed laser deposition (PLD)[18] and sol-gel method[19]. Among these, sol–gel method is one of the most unpretentious techniques for In_2O_3 thin films preparation compared to others deposition methods, becauseof its significant advantages such as simple, economical method, relatively cost-effective processing, and easy precise control of material composition and permits to produce films with a good quality [20,21].In our present work, will be chose the sol-gel spin coating method to prepare films of indium oxide on glass substrates .Then will be studied some of the structural, optical and electrical properties of these films for use it in photovoltaic and optoelectronics applications.

B. Research Aims

The goal of this research is to attain optimization of optical, structural, morphological and electrical properties of undoped and doped indium oxide thin films using sol gel spin coating method, and that's by changing a several parameters such as:

- Film thickness.
- pH precursor solution.
- Molar concentration of precursor.
- Antimony doped indium oxide films.
- Barium doped indium oxide films.

These parameters have been varied to make In_2O_3 thin films a proved for optoelectronic and photovoltaic applications such as: solar cells, buffer layers and gas sensors..., etc.

C. Structure of the Thesis:

This thesis is divided of four chapters organized as follows:

It was starting with a broad introduction.

In the first chapter, we will provide a review of In_2O_3 thin films for last studies. Then we will explain the different methods for deposit the indium oxide thin films, followed by an explanation of structural, optical and electrical properties of films prepared at several processes. At the end of the chapter, it will summarize the multiple applications of these films in optoelectronic and photovoltaic fields.

The second chapter contains some steps of sol-gel spin coating. The different procedure effects for deposit undoped and doped indium oxide thin films. In the present study, the obtained films will characterize using X-ray diffractometer (XRD), scanning electron microscopy (SEM) and energy dispersive X-ray spectroscopy (EDX) techniques. The electrical and optical properties of the films will study using a four probe set up and UV-Visible spectrophotometer, respectively.

The third chapter included the detailed results, explanation and studies the structural, electrical and optical properties of prepared undoped indium oxide thin films at the variation of film thickness and pH solution.

The fourth chapter has an explanation the results of In_2O_3 films prepared at different molar concentration precursors (indium chloride and indium acetate).

The fifth chapter has the detailed results and interpretation of Sb, Ba doped indium oxide thin films.

Finally, there is a conclusion that includes a summary of the main findings, concluding remarks, and recommendations for further research.

CHAPTER 1
Literature review of indium oxide thin films

Introduction:

In the few years later, the research and industry had interesting about the semiconductor materials which have an interesting benefits for the difference applications. They are thinking to improve those materials , which have many properties under extreme environmental conditions .One of the most important semiconductor material is (TCOs) transparent conducting oxides , which have a wide band gap semiconductor , it's because the conduction band has a high concentration of free electrons. These are caused by either material defects or exogenous dopants, whose impurity levels are near the conduction band edge[22]. TCOs are an essential in technology applications, it is represented a compromise between high transparency in the visible wavelength and electrical conductivity ($>10^3\Omega^{-1}Cm^{-1}$). However , that have succeed with a wide band gap oxide by using substitutional dopants [23] , the TCOs have a wide band gap (>3eV) at room temperature in the undoped state that is doped to be degeneracy by increasing the free carrier density enough to move the Fermi level into the conduction band [24].Among them, In_2O_3 is one of the most useful transparent conducting oxides (TCO) having high optical transmittance (>80%), large optical direct band gap 3.5 - 3.7eV [8] ,low electrical resistivity(1– 2 × 10-4 Ω cm) , a cubic structure with lattice constant 1.0117 nm and dielectric constant of 8.9[25]. Moreover, the researchers are interesting to use in various applications the In_2O_3 thin films such as solar cells[26], light emitting diode (LED) ,gas sensors and anti-reflecting coatings [27] . The major goal of this study is to investigate the properties of In_2O_3 thin films based on previous research; we have proposed a review of original research to nanostructure In_2O_3 thin films using various ways and methods.

1.1 The types of precursor (In_2O_3):

In_2O_3 solution can prepared by various precursor such as indium acetate , indium nitrate , indium chloride and various solvents such as ethanol, water ,methanol ,propanol, acetylacetone ...etc in some methods see table1.1.

Table 1.1: The different precursor of indium metals.

Molecule	Molecular formula	Molar mass	Appearance	Solubility in water	Purity
Indium chloride	$InCl_3$	221,177 g/mol	white powder,solid	Very soluble	98+%
Indium actate	$C_6H_9InO_6$	291.95 g/mol	White powder or Crystalline Powder,solid	Soluble , mineral acid and acetic acid.	99.99% Based on trace metal analysis
Indium nitrate	$In(NO_3)_3 \cdot 3H_2O$	354.88 g/mol	White to off-white crystals, powder, or lumps	Insoluble	99.9% trace metal basis

1.2 Methods of In_2O_3 thin films deposition:

In_2O_3 thin films are deposited at three steps: reaction of atomic/molecular/ionic species, (ii) transport of these species through a medium, and (iii) condensation of the species on substrates. These steps have been created by various techniques such as : spin coating process , spray pyrolysis, spin coating , atomic layer deposition (ALD) , electron beam evaporation (EBE), electron beam irradiation ,pulsed laser deposition ,vacuum evaporation and sputtering (magnetron sputtering and ion beam sputtering).

1.2.1 Spin coating:

Spin coating is the most technique in sol-gel method used to deposit thin films; it investigated the uniform and homogenous surface for photovoltaic and optoelectronics applications. However , spin coating of thin films is done by drops the precursor solution of In_2O_3 , this technique has four steps to deposit thin films , deposition, spin up, spin off, and evaporation of solvent , as shown in Figure 1.1 [28] , this process can produce very fine , thin and uniform coating while

it has a difficult with large area samples [29] . In_2O_3 thin films are deposited by the spin coating process using a different way to produce the precursor solution for good, uniform and smoothing films. The solution precursor was prepared from different ways; it can be summarized in some points:

- Indium nitrate hydrate, $In(NO_3)_3 \cdot xH_2O$, as precursor was dissolved into 2-butoxyethanol , In_2O_3 thin films are deposited on alumina substrates (ceramic Al_2O_3 or co-oriented α-Al_2O_3) of 2.0cm×2.0cm [30].
- Indium acetate (Alpha-aeser,99.9%) and urea (Alpha-aeser ,97%) as the precursor was dissolved in ethanol (99.9%) , which ethanol amine(>98%) was dropped till a clear solution obtained [31].
- $In(NO_3)$ $4H_2O$ was dissolved in 96% ethanol with acetylacetone (hacac) [32].

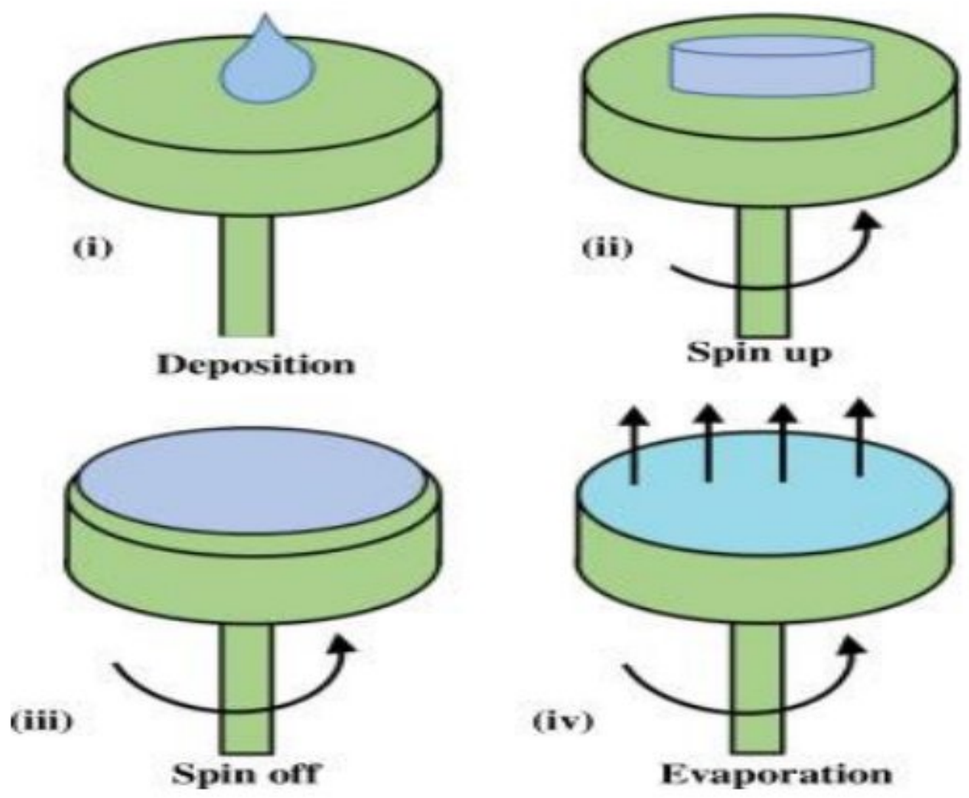

Fig1.1: Stages of spin coating on substrate.

1.2.2 Spray pyrolysis :

The spray pyrolysis technique a low-cost, non-vacuum required, way to synthesize materials in the form of powders and nano thin films [18, 19] , it is a technique based on precursor solution which is formed the aerosol for deposit uniform and homogenous thin films. The generated solution droplets (aerosol) are passing through several stages :(1) the solution (aerosol) is evaporated to the heater substrate ,(2) drying the atomic cloud aerosol containing the precipitated solute ,(3) the precipitate is annealed at high temperature ,(4) formation of In_2O_3 thin films on

the glass substrate[20, 21] .This steps of deposition are showing in figure 2 [37].

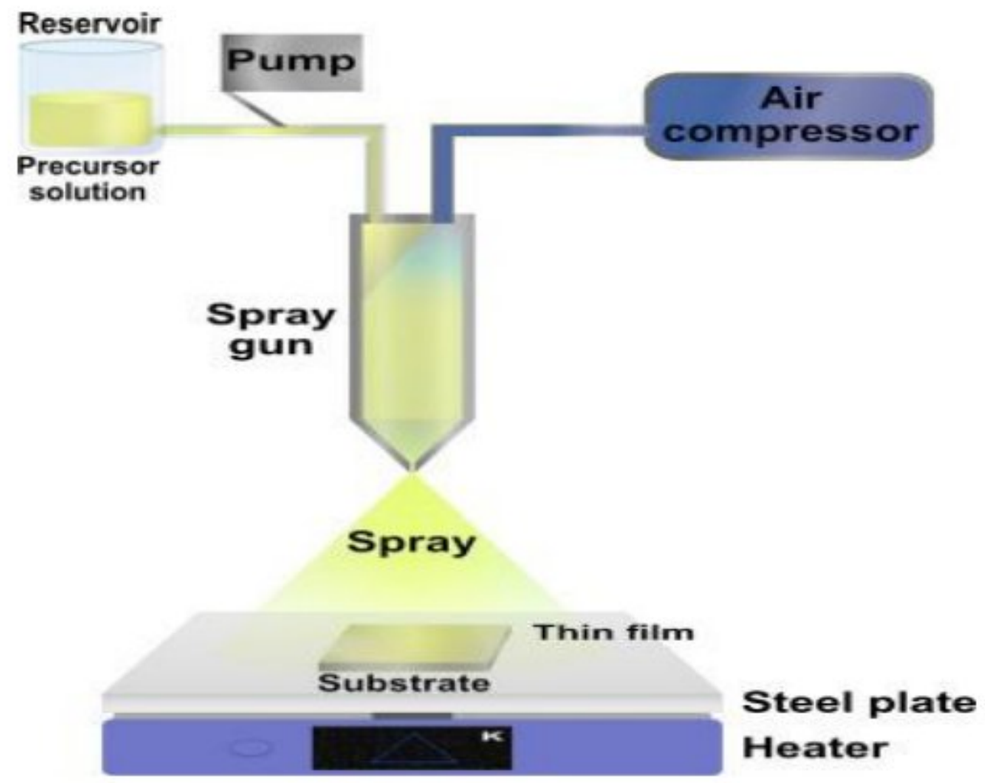

Fig1.2: Schema of a spray pyrolysis system.

The researcher deposit In_2O_3 thin films from different way to obtain homogenous and uniform surface for photovoltaic applications .More recently, the In_2O_3 thin films prepared by spray pyrolysis using a solution of:

- $InCl_3$ precursor was dissolved in deionized water with concentration 0.1M , the films are grown at different substrates with various temperatures from 250°C to 450°C [38].
- Indium (III) acetate trihydrate $In(CH_3COO)_2.3H_2O$ salt was dissolved in deionized water with concentration (0.05M) sprayed at different temperature of substrates (Ts = 350–475 C) [39].
- Indium (III) acetate (0.1M) was dissolved in deionized water with added a few drops of concentrated hydrochloric acid for homogenous solution , after that it was added $TiCl_3$with various concentrations (0-5%) in solution , to obtain In_2O_3 thin films it was sprayed the solution into glass substrates at temperature 450°C[40] .

1.2.3 Thermal evaporation:

Thermal evaporation is a well-known process to deposit a In_2O_3 thin layers , under vacuum chamber 1×10^{-6} torr (1.3×10^{-4} Pa) the source material is evaporated from crucibles heated with electrical current shown in figure 1.3 , which facilitates the vapour particles moving a substrates to obtain a thin films in solid state [27-28-29]. The scientist was deposited In_2O_3 thin films by thermal evaporation explained with some points:

- The source material used to deposit In_2O_3 thin films is indium metal with a purity of

99.99% in the form of band ,which heated in small resistance-heated tungsten boat in a chamber evacuated to a pressure of 5×10^{-5} Torr. Thin films were obtained on glass substrates at room temperature with a deposition rate 6.5A°/s with various oxidation condition by Mihaela Girtan et all [44] .

- Makhija et al[45] used a fine thin powder of indium tin oxide (In_2O_3+17%SnO_2 ,Alfa Johnson Matthey) kept in feeder which was vibrated by electromagnet .Thin films are deposited in vacuum 10^{-4} Pa on substrates heating at 673K after that it annealed at 700K for one hour [45].

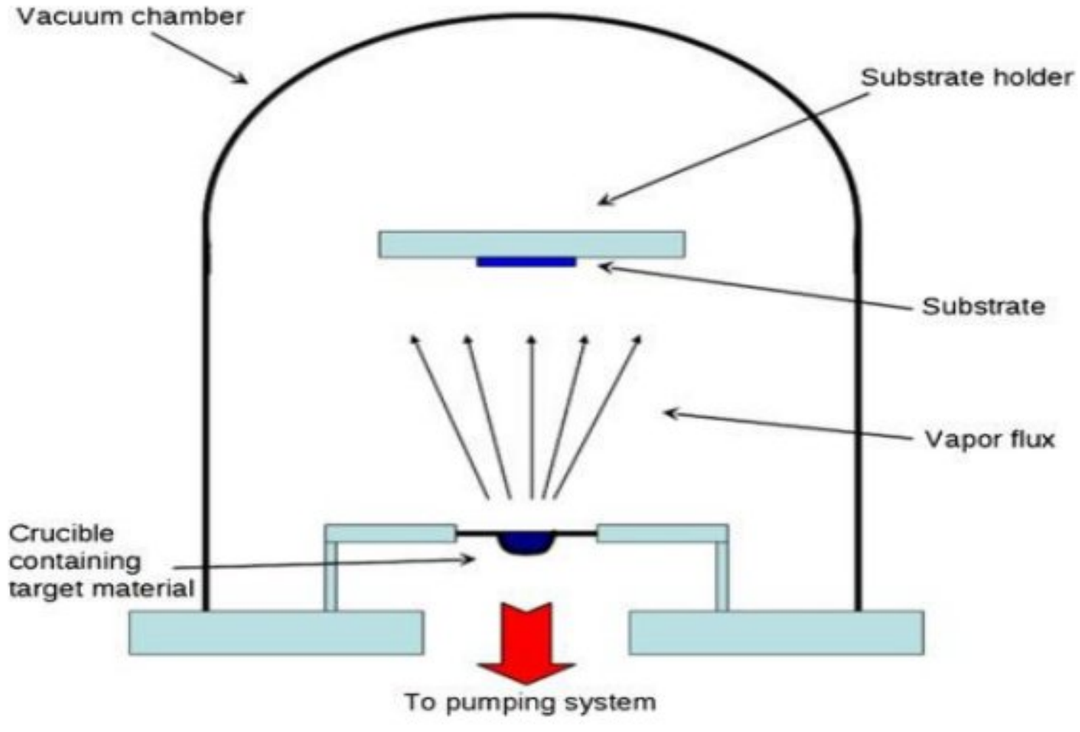

Fig1.3:The phenomenon of thermal evaporation in a schematic[41].

1.2.4 Pulsed laser deposition PLD:

Pulsed laser deposition is a physical vapor deposition technique, it used to growth a high quality of thin films at different materials, and this technique is based on several experimental parameters:

- The laser pulse fluence, wavelength and repetition rate is depending with the physical and chemical properties of target material. During the laser pulses the ablation plume is generated in few seconds , this plume composed a hot bubble of plasma near the target surface[32,33].
- Target material absorb the photons from pulsed laser , the desired of material was transferred as the substrate by laser ablation [46].
- The presence of background gas (N_2, NH_3, O_3 or inert Ar) during PLD growth can effected on the plume composition and control in the stoichiometry of the films ,background gas is depending on the material to deposit [48].

- Substrate temperature is the most important during the deposition of thin films in PLD process.

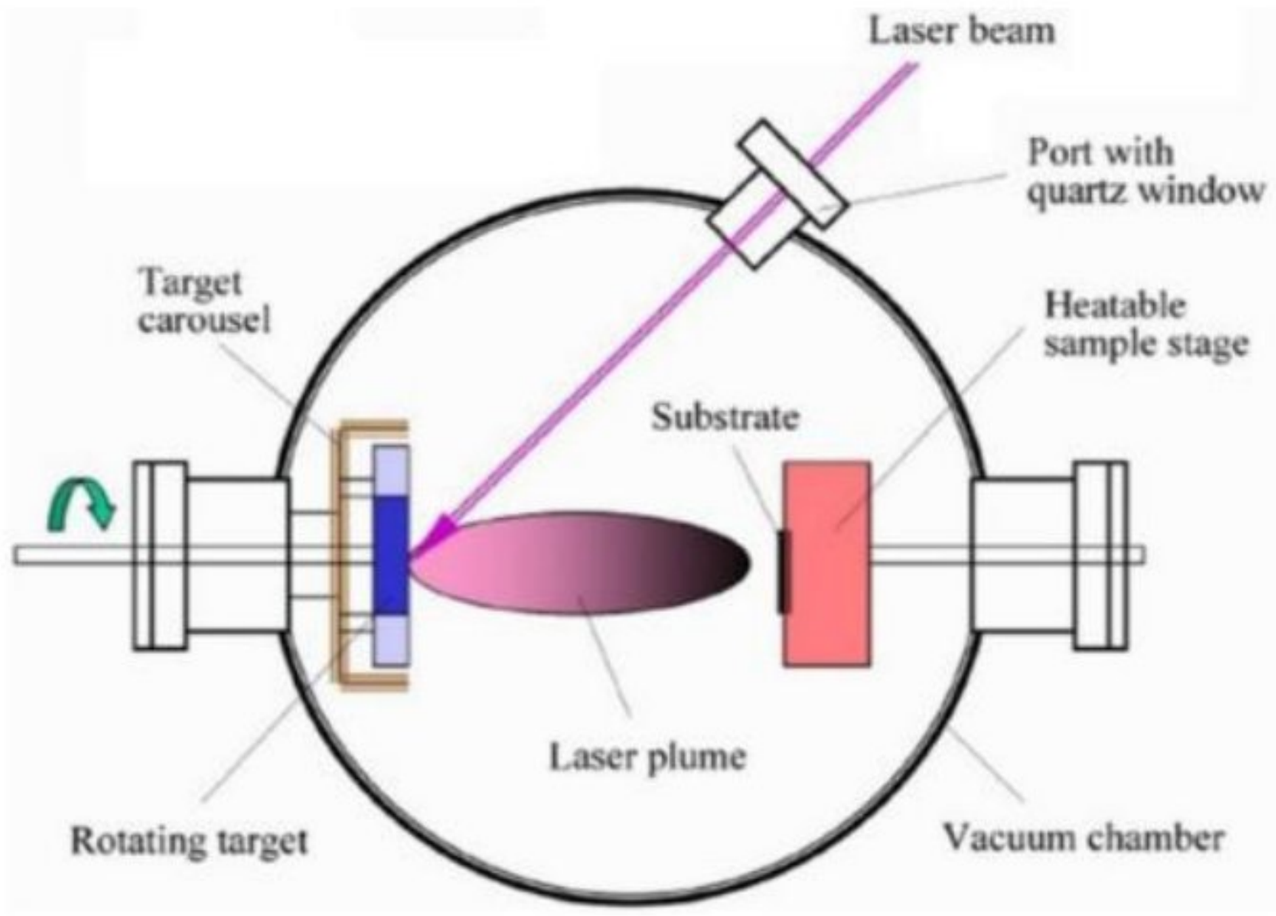

Fig1.4:Technical details of PLD deposition [49].

In_2O_3 thin films was deposited using PLD process (the laser pulse is Kr (248nm) with repetition rate 10HZ , the target material is In_2O_3 (Sigma–Aldrich, 99.99% In2O3 powder) , the target to substrate distance was 5cm , the substrate temperature was fixed at 450°C and the growth produced in 20min , finally the oxygen was maintained at 0.133 Pa) with various substrates such as GaAs , Si, quartz and glass by Neeti Tripathi et al[50] .

1.2.5 Electron beam evaporation:

process using different source material and various parameter (pressure of chamber vacuum , It is a physical vapor deposition to prepared a high thin films with different properties, electron beam evaporation (E-Beam) process consists a chamber vacuum at pressure 10^{-5} Torr or lower, the using of source material is in the form of ingots or a compressed solid. The electron guns based on thermionic emission, field electron emission or the anodic arc method. It is accelerated with high kinetic energy and focused towards the starting material shown in figure 1.5 [51].In_2O_3 thin films were deposited by electron beam evaporation electron guns , acceleration of electron beam) which summarized in some points:

- Mehdi et al[52] were deposited the In_2O_3 thin films on glass substrates using low energy

of 0.8 MeV for three fluencies 4.10^{16}, 35.10^{16} and 42.10^{16}electron/cm^2.

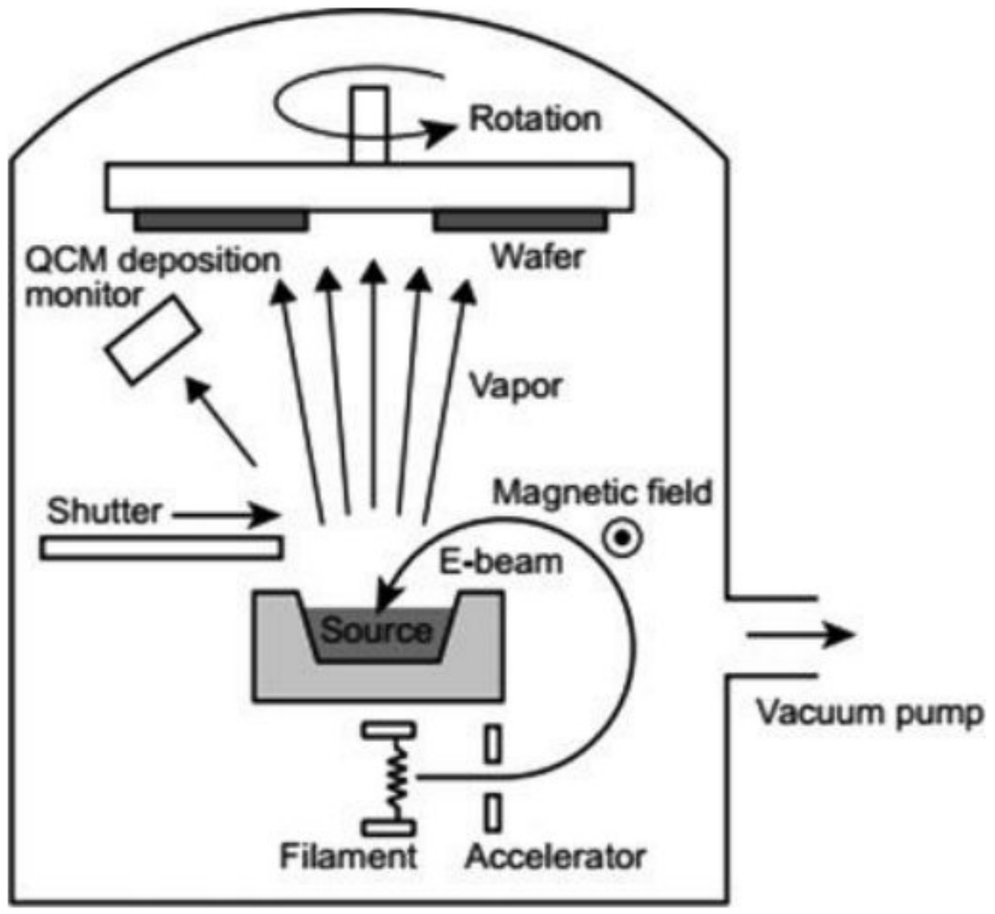

Fig1.5: Electron beam deposition process in schematic[41].

- In_2O_3thin films were synthesized by E-Beam process using high purity of In_2O_3: SnO_2 (respectively 90 wt. % and 10 wt%,) was employed as the source material for evaporation , on the other hand the researchers were used the voltage for the acceleration of electron beam was 5-10KV , the current of electron beam reached 10-14mA [53] .

1.2.6 Sputtering:

Sputtering process or pulvérisation as the French call it, is a vacuum process used to deposit very thin films on substrates for a wide variety of purposes , it is working with several parameters (inert gas usually Argon at ~1Pa for create plasma , the voltage , current ,the target source materials , substrate) shown in figure 1.6. The sputtering process have two type to deposit In_2O_3thin films such as : RF sputtering with standard frequency 13.56MHz is usually applied across the cathode–anode space and DC sputtering is focused on negative bias voltage applied to cathode (the source target) in order to direct the bombardment of Ar+ ions in the plasma toward the source , a stream of ejected materials then traverses across the cathode–anode distance and is deposited onto the substrate[40,41,42].

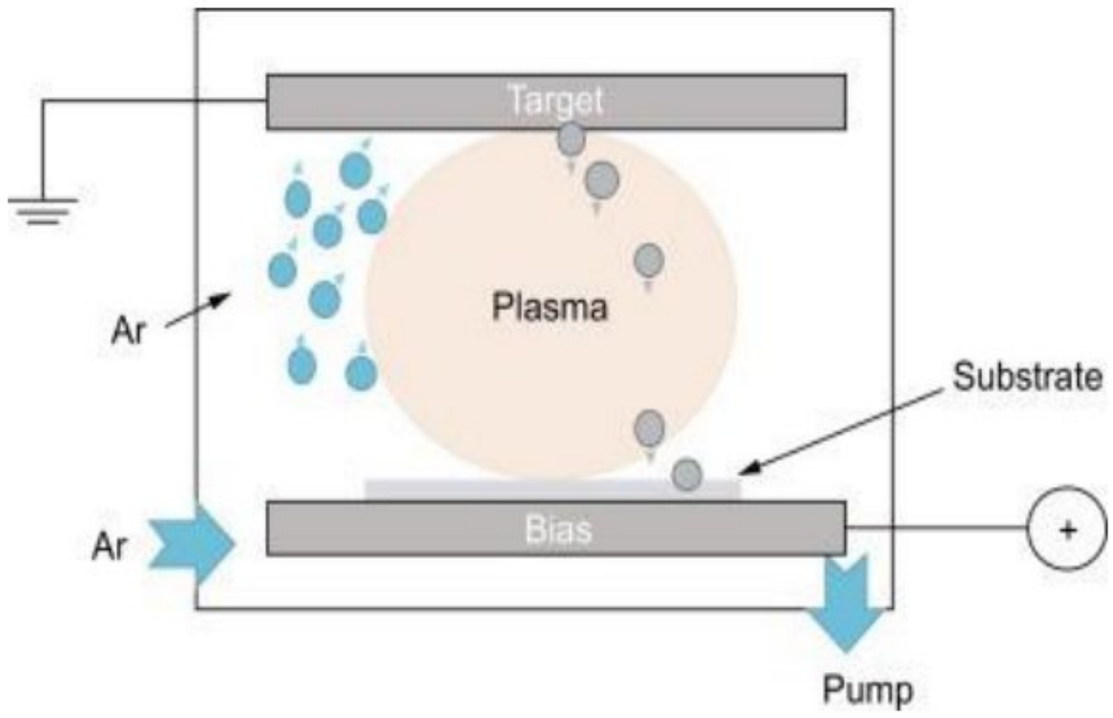

Fig1.6:A schematic representation showing the standard sputtering technique[57].

Many researchers deposited the indium oxide films by sputtering using some effects such as:

- Hadi et al [58] were deposited ITO thin films on Si substrate using RF sputtering process with thickness of 40 nm at room temperature , the ITO target with 90 wt% In_2O_3 and 10 wt% SnO_2 was operated under base vacuum pressure of 2.0×10^{-5} mbar in the pure Ar atmosphere have deposited on cleaned substrates .After the deposition the samples were annealed at temperature between 500°C-700°C .In other hand , In_2O_3 thin films were prepared by RF sputtering process using 2 inch diameter In target (99.999% purity) , this films were deposited on cleaned corning glass 7059 . Mounted behind the substrate holder and was monitored with a thermocouple. The chamber was initially evacuated to a vacuum on the order of 4×10^{-6} Torr by using a turbo-molecular pump. Argon gas was used for sputtering, and oxygen was supplied as a reactive gas. The working pressure was maintained at 20 mTorr with an O_2/Ar ratio = 1:9 at a total flow rate of 60 sccm. The distance between the target and the substrate was fixed at 50 mm[59].
- Xifeng Liet al[60]were deposited In_2O_3 thin films by DC sputtering using pure metal indium sputtering target embedded with 3 wt% pure metal molybdenum was fabricated inhouse on cleaned glass substrates with thickness 3mm in chamber vacuum (2.0×10^{-3} Pa) , the samples have grown at different oxygen partial pressure and temperature substrate .

1.3 The properties of indium oxide thin films:

Since 60 years ago, Rupprecht oxidized an evaporation deposited indium layer at high

temperature in air forming polycrystalline, transparent and conductive material [61]. Also , the amorphous of indium oxide is used for optoelectronics applications [62].However, polycrystalline In_2O_3 have a several properties (structural, optical and electrical) it summarized in table 1 .2 for photovoltaic and optoelectronics applications. The most common type of In_2O_3 is Sn doped In_2O_3, also known as ITO, which has been widely employed in window layers in solar cells, transparent electrodes in liquid crystal displays (LCDs), and organic light emitting diodes (OLEDs) (OLED)[63] . Also , the indium oxide has been doped by other materials such as germanium Ge and titanium Ti to obtain low resistivity of the films [46,22],tungsten applied to investigate the transmittance[65] and iron to increase the electrical mobility [66]. The theoretical properties of In_2O_3 thin films can be listed in table 1.2.

Table 1.2: The theoretical properties of indium oxide.

Parameter	Values	Reference
Chemical formula	In_2O_3	JCPDS Card 044-1087
Space group	Ia3	JCPDS Card 044-1087
Melting point	1913°C	[67]
Crystal type	Cubic (bixbyte)	JCPDS Card 044-1087
Formula unit	16 formula per cell	[68]
Molecular weight	277,64 g/mol	JCPDS Card 044-1087
Structure	Ia-3	JCPDS Card 044-1087
Density(g/cm_3)	7.12	JCPDS Card 044-1087
Lattice constant (Å)	10.117	[69]
Conductivity type	n-type	[70]
Carrier concentration (cm^{-3})	10^{18}-10^{20}	[71]
Optical transmission (%)	75-85%	[72]
Optical band gap (eV)	3.5eV	[72]

1.3.1 The structural properties of In_2O_3 thin films:

In_2O_3 crystallizes in a variety of shapes as a cubic centered and hexagonal [67] see figure 1.7. However, the cubic centered structure of indium oxide is similar to that of the bixbyite

Mn_2O_3(called C-type rare earth oxide structure) which the mesh of In_2O_3 consists of 16 unit formula with 80 atoms as reported by Wyckoff[73]. From this mesh , 8 of 32 In atoms (In1) occupy the centers of the trigonally distorted octahedra (8b position), whereas 3/4 of In atoms (In2) occupy the centers of tetragonally distorted octahedra (24d position), resulting in an axcellent packing ratio (The ratio In1 / In2 = 1: 3)[68] . It is due that 8 b cations are coordinated to six oxygen anions and to two oxygen interstitial sites but the 24 d cations are coordinated to six oxygen anions at three distances and to two oxygen interstitial locations. The 48 oxygen anions are coordinated to four cations[74] . The figure 1.7 reveals the meaning of 8b sites and 24d sites. Moreover, the hexagonal structure of α -alumina is same (corundum). It can be made by using metal dopants or elaborating under high pressure (for example 65 kbar and 1000 ° C).The network parameters are: a = 5.484Å and c = 14.508 Å[75].

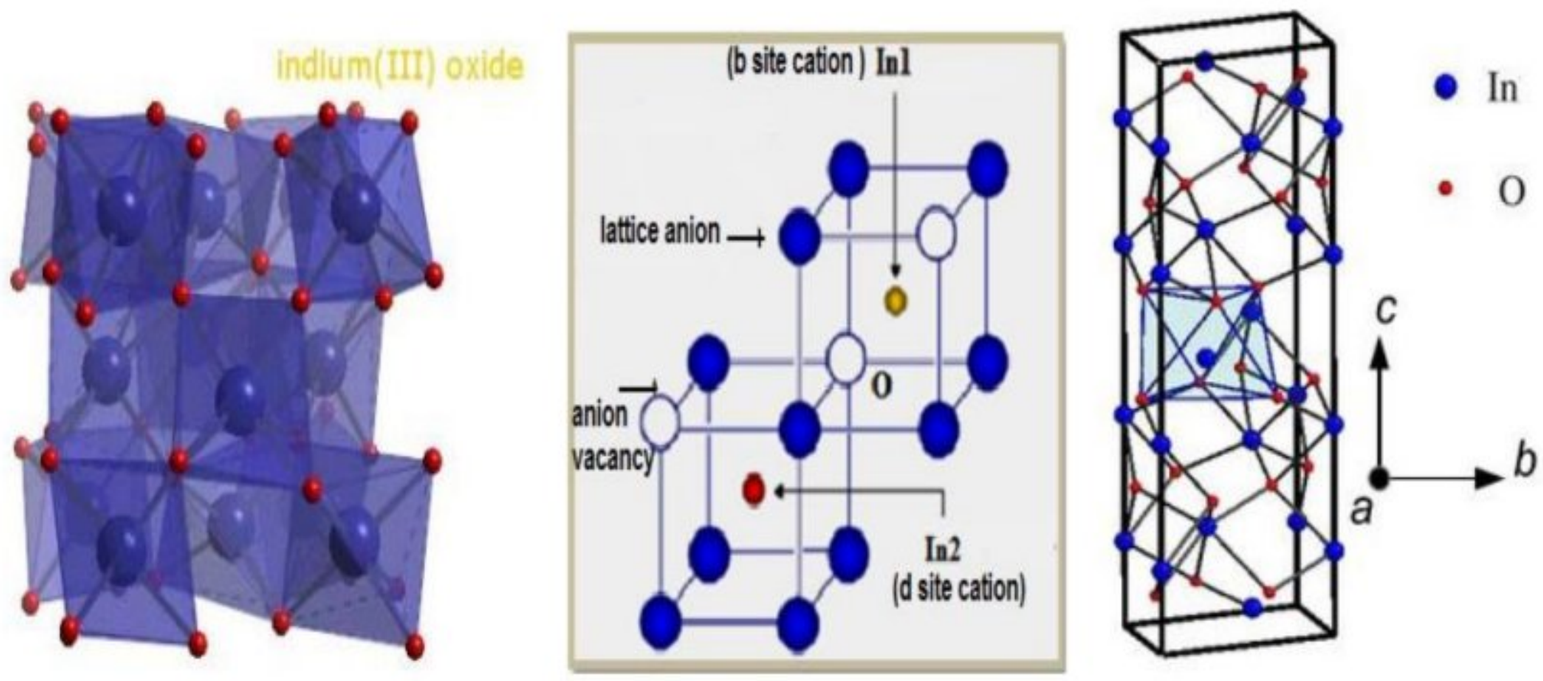

Fig1.7:Crystallographic structure , cubic bixbyte structure of indium oxide(1/16 of the units) and one unit cell of In_2O_3[43, 54].

The In_2O_3 thin films can be characterized from XRD patterns to presented the crystallinity of the films and found the bixbyte structure, it can be calculated the crystallite size, strain and dislocation density from XRD patterns using FWHM of preferred orientation of In_2O_3 films. In previous years, many researcher have studied the structural properties ofIn_2O_3 films to apply and amelioration it in different application. A.Attaf et al[76]has reported the structural characterization of In_2O_3 thin films grown by spray pyrolysis onto different substrates (glass , single crystalline Si , KCl single crystal) . The XRD patterns of In_2O_3 films appeared the orientation peaks at different pervious samples which represented the preferred orientation (222) of In_2O_3/glass films is low intensity located $2\theta=30.76°$ due to cubic structure .Moreover , In_2O_3/Si films show several peaks at 29.61°, 30.76°, 33.06°, 35.76°, and 51.31 , corresponding

to(211), (222), (321), (400) and (440) planes of cubic phase respectively with a Si single crystal peak at 69.54° corresponding to the (400) , finally the In_2O_3/KCl it observed many peaks located at 2θ = 30,69° ,35, 55° and small peak assigned to (222), (400)and (800) planes of In_2O_3 respectively and it observed a KCl peaks at 2θ = 28,42° and 2θ = 58.74° corresponding to the plan(200) and its harmonics (400) respectively (JCPDS 41-1476 file) as shown in figure 1.8.

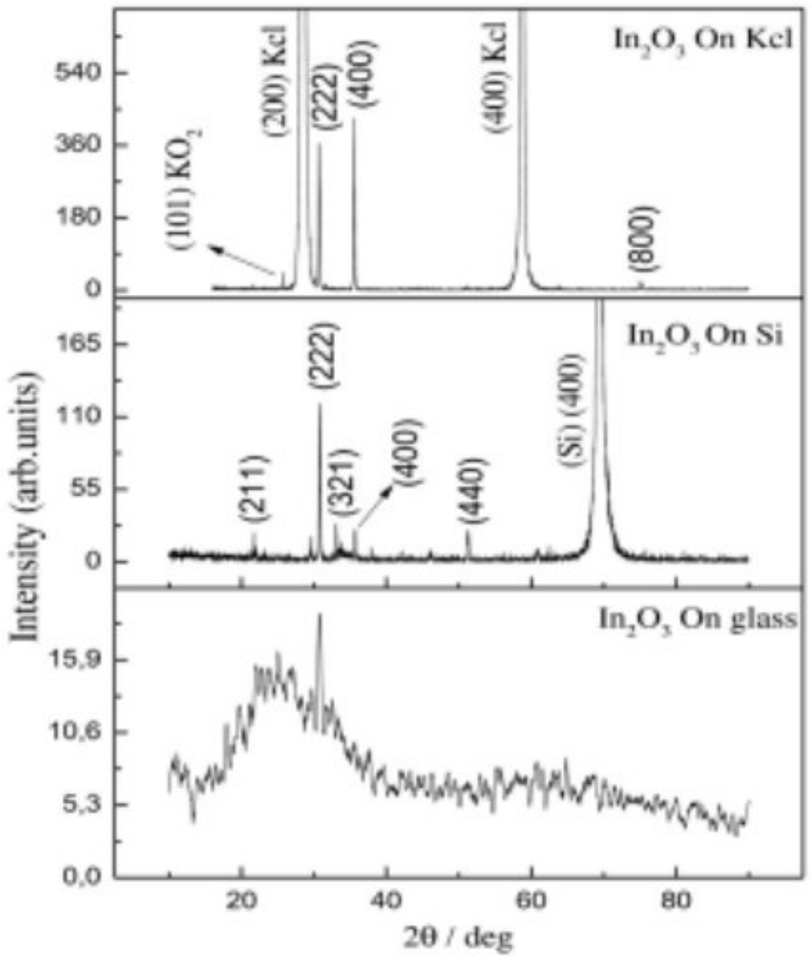

Fig1.8: XRD diffraction pattern of In_2O_3 thin films deposited on glass, single crystalline Si (400) and KCl single crystal substrates [76].

The crystallite size , strain and dislocation density were estimated from the XRD patterns of the films (In_2O_3/glass ,In_2O_3/KCl, In_2O_3/Si) of (222) and (400) , it observed that the average at crystalline size of In_2O_3/KCl films and In_2O_3/Si films are large , they are in the order 70and 62.5 nm respectively .However, the average of crystallite size at In_2O_3/glass films is low crystallite size of 18nm. The strain for (222) orientation and (400) of In_2O_3/KCl films and In_2O_3/Si films are lower (0.42×10^{-3} and 0.62×10^{-3}) than In_2O_3/glass films (2.85×10^{-3}). In addition, the dislocation density is varied between 26×10^{14}, 2.04×10^{14}, 2.56×10^{14} lines/m^2 for In_2O_3/glass films, In_2O_3/KCl films and In_2O_3/Si films. W. Seiler et al[77]deposited the In_2O_3 films by pulsed electron beam deposition method (PED) process with the variation of temperature of substrates at 200, 300, 400 and 500 °C , the XRD patterns shows the intensity of peaks for In_2O_3 films increased with increasing of temperature (figure1.9) , it is due that all the films crystallize in the pure bixbyte structure and it can be say that the increasing is resulting a slight oxygen deficiency

and/or the existence of stresses in the grown films. These peaks can be identified with the (222) and (004) family planes of the In_2O_3 bixbyite indicating preferential (111) and (001) textures. The peak (004) is no longer with increasing of temperature , the 2θ values of (222) is lower than the bulk value (30.58°) for increasing temperature of substrates .The crystallite size was estimated from the preferred orientation (222) using Deby Sherrer equation , it found that the decreasing of values with growth temperature.

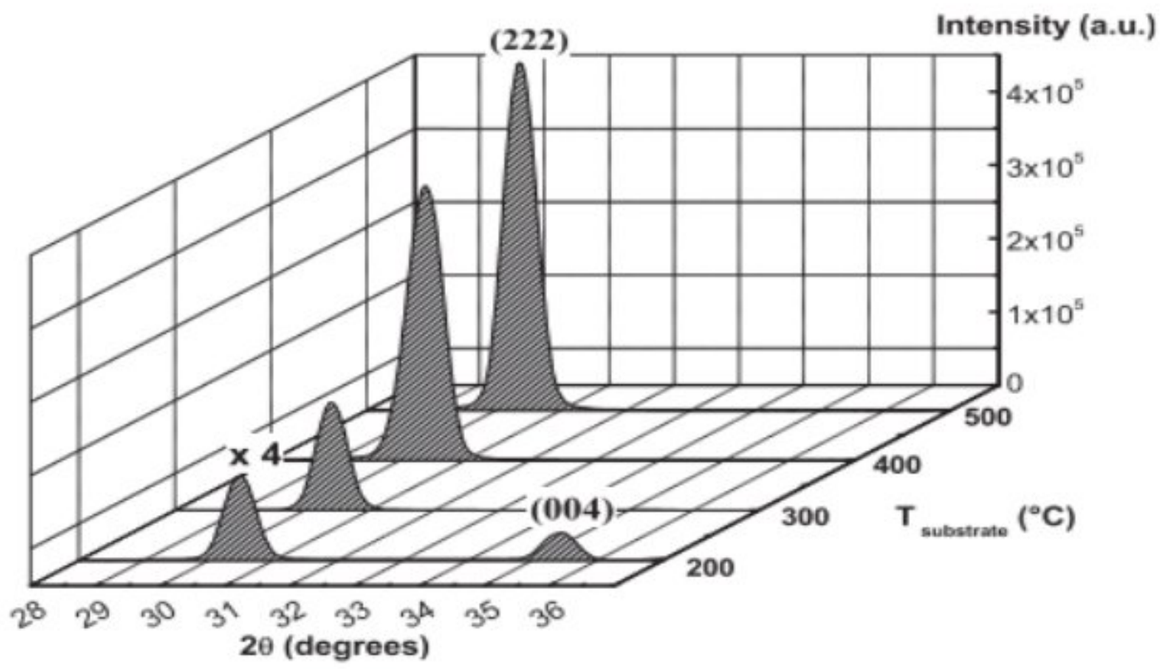

Fig1.9 :θ–2θ X-ray diffraction patterns recorded for In2O3 films grown on c-cut sapphire substrates at 200, 300, 400 and 500 °C[77].

Moreover, the In_2O_3 films were prepared by thermal evaporation in the vacuum of the order of 2 × 10^{-5} mbar on the glass substrate using In_2O_3powder; the films obtained were annealed at different temperatures for one hour in the furnace with thickness 600nm. As the results, the figure 1.10 shows a XRD patterns and SEM micrograph.XRD patterns of films as deposited are presented amorphous in nature; it is due that the films are less crystalline at low annealing temperature which means to defects and lack of enough kinetic energy and mobility of the grains to get oriented at respective planes. In the other hand , the films of In_2O_3annealed at 400°C confirmed a crystalline phase were observed that the films are becoming crystallize in cubic bixbyte structure , the XRD patterns presented a preferred orientation of In_2O_3 thin films along (222) was common in all the films and the intensity of (222) peak gradually increased with the appearance of the other peaks (400) ,(431) ,(440) ,(622) along the increasing of annealing temperature . However , SEM micrographs reveals that the films as -deposited are uniform throughout without grains and that of the films annealed at 400°C has grains with spherical shape , the surface of the films is homogenous and uniform .

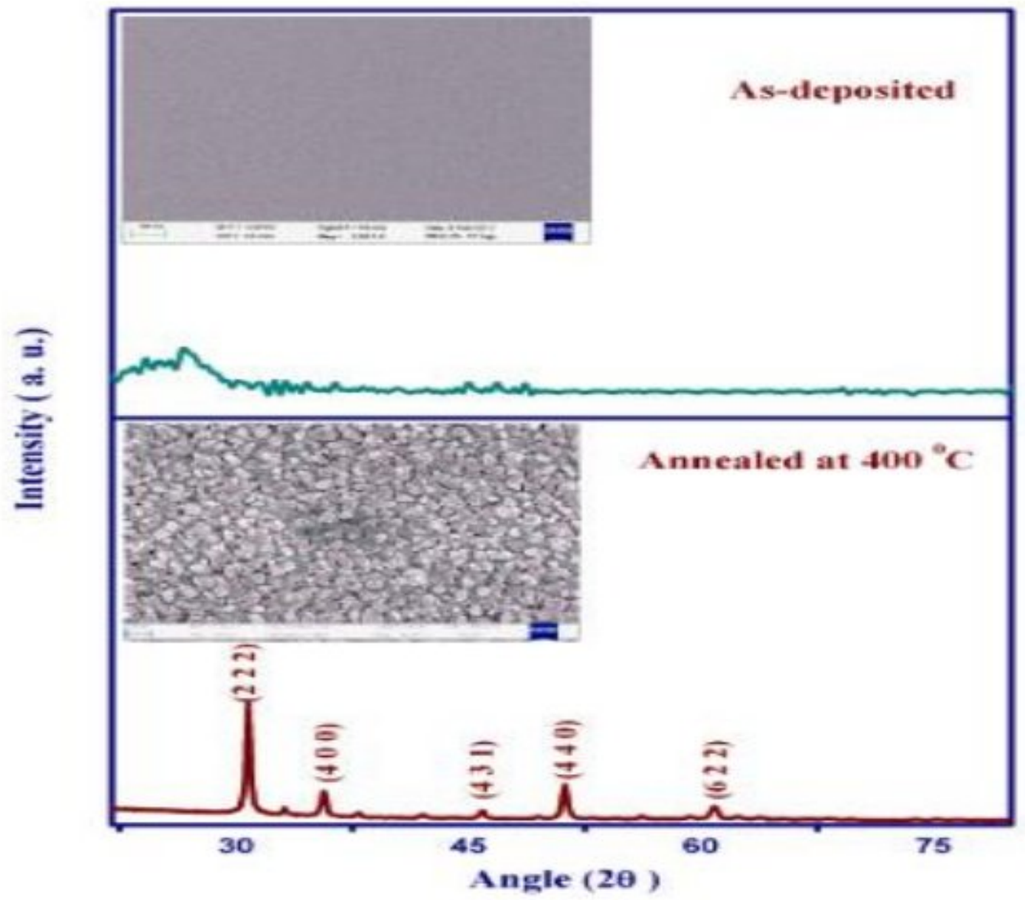

Fig1.10 : The typical XRD patterns and SEM micrographs(as the insets) for the as-deposited In_2O_3 thin films and for the In_2O_3 thin films of thickness 600 nm annealed at 400 °C .

The grain size are estimated from XRD using W-H plot and Debey Sherrer equation for the films annealed at 400°C and SEM micrograph, this values shows in table I.3 this values is good agreement with FWHM from XRD, the average grain size of about 23.2 nm as reported by Sudha et al [5] .

Table 1.3:The structural parameters of indium oxide thin films of thickness 600nm annealed at 400°C.

Grain size (nm)			Micro-strain		Dislocation density (lines/m^2)
Scherrer method	W-H method	SEM images	Scherrer method	W-H method	
22.25	22.21	23.2	0.0063	0.0062	2.02×10^{15}

Also, Lau et al [78] used a spin coater to deposit the indium oxide thin films with various of precursor concentration (0.3- 0.55 M) , they applied the XRD patterns to analyze the films obtained which presented the several peaks such as (211) , (222) , (400) ,(440) all the films while the peak (222) is preferred and strong orientation, it have polycrystalline structures at all the samples with various of concentrations(0.30 – 0.55 M) show good match with pure In_2O_3(PDF card number 01-071-2194)see figure 1.11.

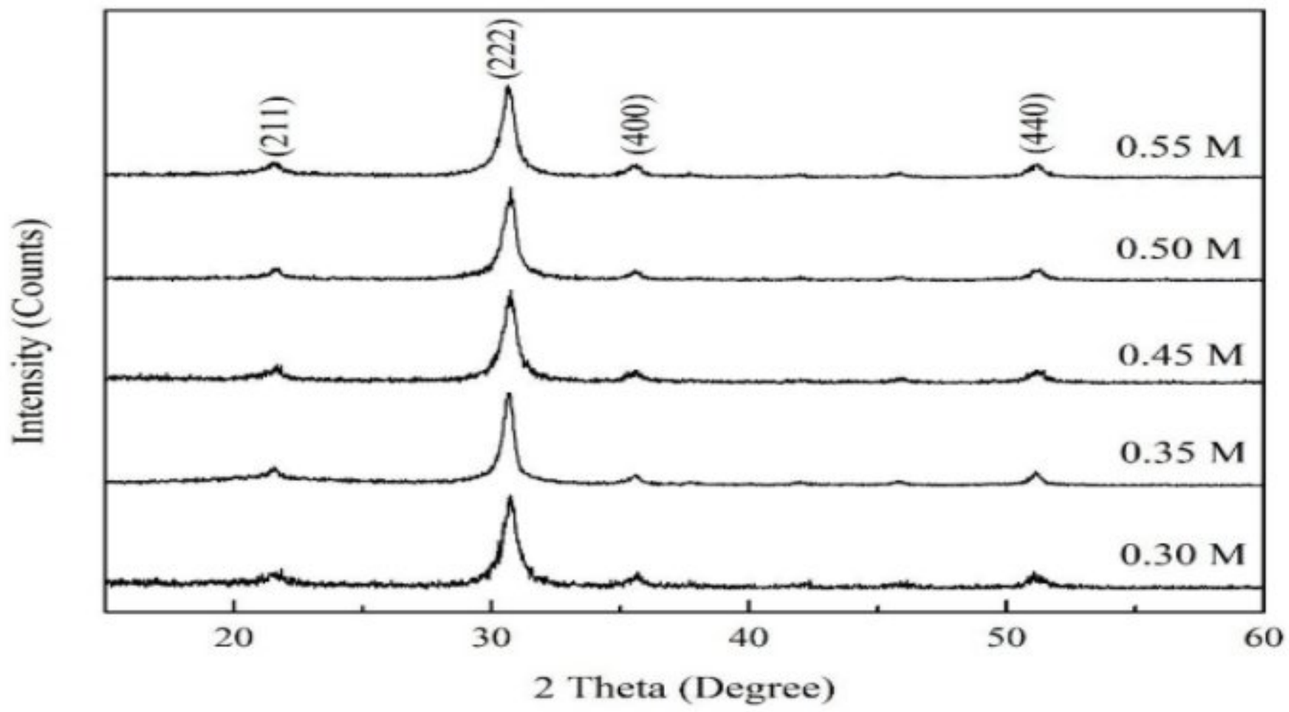

Fig 1.11:X-ray diffraction patterns of In_2O_3 thin films.

the average crystallite size are estimated from XRD patterns using the Sherrer's equation , this values varied non-linearity dependent of precursor concentrations (0.30-0.55 M) and it observed that FWHM is higher at 0.3M which can conclude the crystallite size is the smallest, it is in the range of 10 to 14 nm as tabulated in table 1.4.

Table 1.4: The FWHM, average crystallite size of various molarities of indium oxide thin films.

Molarity (M)	FWHM (°)	Average Crystallite Size (nm)
0.30	0.873	9.43
0.35	0.611	13.49
0.45	0.816	10.10
0.50	0.746	11.04
0.55	0.788	10.45

The degree of crystallinity was determined using the peak intensity ratio between the peaks with the highest peak for all samples whereas high intensity ratio means a better degree of crystalline. All indium oxide thin films show good crystallinity and the crystallinity are non-linearly dependent on precursor concentrations (0.30 – 0.55 M).

1.3.2 The optical properties:

Dependence the optical properties of In_2O_3 thin films deposited on glass by using high gamma

radiations, the In_2O_3 thin films have been doped by iron atomic concentration withy $=\frac{[Fe^{2+}]}{[In^{3+}]}=6\%$ at different gamma doses 1, 5, 10 and 100 kGy. The films are characterized by using UV–Vis–NIR spectra with Perkin–Elmer Lambda 950 spectrophotometer at normal incidence and room temperature in the wavelength range 250–2500 nm. As the result, figure1.12, iron doped indium oxide thin films can be used as optical windows in solar cells which due to the average transmission value increases from 79 to 88 percent after radiation in the wavelength range of 250-600nm, indicating an improvement in optical transmission and proving it belongs to the TCO family.

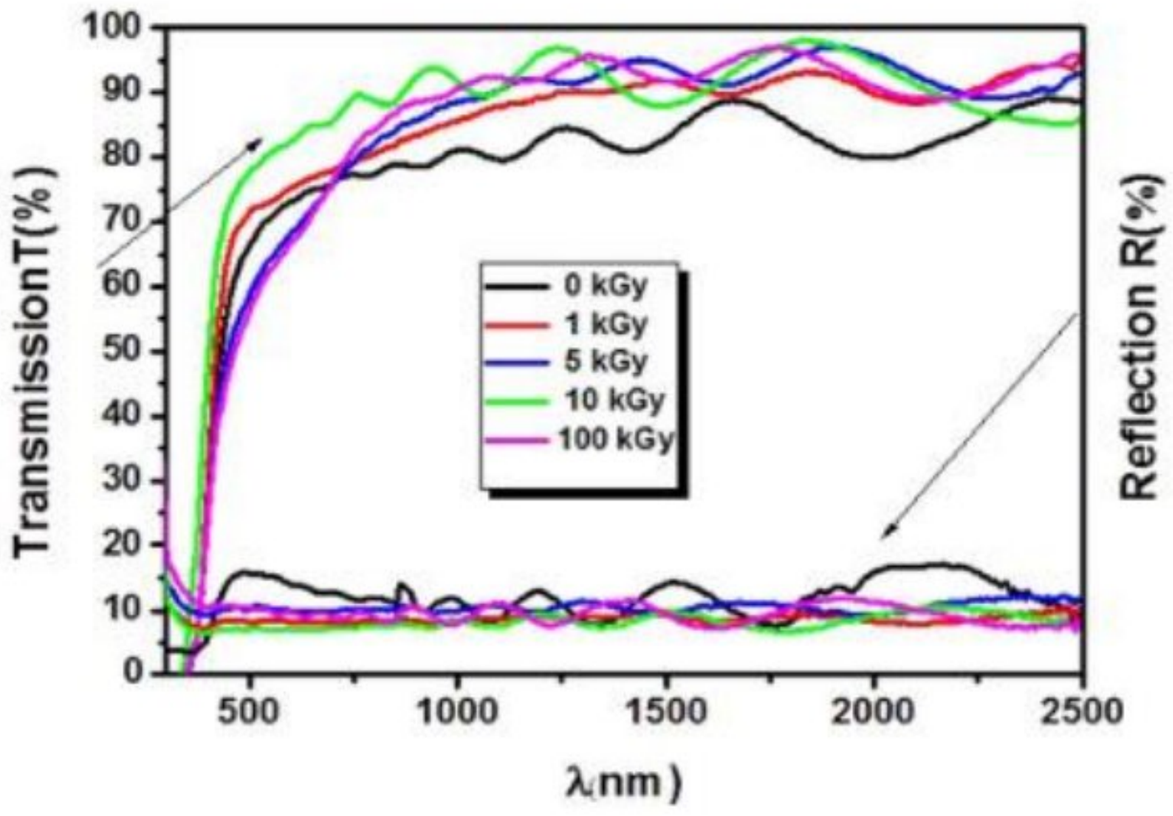

Fig 1.12: Optical spectra of transmittance and reflectance for non-irradiated and irradiated In_2O_3: Fe thin films at gamma doses: 1, 5, 10 and 100 kGy.

The films transmission has improved due to reduced scattering effects, improved crystallinity, and structural uniformity. Even after exposure to intense gamma radiation, the interference in transmission and reflection values of all samples indicates surface homogeneity and uniformity, which is attributed to improved crystallinity. On the other hand, the variation of absorption coefficient α (λ) for non irradiated and irradiated In_2O_3:Fe thin films in the range of [350–600] nm is illustrated in figure1.13. As observed from this figure that α (λ) has been increased after irradiation from 4.5×10^4 to 6.3×10^4 cm^{-1} near the ultraviolet region [300–400] nm corresponding to the high absorption domain, the highest absorption coefficient value was

obtained at 10kGy. The increasing of gamma radiation effected on the sensibility of iron doped indium oxide thin films to the absorption of high ultra-violet wavelength.

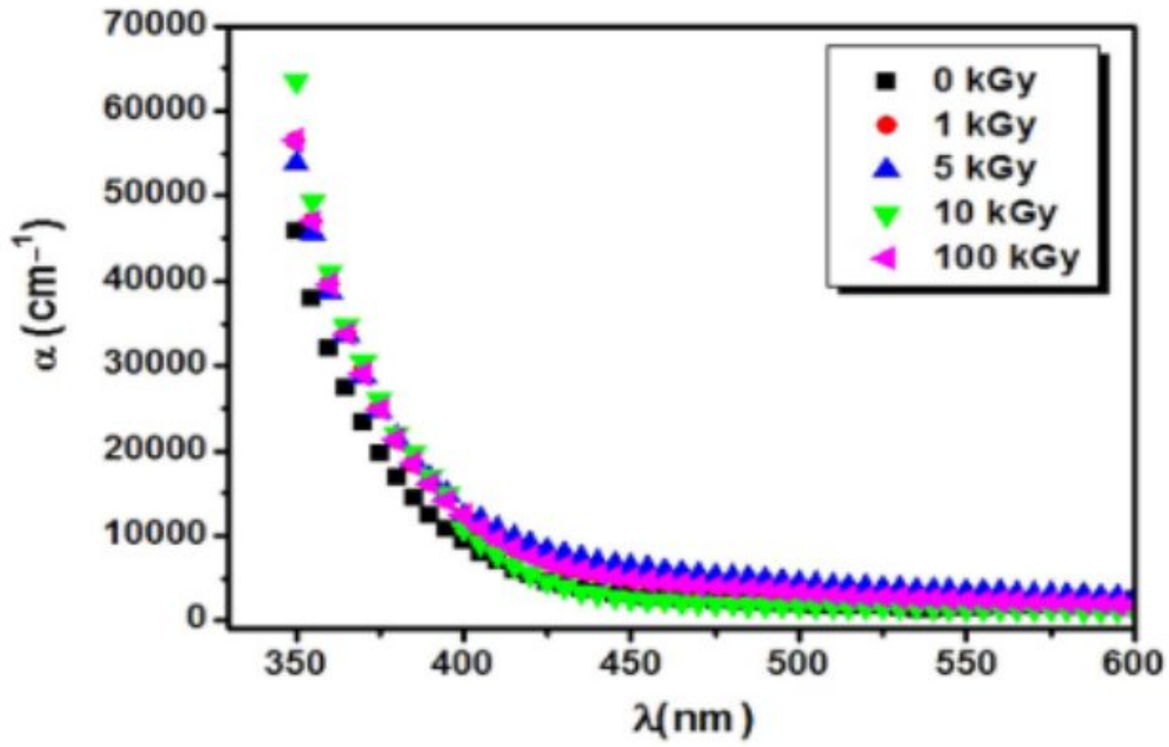

Fig 1.14: Spectral behavior of absorption coefficient (α) with wavelength of non- irradiated and irradiated In_2O_3:Fe at different gamma doses: 1, 5, 10 and 100 kGy.

On the other hand, we discovered that the absorption edge changed following irradiation, indicating that there are differences in band gap energy. The fluctuation of the absorbance coefficient α (λ) for non-irradiated and irradiated In_2O_3: Fe can be used to compute the band gap Eg. It was discovered that after irradiation of Fe thin films in the [350–600] nm region, the energy band gap expanded, as evidenced by the shift of the absorption edge as seen in transmission spectra. This demonstrates that incoming photons have enough energy to move electrons from the valence band to the conduction band. The increase in Fermi level inside the conduction band in degenerated semiconductors promoted the enhancement of crystalline quality of films as shown by XRD and Raman patterns.

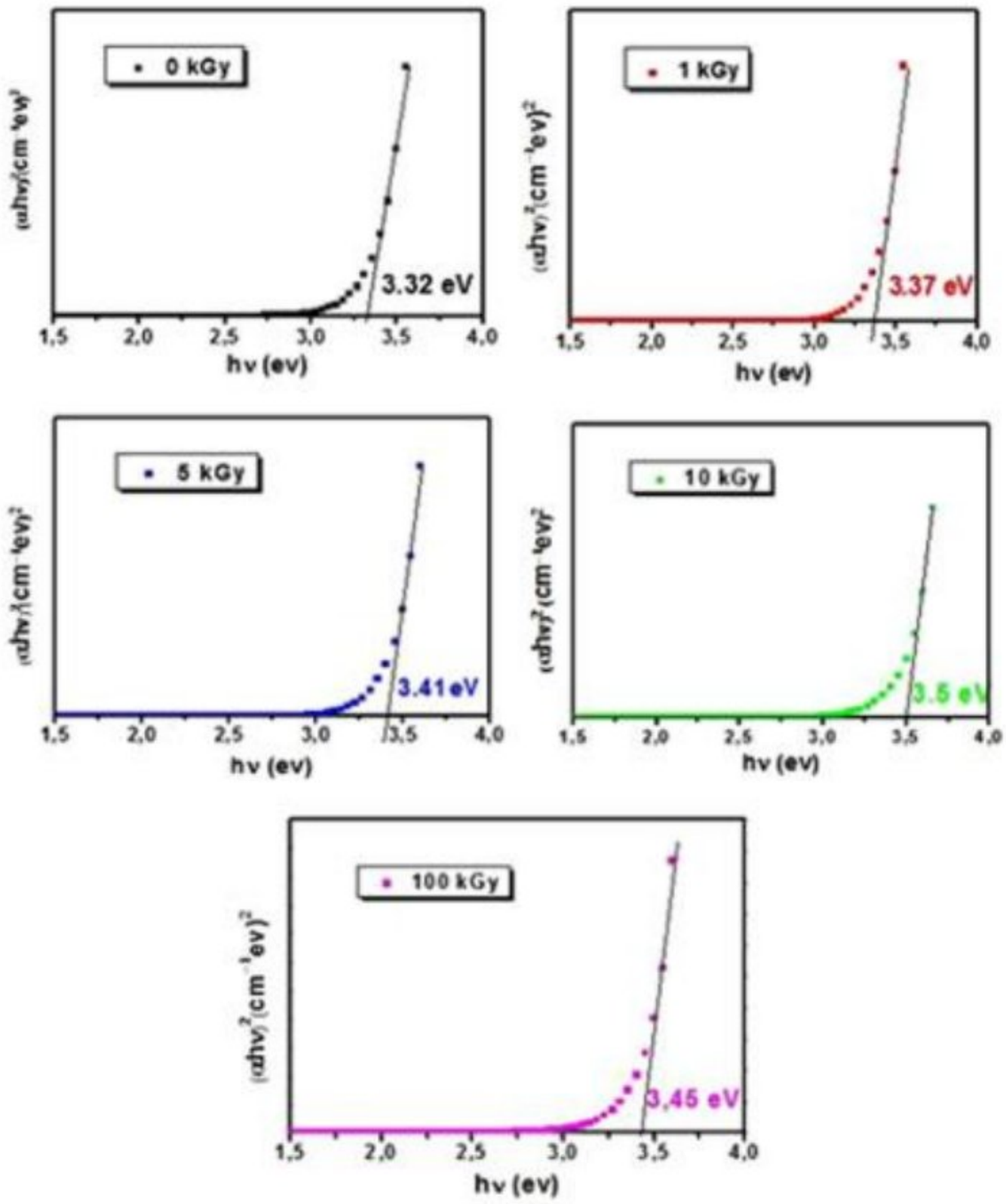

Fig 1.14:Plots of $(\alpha h\nu)^{1/2}$ versus hν for non-irradiated and irradiated In_2O_3:Fe at various gamma doses: 1, 5, 10 and 100 kGy.

Urbach's energy Eu, calculated from the exponential dependency of absorption coefficient vs photon energy, declines for all dosages from 0.57 eV to a minimum of 0.34 eV at 10 kGy, indicating a reduction in crystal lattice defect and degree of structural disorder. The optical band gap has the largest value for dose of 10 kGy, whereas Eu has the lowest value, indicating that In_2O_3:Fe irradiation at 10 kGy has good physical qualities.

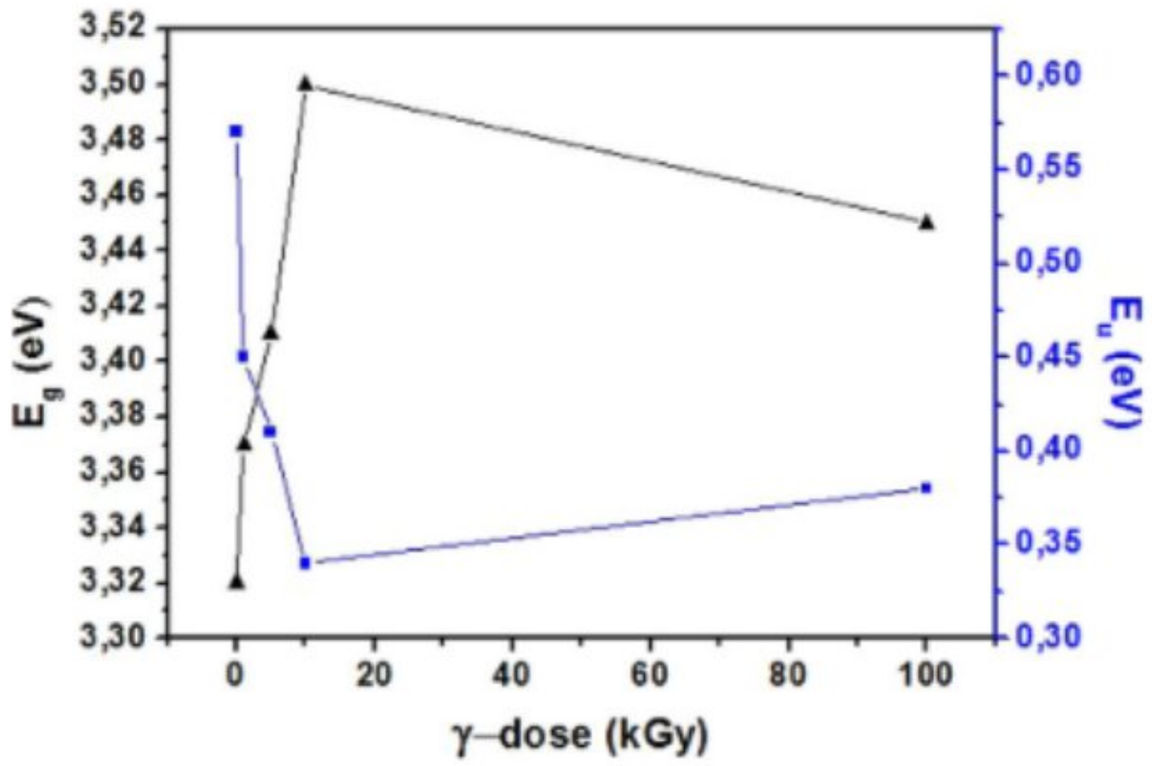

Fig 1.15: Variation of energy band gap values and Urbach energy for non-irra- diated and irradiated In_2O_3: Fe at gamma doses: 1, 5, 10 and 100 kGy.

The refractive index can be related to the optical absorption of the films, the defects located in crystal lattice and the variation of impurities in films. We can observed that the refractive index at 550 nm decreases after irradiation from 2.16 to a minimum value 2.03 when gamma dose is equal to 10 kGy[66] .In the other hand , Senthilkumar et al [79] deposited the In_2O_3 thin films by an electron beam evaporation system in the presence of oxygen with an initial vacuum (base pressure) of 5×10^5 mbar, an accelerating voltage of 1–10 kV. The co-precipitated In_2O_3 powder was used as a target material for evaporation source, it deposited on glass substrates, the samples were annealed at different temperatures in air. The films were characterized by using a UV–Vis-NIR double beam spectrophotometer (Carry 500-VARIAN) to obtain the optical properties of indium oxide thin films. The figure 1.16 shows in UV-Vis region that the transmittance of as-deposited In_2O_3 films is lower than all annealed films , the average transmittance is increased with increasing of annealing temperature from 350°C to 500°C , it is due to the enhancement in crystallinity of the films with rising annealing temperature which can well be related in XRD analysis, the improvement in transparency of the films is due that to decreasing the light scattering which can be applied as transparent electrodes in optoelectronic devices .The refractive indices of indium oxide thin films have been estimated from the weak and medium absorption region, it observed that the values increased from 1.813 to 1.910 by increasing annealing temperature which may be attributed to the improvement in crystallinity. In addition ,

the optical band gap was estimated from $(\alpha h\nu)^2$ versus hν plot this values increased from 3.67 to3.84 eV by increasing annealing temperature. Such a shift in band gap to higher energies is attributed to the increased carrier density due to Brustein–Moss effect.

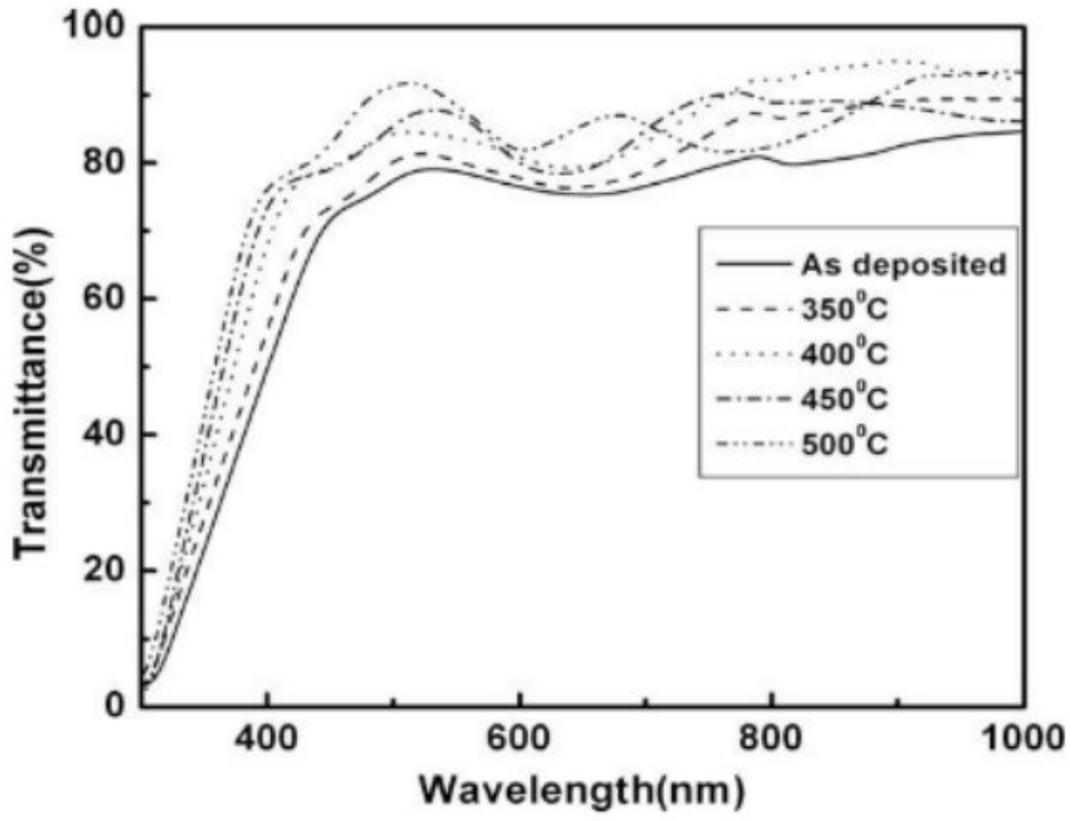

Fig1.16: Optical transmittance spectra of In_2O_3 films formed at different annealing temperatures.

Rambu et al[80] were prepared In_2O_3 thin films by using Vacuum thermal evaporation (the quasi-closed volume technique) ,they used a metallic In ,in the form of pellets it was evaporated from a tungsten crucible, in a vacuum of 4×10^3 Pa at various oxidation temperatures 623 K, 673 K and 700 K .Moreover, the samples characterized to obtain the optical transmittance whereas increased from 60% to75% . Obviously, the presence of the In metallic microcrystallines caused a low transmittance of the films , the un-oxidized indium acts as scattering centers for light and consequently, the optical transmittance is low .As the results , it can be estimated the band gap of In_2O_3 thin films from the absorption edge region while the values is lower than 3.7eV , it is due that increasing of density donor states near the conduction band determined by oxygen vacancies .The refractive index of the films decreases with the increases of wavelength (λ).

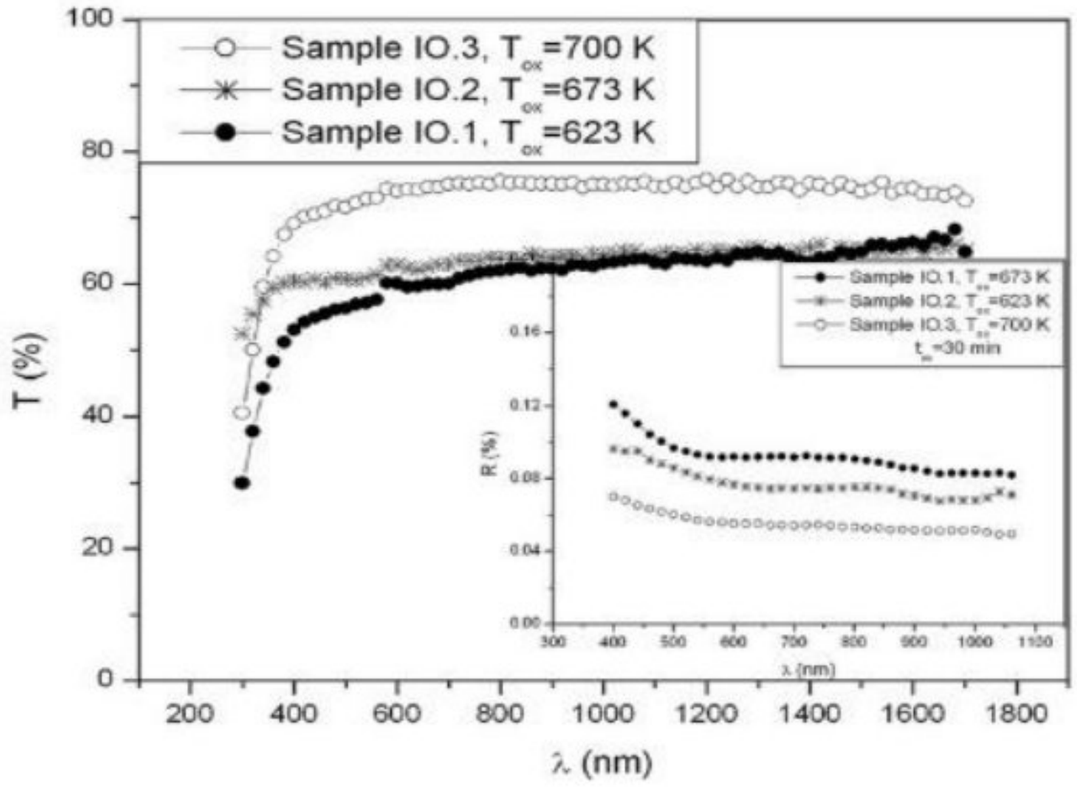

Fig 1.17: Transmission spectra of In_2O_3 analyzed samples (inside are presented reflec- tions spectra for the same samples).

On the other hand, the In_2O_3 thin films prepared by using vacuum thermal evaporation on glass substrates with effect of annealing temperatures from 573-873 K to obtain an optical properties. As the results , figure 1.18 shows that the transmittance is good in the visible range and exhibits interference pattern (the spectra have a high transmittance 85%) it means that the films have less scattering effects, structural homogeneity, high uniform and smoothing and better crystallinity. The band gap varied with increasing of annealing temperature from 2.9-3.5eV, it decreases at high annealing temperature while crystallite size and density of grain boundaries is high reported by Veeraswamy et al[81].

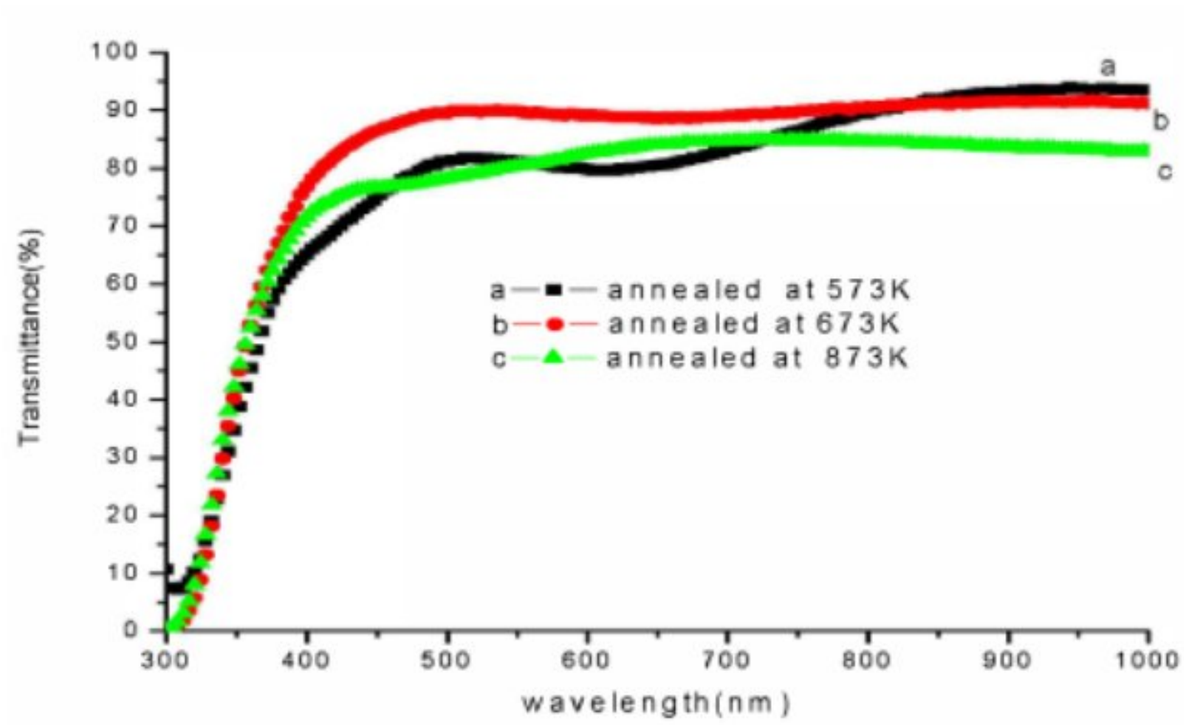

Fig 1.18: Optical transmittance of In_2O_3 films annealed at different temperatures.

1.3.3 Electrical properties:

According to Dey et al [82], Hall measurement results for different substrate temperature with no oxygen gas found that : the reduction of resistivity with increasing of temperature substrates due to high crystallization of the films (confirmed by XRD patterns) , the mobility of the Ce doped indium oxide films increased from 4.43 to 37.8 cm^2/V as the substrate temperature increased from RT to 180 °C and the carrier concentration is higher at room temperature due that low oxygen vacancies at deposition of the films after that carrier concentration decreased with increasing of substrate temperature , the increase in carrier concentration from 2.53×10^{20} cm^{-3} to 2.73×10^{20} cm^{-3} might be due to a larger density of Ce^{4+} ions in In^{3+} substitutional sites as shown in figure 1.19.

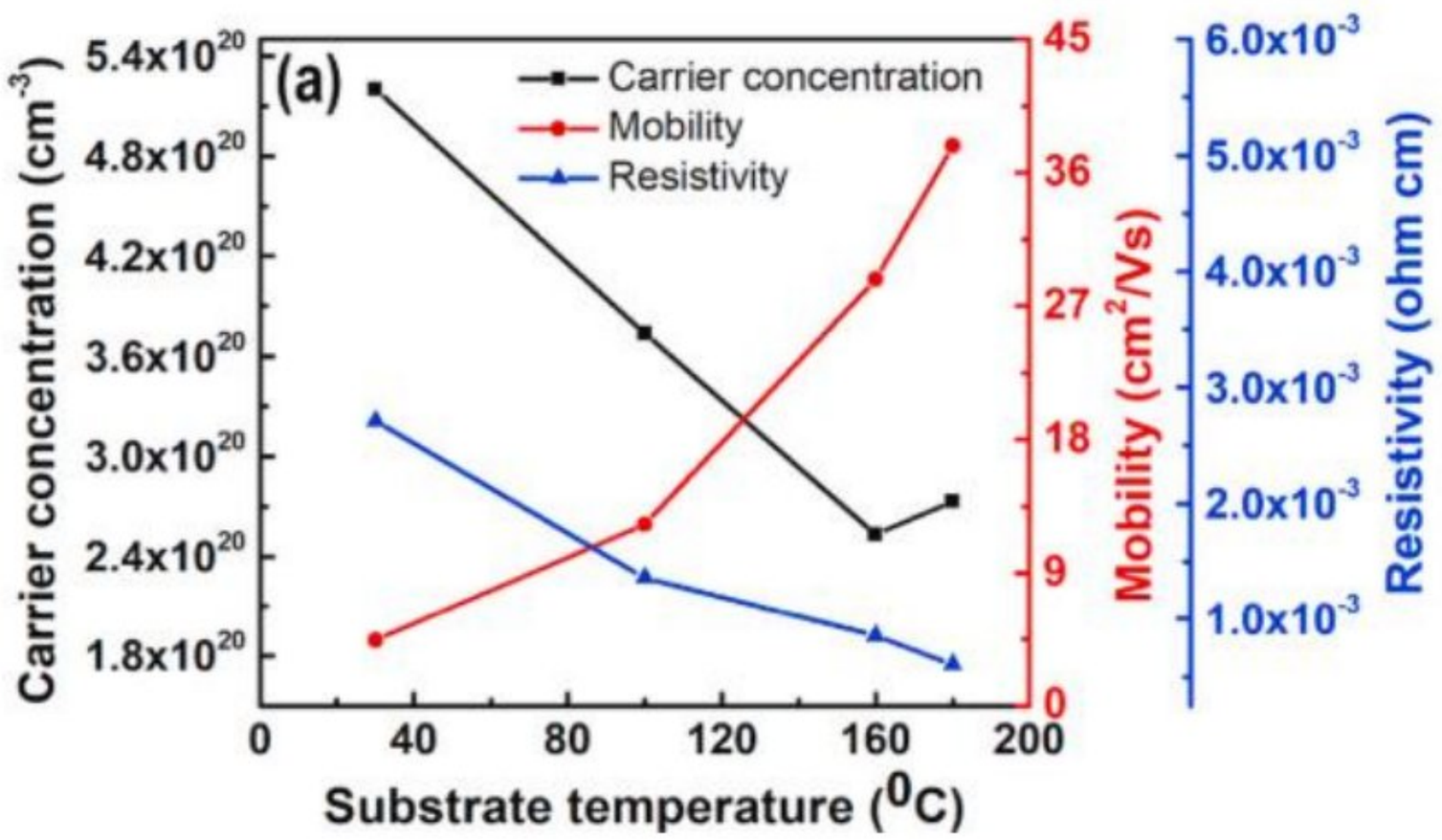

Fig 1.19: Effect of substrate temperature on resistivity, carrier concentration and mobility of ICeO films deposited without any oxygen gas in the chamber.

A second part , Hall measurement results for the oxygen concentration in the sputtering chamber is increased from 0.6 vol% to 2 vol% with the substrate temperature fixed at 160°C found that : the carrier concentration decreases from 2.86×10^{20} to 2.9×10^{19} cm^{-3}which due that a reduction of oxygen vacancies, The mobility of ICeO films increased initially from 36.5 to 51 cm^2/V when the oxygen content in the chamber is varied from 0.6% to 1.4% after that it can be seen the decline of mobility with high oxygen concentration which means to the collisional energy loss of the particles with oxygen during their arrival towards the substrate surface , this results related by XRD patterns of the films and the resistivity increased monotonically with the increasing oxygen

contents in the chamber.

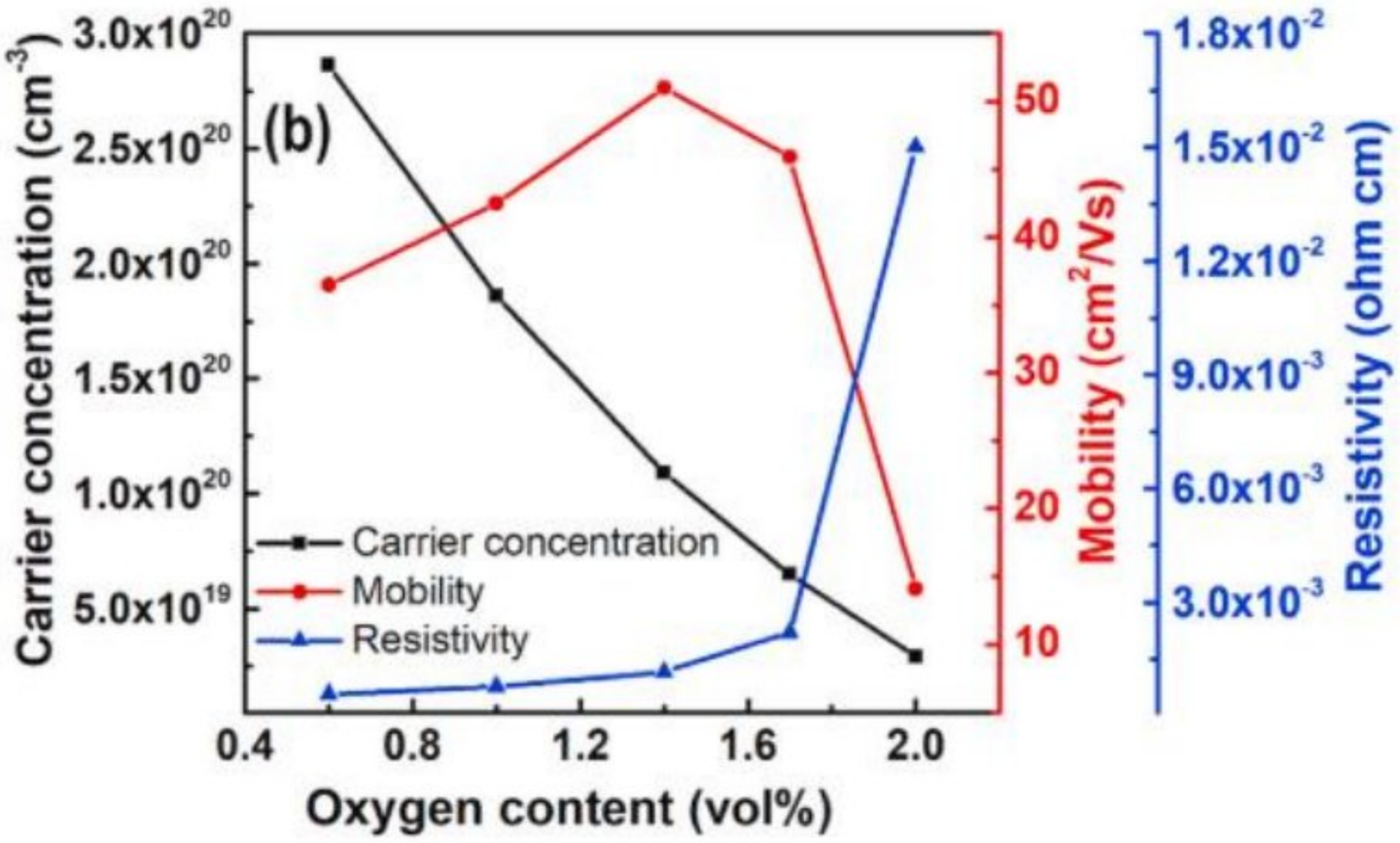

Fig 1.20: Effect of oxygen content on resistivity, carrier concentration and mobility of ICeO films deposited at 160 ◦C.

Ghamari et al [53] were prepared the tin doped In_2O_3 thin films by using electron-beam deposited process with various thickness to obtain the electrical properties. The films have characterized by four point probe technique. As the results, the values of sheet resistance R_s decreased with growing the films thickness, it is confirmed by XRD results which found that the crystallite size increased in order that the grain boundaries density decreased. Therefore , the electrical properties of ITO thin films improved by Hadi et al[58] , they prepared the films by using RF sputtering with variation of annealing temperature , it can be found a several parameters such as : the electrical resistivity varied linearly deceasing with the increasing of annealing temperature from $61.23 \times 10^{-4}\Omega.cm$ to $6.68 \times 10^{-4}\Omega.cm$, the carrier concentration is higher at post-annealed 700°C than the films at as deposited .These results is supported by the mobility characteristics of the ITO samples as the mobility of the post-annealed sample is higher than the as-deposited sample as shown in figure 1.21. It proves that the strong crystalline structure and smoother surface roughness after post-annealing especially at temperature of 700°C helps in improving the transmittance and electrical characteristics of the ITO thin films.

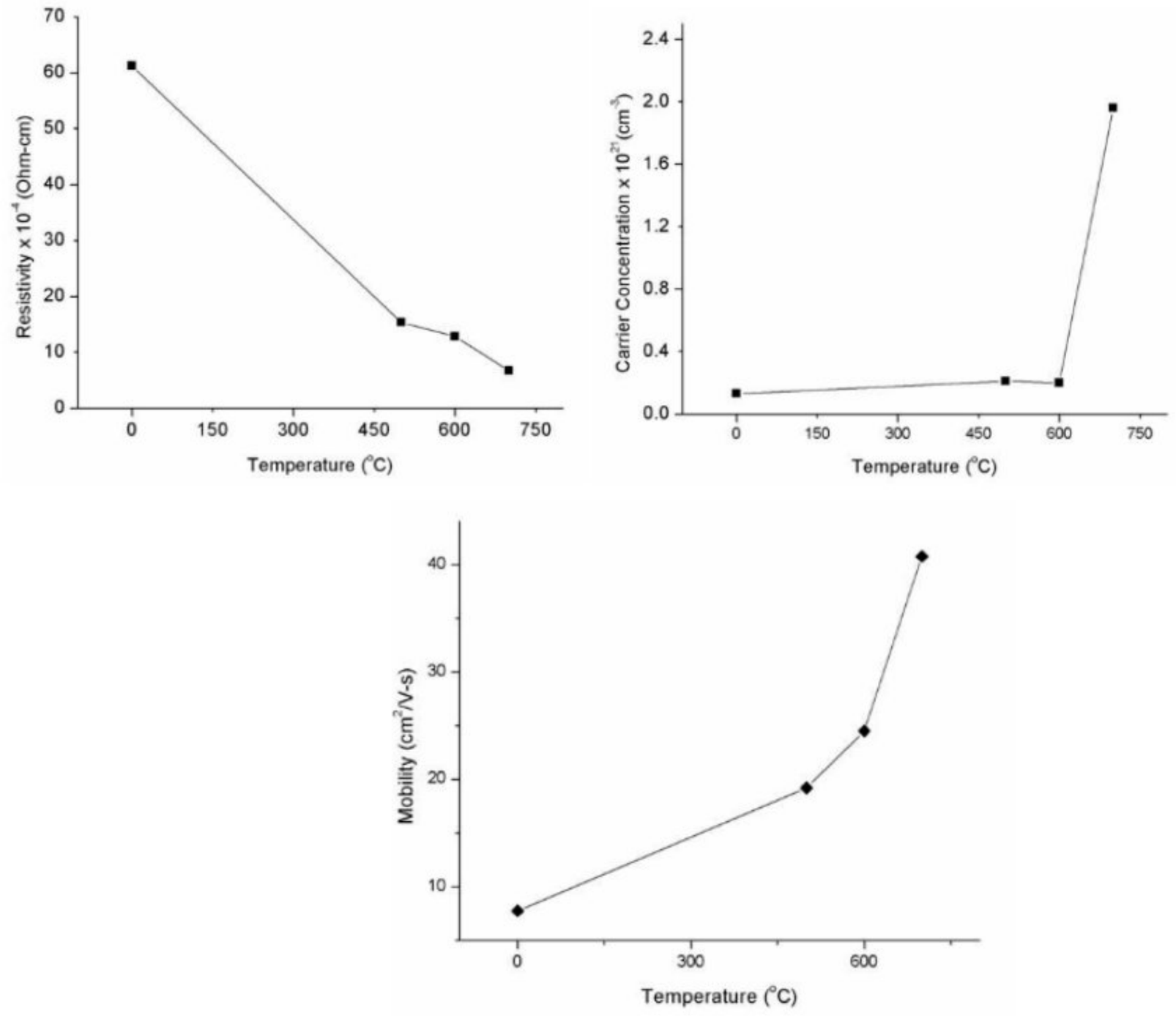

Fig 1.22: The variation of resistivity, carrier concentration and mobility for ITO thin films a function annealing temperature.

However, Nefzi et al [83] reported that the electrical properties of indium oxide thin films improved while varied the parameter of gamma irradiation doses (0 , 1 , 5, 10 , 100 kGy) , it noted that the resistivity reduced with the rising of gamma irradiation doses which attributed the increase of oxygen vacancies and broken bonds. Electrical mobility is also increased significantly but decreased slightly for 100 kGy which due to lattice deficiencies like interstitial indium and the increase of the O vacancies' number. The n-type of indium oxide semiconductor was achieved by sign of Hall Effect measurement.

Table 1.5: Mobility (l), electrical resistivity (q), and volume carrier concentration (Nv) of In_2O_3 material before and after gamma irradiation.

Dose (kGy)	0	5	100
μ ($cm^2\ V^{-1}\ s^{-1}$)	1.17	30.99	7.18
ρ (10^{-2}) (Ω cm)	65.02	1.02	1.40
N_v^* (10^{19}) (cm^{-3})	0.8	1.96	6.19

Neeti et all [50] were deposited the indium oxide thin films by using pulsed laser deposition with different substrate (GaAs , Si , quartz , glass) , they measured the electrical resistivity by four-probe technique and was also reasonably low at around $10^{-3}\Omega$-cm for all the samples .

1.4 Applications of In_2O_3 thin films:

Due to the various properties of indium oxide thin films (high optical transparency and high conductivity); it can apply in several applications such as:

1.4.1 Optoelectronic devices, including solar cells:

TCOs are employed as transparent electrodes in solar cells. They must have a high optical transmission to allow effective photon transport to the active layer, as well as a good electrical conductivity to achieve the lowest possible cost[68].

1.4.2 Gas sensors:

Many years have been spent researching semiconductor materials whose conductance is directly regulated by interaction with an active gas. Certain metal oxides have reversible chemisorptions of reactive gases on their surfaces. In semiconductor sensors, the electron concentration varies less linearly with pressure up to eight decades, but the mobility varies by less than a factor of two over the same pressure range. This shows that gas chemisorptions on the surface of semiconductor materials can be used to make gas-sensing electronic devices. Because of its remarkable sensitivity to the chemical environment, In_2O_3 has been widely used in sensing applications. The electrical characteristics of In_2O_3 are influenced by oxygen vacancies on the surface, which affect the sensing process. Upon oxidation, via adsorption of molecules such as NO_2 at vacancy sites that accept electrons, electrons are withdrawn and effectively depleted from the conduction band, leading to a reduction of conductivity. On the other hand, reducing molecules such as H_2 can react with surface-adsorbed oxygen, leaving behind an electron and hence higher conductivity. In_2O_3 films deposited by spray pyrolysis: gas response to

reducing(CO, H_2) gases have been prepared by Korotcenkov et al[11].

1.4.3 Electronic displays:

Human operators interact with electronic equipment via electronic displays. Liquid crystal displays[89], organic light emitting diodes (OLEDs) [84], electroluminescent displays, plasma and fluorescent displays, and electrochromic displays, among other components and device designs, are required. Transparent and conductive films, luminous or fluorescent films, as well as dielectric and insulating layers are needed to make these displays.

1.4.4 Humidity sensors:

Because moisture is a continual environmental element, accurate measurement and control are critical. Moisture sensors are commonly used in home appliances, medical equipment, agriculture, and automobiles[45]. Electroluminescent devices, anti-reflection coatings, electroluminescent liquid, crystal liquid, crystal displays, electrochromic devices, photo thermal devices, and light-emitting diodes are among the various applications. Because In_2O_3 is mainly employed as a film, it is usually described in terms of thin film properties[68].

Conclusion:

The improvement of properties indium oxide thin films were obtained by using a various preparation technique is reported in pervious study. The different properties such as: structural, optical and electrical are achieved and improved with applied a variation on the method of deposition, various substrates, annealing temperatures and background pressure etc.

CHAPTER 2

Spin coating deposition and characterization methods for In_2O_3 thin films

Introduction:

The growth of In_2O_3 thin films have completed by using a several methods such as reported in pervious chapter .Many scientists use sol-gel (spin coating) to improve the properties of indium oxide thin films for solar cells applications, sensor gas , optoelectronics application and etc .However , this films investigated with applied a some effects on the parameters of spin coating process , it characterized by several methods to found a good results for future application such as: X-Ray diffraction for structural properties ,UV-vis for optical properties , SEM for morphological properties and four probe for technique for electrical properties . Gas sensors, solar cells, and catalysts are just a few of the electronic devices that use In_2O_3 thin films. The first half of this chapter explains the Sol-Gel (spin coating) technique for deposition thin films, while the second portion of the chapter covers several approaches and relationships that are used to describe films.

2.1 Processing steps of preparation In_2O_3thin films using spin coating technique:

Spin coating includes placing a small puddle of fluid resin in the center of a substrate and spinning it at a high speed. This method has the advantage of being simple to execute and requiring just modest investments. On planar substrates with size of the order of cm2, it produces good results [85] as reported in pervious chapter. Obviously, we use this technique to obtain indium oxide thin films at high properties for many photovoltaic and optoelectronic application, figure 2.1 shows the device of spin coating method.

Fig 2.1: Holmarc spin coater.

However, figure 2.2 shows the procedure of spin coating technique for In_2O_3 thin films, on this procedure it can be applied some influence of the main spin coating parameters on properties of the deposited films.

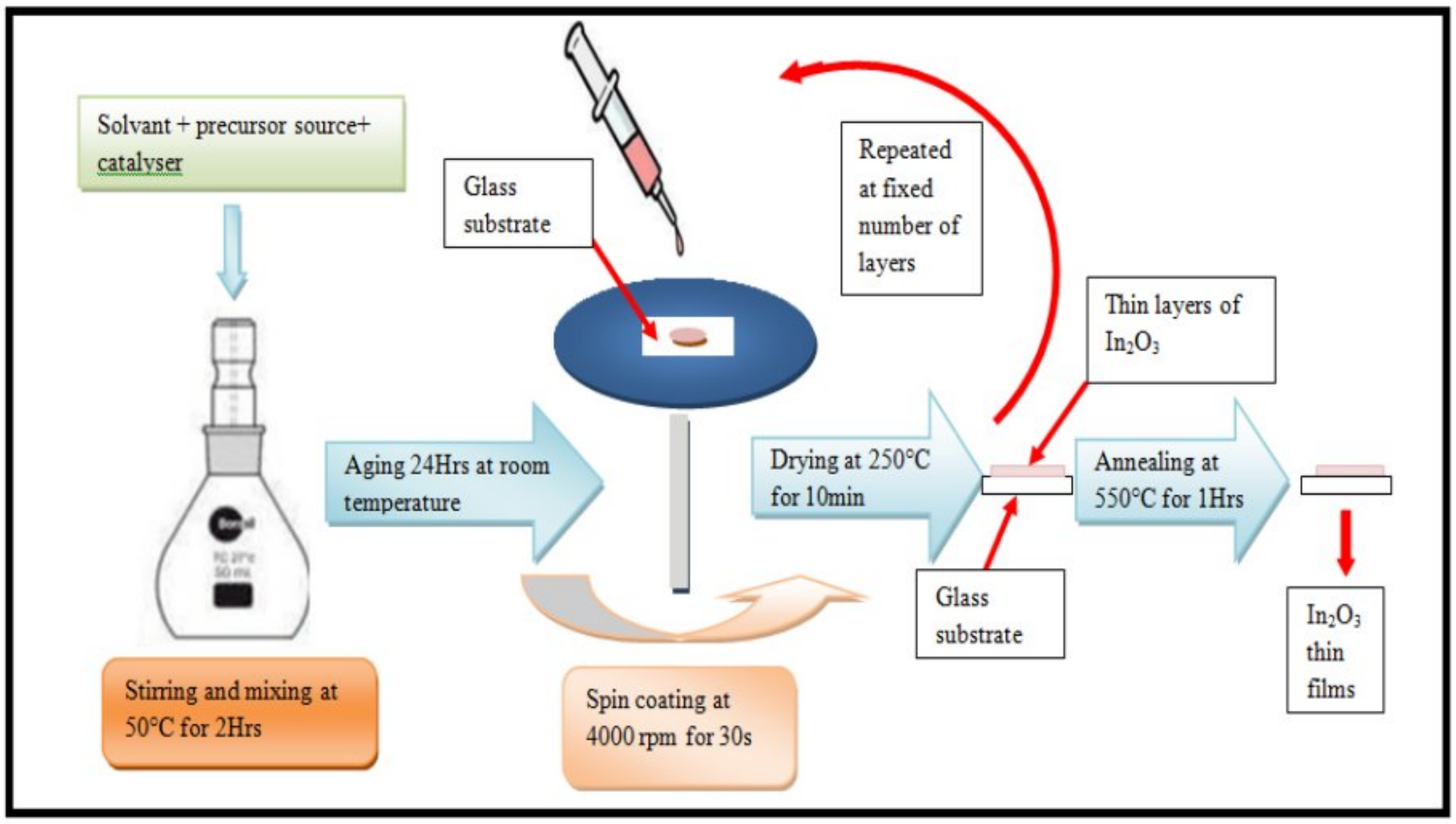

Fig2.2: the sol gel synthesis procedure of prepared In2O3 thin films.

2.2 Influence of films thickness:

To prepare the indium oxide layers, we follow these steps.

2.2.1 Preparation of solution:

The undoped indium oxide (In_2O_3) solution was prepared by Indium (III) nitrate hydratethat was used as source material of In^{+3} and it was dissolved in appropriate amount of ethanol and acetyl acetone as the stabilizer with 0.15 M concentration. The volume ratio of acetyl acetone to ethanol was maintained at 1:10 (see table 2.1).The starting solution was stirred for 2 h at 50°C, then mixed and stirred with a magnetic stirrer for 24 h at room temperature to obtain a transparent solution.

Table2.1: The parameters of chemical products.

Chemical name	Indium (III) nitrate hydrate	ethanol	acetyl acetone
Molecular formula	$In(NO_3)3 \cdot H_2O$	C_2H_6O	$C_5H_8O_2$
Volume	/	9ml	1ml
Weight	0.43 g	/	/

2.2.2 Preparation of the films:

In elaboration of the films, we have deposited the films on glass substrates to obtain good results in their properties. Soda lime glass (SLM) slides were used as substrates with the size of (2.5 cm × 2.5 cm × 0.15 cm). Before the deposition, the glass substrate was cleaned followed by rinsing in methanol and acetone for 10 min then cleaned with deionized water for 5 min and dried in air , the figure 2.3 shows the glass substrate was used .

Fig 2.3: Cut glass substrates using a sharp pen.

Fig 2.4: The cleaning of glass substrate and films deposition.

The prepared solution was dropped onto cleaned glass substrate, with rotation speed of 4000 rpm for 30 s in order to obtain a well coated thin film on glass substrates. Subsequently, the coated films were dried at 250°C for 10 min after each successive coating in a furnace to evaporate the organic solvent. The procedures was repeated 4, 6, 8, 10 and 15 times (number of layers) in order to achieve various In_2O_3 thin film thicknesses. Finally, the film was annealed at 550°C in the furnace for 1 h see figure2.5.

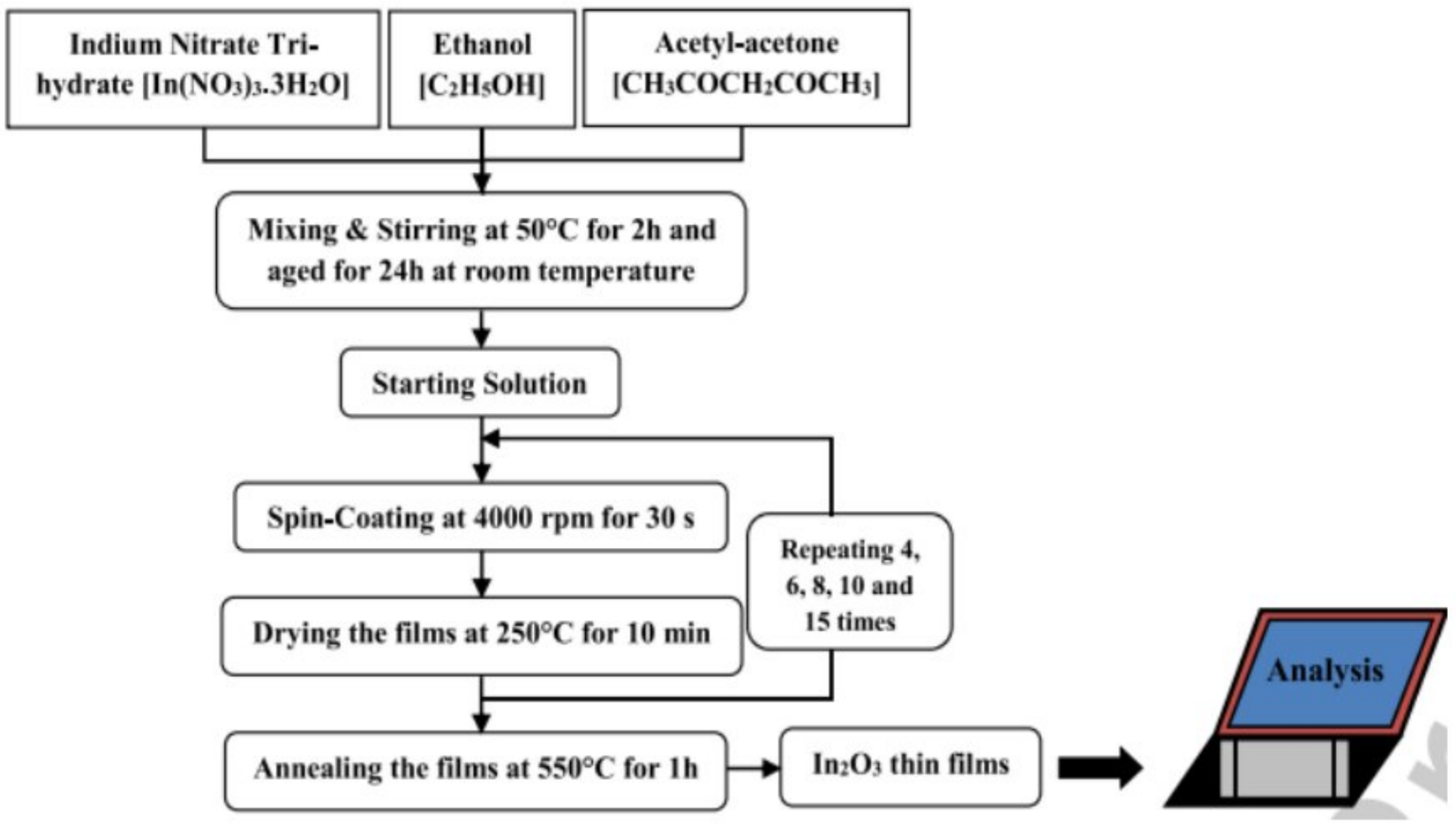

Fig 2.5: Flow chart showing the schematic diagram for In_2O_3 thin films preparation.

2.3Influence of pH solution:

2.3.1 Preparation of solution:

The solution have several parameters to produce thin films by spin coating process such as pH solution dependent with the source precursor , in this section we have use a last solution in previous work .In the other hand , we dissolved a NaOH powder in deionized water with concentration 2mol/L see table 2.2. After stirred and mixed24h for transparent solution, we added droplets of NaOH in indium oxide solution and measured the pH with pH-meter technique; it obtained a various pH solution of indium oxide (0.84, 2.63, 5.01, and 9.58).

Table2.2: The parameters of chemical products.

Chemical name	**Indium (III) nitrate hydrate**	**Ethanol**	**acetylacetone**	**Sodium hydroxide**
Molecular formula	$In(NO_3)3\cdot H_2O$	C_2H_6O	$C_5H_8O_2$	NaOH
Volume	/	9ml	1ml	/
Concentration	0.15mol/L	/	/	2mol/L
Molecular weight	354.88 g/mol		/	

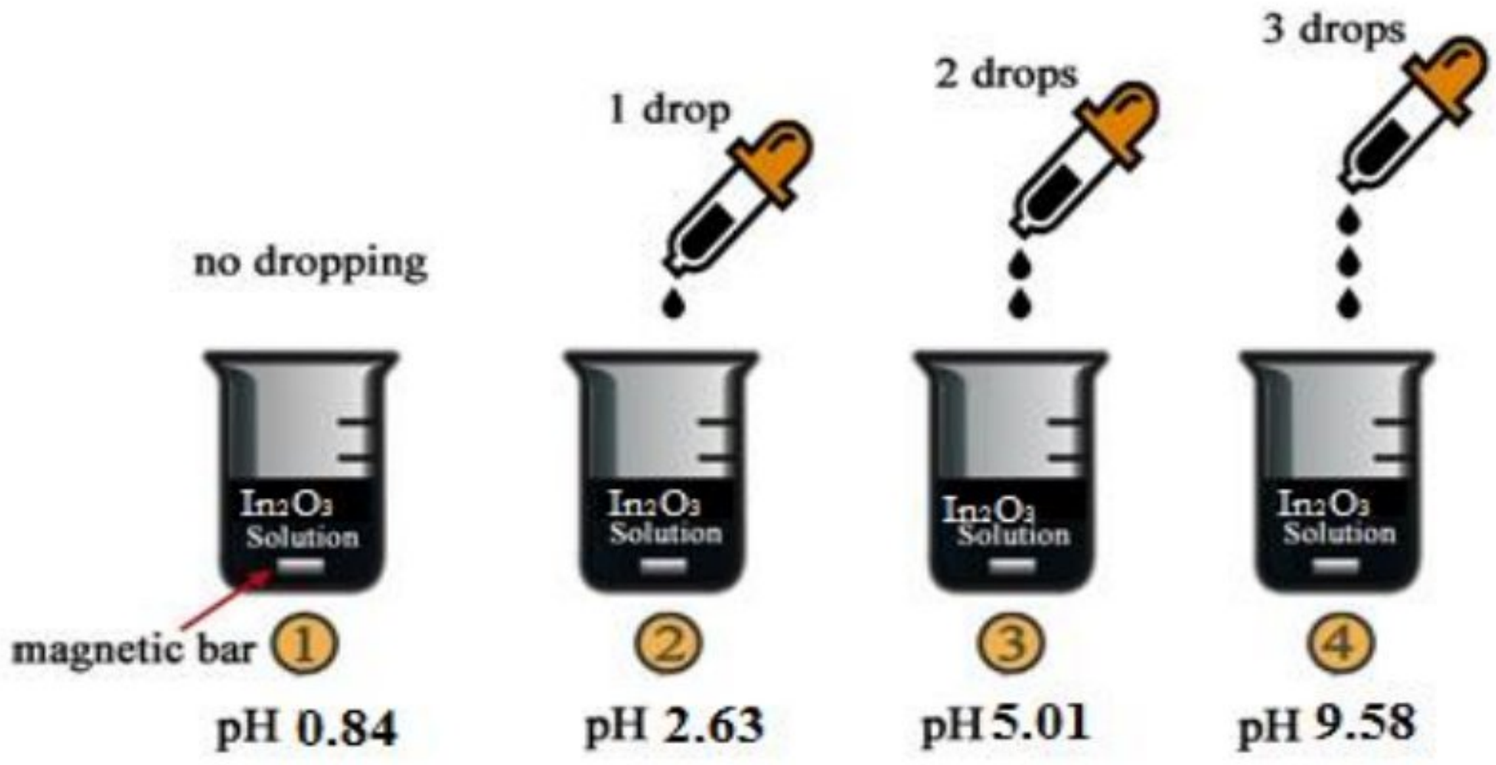

Fig 2.6: Experimental procedure for the pH adjustment in the In_2O_3 solution.

2.3.2 Preparation of the films:

The glass substrates were cleaned at same previous steps. The In_2O_3 thin films was deposited on cleaner glass substrates by using spin coating process with same parameters of deposition (choosing the parameters at film thickness 910nm), the films obtained was annealed at 550°C in the furnace for 1h.

2.4 Influence of precursor source:

2.4.1 Preparation of solution:

In this section, we have to deposit an indium oxide thin films by using a various precursor source (indium (III) acetate, indium (III) chloride (see table2.3)) to obtain a homogenous indium oxide solution see figure 2.7. We use acetyl acetone as solvent to dissolve the several precursor sources such as indium (III) acetate and indium (III) chloride with different concentration (0.5M, 0.1M, 0.15M, 0.2M, and 0.25M).The starting solution was stirred for 2 h at 50°C, then mixed and stirred with a magnetic stirrer for 24 h at room temperature to obtain a transparent solution.

Table2. 3: The parameters of chemical products.

Chemical name	**Indium (III) acetate**	**Indium(III) chloride**	**acetyl acetone**
Molecular formula	$C_6H_9InO_6$	$InCl_3$	$C_5H_8O_2$
Volume	/	/	10ml
Concentration (mol/L)	0.5 , 0.1,0.15 ,0.2 ,0.25	0.5 , 0.1,0.15 ,0.2 ,0.25	/
Molecular weight	291.95g/mol	221.177g/mol	/

2.4.2 Preparation of thin films:

The indium oxide thin films was deposited on cleaned glass substrate (see cleaner procedure is shown in figure 2.4)with the several parameters of spin coating technique (4000rpm , 30s , 6 layers), the samples was drying at 250°C for 10min , the final films was annealing at 550°C for 1Hrs .

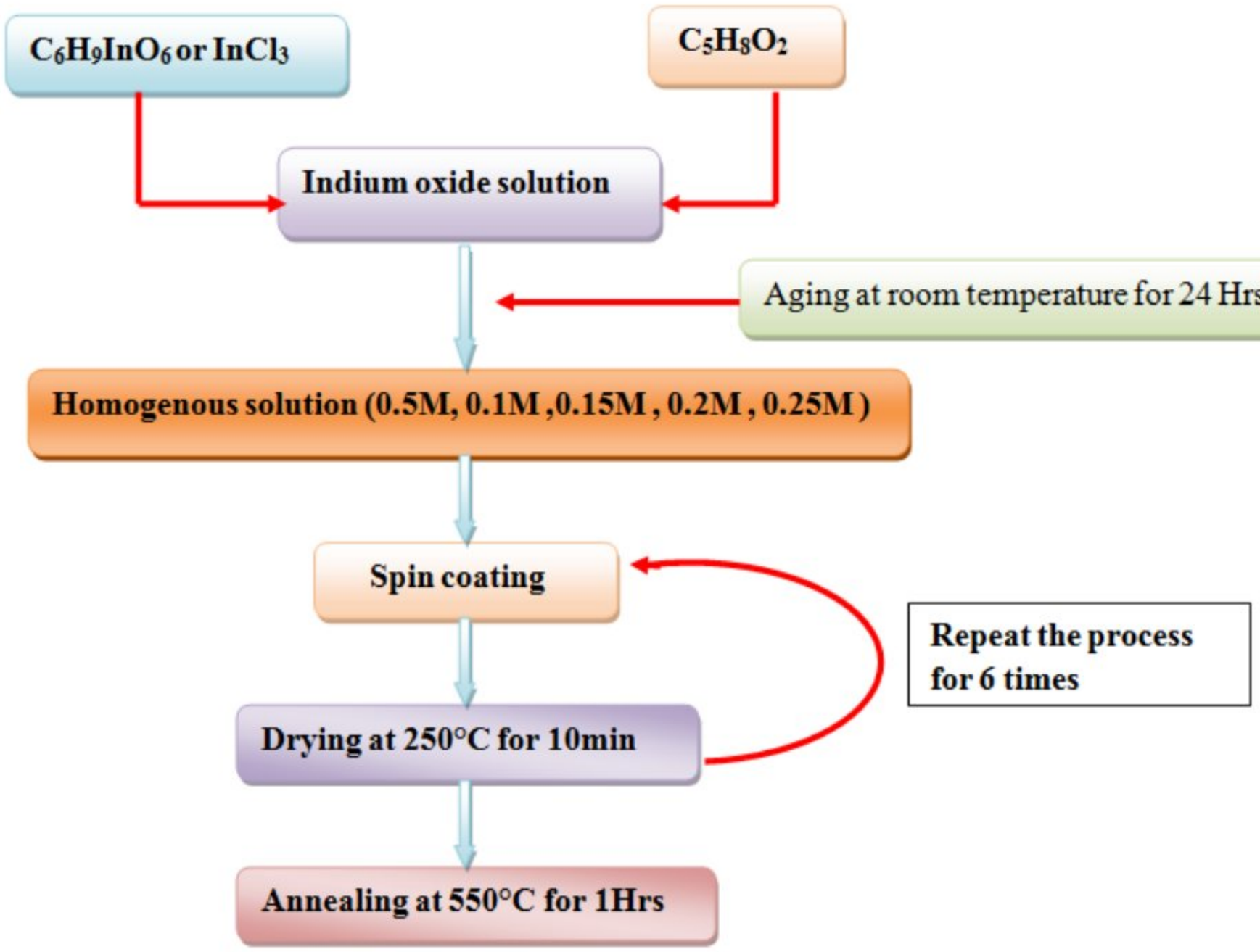

Fig 2.7: The sol gel synthesis procedure of prepared In_2O_3 thin films.

2.5 Influence of doping In_2O_3 thin films:

2.5.1 Preparation of solution:

Preparation of Sb and Ba doping In_2O_3 solution

- Sol gel spin coating was used to make antimony doped indium oxide thin films with varied concentrations (0, 3, 6, 9 mol%) on glass substrates. The initial materials, solvent, and antimony doping supply were indium III chloride anhydrous ($InCl_3$), absolute acetyl acetone ($C_5H_8O_2$), and antimony (III) chloride ($SbCl_3$), respectively. The indium (III) chloride concentration was 0.15 M, and the volume of actylacetone was 10ml. To obtain clear and homogeneous solutions, the prepared solutions were agitated at 50 °C for two hours.
- Sol gel spin coating was used to create barium doped indium oxide thin films with various concentrations (0, 3, 6, 9 mol%) on glass substrates. The initial precursors, solvent, and antimony doping source were Indium III chloride anhydrous ($InCl_3$), absolute acetyl

acetone ($C_5H_8O_2$), and Barium chloride ($BaCl_3$), respectively. The indium (III) chloride concentration was 0.15 M, and the volume of acetylacetone was 10ml. To obtain clear and homogeneous solutions, the prepared solutions were agitated at 50 °C for two hours.

Table2.4: The parameters of chemical products.

Chemical name	**Indium(III) chloride**	**acetyl acetone**	**Antimony chloride**	**Barium chloride**
Molecular formula	$InCl_3$	$C_5H_8O_2$	$SbCl_3$	$BaCl_2$
Volume	/	10ml	/	/
Concentration(%.mol)	/	/	0,3,6,9	0,3,6,9
Molecular weight (g/mol)	221.177	/	228.11	244.28

2.5.2 Preparation of thin films:

The resulting solutions were dropped onto cleaned glass substrates and spun at 4000 rpm for 30 seconds after maturing for 48 hours at room temperature. The films were dried at 250°C for 10 minutes after each coating stage to evaporate the solvent and eliminate organic residues. To reach the necessary film thickness, the spin coating process was done six times. To generate good crystalline films, all of the samples were annealed in a furnace at 550 °C for 1 hour.

2.6 The adhesion test:

The adhesion test for thin films is an interesting step; It is an essential parameter in the reliability of the deposited films, there are two methods: the test which damages the films "destructive methods", and the other which keep the films intact "Non-destructive methods». But these types are expensive material and we don't have them. For this, we used the simple adhesion tests such as; the stick tape test which sees the films that adhered well the substrate. In this work, all the films was very well bonded to the substrate and this allowes us to continue our study.

2.7 Film thickness:

Many approaches, such as the optical method based on the interference fringe, the perpendicular section of this thin layer from a SEM micrograph (explained later), and the gravimetric method based on the relation, are used to determine film thickness.

$$d = m / (\rho S) \qquad (2.1)$$

Where (S) and (ρ) are respectively the surface and the density of the thin layer studied.

2.8 Film characterization technique:

The indium oxide films obtained are analyzed to achieve their properties (structural, optical, morphological, and electrical) such as:

1. Scanning electron microscopy (SEM) is applied to find surface morphology and energy dispersive X-ray (EDX) (attached to SEM) to study films elemental composition.
2. The crystalline structure have been obtained by X-ray diffraction(XRD)
3. UV-Visible spectra photometer is used to achieve the transmittance in visible region (400nm-800nm) and absorbance spectra to find a several parameters from them.
4. The Four point probe technique is employed to measure electrical conductivity of the films.

2.8.1 Scanning electron microscopy (SEM):

Scanning electron microscope (SEM) is one of the common methods for imaging the microstructure and morphology of the materials[58]which can provide information on surface topography, crystalline structure, chemical composition and electrical behavior of the top 1 urn or so of specimen[59].The electrons interact with the different atoms presented at the sample surface, producing various signals that reveal information on the sample surface morphology and composition. In fuel cells, it is used during the materials development stage, providing characterization in terms of morphology, composition, and analogous abilities[60](see figure2.8).

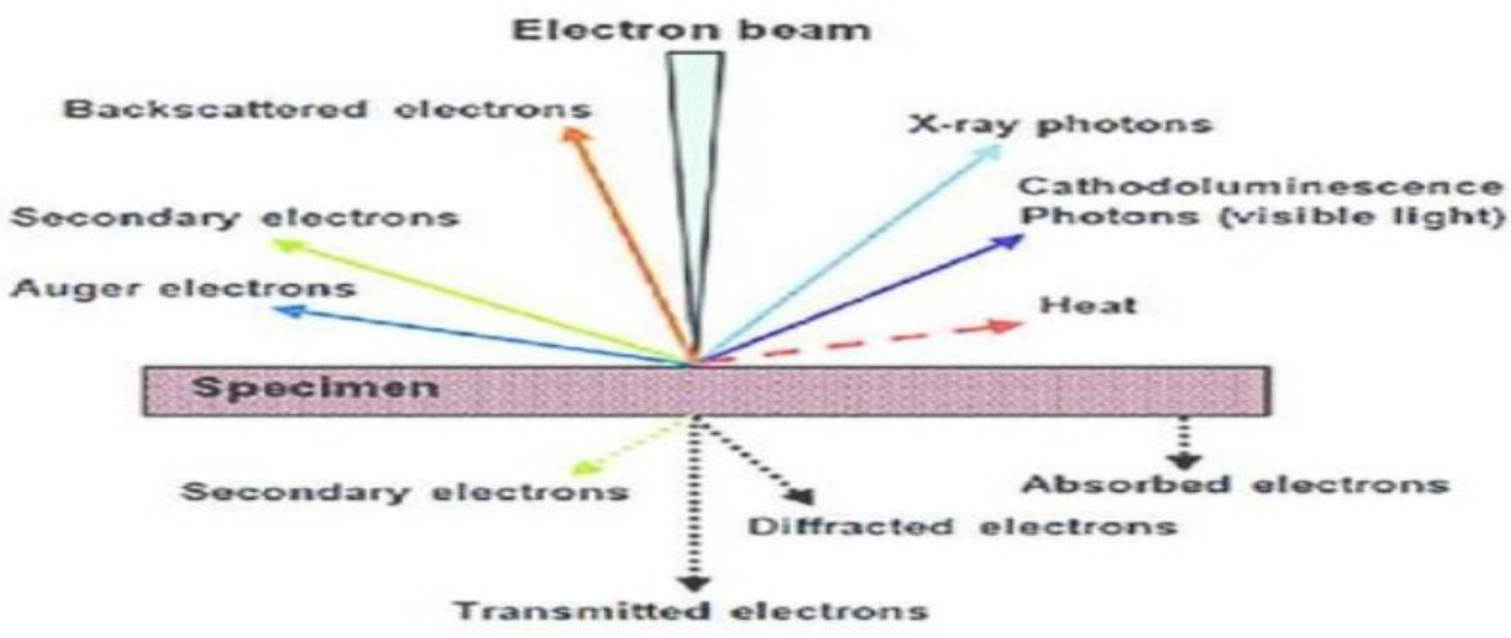

Fig2.8:Variety of interaction products evolved due to interaction of a primary electron beam and specimen (sample).

2.8.2 Energy dispersive X-ray spectroscopy (EDS or EDX)

Energy-dispersive X-ray spectroscopy (EDS, EDX, or XEDS) is an analytical technique used for the elemental analysis or chemical characterization of a sample. It relies on the investigation of an interaction of some source of X-ray excitation and a sample. Its characterization capabilities are due in large part to the fundamental principle that each element has a unique atomic structure allowing unique set of peaks on its X-ray spectrum. To stimulate the emission of characteristic X-rays from a specimen, a high-energy beam of charged particles such as electrons or protons, or a beam of X-rays is focused into the sample being studied[89]. In quantitative analysis, the concentration of a specific element present in a sample is measured by the intensities of peaks. Since each element has a unique atomic structure allowing a unique set of peaks on its electromagnetic emission spectrum, in qualitative analysis, different X-ray peaks with specified positions in a spectrum are identified [90], the procedure of X-ray dispersive is shown in figure 2.9.

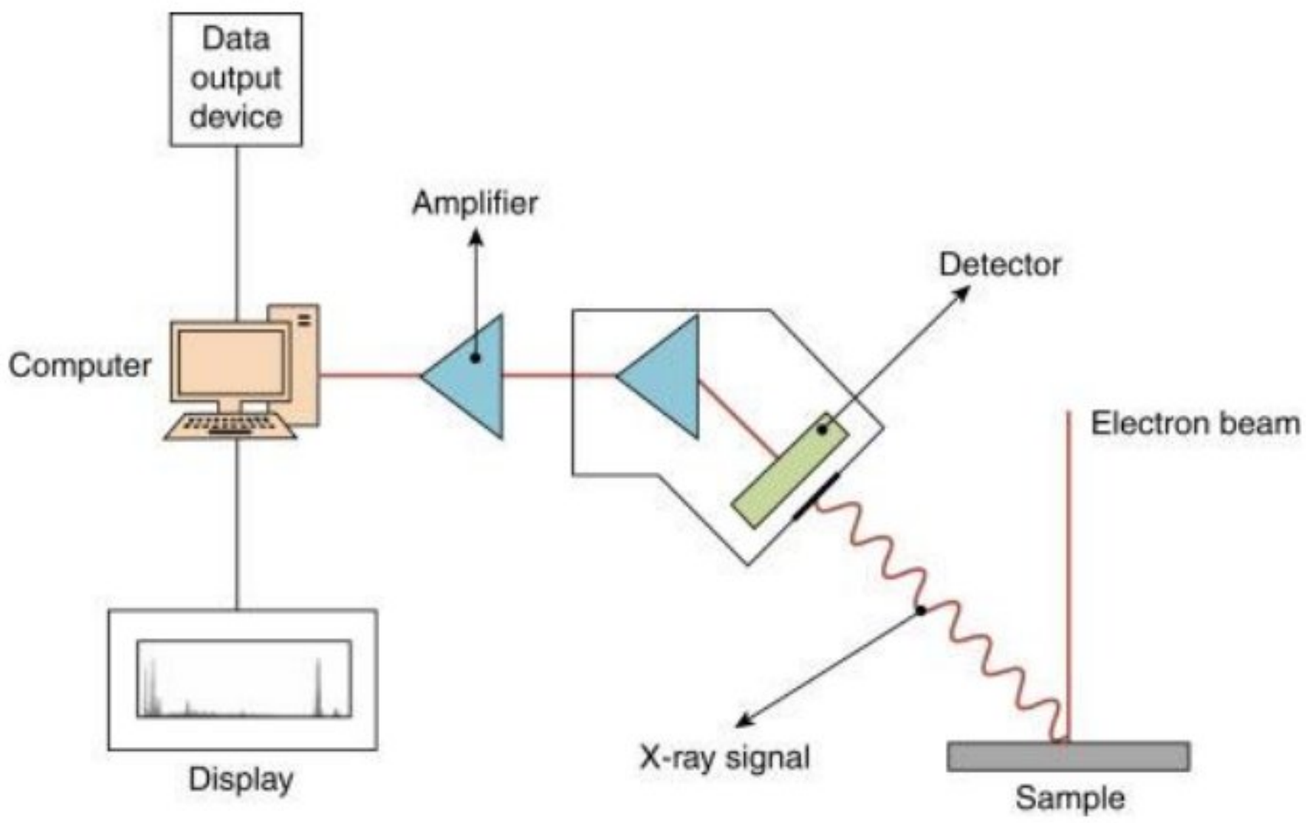

Fig 2.9:Energy dispersive X-ray spectroscopy[91].

2.8.3 X-ray diffraction (XRD):

XRD is a technique used to find out the nature of the materials as crystalline or amorphous. It will define the quantification of cementations materials. The XRD analysis is done with an X-ray source of Cu Kα radiation ($\lambda = 1.5406$ Å). It will analyze and identify the unknown crystalline compounds by Brag Brentano method [92]. The crystalline phases of the materials is based on Bragg law's .As shown in figure 2.10 condition at which diffraction occurs in a crystalline

material satisfying the Bragg‟s law is described as:

$$n\lambda=2d_{hkl}^{exp}\sin(\theta_{hkl}^{exp}) \qquad (2.2)$$

Where(λ) is the wave length of the X-ray beam, (d_{hkl}) is the spacing between the parallel planes in the atomic lattice, (*h,k and l*) are the miller indices of the corresponding lattice planes (*hkl*), θ_{hkl} is the angle between the incident ray and the scattering planes, and *n* is an integer[93].

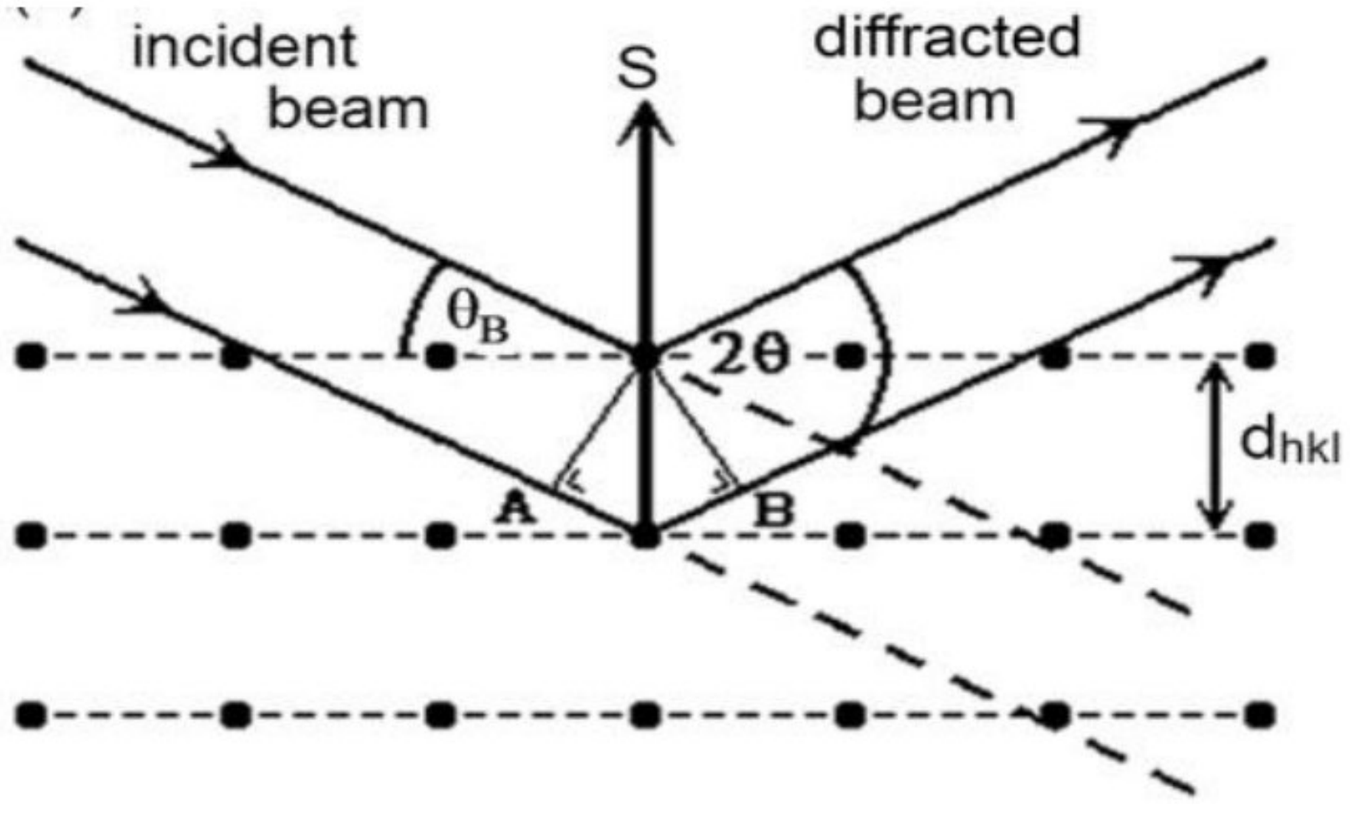

Fig 2.10:Schematic of X-ray diffraction According to Bragg.

In the thin-film geometry, the specimen should be in the form of a thin-film deposited on to the substrate. In this geometry, especially the X-ray beam enters the specimen with a small angle of incidence from the surface which is shown in figure 2.11.In the other hand, X-ray diffraction techniques are widely applied to characterize the material properties of nanostructured thin films and bulk crystal samples. The essential information which can be extracted by using XRD techniques include (i) phase identification, (ii) degree of crystallinity, (iii) structure determination, (iv) determination of lattice parameters, (v) crystallite size and strain determination, (vi) uniform and non uniform strains, (vii) preferred orientation parameter for example texture coefficient and (viii) residual stress[94] .

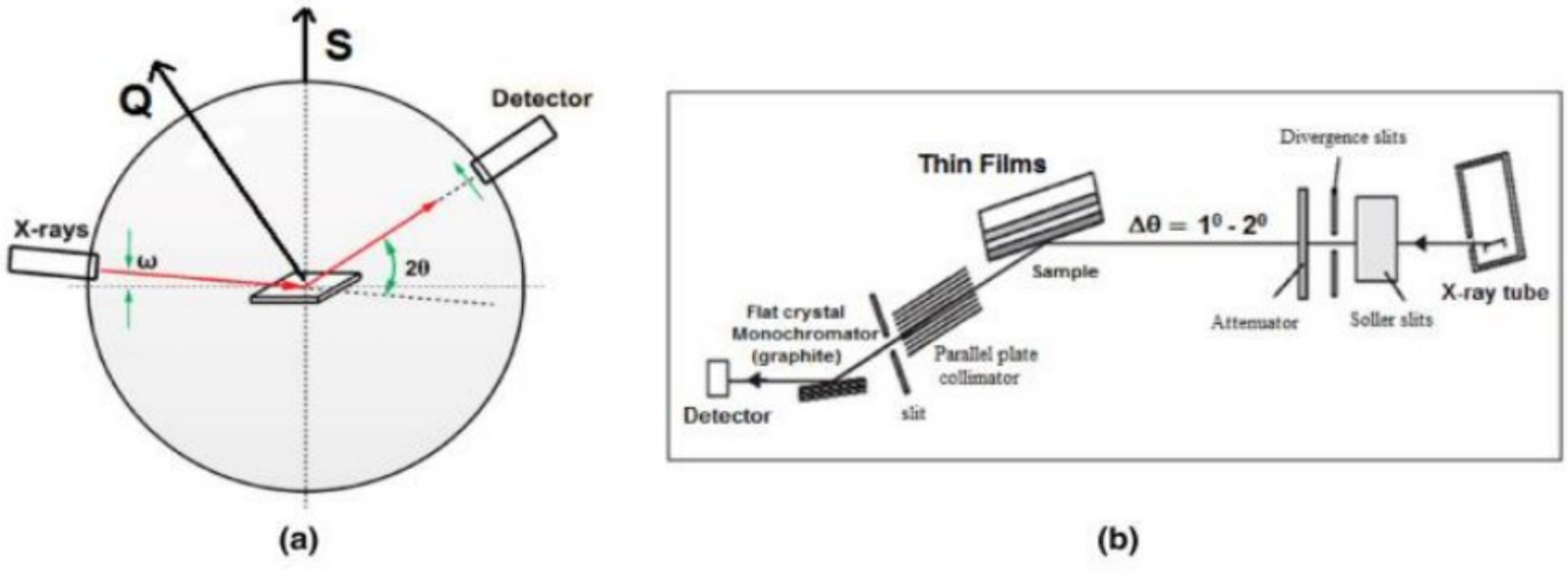

Fig 2.11: Schematic diagram of thin-film grazing incidence X-ray diffraction (a)using diffractometer circle Q is the scattering vector and S is the surface normal which is not parallel for each other. (b) Experimental setup of GIXRD.

The main parameters are discussed from XRD analyzes as follows:

Lattice parameters determination:

The set of lattice planes (hkl) is determined from the standard data and the lattice parameters are derived using the relations for deriving the lattice parameters from X-ray reflections using (d hkl_{exp}) values from Bragg's law. The experimental lattice parameter for a cubic crystal structure can be calculated using the relation[95]:

$$\frac{1}{d_{hkl}^{exp}} = \frac{h^2+k^2+l^2}{a_{exp}^2} \qquad (2.3)$$

Where, *h*, *k* and *l* are the indices of the crystal planes, *d* is the inter-planar spacing and *a* is the lattice constant. The crystallite size of the elaborated sample is estimated from the full width at half maximum (FWHM) of the most intense diffraction line see figure 2.12 by Debay Scherrer's formula as follows[96]:

$$D=\frac{0.9\lambda}{\beta cos\theta} \qquad (2.4)$$

D: The crystallite size (nm or A°).

λ: The wavelength of X-ray (nm or A°).

β: The full width at half maxima of the peak (FWHM) in radians.

θ: TheBragg's angle (rad).

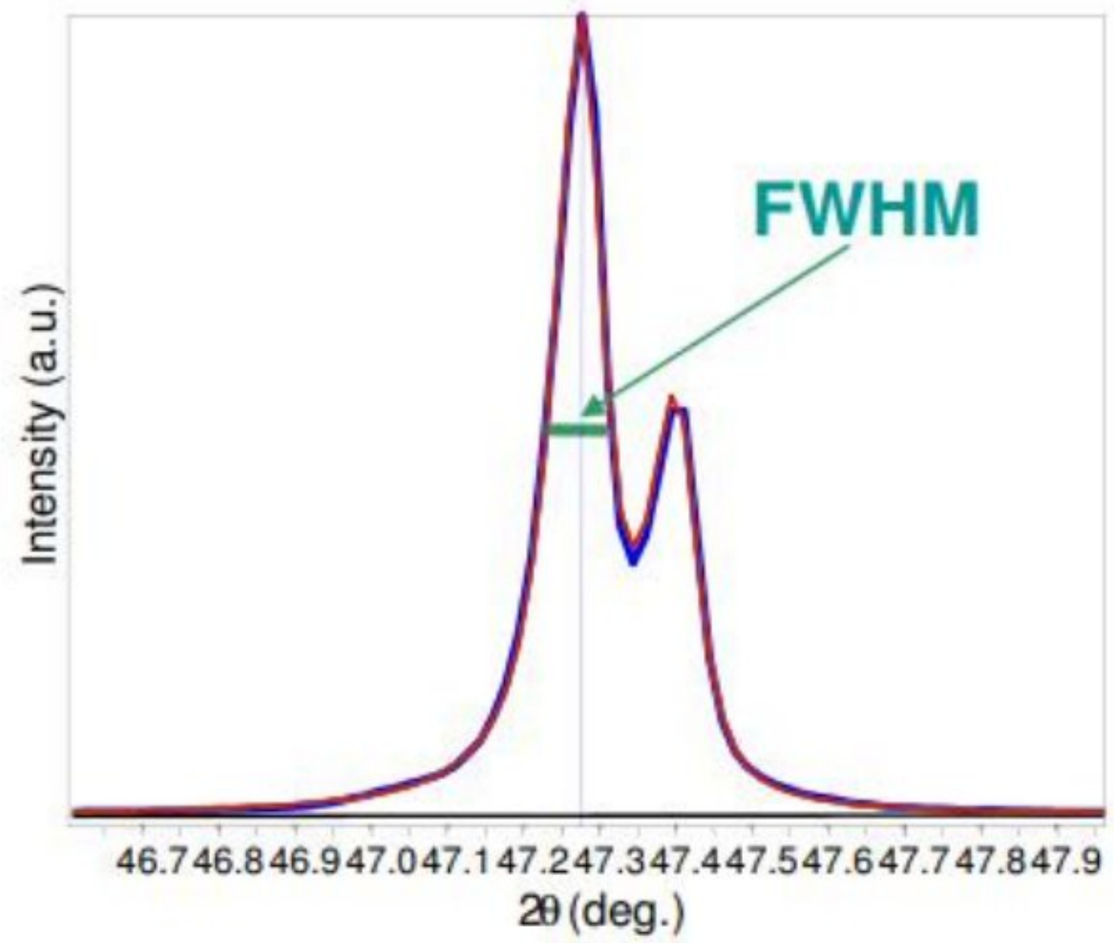

Fig 2.12: Determination of β from stranger orientation [74].

On the other hand ,the lattice parameters dependent with the substrate which means that there is mismatch between substrate and the deposited thin films , this different is responsible of strains and stresses , it can be estimated the strain from XRD patterns from stronger peak using [68,69]:

$$\varepsilon = \frac{\sin\theta}{4\beta} \qquad (2.5)$$

Where (ε) is the mean strain in thin films, a_{hkl}^{exp} is the lattice constant of thin films measured from the XRD and a_{hkl}^{the} the lattice constant of bulk (10.118 A°).

The change in the bulk value of lattice parameters is due to the stress and strain that are produced during the crystal formation. The intrinsic stress developed in the thin films were calculated according to the following relationship[99]:

$$\text{Stress} = \frac{Y\,\varepsilon}{2\gamma} \qquad (2.6)$$

Where Y is Young's modulus of In2O3 (145 GPa)[100] and γ is the Poisson's ratio (0.31) for In_2O_3[101] . The dislocation density (δ) was calculated from D using the equation [102] :

$$\delta = \frac{1}{D^2} \text{ (lines/m}^2\text{)} \qquad (2.7)$$

Texture:

The crystallographic texture of an anisotropic solid is described as the relative "organization" of the grains, which has a significant impact on its physics and mechanical properties. The bulk of polycrystalline materials are like this: Rocks, ceramics, metals, polymers, and other materials. The texture coefficient (TC) represents the texture of a specific plane, which is indicating a preferred growth. Quantitative data on the preferable crystallite is available. The varied texture coefficients were used to determine the orientation. TC(hkl) is described as[103]:

$$\text{TC (hkl)} = \frac{\text{I(hkl)}/\text{I}_0\text{(hkl)}}{\text{N}^{-1}\sum_n \text{I(hkl)}/\text{I}_0\text{(hkl)}} \qquad (2.8)$$

Where I(hkl) is the measured relative intensity of a plane (hkl), I_o(hkl) is the standard intensity of the plane (hkl) taken from the JCPDS data, N is the reflection number and n is the number of diffraction peaks.

2.8.4 UV-Visible spectroscopy:

The technique of UV-VIS spectroscopy is beneficial for identifying pure medicinal molecules. Many compounds have chromophores that absorb ultra violet or visible light at specific wavelengths. The absorption of spectra obtained from these samples at given wavelengths can be directly attributed to the sample concentration using the Beer Lambert law. Normally, UV and UV-VIS spectra are recorded at high and low pH, and the results of both are compared to recognized standards for the sample in issue. UV-VIS is a simple and inexpensive technology that provides for sample recovery and effective separation of pure chemicals without derivitisation. For street samples with complicated mixtures, it is less useful[104].In our case, we used a dual-beam recording spectrophotometer, whose operating principle is depicted in (Figure2.13), to plot curves representing the variation of transmittance as a function of length in the UV-Visible and near-infrared spectrums (200-800nm). These curves can be used to estimate the thickness of the material. To determine the optical properties of the film, such as optical absorption, absorption Urbach energy, coefficient, band gap width, and refractive

index[105].When a beam of monochromatic light passes through a homogeneous medium of an absorbing substance, the rate of decrease in intensity of radiation with respect to thickness of the absorbing medium is directly proportional to the intensity of incident radiation as well as the concentration of the medium, according to the UV-VIS Spectroscopy principle.

$$I=I_0e^{-\alpha d} \qquad (2.9)$$

Where α is the absorption coefficient, d is the thickness of the film, I_0 and $I$are the intensity of the incident and the transmitted beams, respectively.

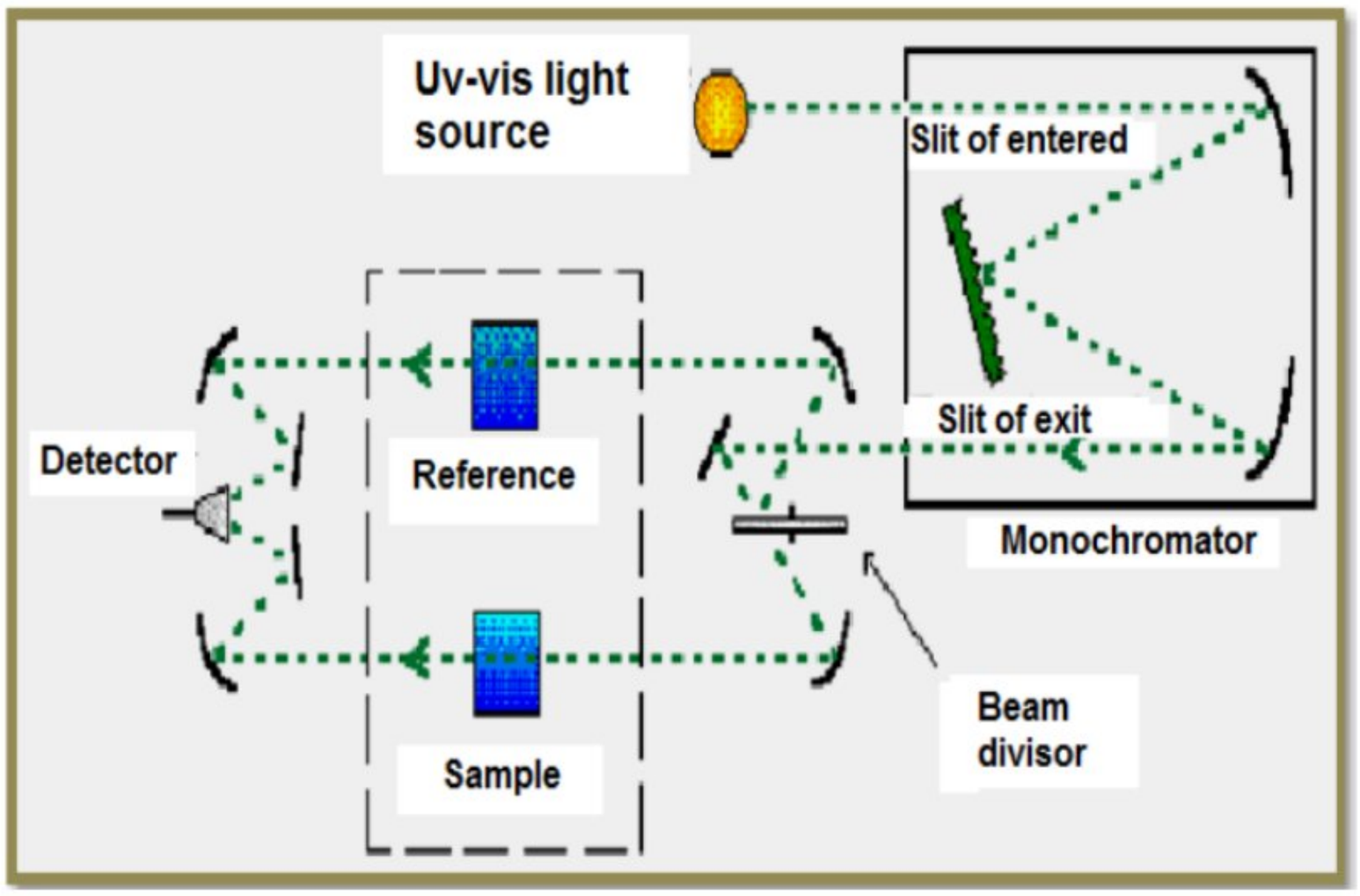

Fig 2.13: Schematic representation of the UV-Visible spectrophotometer[105] .

The absorption coefficient (α) can be calculated using the following expression:

$$\alpha = \frac{1}{d}\ln\frac{100}{T(\%)} \qquad (2.10)$$

where $T(\%)$ is the transmittance (quantity of the transmitted light), and can be directly measured by[106] :

$$\mathrm{T}\ (\%) = \frac{I}{I_0} \times 100 \qquad (2.11)$$

2.8.4.1 Optical band gap:

The basic absorption in a polycrystalline semiconductor is connected to band-to-band transitions, the excitation of an electron from the valence band to the conduction band. As a result, the basic absorption can be utilized to calculate the semiconductor's energy gap[107].The absorption coefficient α data was used to determine the energy gap (Eg) using the relation:

$$\alpha h\nu \approx (h\nu - Eg)^{1/2} \qquad (2.12)$$

Where, $h\nu$ is the photon energy.The values of direct bandgap were estimated by extrapolation of the linear region of the plots to zero absorption(($\alpha h\nu)^2 = 0$) [108] see the example in figure .

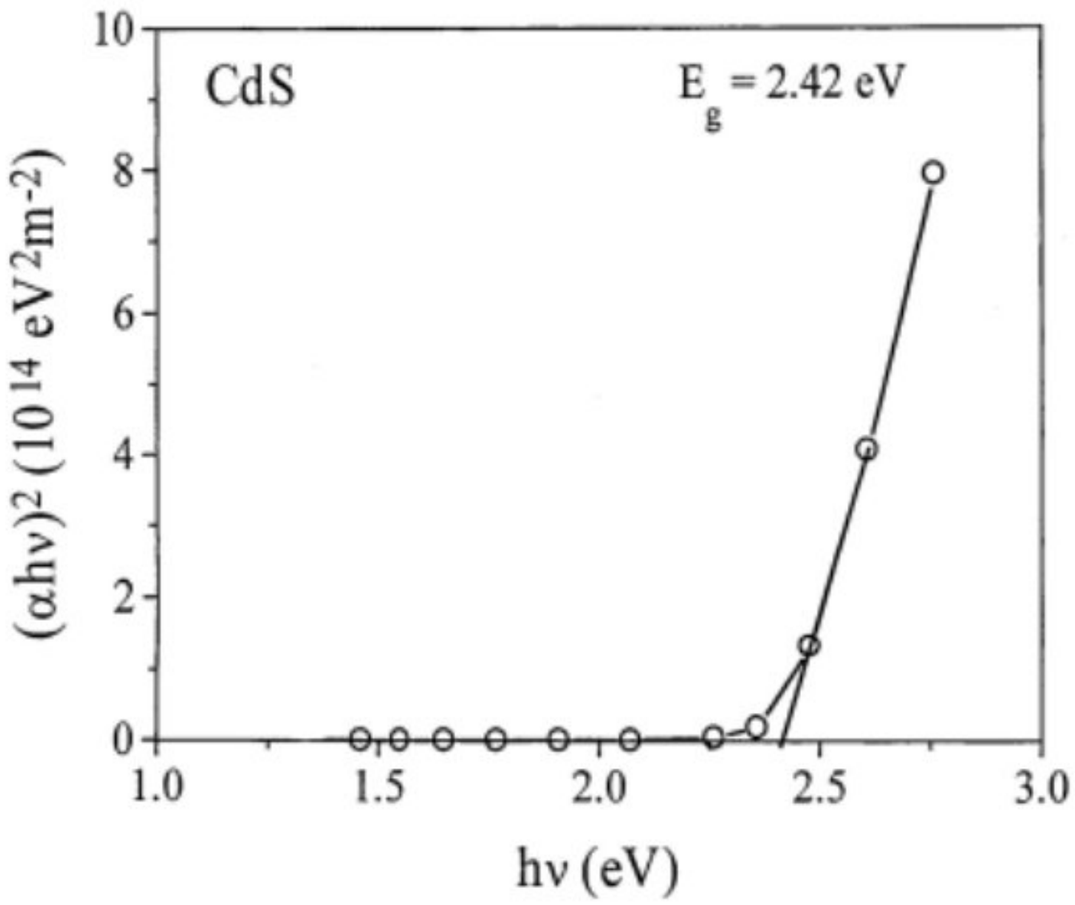

Fig2.14 :Plot of $(ah\nu)^2$ vs. hν for the vacuum-evaporated CdS film[109].

2.8.4.2 Energy Urbach :

Band tailing can be explained as local perturbation of the band edges by the effect of impurities or any other defect. Density-of-states distribution integrates the number of states ateach energy level inside the whole volume and shows that thereare conduction band states at relatively low potentials and valance band states in high-potential regions as shown in figure below [110].

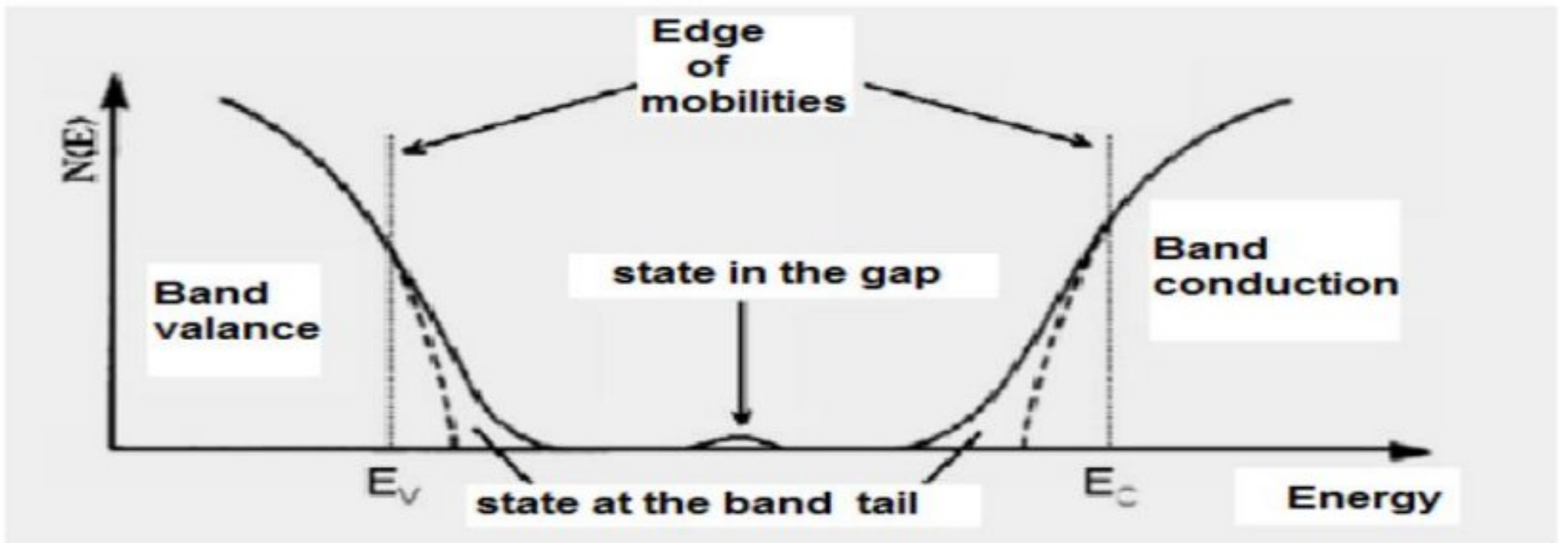

Fig 2.14: Function of distribution of the energy states in the bands[75].

In the other hand, the energy Urbach can be calculated via the equations below:

$$\alpha = Bexp\left(\frac{h\nu}{Eu}\right) \qquad (2.13)$$

Where *B* represent constant and α is optical absorbance ,it can be obtained by taking the reciprocal of the gradient of slope from the plot lnα against hν curve as shown in figure 2.15[111].

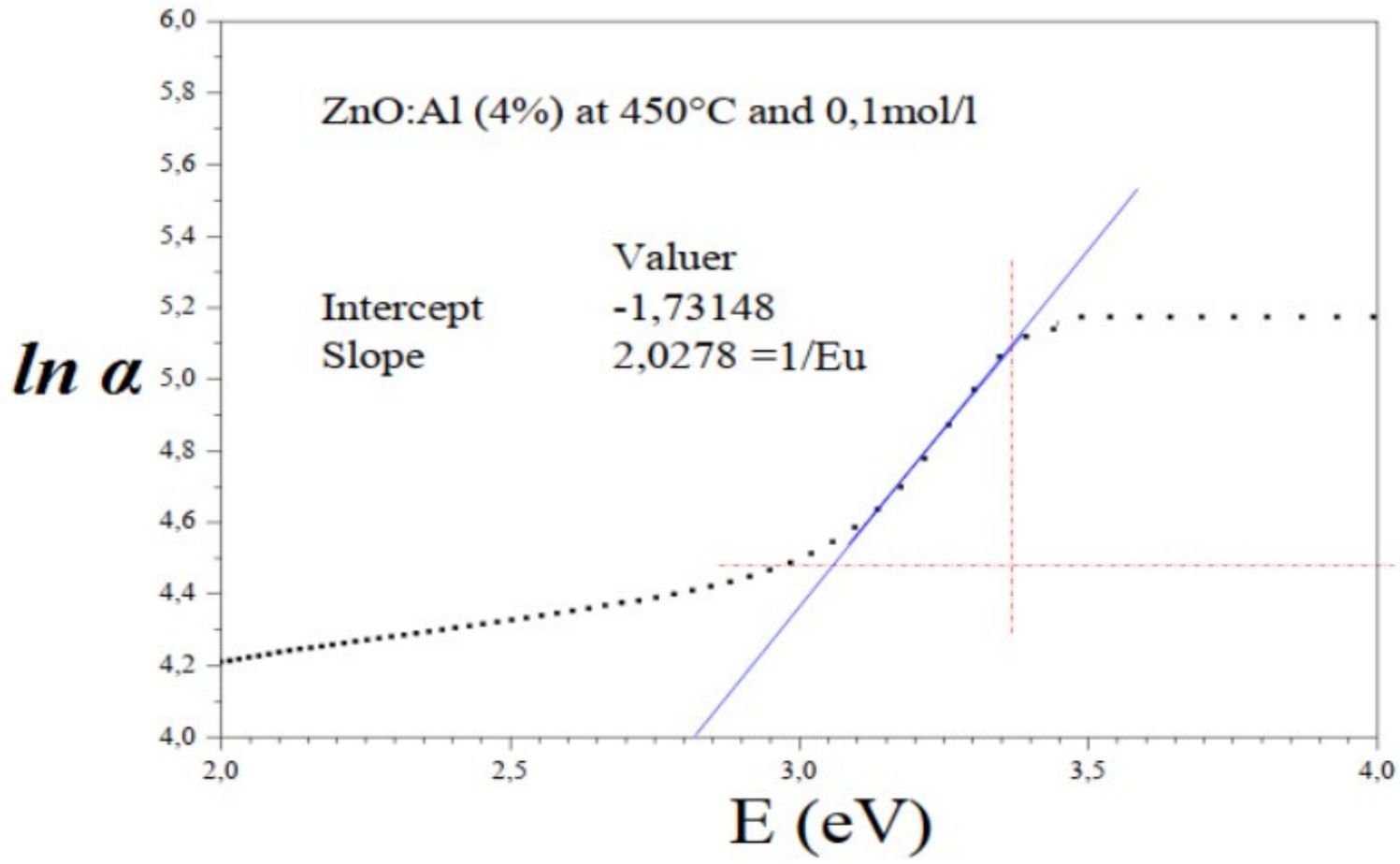

Fig 2.15: Determined the Urbach energy for ZnO:Al [112].

2.8.5 Electrical properties:

The four-point method can be used either for thick material or a thin layer deposited on an insulating substrate or isolated by a junction. We apply the four-point aligned on the In_2O_3 film

deposited on glass substrate, the distance s between the points being 1 mm (Figure 2.16). The two outer points (1, 4) are used to inject current I, the two other points (3, 2) are used to take the drop in potential ΔV.

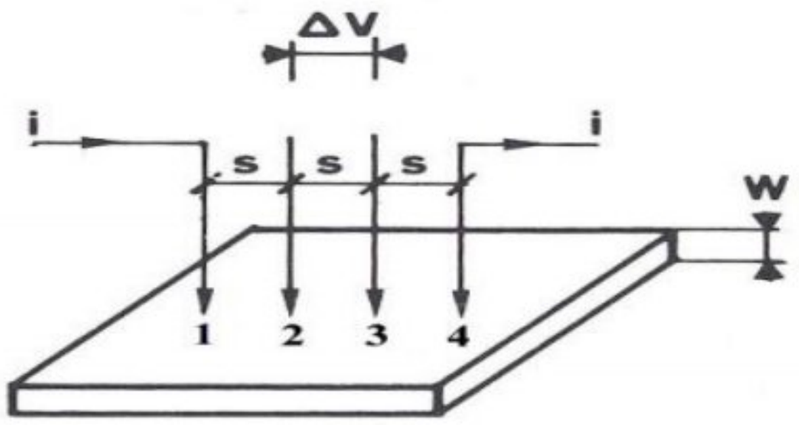

Fig 2.16: four-points method.

The ratio ΔV/I are measured. Our samples are two-dimensional (the thickness w is small in front of s); the equipotentials of the current injected in (1) are cylindrical. The current density at a distance r from the point is:

$$J = \frac{I}{2\pi r w} \qquad (2.14)$$

The potential drop between r and r+dr is equal to:

$$dV = -\frac{\rho I}{2\pi r w}\, dr \qquad (2.15)$$

Where ρ is the resistivity , It follows that the potential dV difference between points 3 and 2 due to the flow of the current injected into (1) is:

$$V`_{32} = \int_s^{2s} -\frac{\rho I}{2\pi r w}\, dr = -\frac{\rho I}{2\pi w} \ln 2 \qquad (2.16)$$

Similarly, the dV between 3 and 2 resulting from the current I extracted at 4 is:

$$V¨_{32} = -\frac{\rho I}{2\pi w}\, ln2 \qquad (2.17)$$

Finally by the superposition theorem:

$$\rho = \left(\frac{\pi}{ln2}\right) w \frac{|\Delta V|}{I} = 4.53 w \frac{|\Delta V|}{I} (\Omega cm) \qquad (2.18)$$

The resistance per square R is, therefore:

$$R_{\blacksquare} = 4.53\ \frac{|\Delta V|}{I} = \frac{\rho}{w} (\Omega\ ) \qquad (2.19)$$

If we know the thickness w, we can thus deduce the resistivity ρ from $R_{\blacksquare}$ [113] .

CHAPTER 03

Effect of film thickness and pH solution

Introduction:

Last studies, In_2O_3 thin films were prepared by using the spin coating process at many effects such as : annealing temperature[114], molar concentration[115] and varied a deposition parameter (sputtering powers[116]) to obtain a good properties for applied in different applications such as solar cells, gas sensor, flat panel displays and anti-reflecting coating….etc [117]. In this chapter have a various steps of the preparation of In_2O_3thin films on glass substrates by spin coating and its characterization techniques used to measure their optical, structural, morphological and electrical properties are discussed below. This chapter discusses and interprets the results of characterization for undoped In_2O_3 thin films deposited by spin coating method at many affects (film thickness and pH solution) for the amelioration their properties for different application.

3.1The influence of film thickness:

Indium oxide thin film was prepared by using spin coating process at various of film thickness, this films characterized by XRD patterns, SEM, UV-Vis spectroscopy and four probe point. The results obtained are discussed below.

3.1.1 Structural properties:

To films thicknesses of In_2O_3 thin films were controlled by varying the number of the layers from 4to 15 layers. The film thickness was determined using SEM cross sections by calculating the average thickness from one end to the other as depicted in Figure 3.1. As shown in Figure 3.2, the thickness of the films increases with the number of the layers, the variations follow a quasi linear behavior with a rate of58 nm per cycle. Form the linearity depence one can choose the number of cycle suitable to obtain a desired thickness. The crystal structure and orientation of the In_2O_3 thin film were investigated by X-ray diffraction (XRD) pattern. The XRD pattern of all In_2O_3 films prepared at different film thickness (175, 330, 520, 690 and 910 nm) on glass substrate are shown in Figure 3.3. As can be observed in the graphic, the samples have a polycrystalline structures with five peaks shown in Figure 3.3, assigned to (211), (222), (400), (440) and (622) diffraction planes, matching with a body cantered cubic (BCC) phase of In_2O_3 with a space group of Ia3(206) (JCPDS Card No. 06-0416, space group, a = 10.118 A˚)[118]. However, no peak related to a secondary phases such as In or InO is observed. Similar result has been observed in our earlier work and other work[96,97].

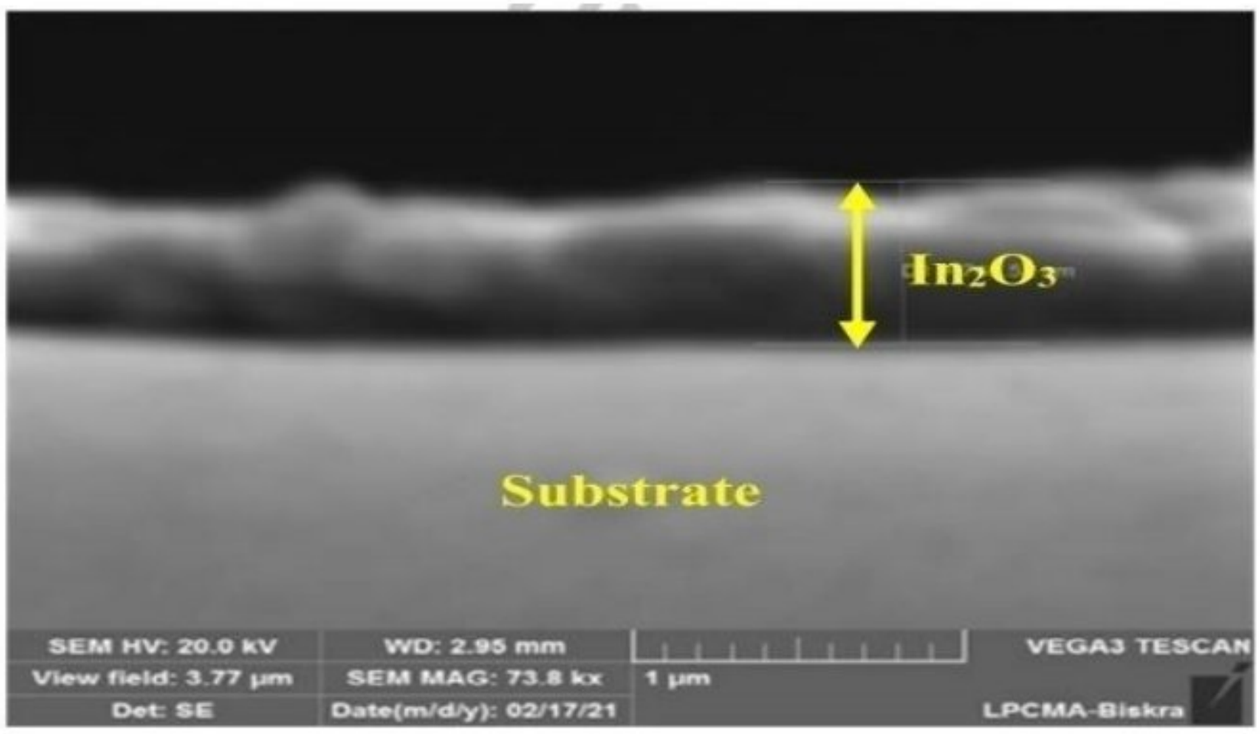

Fig 3.1: Direct thickness measurement of the film of In_2O_3 from the cross sectional SEM images.

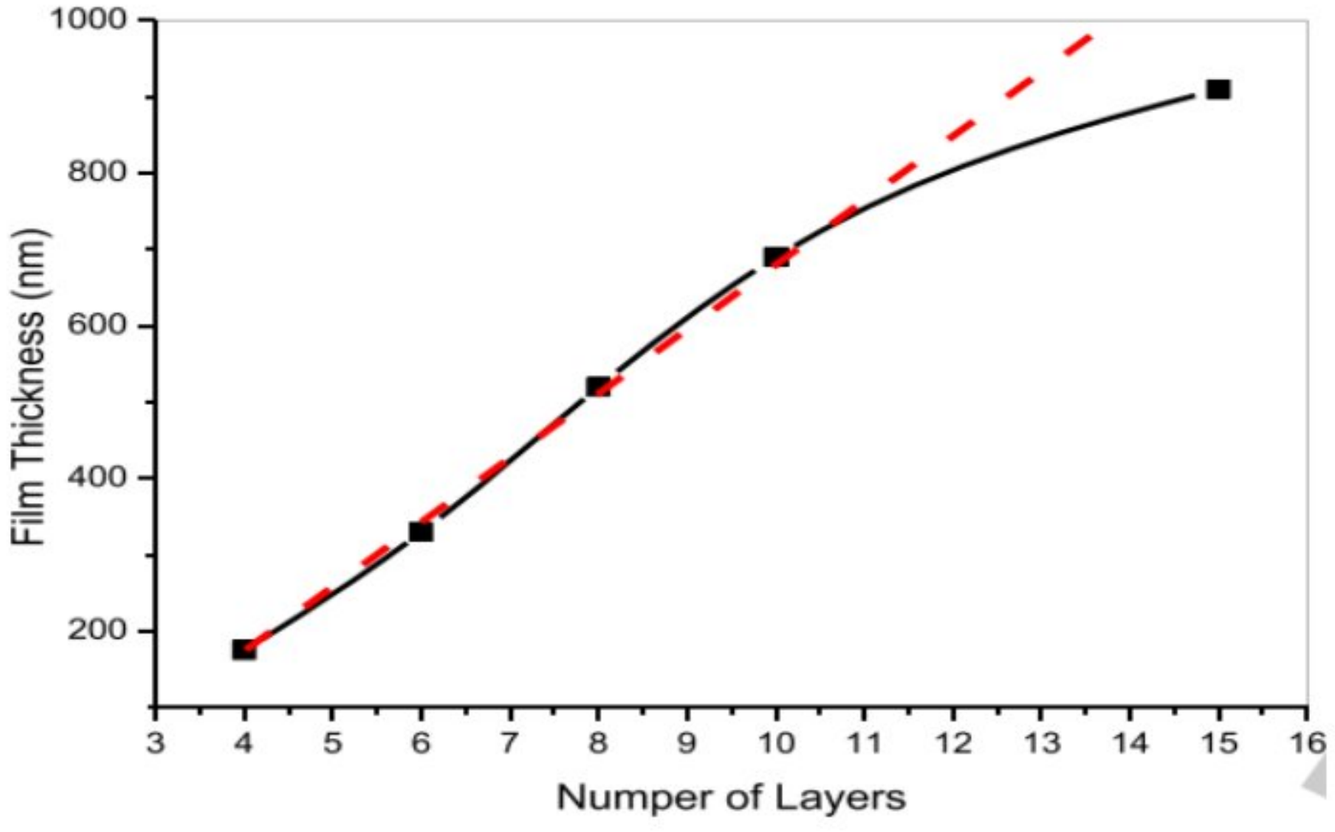

Fig 3.2: Variation of the film thickness with the number of layers.

Moreover, Figure3.3 reveals that the samples have an intense peak originating from the (222) diffraction plane, it becomes narrower, intense when the film thickness increases, suggesting the films crystallinity improvement. The preferential growth along (222) direction may be due to the reasons that the plan(222) requires the lowest free surface energy formation[98,99]. The data also shows that the peak position slightly shifts to a lower 2θ value as shown in Figure 3.4, this is probably due to stress created during the films growth.

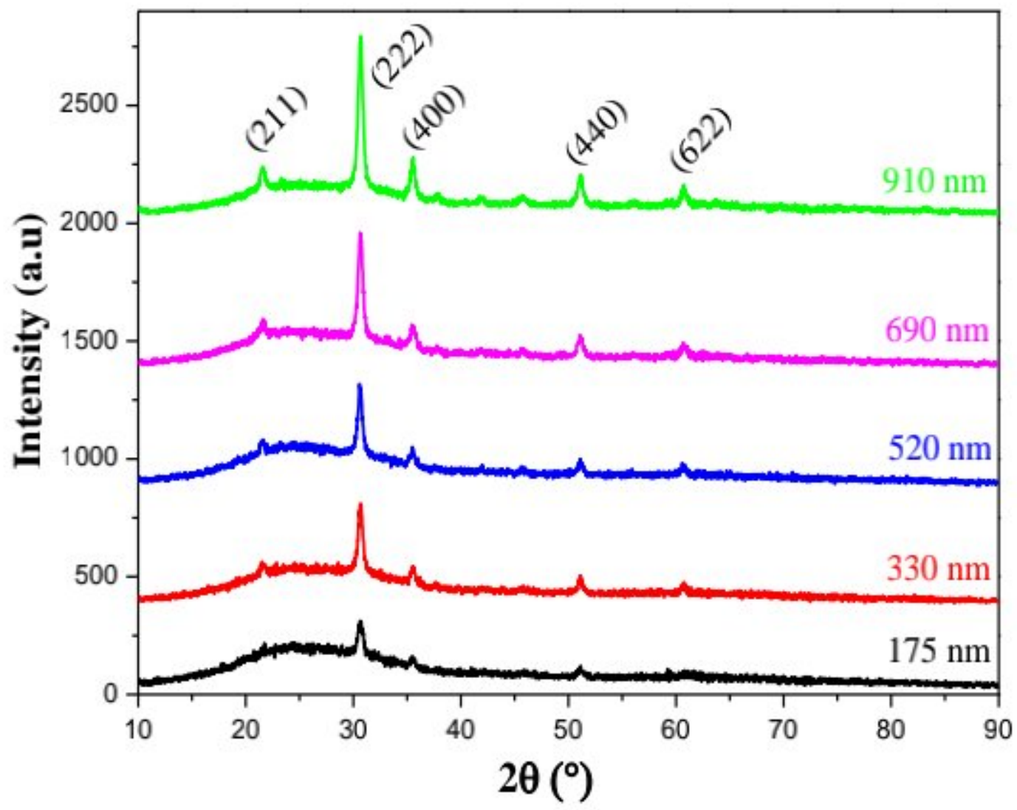

Fig3.3: XRD patterns of nano-crystalline In2O3 thin films for different film thickness.

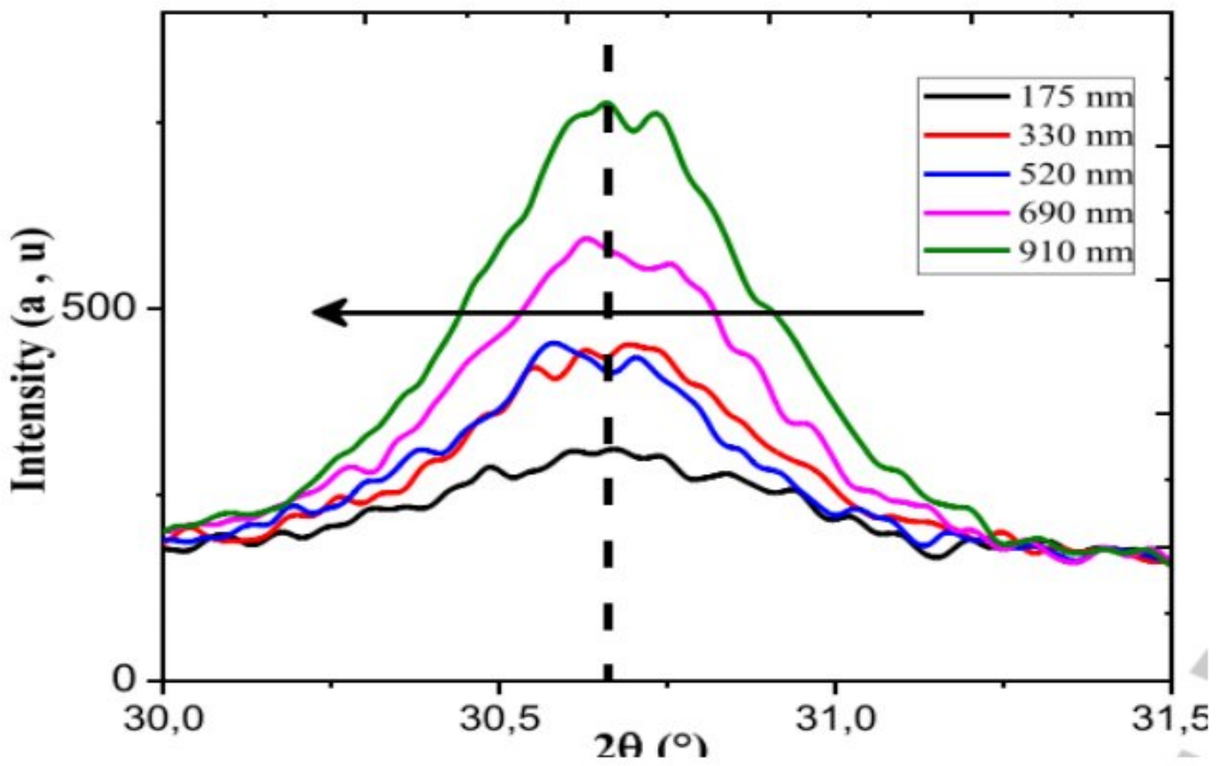

Fig 3.4:Variation of peak (222) position of In_2O_3 thin films at different film thickness.

To describe the preferred growth orientation (*h k l)*, we calculated the texture coefficient from the X-ray data using the equation. The obtained results summarized in the Figure 3.5. It is clear that the (222) direction has the highest texture coefficient comparing with other peaks, which increases drastically with increasing film thickness. It is well known that the films texturation is usually related to two factors: the growth and nucleation. The increase in the preferred orientation of (222) plane is attributed to the increasing in the growth along this direction on the detriment other planes.

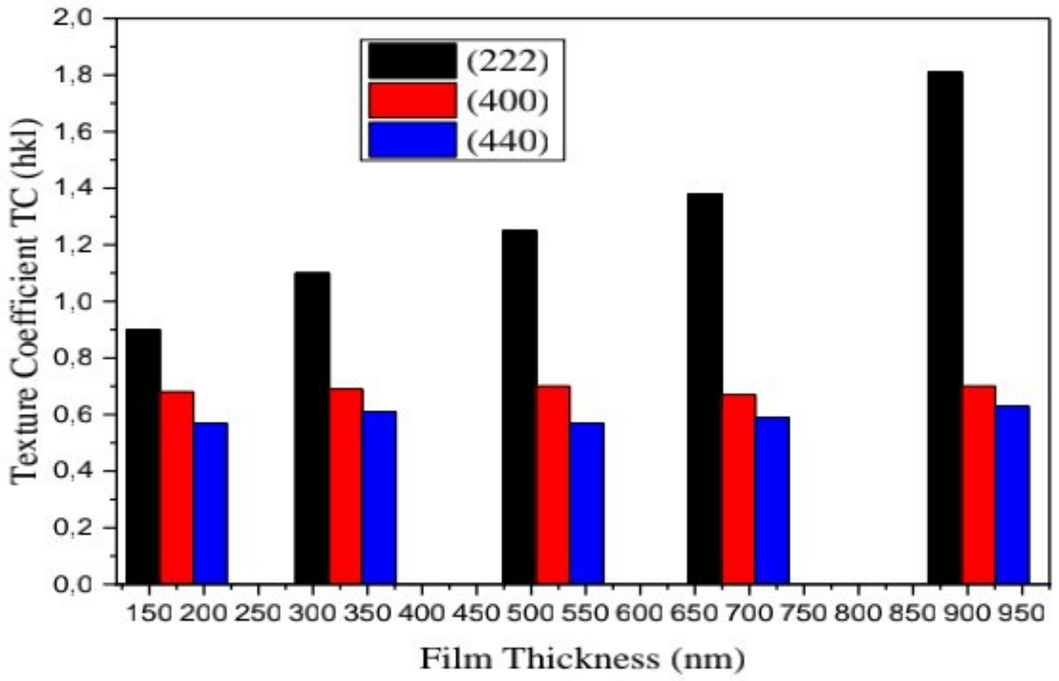

Fig 3.5: The texture coefficient of In_2O_3 thin films as function of film thickness along (222), (400) and (440) directions.

The calculated crystallite sizes, strain and dislocation density is listed in Table 3.1. It is evident from the contents of Table 3.1 and Figure 3.6, that as the films thickness increases, the crystallite size enlarges, while the strain decreases. The same behavior is reported by Goswami et al. In his study on In_2O_3 thin films prepared by pulsed laser deposition technique [123]. On opposite, in our previous work[124] we have noticed a decrease in crystallite size with molar concentration increase. The observed improvement in crystallite sizes is commonly attributed to sufficient supply of thermal energy to the coalescence the atoms over the surface substrate and this facilitate the merging of the smaller particles into larger ones, as the results, the crystallite sizes increases[102,103]. The decrease in strain formed in the crystal could be related to improvement of the crystallinity, which results to produce more organized films with less point defect.

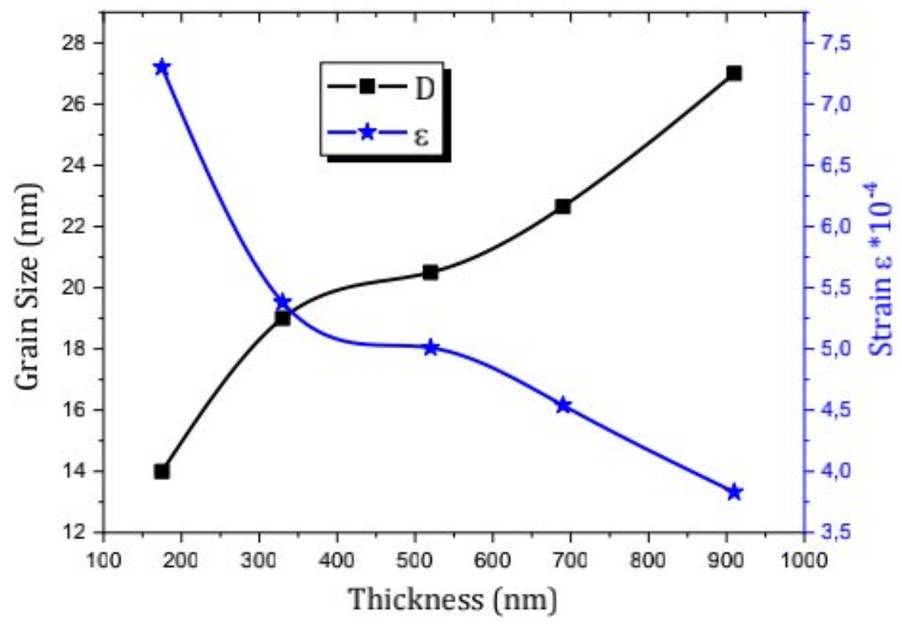

Fig 3.6: Evolution of grain sizeand strainof In_2O_3 thin filmsat different film thickness

Table3.1:Crystallite sizes, dislocation density and strain values of In_2O_3 thin films extracted from XRD analysis.

Thickness (nm)	Peak (hkl)	2θ°	FWHM (β°)	D (nm)	δ x10^{15} (Lines /m^2)	ε x10^{-4}
175	(222)	30.66	0.61	14 ±0.2	5.1	7.3
330	(222)	30.62	0.45	19 ±0.2	2.77	5.38
520	(222)	30.59	0.42	20.5 ±0.2	2.38	5.01
690	(222)	30.57	0.38	23 ±0.2	1.89	4.54
910	(222)	30.54	0.32	27 ±0.2	1.37	3.83

The calculated structural parameters from XRD pattern of In_2O_3 films are summarized in Table 3.2. As can be seen from Table 3.2 the α lattice parameter of pure In_2O_3 thin films increases with the films thickness. At the same time, the internal stress changes from compressive (negative) to tensile (positive). The similar result observed in previous study[104,105]. It can be seen that the compressive stress in the films decreases and in contrary, the tensile stress increases with increasing films thickness.

Table3.2: Structural parameters information of prepared In_2O_3thin films for different films thickness.

Thickness (nm)	*h k l* planes	2θ(degree)	Calculated parameters		Reference parameter (JCPDS card No 06-0416)	Stress (Gpa)
			Lattice constant *a* (Å)	d-spacing (Å)		
175	(222)	30.66	10.101 ±0.01	2.916		-0.39
330	(222)	30.62	10.112 ±0.01	2.919	a_0 = 10.118 Å	-0.14
520	(222)	30.59	10.122 ±0.01	2.922	*d* = 2.921 Å	0.09
690	(222)	30.57	10.129±0.01	2.924	2θ = 30.58	0.25
910	(222)	30.55	10.136 ±0.01	2.926		0.42

3.1.2 Morphological properties:

The surface morphology images of as grown In_2O_3 thin film having different thickness is presented in Figure 3.7 (a)-(e). It can be seen that all the films have a uniform, smooth, continuous and homogenous surface morphology with particle distribution consisting of spherical and triangular shapes without any voids and cracks. However, with the increases of film thickness, a large number of granular and dense grains are formed on top of the film. As can be seen, the grain size increases with increasing of film thickness. This result is supported by obtained results in the XRD analysis.

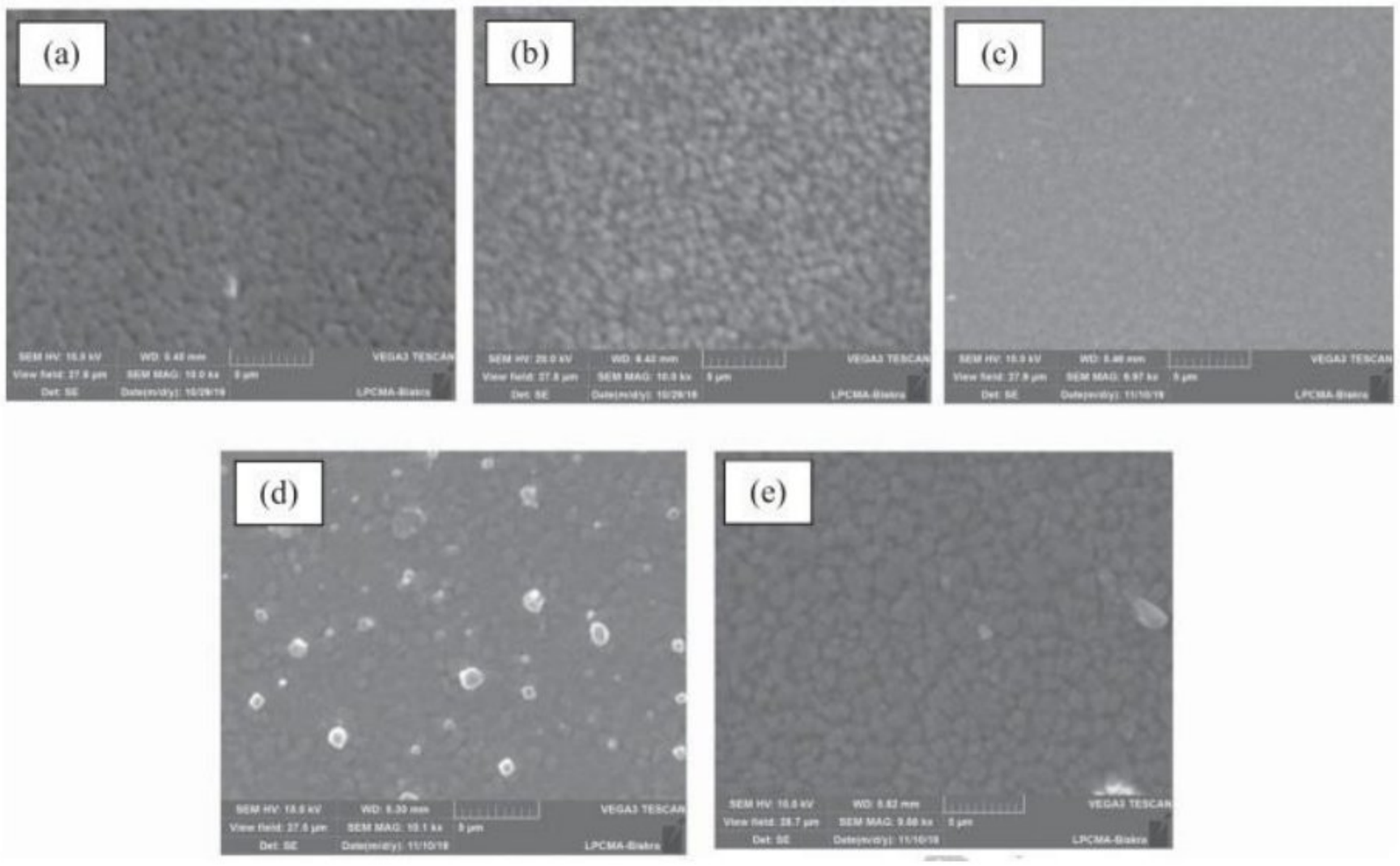

Fig 3.7: SEM micrographs of the In_2O_3 thin films at different film thickness: (a) 175 nm, (b) 330 nm, (c) 520 nm, (d) 690 nm and (e) 910 nm.

3.1.3 Compositional properties:

The EDX spectra of In_2O_3 thin film deposited with different films thickness are reported in Figure 3.8. The EDX study confirms the presence of indium (In) and oxygen (O) necessary for In_2O_3 formation. The silicon originates from the glass substrate. In a stoichiometric In_2O_3 the atomic percentage should be 60% and 40% for Oxygen and Indium, respectively. However, according to the EDX spectra (Figure 3.8) the films contain an excess of oxygen, this might be due to the contribution of oxygen originating from the substrate as well as Si atoms. On the other hand the excess of oxygen may also originate from the existence of oxygen vacancies[128].

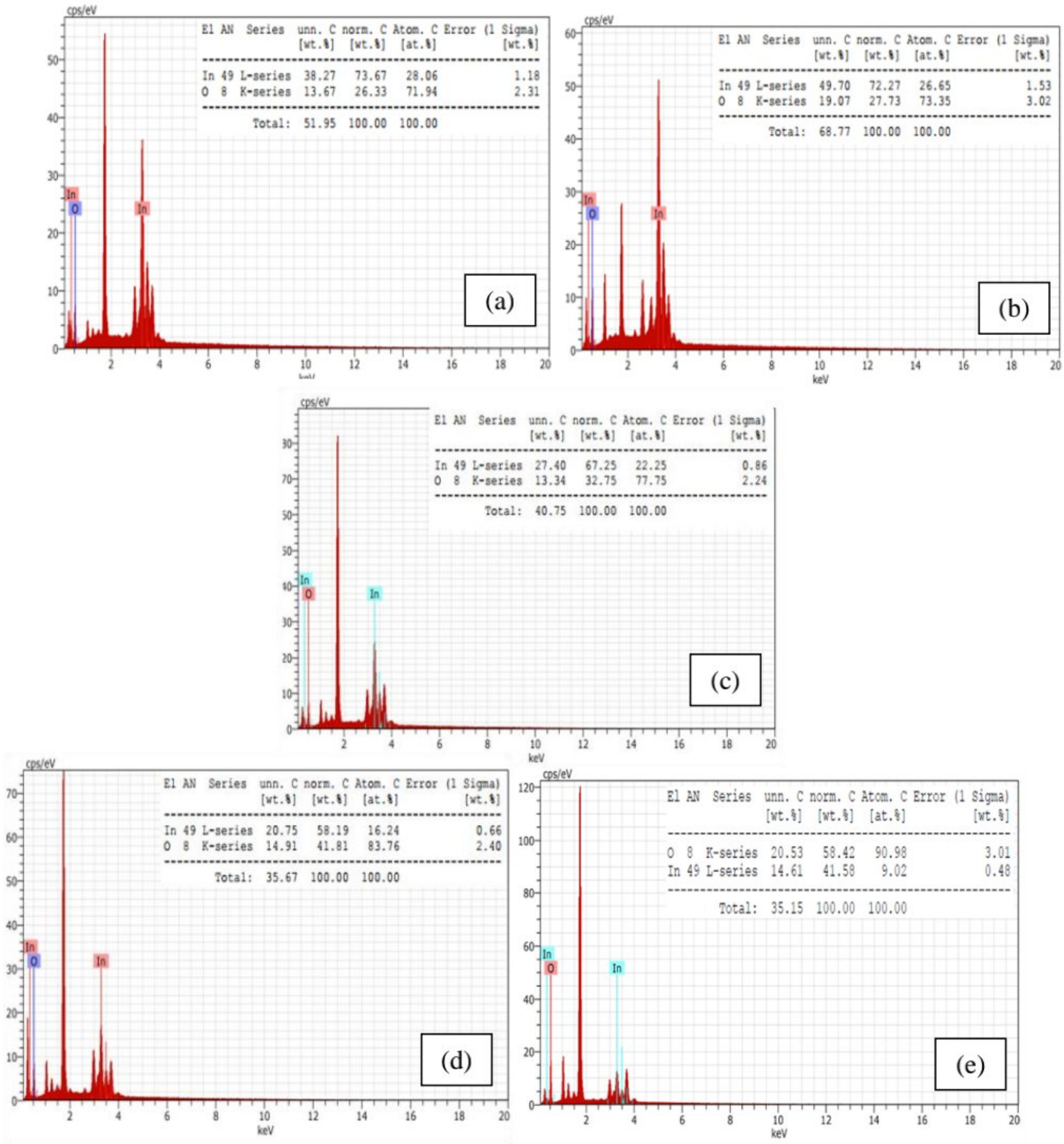

Fig 3.8:EDX spectrum ofthe In_2O_3 thin films at different film thickness:(a) 175nm, (b) 330nm, (c) 520nm, (d) 690nm and (e) 910nm.

3.1.4 Optical properties:

The transmittance spectra of the indium oxide thin films in the wavelength range of 200–1000 nm are shown in Figure 3.9. All of the samples exhibit high optical transmittance more than 75% in the visible wavelength region (400 to 800 nm). The high transmittance of these films can be

appropriated as transparent electrode of the solar cell application[129]. Interference fringes are noticeable in the visible region, these indicatives of uniform and homogenous obtained films which are characteristically smooth[107,108]. Hence, the reduction in the light scattering losses due to the films smoothness is the principal reason of the films transmittance improvement. Besides, the transmittance spectra of our samples revealed strong absorption edges in the UV region (λ< 380 nm), which suggesting the blue-shifted absorption edge with the increasing films thickness, as shown in the inset of Figure 3.9. This phenomenon has been reported in other TCO thin films [109,110]. From the curve of $(\alpha h\nu)^2$ as function ($h\nu$) which depicted in Figure 3.10, the optical band gap (Eg) can be determined by the extrapolation of the linear region of the curves to intersect at hν axis following Tauc relationship (2.12).

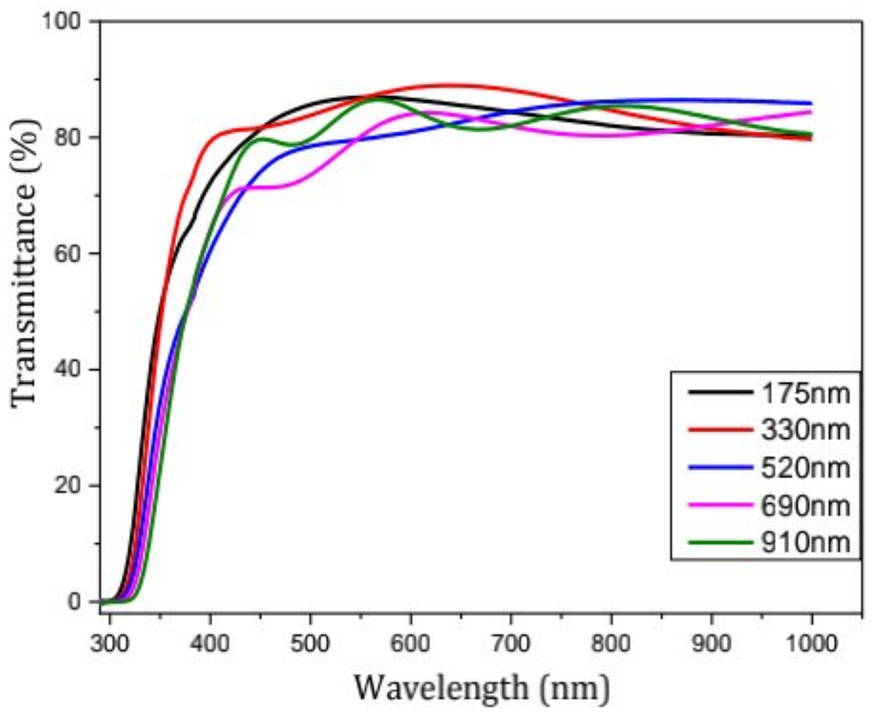

Fig 3.9: The transmittance spectra of In_2O_3 thin films prepared with various film thickness.

The inset image as shown in Figure 3.10 represents the calculated band gap values dependence on the films. The observed band gap values are in good agreement with the reported value for the ITO films deposited by electron beam evaporated and RF sputtering technique [112,113]. The broadening of band gap energy with the increasing films thickness can be due to the Burstein–Moss effect [114,115]. This phenomenon is related to increased carrier concentration which leads to shifts the Fermi level to higher energy [116,117].

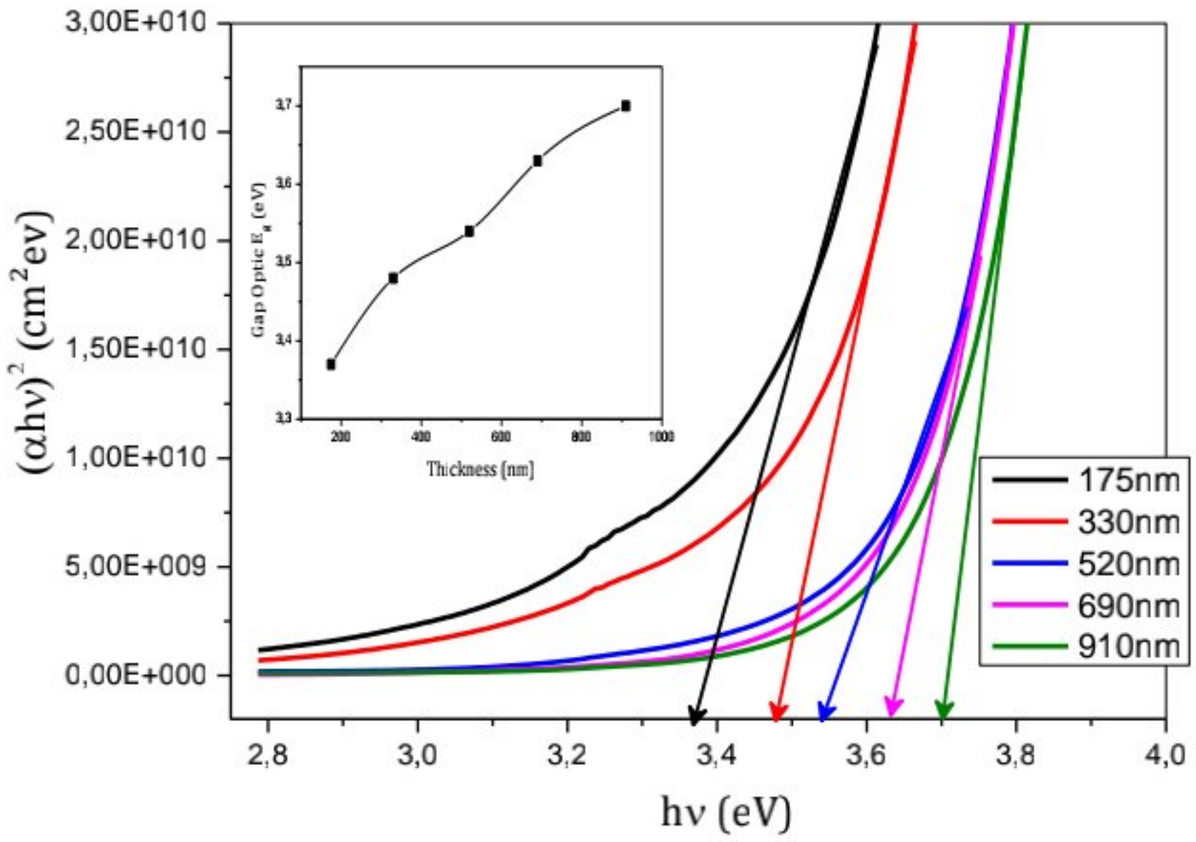

Fig 3.11: The plot of (hν) 2 against hν of In_2O_3 thin films and inset shows the variation of optical band gap (Eg) as a function of film thickness.

3.1.5 Electrical properties:

Table 3.3 illustrates the variation in resistivity (ρ), carrier concentrations (n), and Hall mobility (μ)of In_2O_3 thin films as a function of films thickness. As shown in Table3. 2, the resistivity decreased from $1.5 \times 10^{-3}\Omega\cdot$cm at 175 nm to $1.5 \times 10^{-4}\Omega$.cm at 910 nm. At the same time, both of the carrier concentration and mobility of the films rapidly increase from 1.24×10^{21} cm^{-3} to 6.43×10^{21} cm^{-3} and 0.65 $cm^2/V.S$ to 33.7 $cm^2/V.S$ with increasing thickness, respectively. Similar results were reported in previous literature[111,112]. The resistivity reduced can be attributed to the films crystallization improvement, which leads to the enlargement in crystallite sizes which consequently reduces the free electron scattering at grain boundaries[142]and then the carriers mobility enhancement. On other hand, the presence of oxygen vacancies and/or interstitial indium acts as charge donor centers in the system consistent with the observed increase of the charge carrier density and mobility[121,122]The free carriers enhancement with the thickness is in good agreement with the films band gap broadening as deduced from the optical characterization results.

Table 3.3:Electrical resistivity, carrier concentration and carrier mobility values of In_2O_3 thin films deposited using sol-gel spin coating method.

Thickness (nm)	Resistivity ρ (Ω.cm)	Carrier concentration n (cm^{-3})	Carrier mobility μ (cm^2/VS)
175	1.50×10^{-3}	1.24×10^{21}	0.65
330	1.03×10^{-3}	1.63×10^{21}	1.78
520	5.20×10^{-4}	2.16×10^{21}	5.56
690	2.80×10^{-4}	3.41×10^{21}	13.70
910	1.50×10^{-4}	6.43×10^{21}	33.70

3.2The influence of pH solution:

The ph solution of In_2O_3 is one of the contributing parameter to obtain indium oxide thin films. So, it effects on structural, optical, morphological and electrical properties of the films with the best possible characteristics for optoelectronic and photovoltaic applications.

3.2.1 Structural properties:

The XRD patterns of In_2O_3 films deposited at various pH solutions is shown in fig3.11. As the result, the diffraction patterns were well matched with the standard JCPDS data file reference code: 0416-006-00 for bixbyte structure in the lower pH solution[145]. It observed that all the samples have a preferred orientation along (222) .The XRD patterns at pH=0.84and pH=2.36 (without adding of NaOH solution) have a strong polycrystalline structure with high and preferred orientation along (222) at 2θ=30.54° and another peaks such as (211), (400), (440),(622) which corresponds to (21.55°) ,(35.53°), (51.14°), (60.70°), which proves the crystallization degree of the films is highest, it means that the films deposited from the sol having a lower pH (0.84 -2.36) have more grain growth. The smallest peaks and the intensity of preferred diffraction peak plane (222) are disappeared with increasing of pH solution which revealed that the crystallinity decreases with higher pH solution. This phenomena is related with research of Werta et all[146] , they reported that the presence of more OH- in the solution (as the similar result for addition a more NaOH solution for the pH adjustment), this causes a slow growth of the layers, which leads to reduced of thickness (see figure 3.12).In the other hand , the table3.4shows the lattice parameter α and stress σ of the samples for pure In_2O_3 thin films with different pH solution , as can be seen the lattice parameter of In_2O_3 decreases with increasing of

pH solution. In the other hand, it can clearly noticed the stress decreases with increasing of OH^- in the solution, this is due to the internal stress varies from tensile (positive) to compressive (negative) .

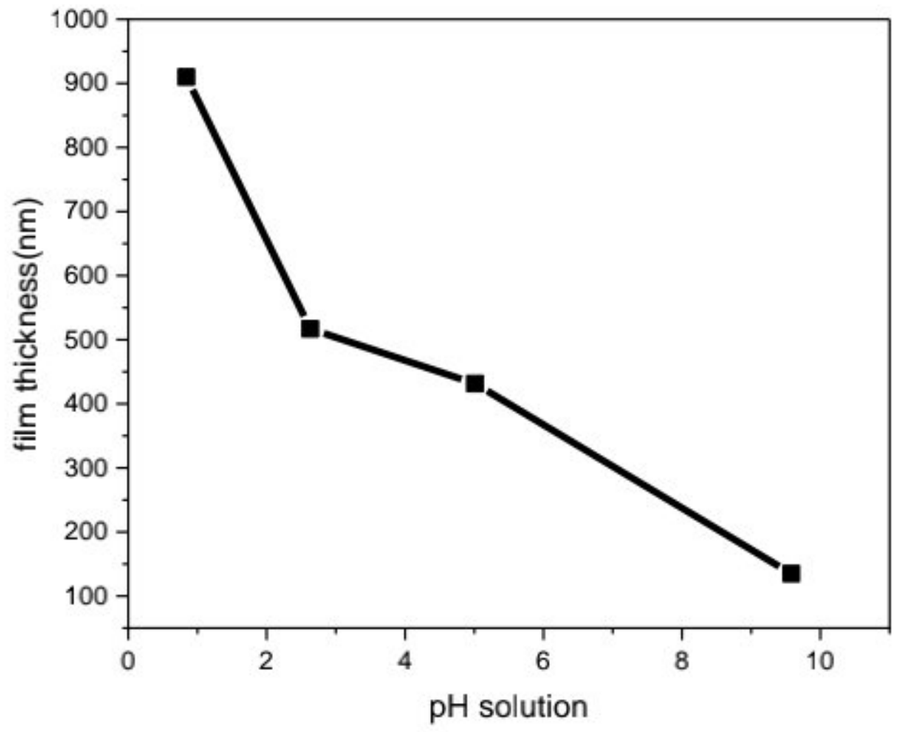

Fig 3.12: The variation of film thickness for In_2O_3thin films at various pH solution.

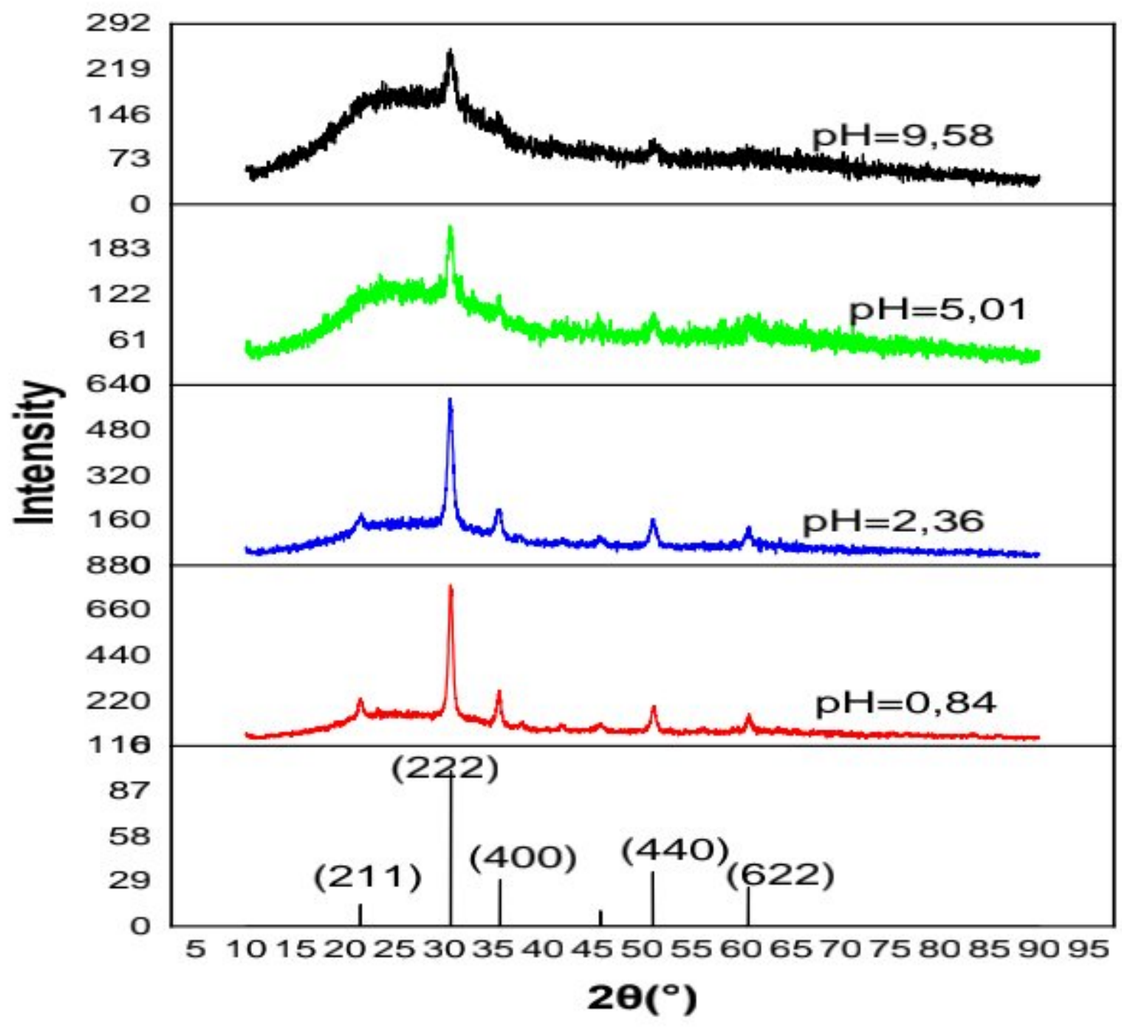

Fig 3.13: The XRD results of In_2O_3 thin films with various of pH solution.

At the same time, the lattice parameters of In_2O_3 thin films decreases with increasing of pH solution these results are dependent with the variation of internal stress.

Table 3.4: Structural parameters information of prepared In_2O_3thin films for different pH.

pH solution	*h k l* planes	2θ(degree)	Calculated parameters		Reference parameter (JCPDS card No 06-0416)	Stress (Gpa)
			Lattice constant *a* (Å)	d-spacing (Å)		
0.84	(222)	30.55	10.136 ±0.01	2.926		0.42
2.63	(222)	30.66	10.093 ±0.01	2.913	a_0 = 10.118 Å	-0.055
5.01	(222)	30.74	10.067 ±0.01	2.906	*d* = 2.921 Å	-0.112
9.58	(222)	30.65	10.096±0.01	2.914	2θ = 30.58	-0.048

The table 3.5 shows the variation of several parameters (crystallite size D, full width maximum FWHM of preferred orientation(222), dislocation density δ and strain ε), it is clearly noticed that the FWHM increased with decreasing of intensities of all peaks for the samples at rising pH solution attributed to deterioration of the crystallinity of indium oxide films revealed the incorporation of defects in the structure[147].In the same time, figure 3.12 represents the reduction of crystallite size with increasing of pH sol while the strain and dislocation density increases due to increase the defects and impurities in films, this is demonstrate the less crystallinity of In_2O_3 thin films which confirmed by XRD patterns.

Table 3.5: The crystallite size D, FWHM, strain and dislocation density for In2O3 thin films prepared at different pH solution.

pH solution	Peak (hkl)	FWHM (β°)	D (nm)	δ x10^{15} (Lines /m^2)	ε x10^{-3}
0.84	(222)	0.32	27	2.77	0.538
2.63	(222)	0.39	21.85	2.28	2.31
5.01	(222)	0.55	15.61	4.47	3.28
9.58	(222)	0.78	10.92	9.13	3.31

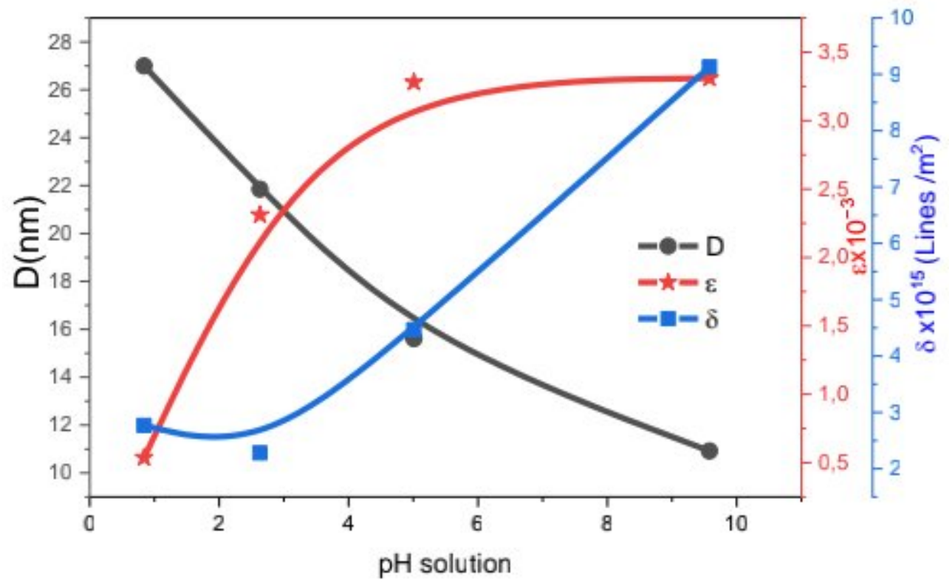

Fig 3.14: the variation of crystallite size, strain and dislocation density against the pH solution.

3.2.2 Optical properties:

The figure 3.15 shows the transmittance of In_2O_3 thin films deposited at different pH solution in the region of wavelength (400-800nm), the transmittance obtained decreases from 80.55% to 70.96% with increasing of pH solution (the adding of NaOH into the prepared solution of indium oxide). This leads to increase in vacancy defects, which due to increase in absorption[148]. At the same time, it may be probably causes the reduction in crystallinity of the films with rising of pH solution which can be related in XRD analysis. The light scattering increases with the reduction in degree of crystallinity for indium oxide thin films, which leads the lower transparency. A low transparency for the In_2O_3 thin films in the visible range is not expected for applications as transparent electrodes in optoelectronic devices.

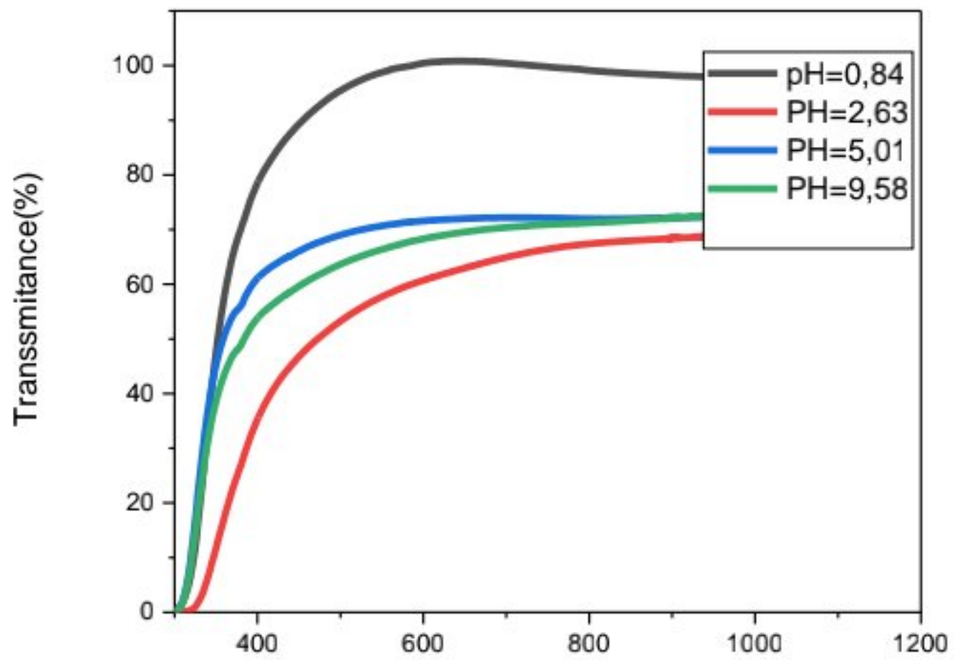

Fig 3.15: The transmittance of In_2O_3 thin films with different pH solution.

The optical band gap was estimated using the equation (2.11) from the edge absorption which can be plot $(\alpha h\nu)^2$as function hν (see figure 3.16). In the other hand, the Urabch energy was calculated using the function(2.12) from the edge absorbance at UV wavelength (λ<380nm) of In_2O_3thin films (figure 3.17),which suggesting the blue-shifted absorption edge (for band gap values) with the increasing of pH solution (in acid medium pH= 0.84, 2.36 and 5.01) and red shifted absorption edge(for band gap values) in basic medium (pH=9.58),the values of band gap are illustrated in figure 3.18. It observed the values of band gap increase with increasing of pH solution at acid medium, this variation is confirmed the Burstein-Moss effect [149] and decrease at basic medium (pH=9.58). A minimum value of optical band gap (2.95eV)can be attributed the change in crystallite size[150].

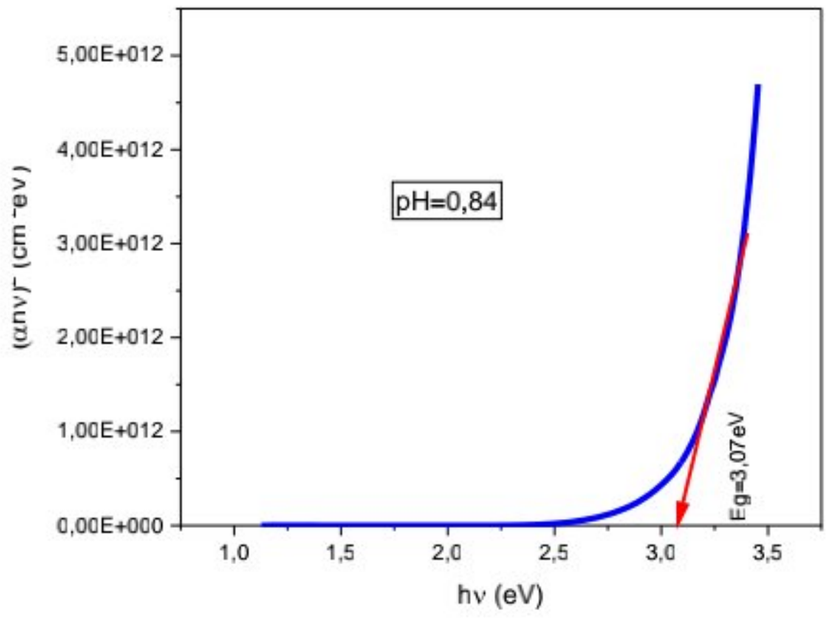

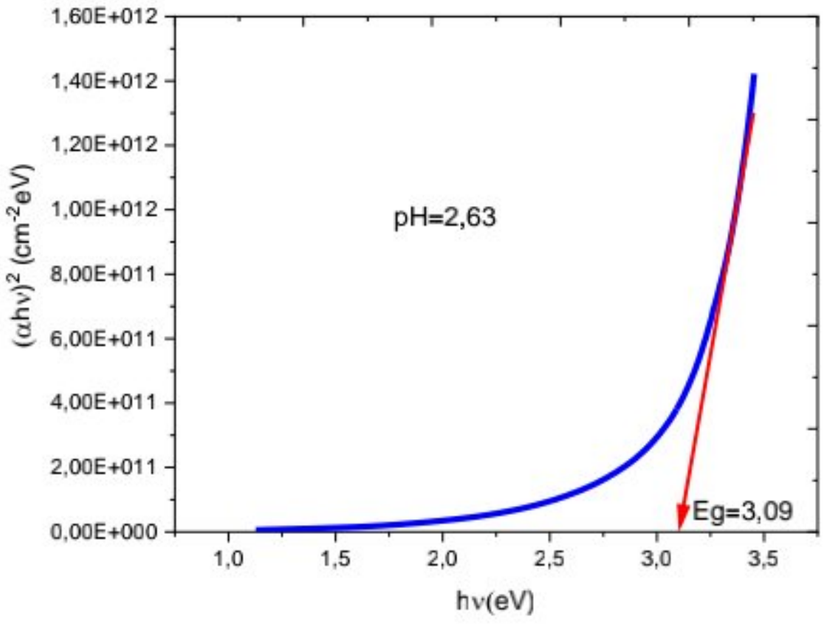

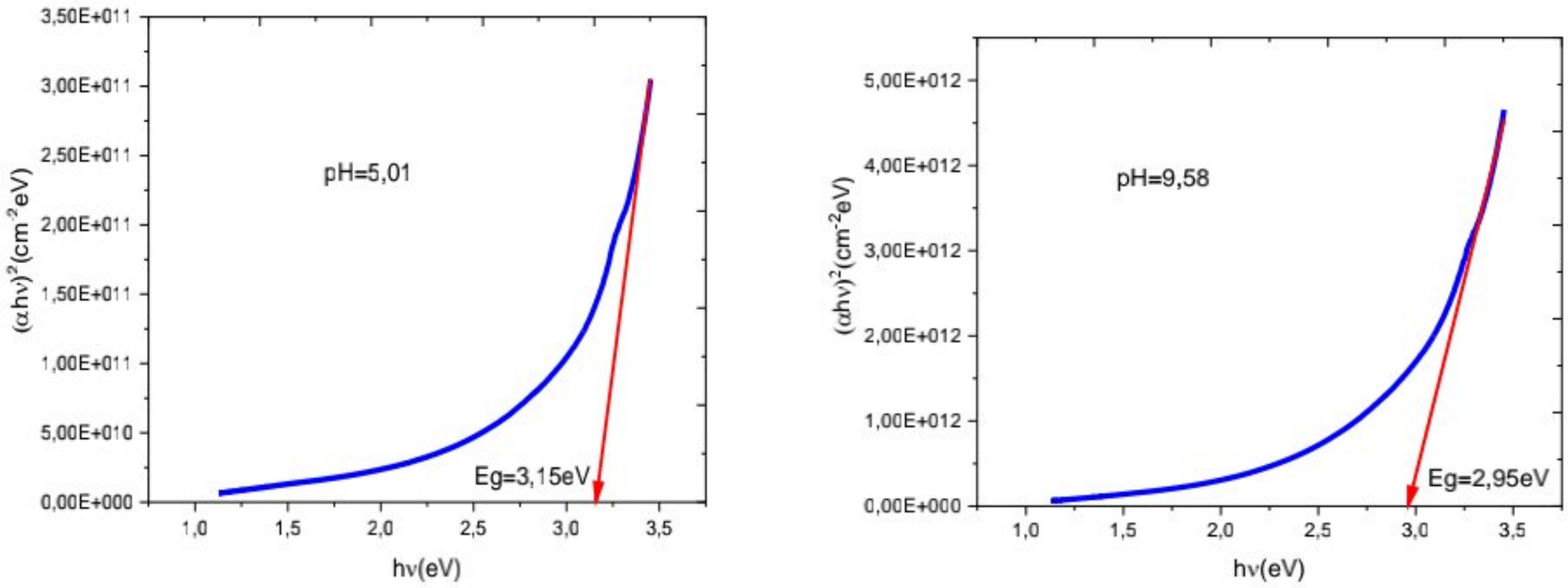

Fig 3.16: The tauc plot of $(\alpha h\nu)^2$ as function hν at different pH solution.

However, Urbach energy values increases from 0.15 to 0.38 eV at with increasing of pH solution from (figure 3.18) due to increase the disorder in structure of indium oxide thin films which related with XRD results.

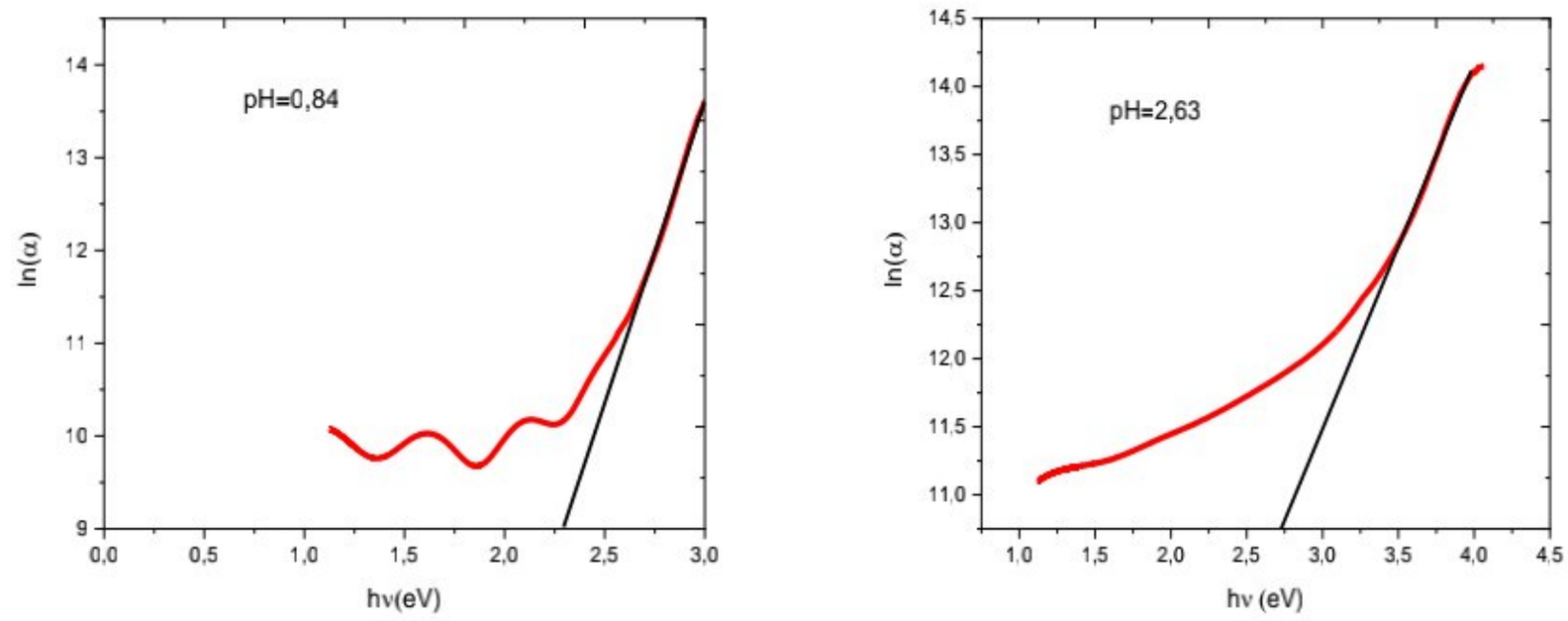

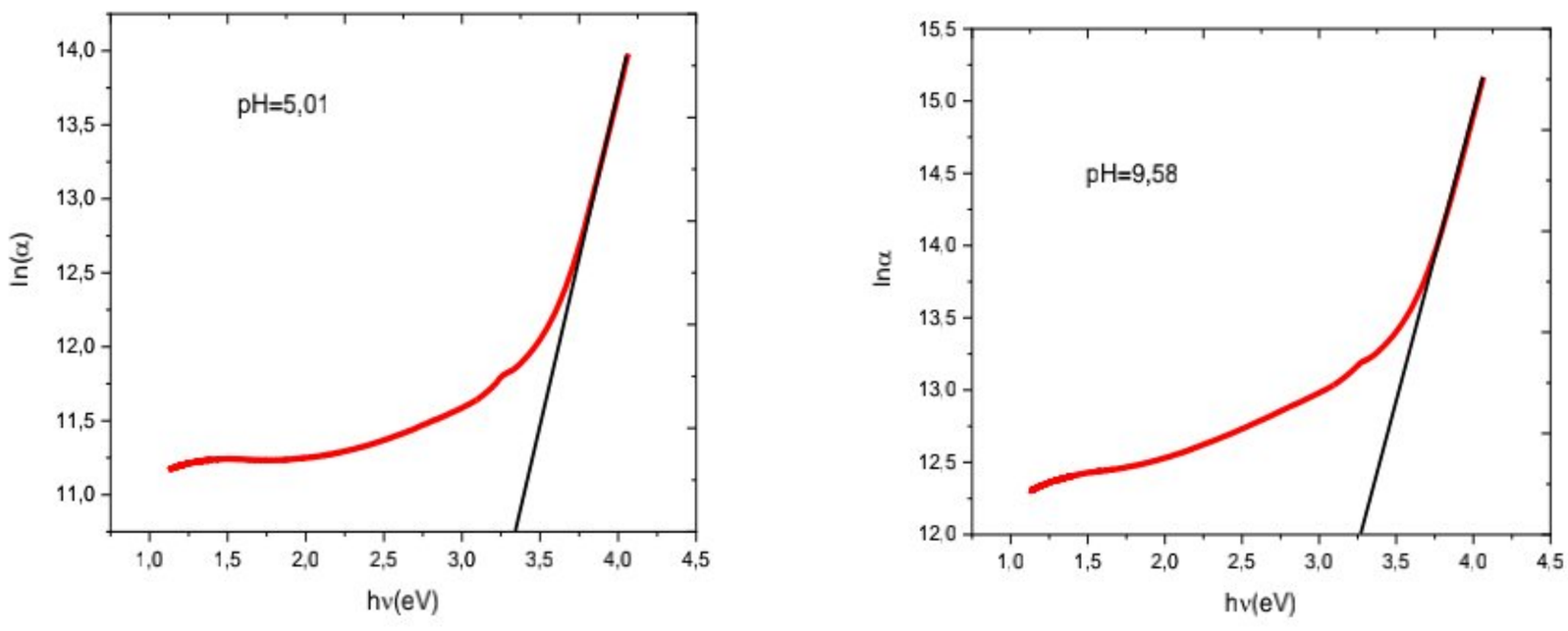

Fig 3.17: The plot ln(α) as function photon energy (hν) at different pH solution.

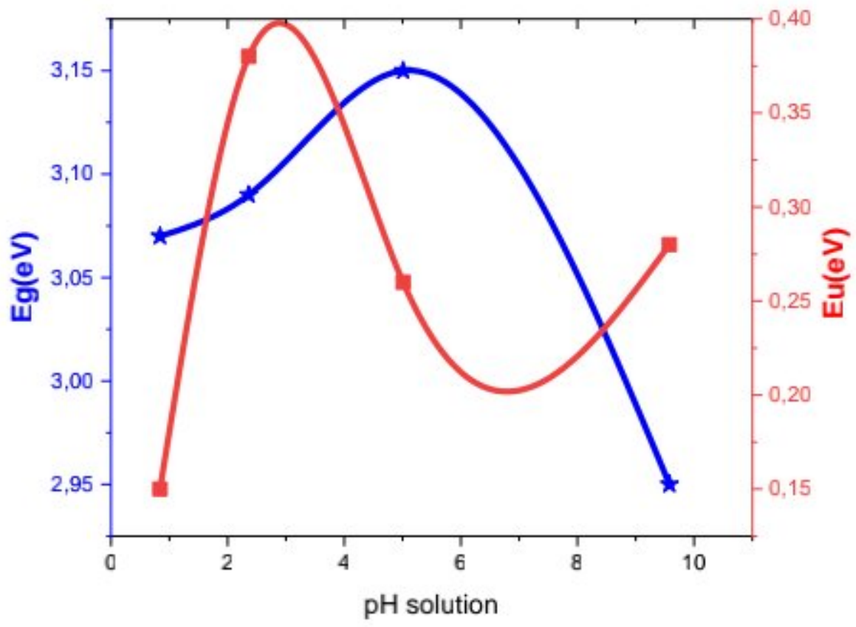

Fig 3.18: The variation of band gap Eg and Urbach energy Eu at different pH solution.

3.2.3 Morphological properties:

The morphological of In_2O_3 thin films shows in fig 3.19, it can be seen the films have a homogenous, smoothing surface and uniform distributed of grain size without any cracks or pin holes at lower pH solution and higher pH. Also, the SEM measurement confirmed that the results of XRD patterns (the variation of crystallite size) [99,100] ,at lower pH solution it clearly see the grain size is the biggest this related with the good crystallinity of indium oxide thin films which the values of crystallite size is bigger (27nm) at pH=0.84 than the other values for pH solution (2.36, 5.01, 9.58) .In the other hand , the films obtained at higher pH solution have a smallest grain size which is good agreement with the decrease of crystallite size with increasing of pH solution , this is attributed of incorporation of more NaOH solution in the original solution.

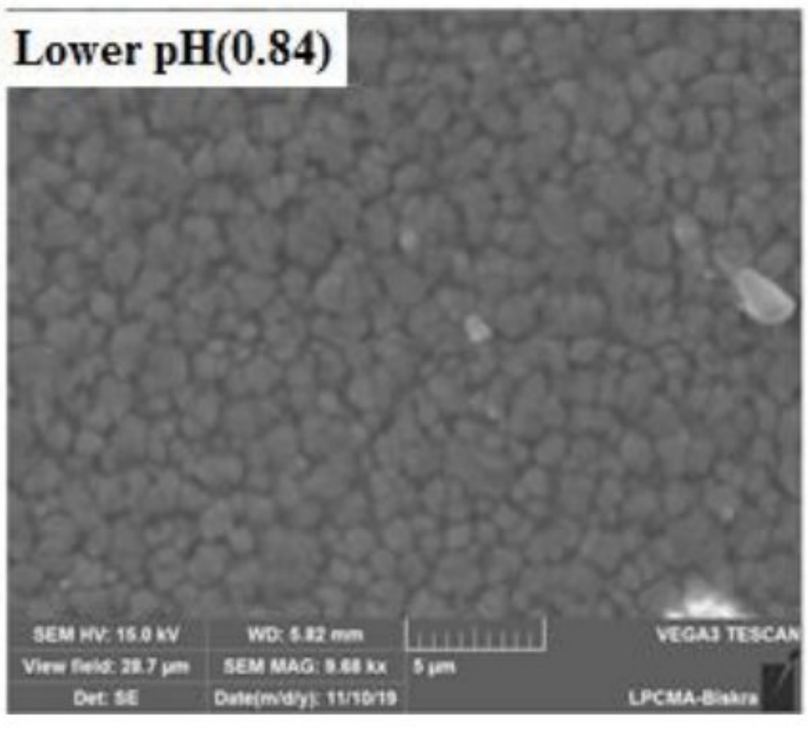

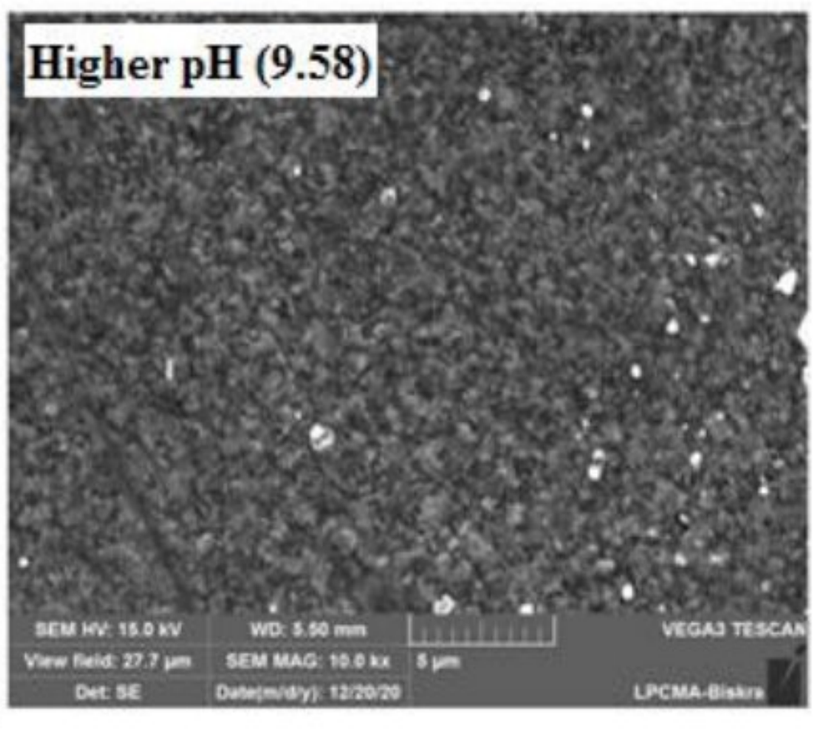

Fig 3.19: The SEM images of indium oxide thin films at lower pH (0.84) and higher pH (9.58).

3.2.4 The compositional properties:

The EDX analysis confirms the presence of In and O in the films at lower pH and higher pH solution (figure 3.20).The Na atoms appeared in the films at higher pH due to the more adding of NaOH sol in the prepared solution for deposited In_2O_3thin films. The atomic and weight percentage of O and In given in table 3.6. Obviously, it observed that the percentage of O atom increases with the increasing of pH solution due to increase the OH^- ion in the reaction while the percentage of In reduces with the rising of pH solution. These results related with XRD patterns of indium oxide thin films.

Table 3.6: The atomic and weight percentage of oxygen and indium.

pH solution	Elements					
	Wt%			at%		
	In	O	Na	In	O	Na
0.84	72.27	27.73	0	26.65	73.35	0
9.58	47.74	34.49	17.76	12.43	64.46	23.10

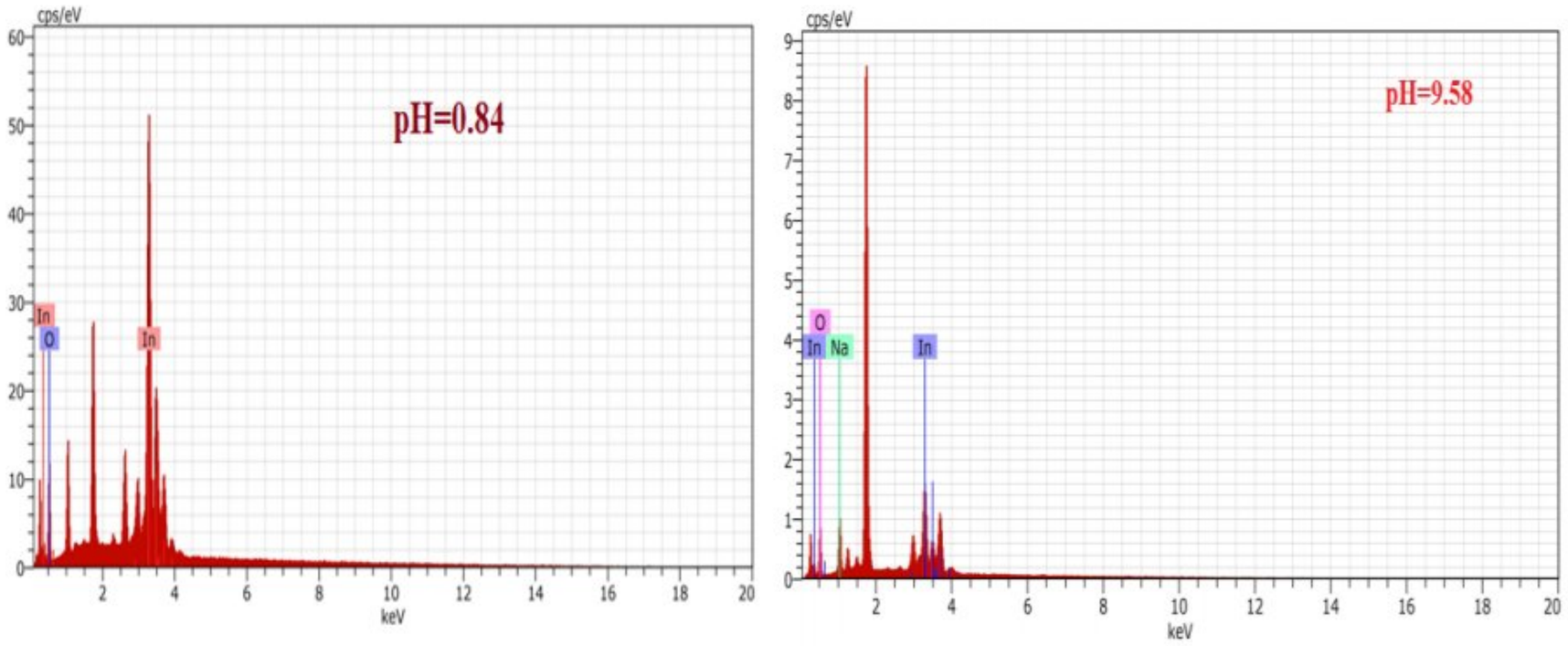

Fig 3.20 : The energy dispersive of lower pH and higher pH solution for indium oxide thin films.

3.2.5 Electrical properties:

The figure 3.21 presents variation of resistivity (ρ) and conductivity (σ) of In_2O_3 thin films at varied pH solution. As the results , the resistivity increases from $1.5\times 10^{-4}\Omega$.cm to 0.059Ω.cm

with increasing of pH solution for indium oxide thin films while the conductivity decreases accordingly. The increasing in resistivity may be attributed the detrioration of crystalline quality and increase of total grain boundary fraction in the films, which can enhance grain boundary scattering, thus , result in a decrease of electrical conductivity[153].

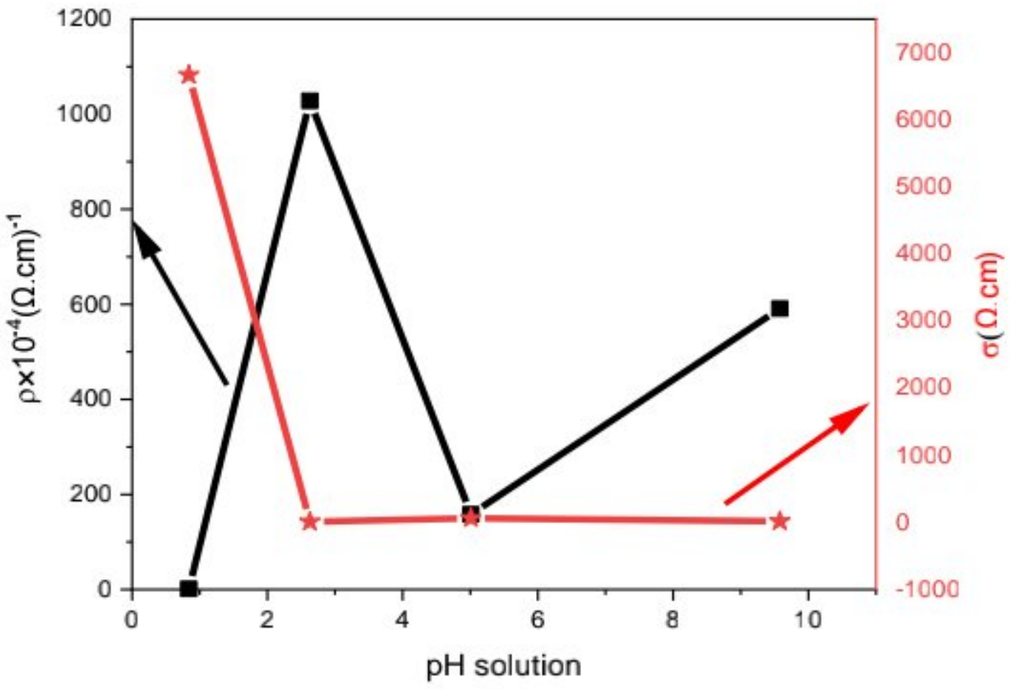

Fig3.21: The variation of resistivity as function pH solution for indium oxide thin films.

Conclusion:

The variation of film thickness is found to have effect on structural, optical morphological and electrical properties. X-ray diffraction shows the strong crystallinity of the films with rising the film thickness and a preferred orientation along (222) for growth the film. The transmittance of the films is higher in the visible region with increasing of band gap. The surface morphology of the films is uniform and smoothing with increasing of grain size. The electrical resistivity reduces with increasing of film thickness. The influence of pH solution investigated that the XRD patterns presented that the films have a polycrystalline structure with preferred orientation along (222) plane corresponding to In_2O_3 cubic structure. The crystallinity of the films reduces at higher pH solution. SEM images showed homogenous surface and reduction of grain size. EDX spectra revealed the presence of In and O elements in the prepared films and Na element start appeared at the adding NaOH solution with their atomic (at %) and weight (wt %) percentage. The transmittance of the films is higher in the visible region with increasing the optical band gap. The electrical measurement showed that the electrical conductivity decreases with rising pH solution. From this result, we conclude that the prepared In_2O_3 films can be used as a window in solar cells device.

CHAPTER 4:
Effect of molar concentration precursors

Introduction:

The precursor solute concentration is one of the important process parameters that determines the indium ion concentration and hence the film growth, structure and characteristics. So, the influence of the precursor solute concentration on the In_2O_3 film characteristics has been studied with a view to optimize the solute concentration to obtain films with the best possible characteristics.

4.1 Precursor In_2Cl_3:

The precursor is one of the important parameter to obtain the indium oxide thin films, it can be optimized by varied the molar concentration precursor solution for given the best properties of In_2O_3 thin films to applied in photovoltaic and optoelectronic applications. We have studied the effect of molar concentration precursor (In_2Cl_3) on structural, optical, morphological and electrical properties of undoped indium oxide thin films.

4.1.1 Film thickness:

The film thickness of indium oxide films deposited at different molar concentration precursor was calculated by using the equation (2.1). As the result, the figure 4.1 shows the variation of film thickness for In_2O_3 films deposited at different molar concentration precursor (0.05M, 0.1M, 0.15M, 0.2M, and 0.25M), it noted the film becomes thicker as the precursor increases, film thickness increases from 67.41to 382.24nm when the molarity was increased . Nevertheless, it means that nucleation of In^{3+} and O^{2-} improves with the growth of In_2O_3 thin films; this is because the molar concentration precursor increases with the enhancement of the films.

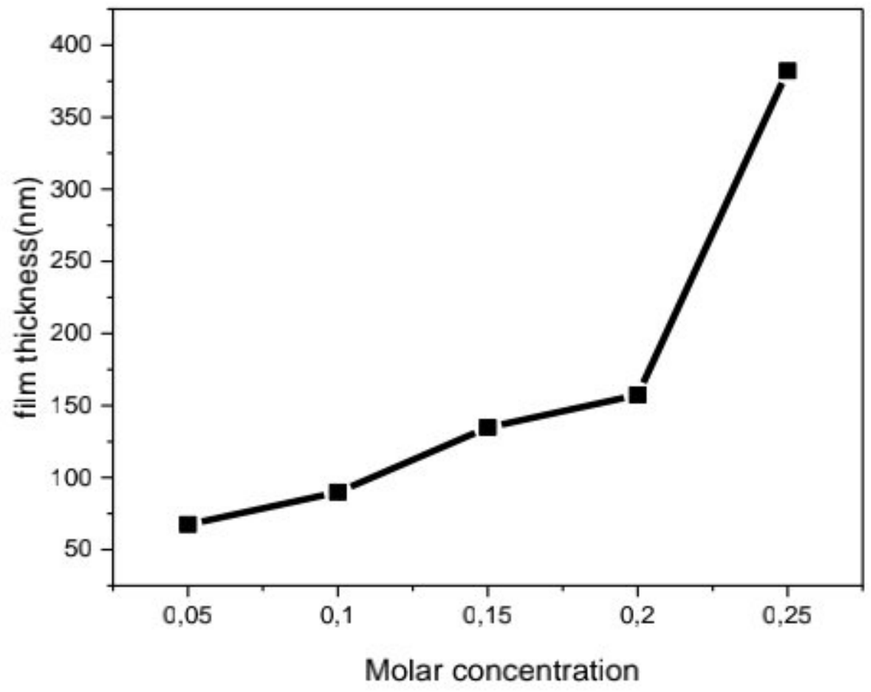

Fig 4.1: The variation of film thickness when the molarity increases.

4.1.2 The structural properties:

The figure 4.2 shows the results of XRD patterns for deposited In_2O_3thin films at different molar concentration precursor ($InCl_3$) 0.05M, 0.1M, 0.15M, 0.2M and 0.25M, it is clearly see the films at less molar concentration (0.05M) is amorphous with more impurities, this due to reduction of In^{3+} and O^{2-} ions in solution for coated on glass substrate to obtain indium oxide thin films. In the other hand, the orientations plane of In_2O_3 thin films appeared at 0.1M and increased with increasing of molar concentration (0.15M, 0.2M, 0.25M), it is indicated the polycrystalline in nature. The XRD patterns presented peaks corresponding to (211), (222), (400), (440), (622) planes of crystalline $In_2O_3$with body centered cubic (BCC) structure [(JCPDS) data card No. 06-0416] , it noticed the films improved at 0.1M and 0.15M and have a preferred , strong orientation along (222), the films at (0.2M,0.25M) have a strong and highest orientation along (400). As molar concentration increases the orientation (222) plane has appeared, and the most preferred orientation was found along (400) plane this may be due to more $In^{3+}$and O^{2-} ions in films. Aparna et al[154] were deposited indium oxide films by using In_2Cl_3 as precursor and reported the nucleation along (400) plane contributed to extended diffusion length and increased mobility of the atoms.Table4.1 shows the lattice parameters calculated using equation(2.2) of In_2O_3 thin films deposited at various molar concentration precursor , it observed that the lattice constant decreases form 10.15to 10.09A° with increasing of molar concentration from 0.1 to 0.15M which the values lower than α_0 (10.118A°) . This can be explained by internal stress calculated which is tensile with positive value at 0.1M and compressive (negative) for indium oxide films deposited at 0.15M, 0.2M, 0.25M contributed to more In^{3+} and O^{2-} in lattice structure that leads to pressure on lattice structure of In_2O_3 . It also observed the values of compressive stress reduced from 0.15 to 0.25M and have a variation inverse with crystallite size and lattice constant which proves that the grain boundaries decreased. Thus, when the crystallite size increases, which indicates the improvement of the crystallinity and the number of defects decreases, it is means the reduction in stresses[155].On the other hand, the figure 4.3 shows the variation of crystallite size calculated from XRD patterns increases from 14.92nm to 70.60nm with increasing of molar concentration precursor, In_2O_3 thin films can be viewed as high crystalline structure, which leads to the reduction of the strain as well as the stresses in the crystal lattice of the films and consequently to the improvement the crystallinity of In_2O_3 films has been well confirmed with XRD patterns.

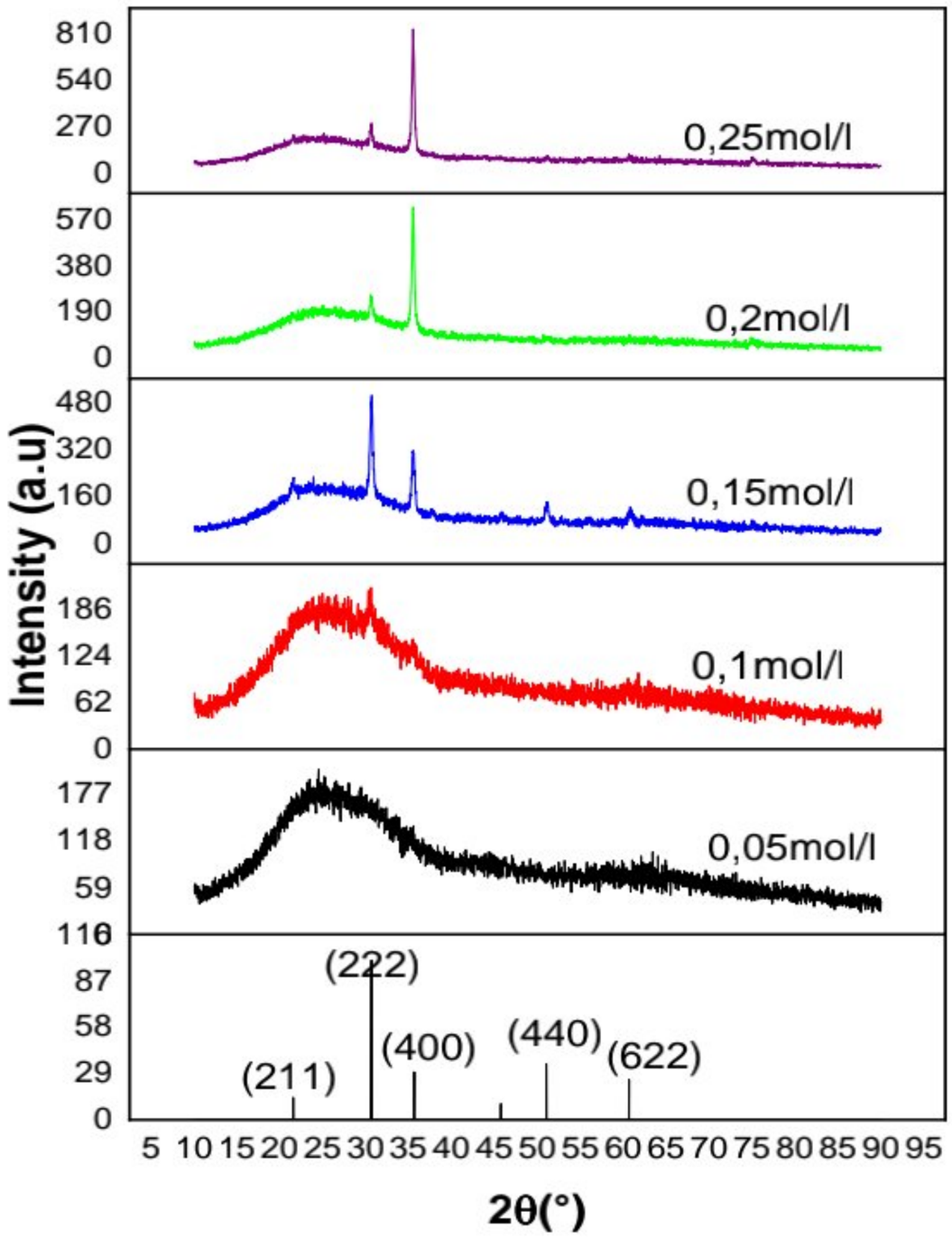

Fig 4.2: The XRD patterns of In_2O_3 thin films at different molar concentration.

The strain ε and dislocation density δ decrease with a variation of molar concentration precursor, this due to the amelioration of crystallinity in films.

Table4.1: The lattice parameters of In_2O_3 thin films with variation of molar concentration precursor.

Samples	*h k l* planes	2θ(degree)	Calculated parameters		Reference parameter (JCPDS card No 06-0416)	Stress (Gpa)
			Lattice constant *a* (Å)	d-spacing (Å)		
0.05M	/	/	/	/		/
0.1M	(222)	30.46	10.15	2.9314	a_0 = 10.118 Å	0.0814
0.15M	(222)	30.694	10.09	2.9128	d = 2.921 Å	-0.647
0.2M	(400)	35.502	10.11	2.528	2θ = 30.58	-0.138
0.25M	(400)	35.509	10.11	2.5281		-0.138

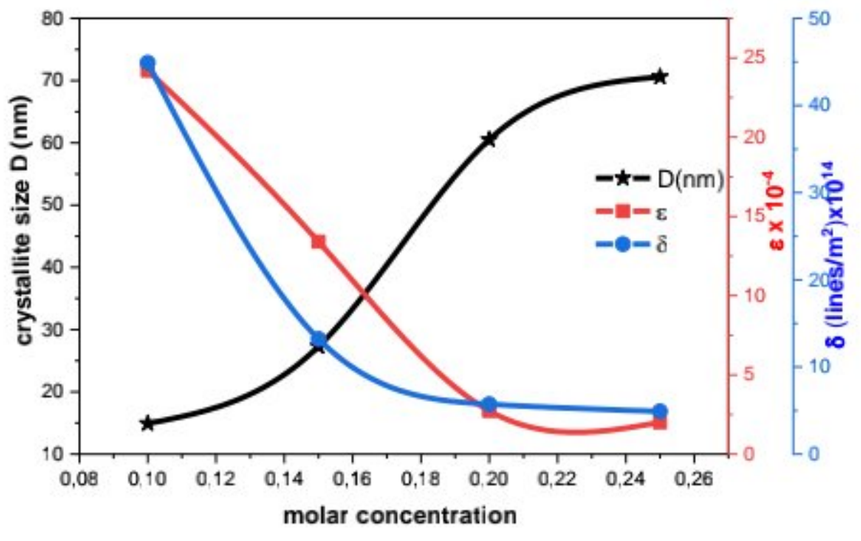

Fig 4.3: The variation of crystallite size D, strain and dislocation density as function molar concentration precursor.

The calculated texture of the films prepared at molar concentration precursor ($InCl_3$) is shown in figure 4.4, it can be seen the texture coefficient have a larger value at orientation (222) at 0.1Mand 0.15M due to textured growth dominant .These value increases for the orientation (400) at higher molar concentration precursor (0.2M and 0.25M) which is the preferred growth of the films. The low concentration of oxygen vacancies at 0.1 M and 0.15M investigates to more favour to the [111] textured In_2O_3 growth at low molar concentration due to the high atomic density [111] plane present a lower surface free energy than the [100] plane. It also noted at 0.2M and 0.25M the oxygen vacancies increases with molar concentration precursor consequently the

[100] textured the growth of In_2O_3 films. Moreover, the rising of molar concentration leads to In rich conditions preferred the direction [100] for the growth of indium oxide thin films[156].

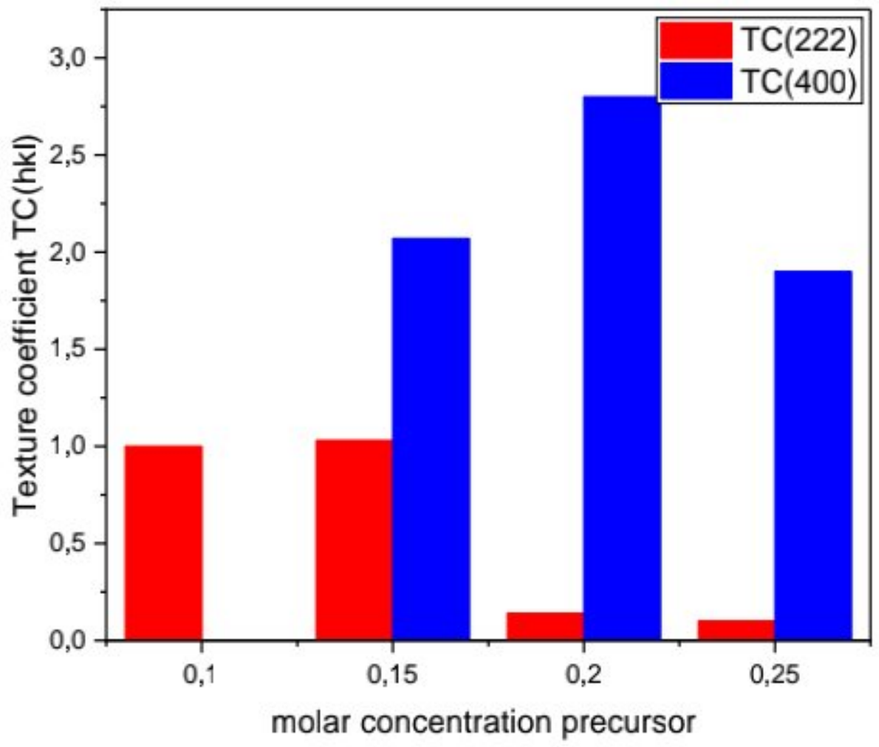

Fig 4.4: The texture coefficient TC(hkl) of In_2O_3 thin films at different molar concentration precursor.

4.1.3 Morphological properties:

The morphological properties of In_2O_3 thin films deposited at varied molar concentration precursor are shown in figure 4.5, it can be noted the films at low molar concentration precursor (0.05M) have not grain in surface. However, The SEM images of In_2O_3 films deposited at high molar concentration precursor (0.1M, 0.15 M, 0.2M, and 0.25M)presented that the films have a smoothing, uniform and roughness surface, it is clearly observed the grains was appeared at 0.1M and increased at high molar concentration precursor and have a spherical shape. Similarly, the enhancement in morphological properties related with increasing of molar concentration which confirmed with XRD results.

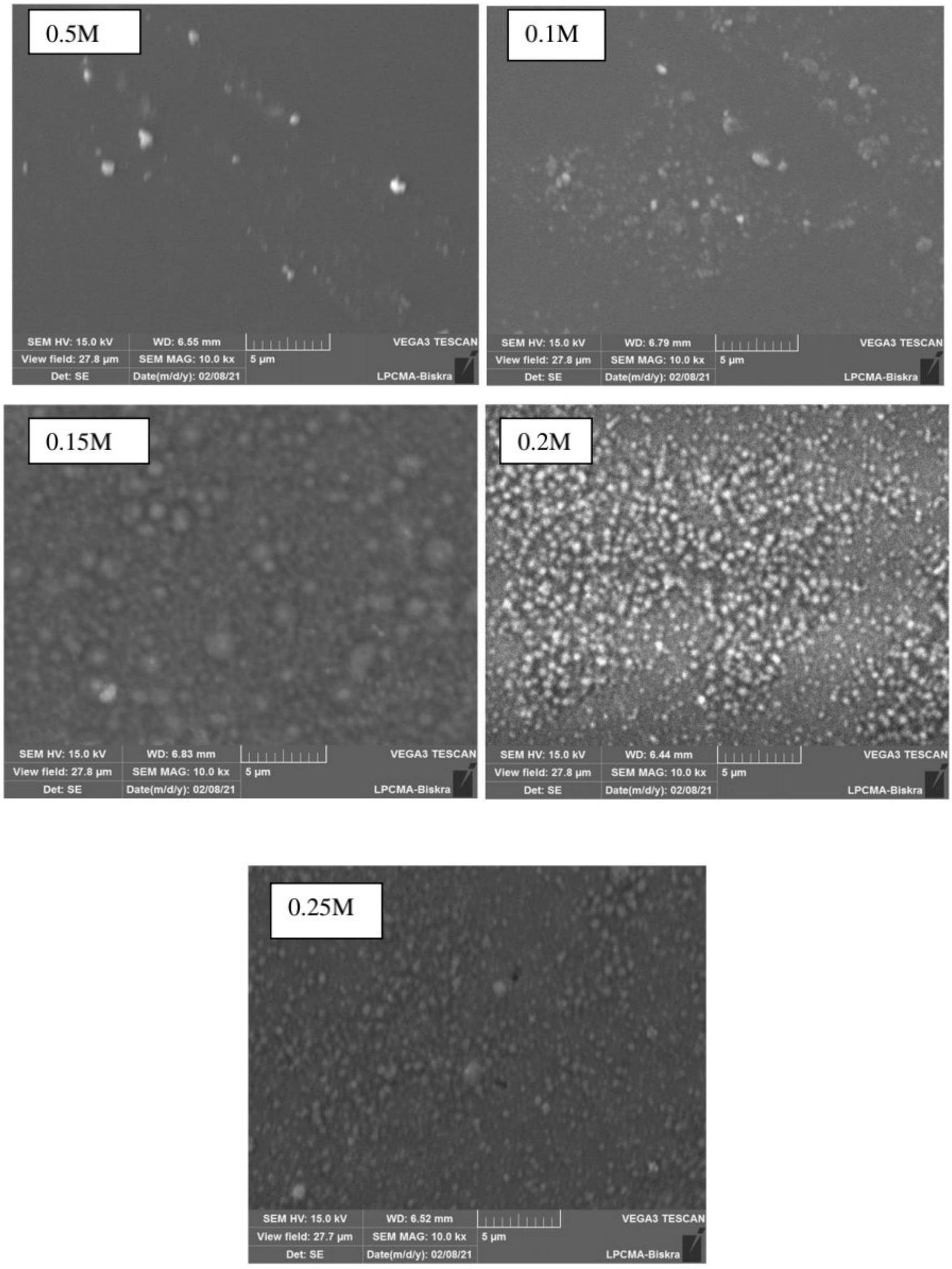

Fig 4.5: The SEM images of In_2O_3 thin films deposited at various molar concentration precursor (0.05M, 0.1M, 0.15M, 0.2M, and 0.25M).

4.1.4 Compositional properties:

The chemical compositions of the synthesized thin films were identified using EDX analysis and the obtained EDX spectra are presented in figure 4.6, it shows the presence of In and O in all the films with variation of molarities from 0.05M to0.25M. Furthermore, the table 4.2 illustrates the atomic and weight percentage of In increases with the increase of molar concentration precursor while the percentage of O decreases, this results(EDX) are in good agreement with XRD analysis which reported that in last studies by Isiyaku et al[157].

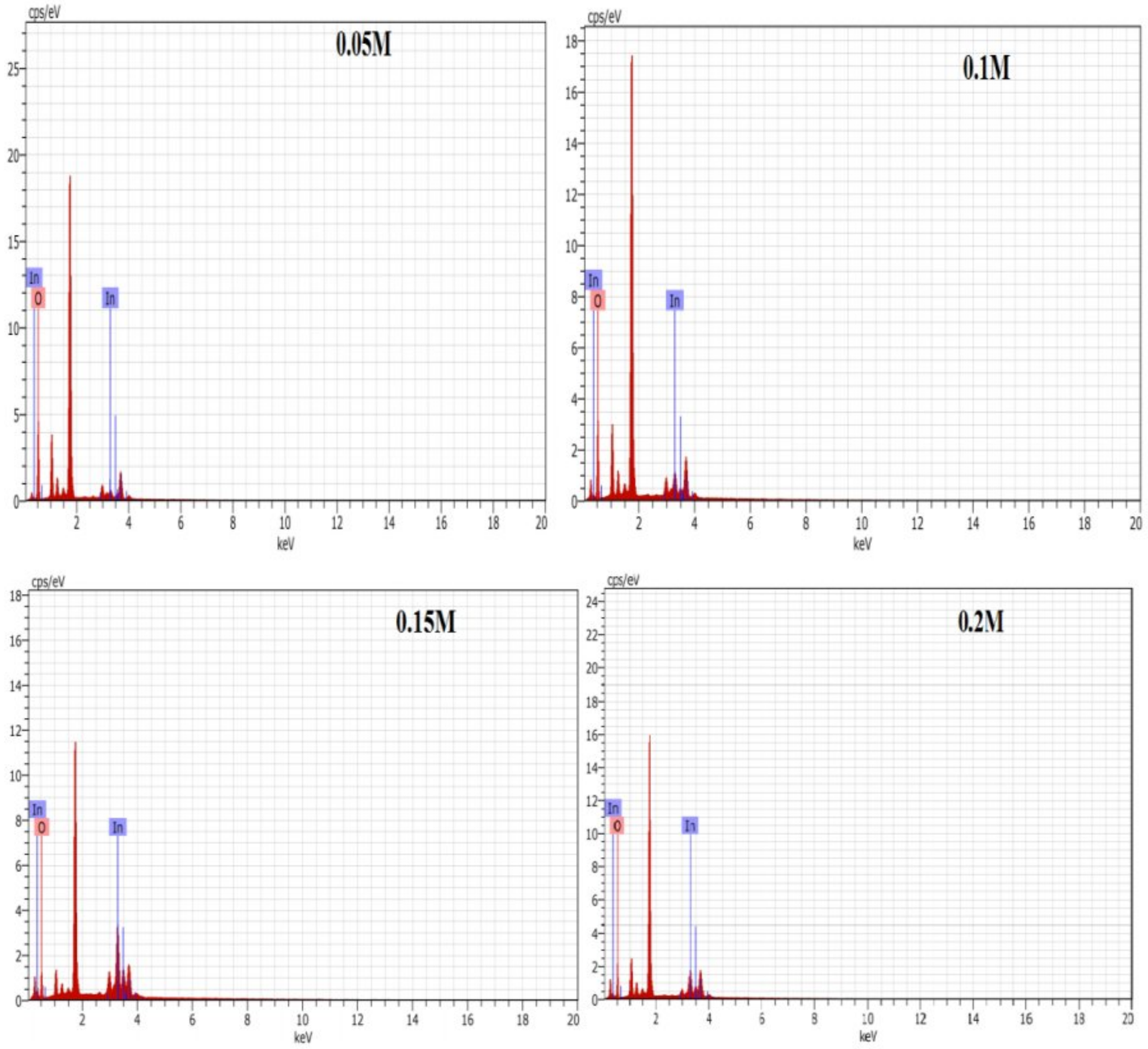

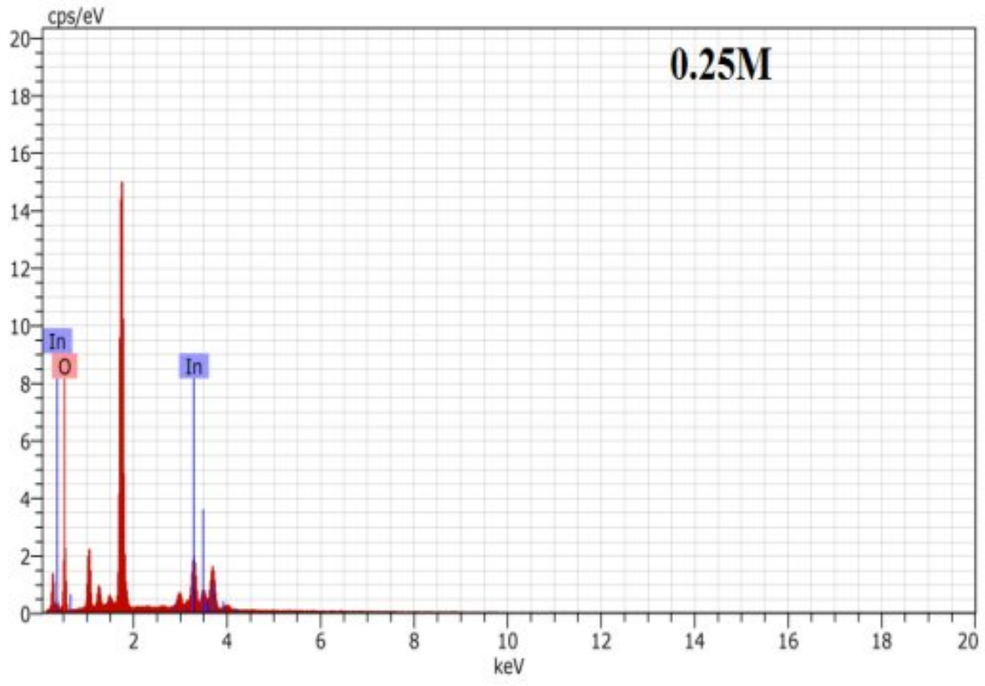

Fig 4.6: The EDS of indium oxide films deposited at different molar concentration precursor (0.15M, 0.2M and 0.2M).

Table 4.2: The weight percentage of In and O for In_2O_3 films deposited at different molar concentration precursor.

Molar concentration	Elements			
	Wt%		at%	
	In	O	In	O
0.05	18.47	81.53	3.06	96.94
0.1	30.02	69.98	5.64	94.36
0.15	63.39	36.61	19.44	80.56
0.2	39.55	60.45	8.35	91.65
0.25	42.79	57.21	9.44	90.56

4.1.5 Optical properties:

The transmission of In_2O_3 thin films deposited at various molar concentration precursors from 0.05M to 0.25M is shown in figure 4.7; it is clearly observed the transmittance of all samples have a highly transparency in the visible wavelength region (400nm -800nm). High transparency of the film can be attributed to less scattering, high crystallinity and homogeneity. Hence, the transmission decreases with the increase of molar concentration precursor from 95.88% to 80.84%, it is due to increase the film thickness. This result has been reported with ITO films [97,104], the transmittance spectra of films have a strong absorption edges in the UV region (λ<400nm) which investigating the red-shifted absorption edge with increasing molar

concentration precursor.

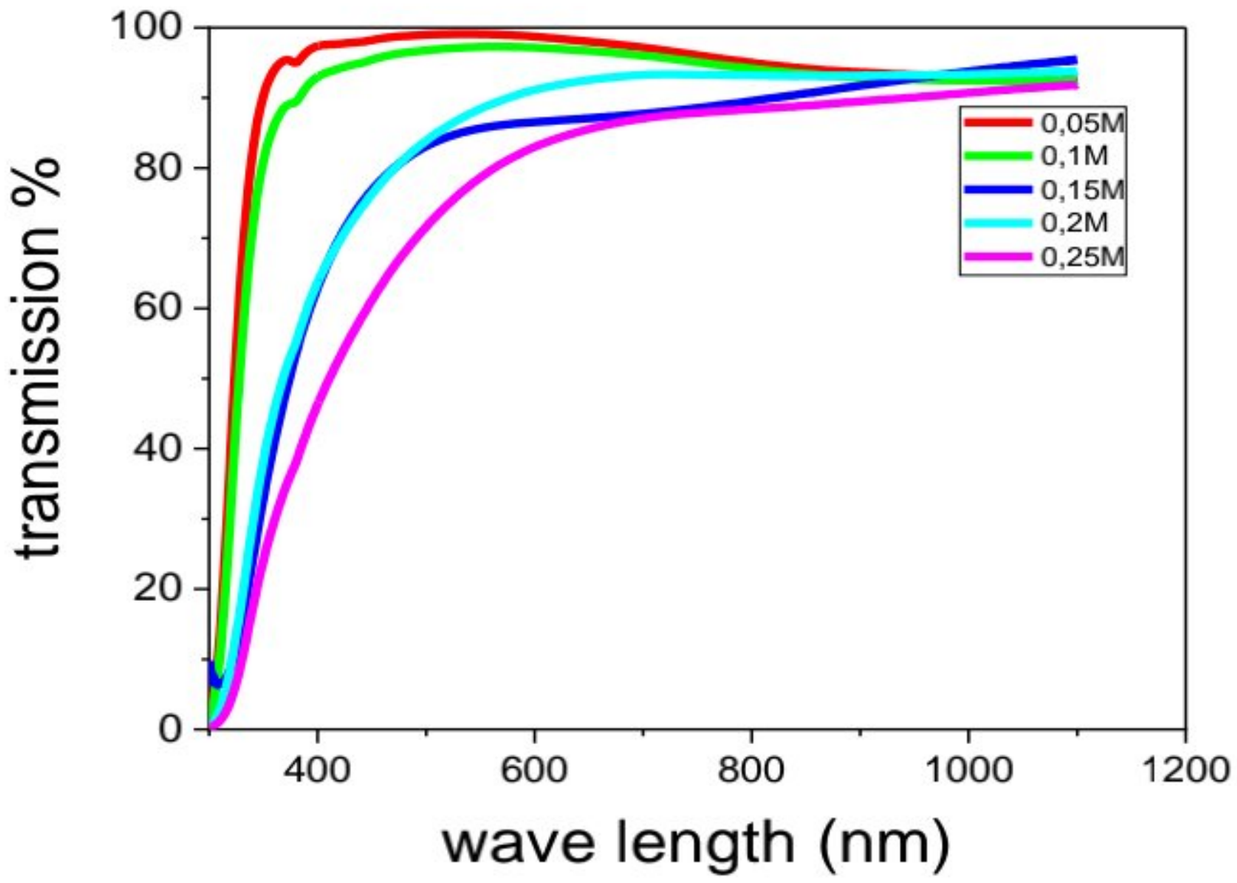

Fig 4.7: The transmittance spectra of In_2O_3 thin films deposited at different molar concentration precursor.

Besides, the band gap can be calculated using the plot $(\alpha h\nu)^2$ as function $(h\nu)$ by applied the equation (2.11) as shown in figure 4.8 and energy Urbach was estimated by using the plot $(\ln\alpha)$ as function $(h\nu)$ by applied the equation (2.12) see figure 4.9.

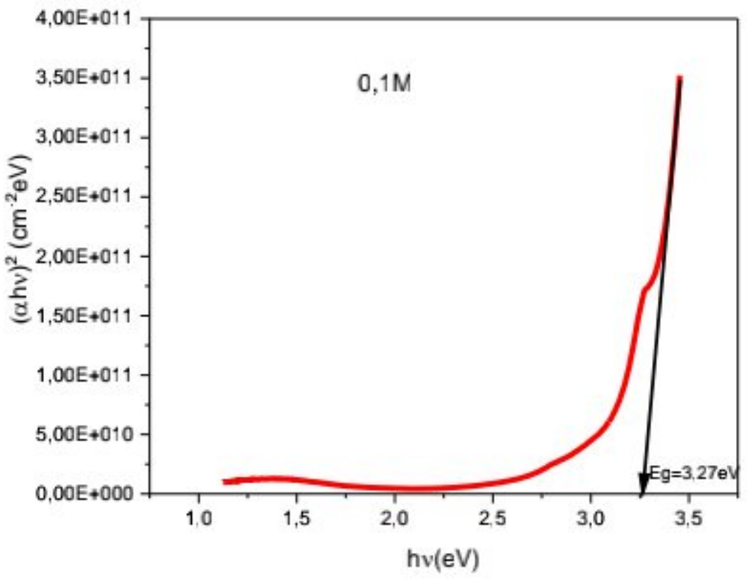

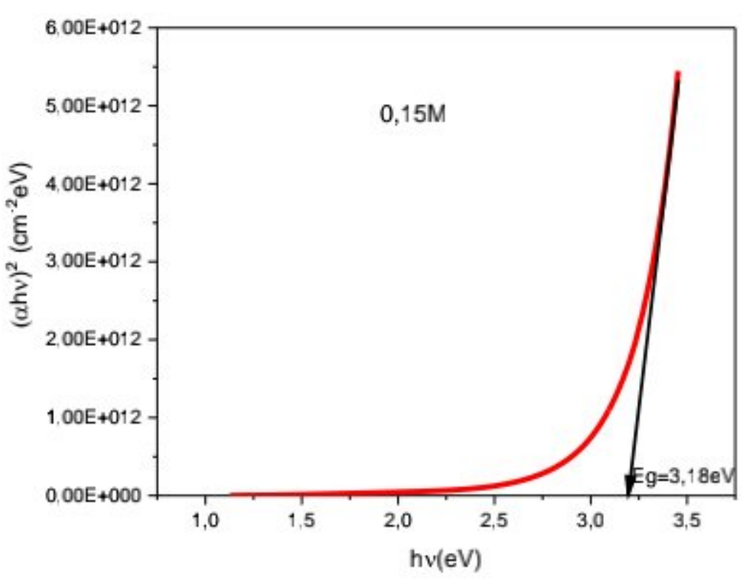

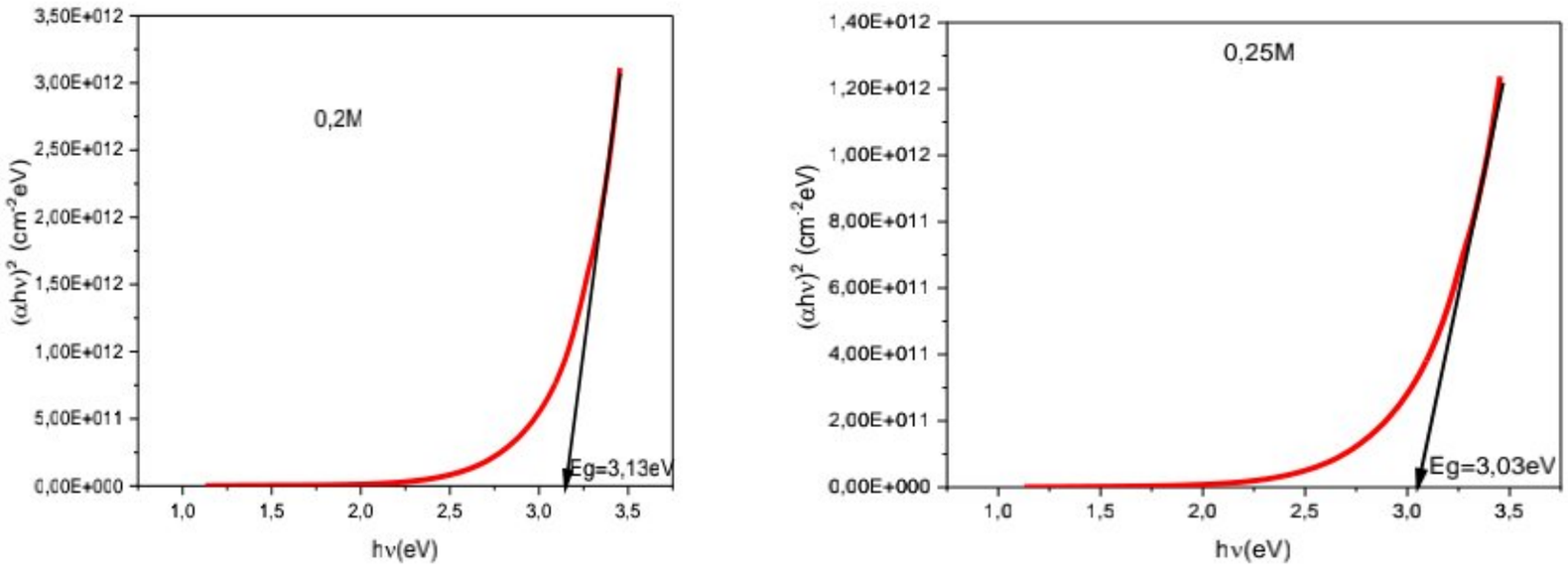

Fig4.8: The plot$(\alpha h\nu)^2$ as function (hν) for In_2O_3 films deposited at different molar concentration precursor (0.1M, 0.15M, 0.2M and 0.25M).

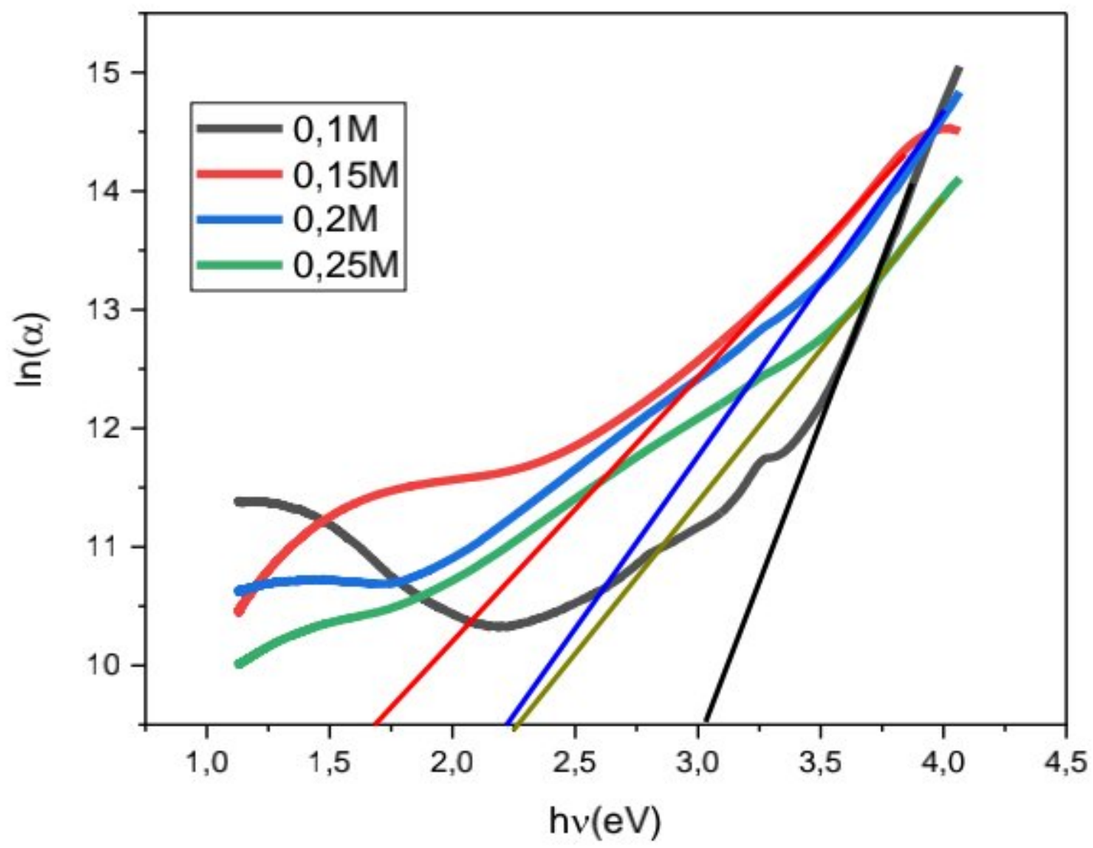

Fig 4.9: The plot ln(α) as function (hν) for In_2O_3 films deposited at different molar concentration precursor (0.1M, 0.15M, 0.2M and 0.25M).

The figure 4.10 shows the variation of band gap energy and Urbach energy, it is clearly noted the band gap was reduced (from 3.27eV to 3.01eV) with increasing of molar concentration precursor and Urbach energy was inversed with band gap(from 0.2eV to 0.719eV), this reduction of band gap revealed the improvement in crystallite size, it can be explained using quantum confinement theory according to which band gap energy and crystal size show an inverse relation[159], increasing molar concentration precursor rising Urbach energy which appeared due to disorderliness in the system and due to the local states formed in the band gap region with

perturbation[160].

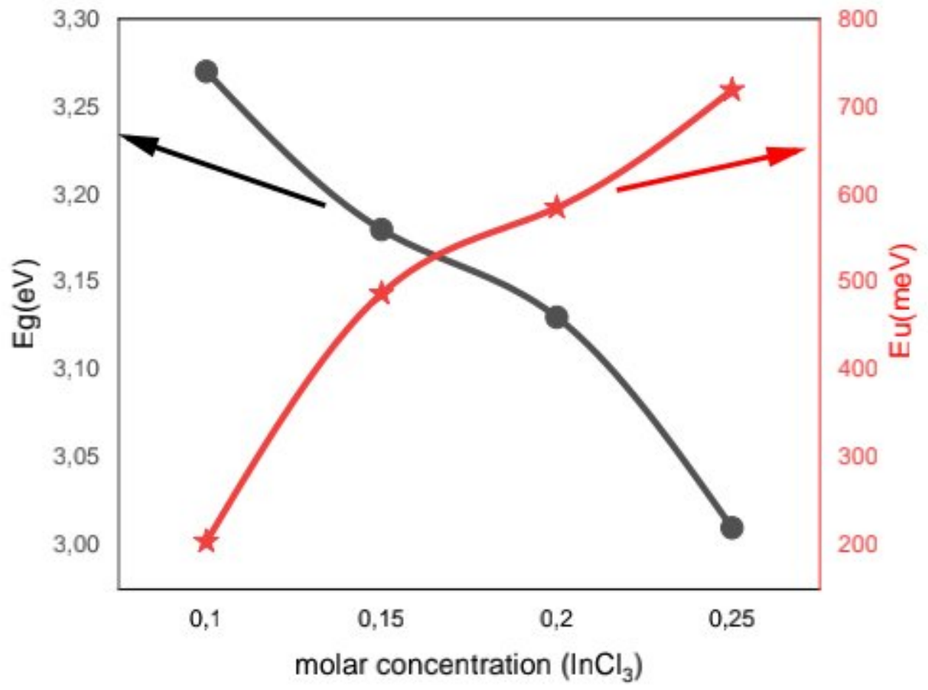

Fig 4.10: The variation of band gap energy and Urbach energy with different molar concentration precursor.

4.1.6 Electrical properties:

The results of electrical measurement on In_2O_3 thin films coating are shown in figure 4.11, the observed electrical resistivity (calculated by using the formula (2.18)) reduced with increasing molar concentration precursor (from 0.0309Ω.cm to 0.0021Ω.cm), it may be related with improvement in crystallinity of the films deposited at different molar concentration (increasing in crystallite size) which leads to decrease of grain boundary and defects in the structure of the films. The reduction of electrical resistivity attributed to the enhancement of free carrier concentration[161].However, the electrical conductivity increases with increasing of molar concentration precursor ($InCl_3$) revealed that the n- type conductivity in In_2O_3 is owing to oxygen vacancy and interstitial indium atoms, both acting as donors. Hence, it gives rise to higher carrier concentration as In and O concentration increases[162].

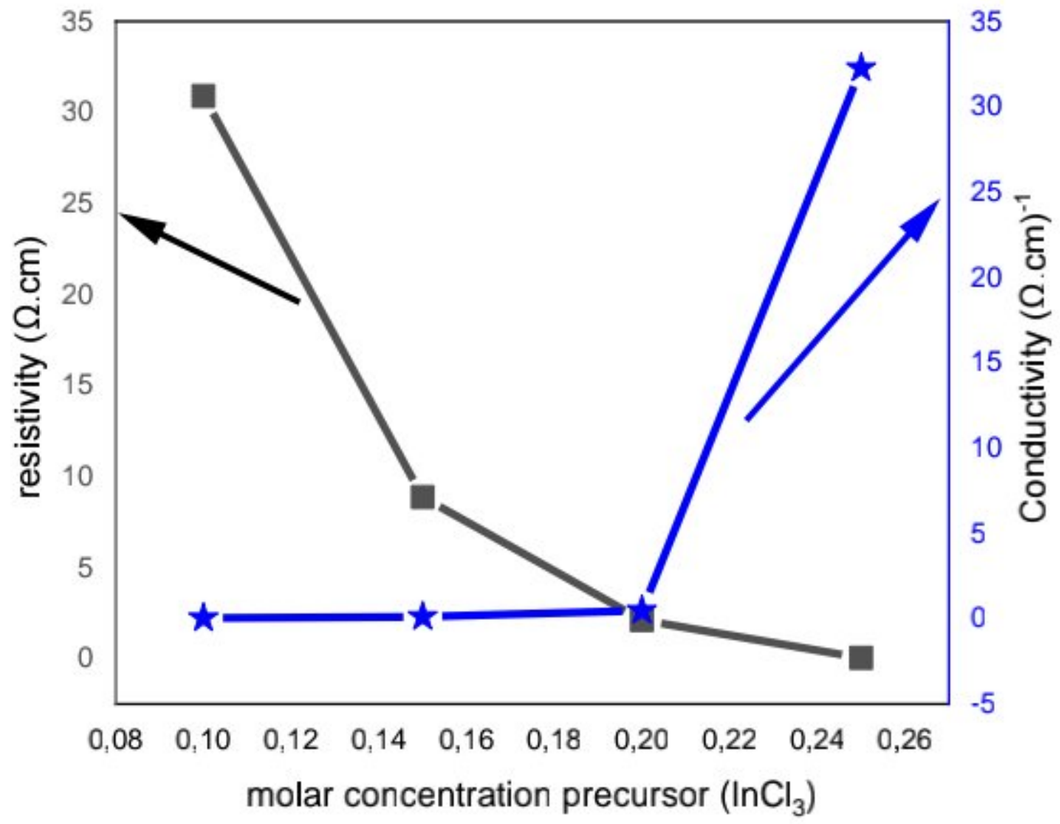

Fig 4.11: The variation of resistivity for In_2O_3 films deposited at various molar concentration precursor.

4.2Acetate Indium precursor:

In previous work, we were deposited In_2O_3 thin films by using the chloride indium In_2Cl_3 as precursor with variation of molar concentration after that these films can be deposited by using indium acetate as precursor by vary the molar concentration of solution prepared and estimated the best properties to apply it in photovoltaic and optoelectronic application.

4.2.1 Film thickness:

The film thickness was estimated from using the equation (2.1), the variation of film thickness as function molar concentration is given in figure 4.12. It is clearly see the calculation film thickness increases from 40.85nm to 202.24nm with increasing of molar concentration precursor, the film obtained at 0.25M appears thicker compared to the other films due to roughness and morphology property (see figure 3.35). However, this variation of film thickness can be attributed to the molar concentration precursor on nucleation, diffusion, adsorption and desorption of atoms[163].

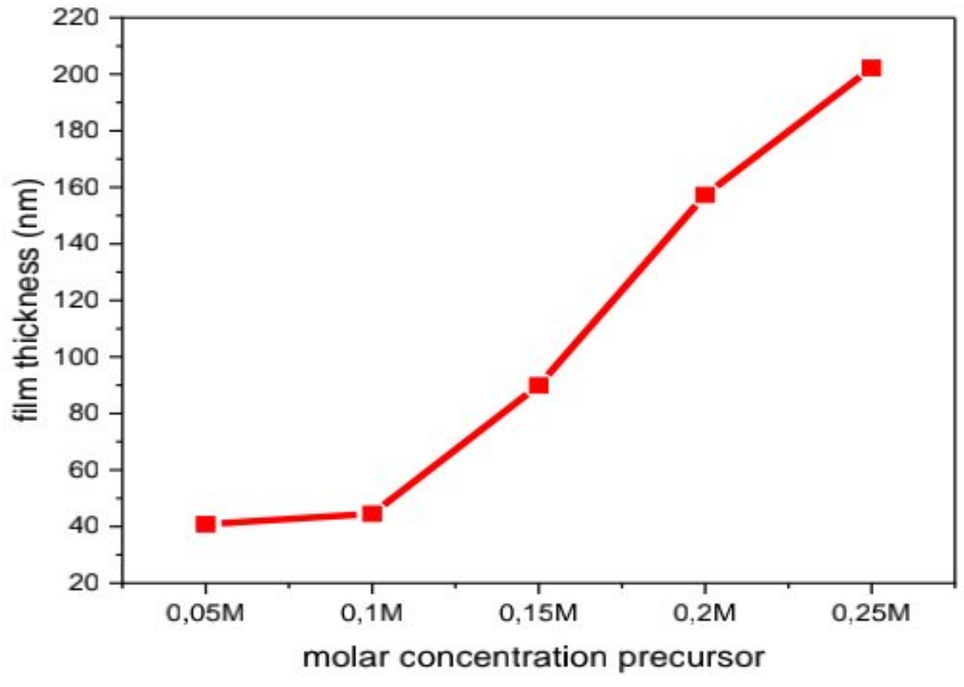

Fig 4.12: The variation of film thickness as function molar concentration precursor.

4.2.2 Structural properties:

The XRD results of indium oxide films deposited at different molar concentration precursor (acetate indium) on glass substrate are given in figure 4.13, it observed that there is no peak at 0.05M which attributed that the films are amorphous this due the less quantity of In^{3+} and O^{2-} ions in solution. However, the orientation peaks ((222) and (400) planes corresponds a different angle see table 4.3) was appeared in the films deposited at higher molar concentration (0.1M, 0.15M, 0.2Mand0.25M),all the samples have a preferential crystal growth along the (222) orientation, the intensity of this orientation peak along (222) increased with increasing of molar concentration precursor which confirmed that the In_2O_3 films have a good crystalline structure at rising of molar concentration precursor related with JCPDS data file reference code: 0416-006-00 for bixbyte structure. As reported by Paz et al[164], the orientation of the grains in specific crystallographic directions is related with minimization of free surface energy density of the film and the energy density of the interface between the film and substrate. From the high intensity of the (222) peak, it can be seen that [111] is the preferred direction of crystal growth in all these films. In contrast, the crystallite size, strain and dislocation density were estimated by using the equation ((2.3), (2.4), (2.5)) respectively from XRD results. The variation of crystallite size, strain ε and dislocation density δ were given in figure 4.14, it is also observed the crystallite size increases from 11.15nm to 34.85nm with increasing of molar concentration precursor due to increase in amount of oxygen atoms into the thin film particles, non uniform distribution of oxygen vacancies and the defects in the films decrease and the crystal quality is

enhanced[165,101]. In addition, the variation in strain and dislocation density have an inverse relation with crystallite size (see figure 4.14), the reduction in strain and dislocation density prove the high quality of crystallinity. Moreover, the table 3.9 shows the variation of lattice parameter and the values of stress, it noted stress has a negative values at 0.1M and 0.2M due to compressive in the structure of films and a positive value at 0.25M and 0.15M due to tensile in structure of the films. The lattice parameter has a different value along the variation of molar concentration precursor (indium acetate) which has a bigger value at 0.15M and0.25M than the bulk value (10.118A°) improves that the tensile stress in the lattice structure and the smallest values of lattice constant confirmed the compressive stress in the lattice structure of indium oxide thin films.

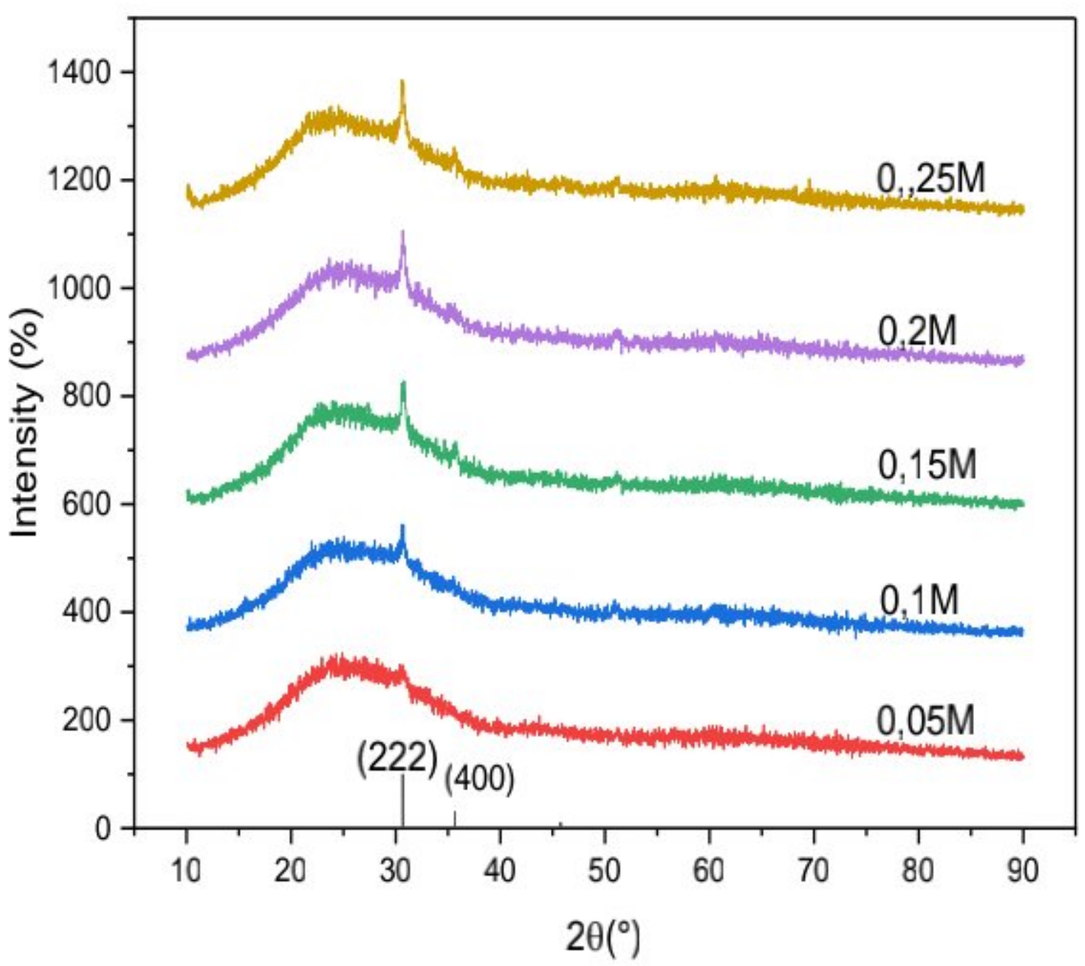

Fig 4.13: The XRD patterns of In_2O_3 thin films deposited at different molar concentration precursor.

Table4.3: The lattice parameters of In_2O_3 thin films with variation of molar concentration precursor.

Samples	*h k l*planes	2θ(degree)	Calculated parameters		Reference parameter (JCPDS card No 06-0416)	Stress (Gpa)
			Lattice constant *a* (Å)	d-spacing (Å)		
0.05M	/	/	/	/		/
0.1M	(222)	30.64	10.09	2.9146	$a_0 = 10.118$ Å	-0.0468
0.15M	(222)	30.715	10.893	2.9108	$d = 2.921$ Å	1.7148
0.2M	(222)	35.691	10.091	2.9131	$2\theta = 30.58$	-0.0593
0.25M	(222)	35.597	10.121	2.9218		0.0075

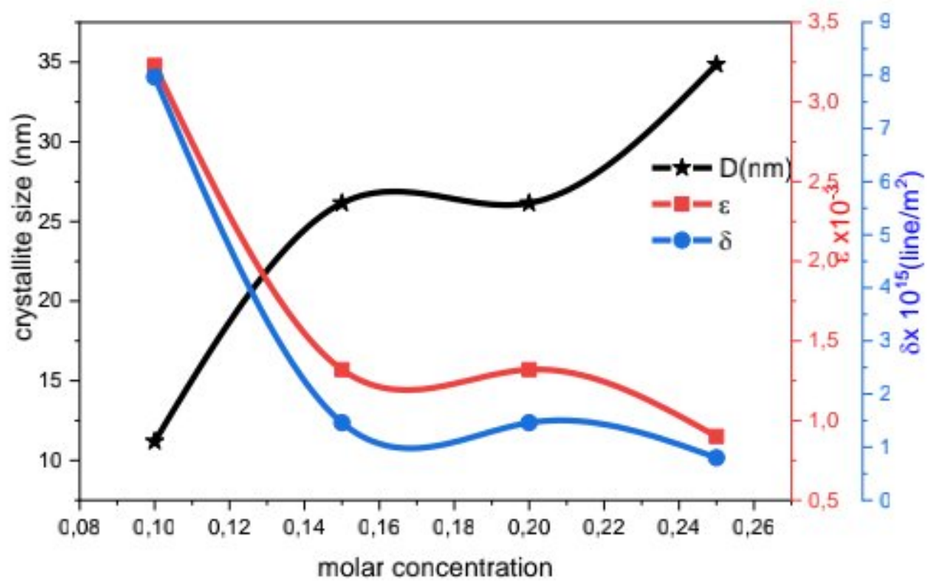

Fig4.14: The variation of crystallite size, strain and dislocation density with several values of molar concentration precursor.

4.2.3 Morphological properties:

The SEM images of In_2O_3 thin films at different molar concentration precursor (Indium acetate). It is obvious that all the films have homogenous, uniform and dense surface without any pin holes and cracks indicating that the films are well adherent to the substrates. As the result, it is clearly see the films at 0.05M have a smooth surface without clearly visible particles confirmed the amorphous structure (related with XRD results), the surface morphology of all the samples

(0.1M,0.15M,0.2M and 0.25M) presented a rough surface morphology with a small grains size. Obviously, the grain size increases at high molar concentration precursor due to crystallinity improved in the films which related by XRD results.

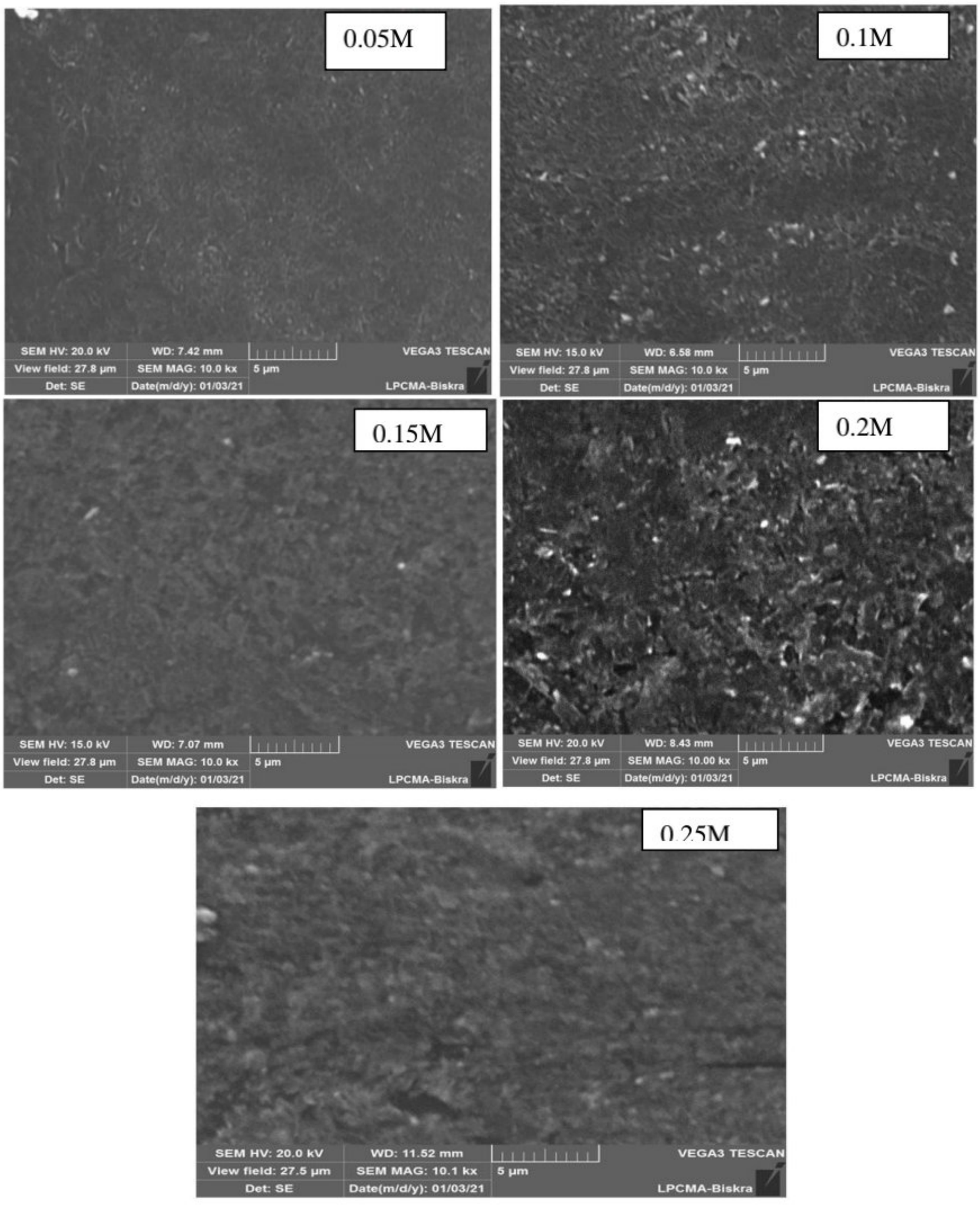

Fig 4.15: The SEM images of In_2O_3 thin films deposited at various molar concentration precursor (0.05M, 0.1M, 0.15M, 0.2M and 0.25M) for indium acetate.

4.2.4 Compositional properties:

The chemical compositional analysis of In_2O_3 thin films prepared at various molar concentration

precursors are presented in figure 4.16, it shows the presence of In and O in all the samples at different molar concentration precursor (from 0.05M to 0.25M). Also, the atomic and weight percentages of these elements in the films were tabulated in table 4.4. The atomic and weight percentage of In increases with rising of molar concentration while the films are rich of O atoms. Thus, EDX elemental analysis confirmed the In/O atomic ratio increases (defined as In concentration in O) as~ 0.034%, 0.04%, 0.05%, 0.049% and 0.06% in In_2O_3 thin films deposited at various molar concentration 0.05M, 0.1M, 0.15M, 0.2M and 0.25M respectively.

Table 4.4: The atomic and weight percentage of In and O for In_2O_3 thin films at different molar concentration.

Molar concentration	Elements			
	Wt%		at%	
	In	O	In	O
0.05	3.33	96.67	3.33	96.67
0.1	4.6	95.40	4.60	95.40
0.15	5.15	94.85	5.15	94.85
0.2	4.76	95.24	4.76	95.24
0.25	6.50	93.5	6.50	93.50

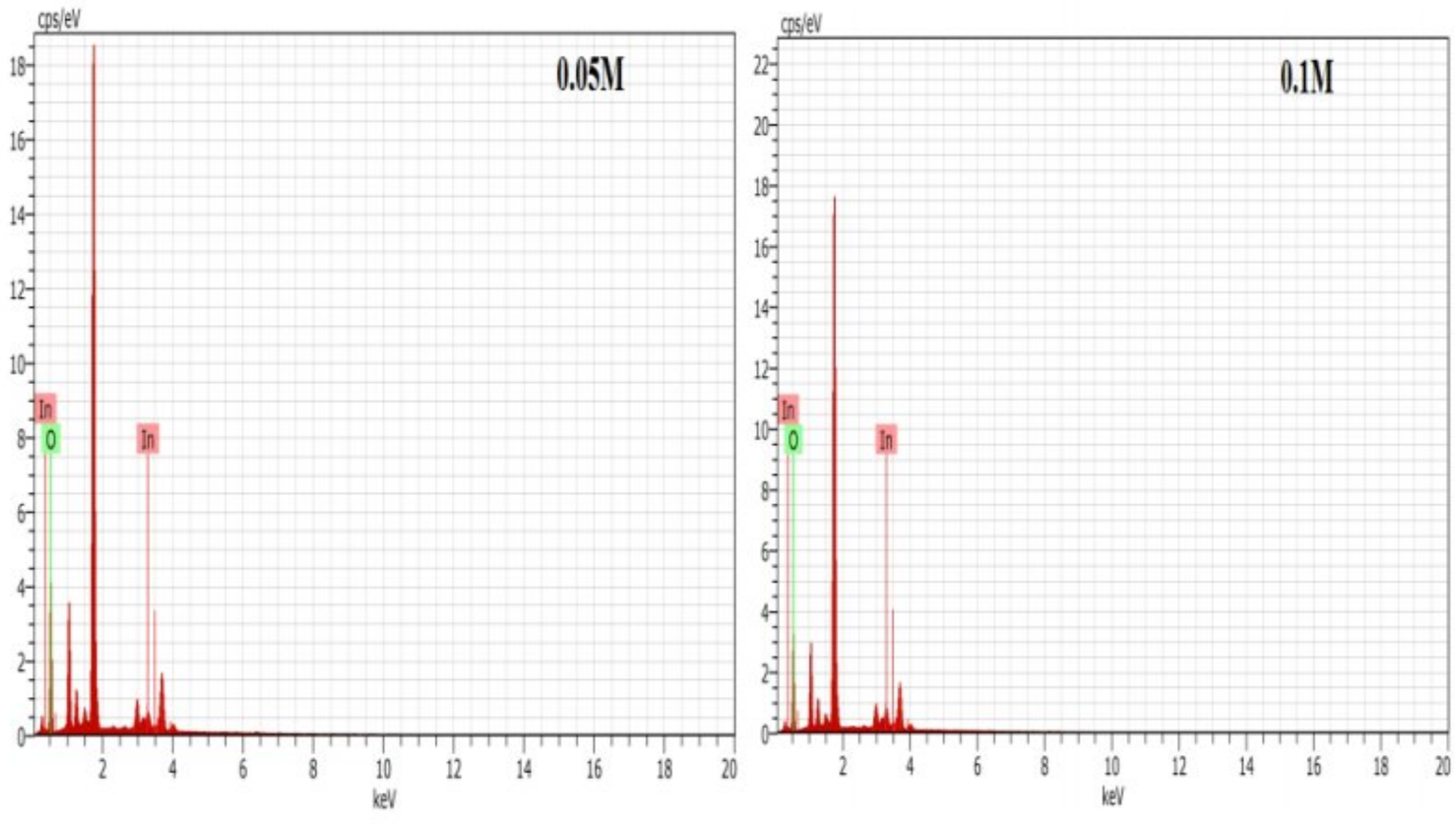

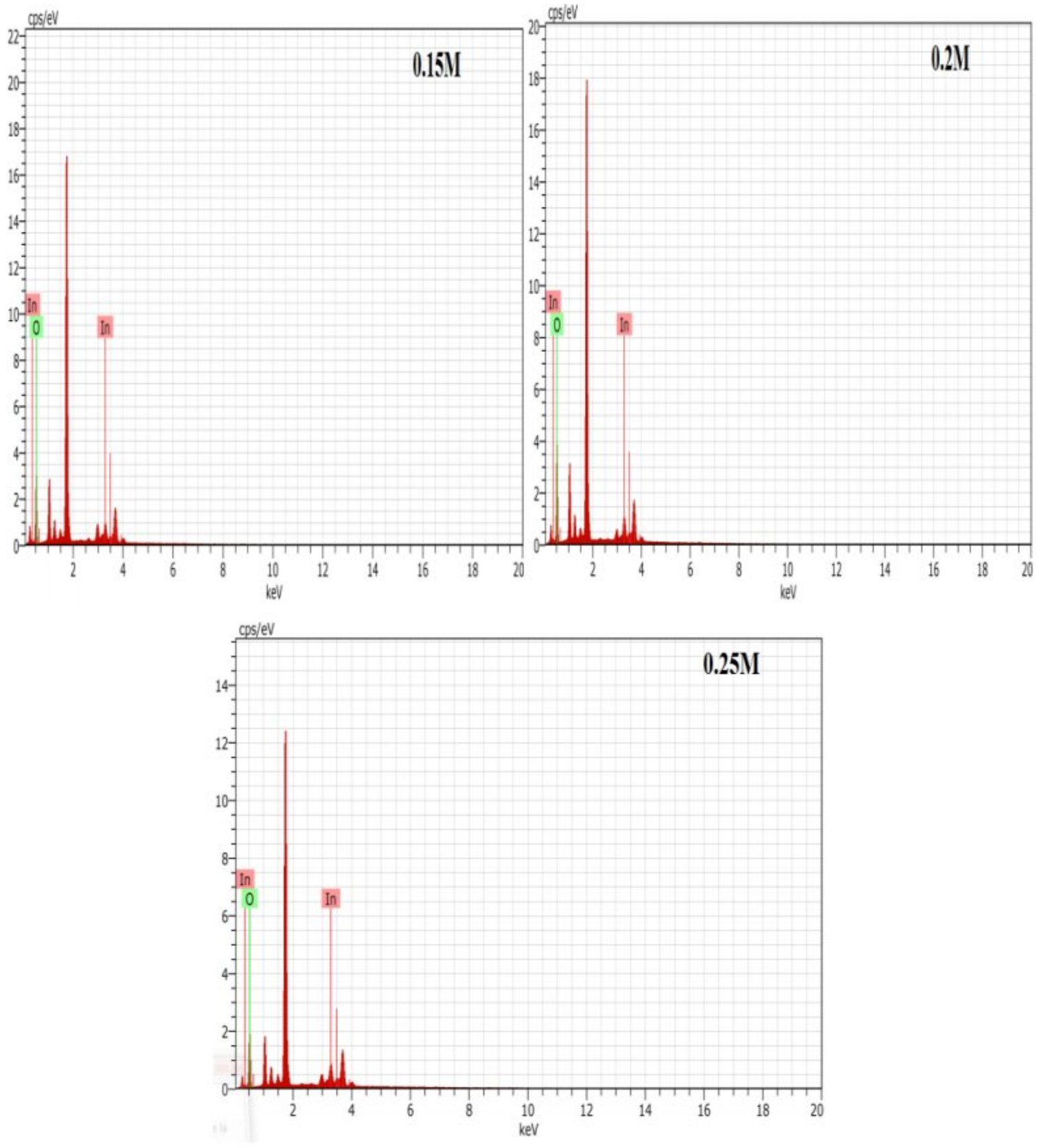

Fig 4.16: The EDX spectra of indium oxide thin films prepared at various molar concentration precursors.

4.2.5 Optical properties:

The optical transmittance spectra with a wavelength from 290nm to 1100nm of In_2O_3 thin films obtained at various molar concentration precursors are shown in figure 4.17. This figure shows that all the samples have a good transmittance in the visible region (400nm-800nm). The transmittance value was found higher in the range 87.18%-92.51%in the visible region with a sharp fundamental absorption edge. So, the transmittance of the films has been found higher due to improvement of crystallinity leads to decrease in optical scattering and defects [111,112]. The absorption edge in the region (λ<400nm) investigated the red shifted with increasing molar concentration precursor.

The band gap of In_2O_3 thin films was calculated from the $(\alpha h\nu)^2$ versus photon energy ($h\nu$) by extrapolation of the straight line of the plot $(\alpha h\nu)^2$ versus photon energy ($h\nu$) for the different molar concentration precursor, as shown in figure 4.18. The variation of energy band gap for indium oxide thin films as a function of molar concentration precursor is presented in figure 4.20. It is observed that the values of band gap reduces from 3.13eV to 2.97eV , this variation attributed the improvement of crystallinity and increases of crystallite size of the films which leads the quantum confinement[169].Ali et al [170] reported that the increasing molar concentration precursor causes an increase in the density of charges and then every electron is effectively surrounded by an exchange and correlating hole that lowers the energy level of the electrons, and the conduction band is shifted downwards.

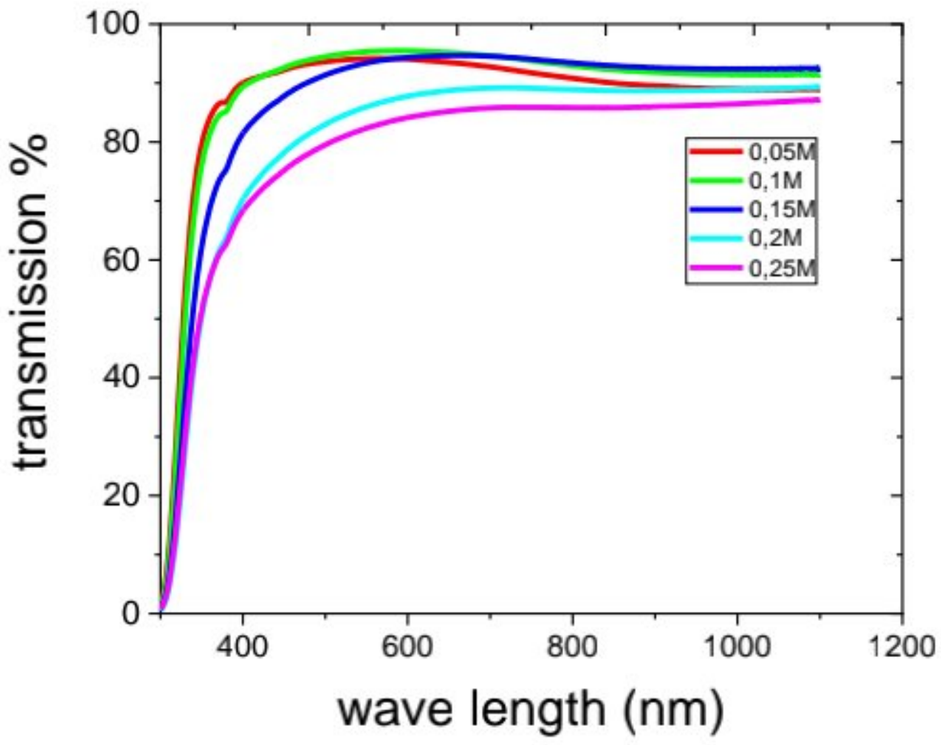

Fig 4.17: The transmittance spectra of In_2O_3 thin films prepared at different molar concentration precursor.

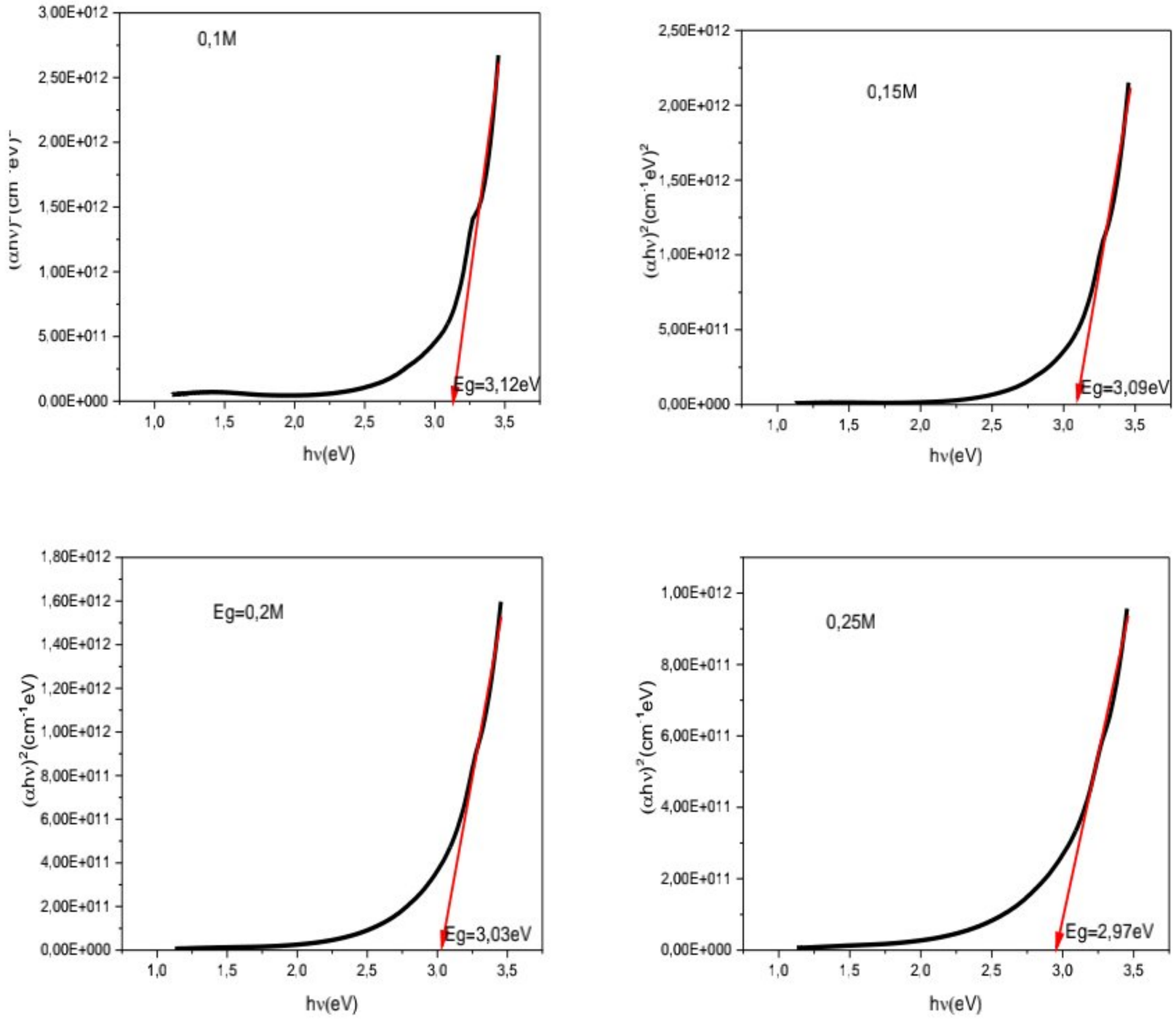

Fig 4.18: The plot$(\alpha h\nu)^2$ versus photon energy (hν) of In_2O_3 thin films prepared at different molar concentration precursor (0.1M, 0.15M, 0.2M and 0.25M).

The Urbach tail was estimated from the (lnα) versus photon energy (hν) by taking the reciprocal slope of the straight line for indium oxide thin films deposited at various molar concentration precursors as shown in figure 4.19, the variation values of width of band tail as function molar concentration precursor increases from 0.233eV to 0.307eV with rising of molar concentration precursor.

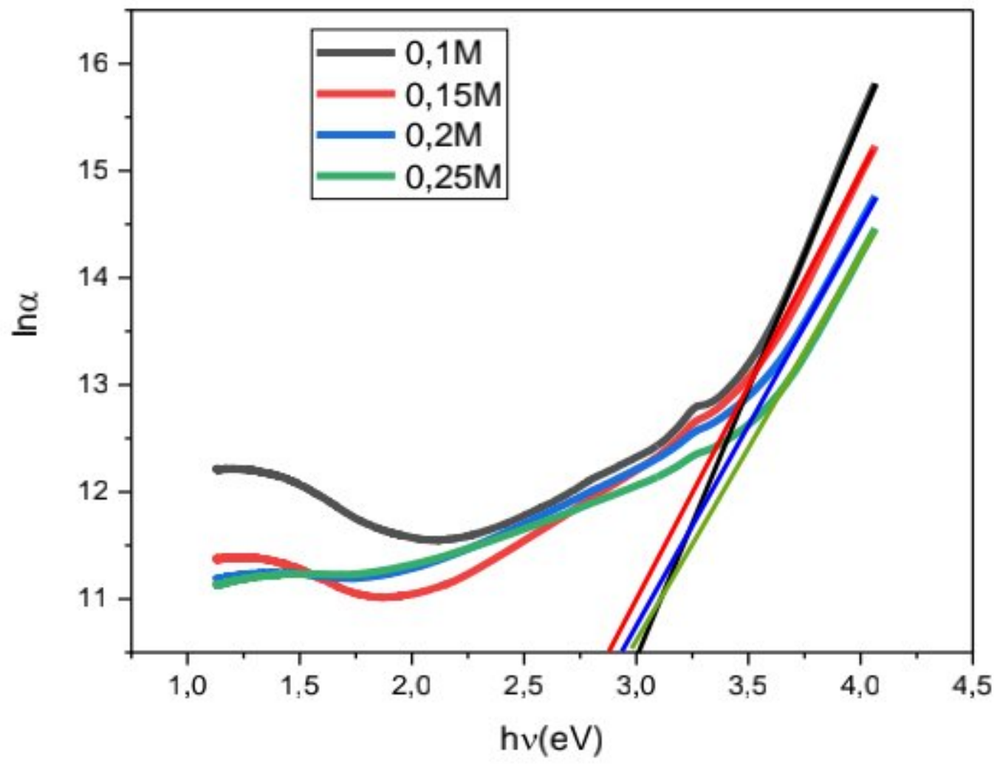

Fig 4.19: The plot of ln(α) as function molar concentration precursor (indium acetate).

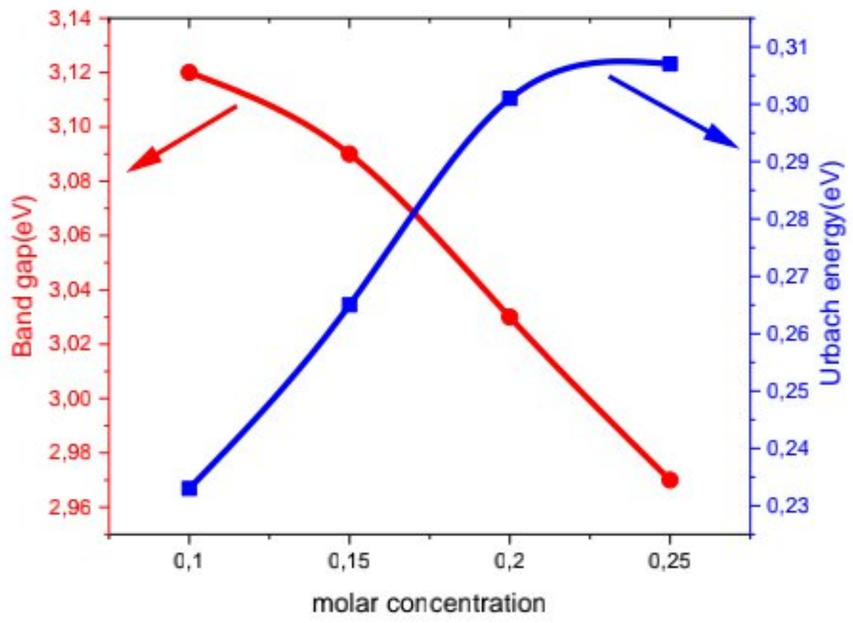

Fig 4.20: The variation of band gap energy Eg and Urbach energy Eu as function molar concentration precursors.

4.2.6 Electrical properties:

The figure 4.21 presents the variation of electrical resistivity at different concentration precursor (indium acetate). As the result, the electrical resistivity is reduced from 6.46×10^{-2} to 1.13×10^{-2} Ω.cm at molar concentration precursor from 0.05M to 0.25 M, it proves that the improvement in crystalline quality. This result is good agreement with last studies of prepared cobalt oxide thin films[171]. RaviShankar et al [172] reported that the electrical resistivity of the films decreases with increasing film thickness. Grain boundary scattering of free electrons in thicker films is less than in thinner films because of larger crystallite sizes.

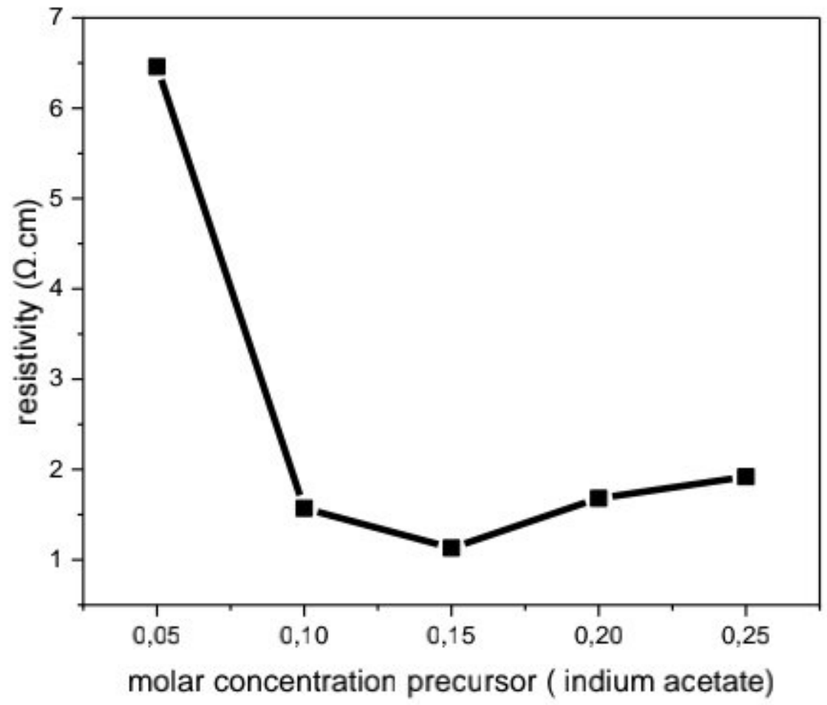

Fig 4.21: The variation of electrical resistivity at various molar concentration precursors (indium acetate).

4.3 Comparison:

The previous literature , Yahia et al [124] prepared the indium oxide thin films at different molar concentration precursor (they used nitrate indium as a precursor)by sol-gel spin coating process. They found that:

1. Indium oxide films have a polycrystalline structure with a preferred orientation along (222) at all the samples with the decreasing of crystallite size.
2. High transmission in the visible wavelength (400-800nm) with narrowing of optical band gap (4.04-3.88eV).
3. The electrical conductivity increased from 5.8 to 25 $\Omega.cm^{-1}$with increasing of molar concentration precursor.

We deposited the indium oxide films at various molar concentration precursor (used the indium chloride as precursor) by sol-gel spin coating process. We obtained that:

1. The films have a strong crystallinity at all the samples with change the growth direction from [111] to [100]. The crystallite size increased with the increase of molar concentration precursor. The films shows a strong crystalline.
2. All the samples have a good transmission in the visible wavelength region with the reduce of optical band gap.
3. The electrical resistivity decreased with increasing of molar concentration precursor.

Indium oxide films deposited by using acetate indium as precursor with varying of molar concentration, we found that:

1. The films have a crystalline structure with preferred orientation along (222) and the increase of crystallite size.
2. All the samples have a high transparency in the visible region (400-800 nm) with a red shifted of optical band gap.
3. The reduction of electrical resistivity from 6.46×10^{-2} to 1.13×10^{-2} Ω.cm.

As the result, we deduce that the films prepared at $InCl_3$precursor are better than the films deposited at indium acetate and indium nitrate precursor to continue the other effects. These films can be applied in photovoltaic and optoelectronic applications.

Conclusion:

The effect of molar concentration precursor for indium chloride ($InCl_3$) and indium acetate $C_6H_9InO_6$ achieved that the rising of film thickness. The X-ray diffraction presented the polycrystalline structure of the films for each precursor (indium chloride, indium acetate). For the precursor $InCl_3$ the films change the direction growth from [111] to [100], at 0.15M the films have a strong crystallinity when the weak peak appeared, but regarding the precursor indium acetate the films have a strong and preferred orientation along (222) with disappeared of weak peak . The surface morphological of In_2O_3 thin films at each precursor ($InCl_3$and$C_6H_9InO_6$) is uniform and homogenous with increasing of grain size. The films at each precursor s solution have a good transmittance in the visible wavelength (400-800nm). The optical band gap reduces with increasing molar concentration precursor. The increasing of molar concentration precursors ($InCl_3$ and $C_6H_9InO_6$) improves the electrical conductivity with the reduction of electrical resistivity.

CHAPTER 05

Sb and Ba doped indium oxide thin films

Introduction:

It is axiomatic that the properties of In_2O_3 thin films have optimized by synthesized different deposition parameters such as molar concentration precursor, film thickness, pH solution, annealing temperature and dopant concentration, etc. However, Indium oxide doped with metals has been widely used for numerous applications in optoelectronic devices (Sn doped In_2O_3 and Cd doped In_2O_3)[115,116], in humidity sensor (Ni doped In_2O_3)[175], used as electrodes (Zn doped In_2O_3)[176] and etc. This part illustrates the detailed results and interpretation obtained from the preparation and characterization of Sb-doped In_2O_3 thin films and Ba-doped In_2O_3 thin films deposited using sol-gel spin coating method. Doping with Sb and Ba is primarily done to achieve high transparency, crystallinity and high conductivity of indium oxide thin films to apply in the optoelectronic and photovoltaic applications.

5.1 Influence of Sb-doping In_2O_3:

At our studies, we have doped In_2O_3 by Sb while Sb have a smallest ionic radius than In, the films were deposited by sol gel spin coating method to improvement the structural, optical, morphological and electrical properties. However, the influence of Sb concentration on the properties of In_2O_3 thin films is also discussed in detail and to achieve high quality of properties for optoelectronic application.

5.1.1 Structural properties:

The X-ray diffraction spectra for undoped and Sb-doped indium oxide thin films deposited on glass substrates by sol gel technique are given in figure 5.1. The spectra indicate that all the films are polycrystalline in nature and crystallize in a cubic structure according to JCPDS card (06-0416).No phases corresponding to antimony or any other antimony compound have been detected in the XRD patterns. In contrast, the films at0% and 3%Sb concentration have a preferred orientation along (222) plane. The growth along the predominant (222) plane may be attributed to minimization of the crystal surface free energy[177], it is clearly observed at 6% and 9% Sb concentration have a preferred orientation along (400) plane which revealed that the growth of the films change the direction from [111] to direction [100], The other weak peaks in XRD patterns correspond to (211), (440) and (622) planes appeared in samples obtained at undoped and Sb-doped In_2O_3(3%concentration). This peaks revealed the strong crystallization of the films. However, the increasing of doping by Sb lead to disappearance in intensities of XRD peaks corresponding to lattice planes such as (211), (440) and (622), it attributed to imply the presence

of a large number of vacant lattice sites, destroyed periodicities in some crystal planes and local lattice disorders[136]. The XRD patterns shows no diffraction peaks for Sb_2O_3 phase which due the complete miscibility of Sb components in the proposed composition [178].

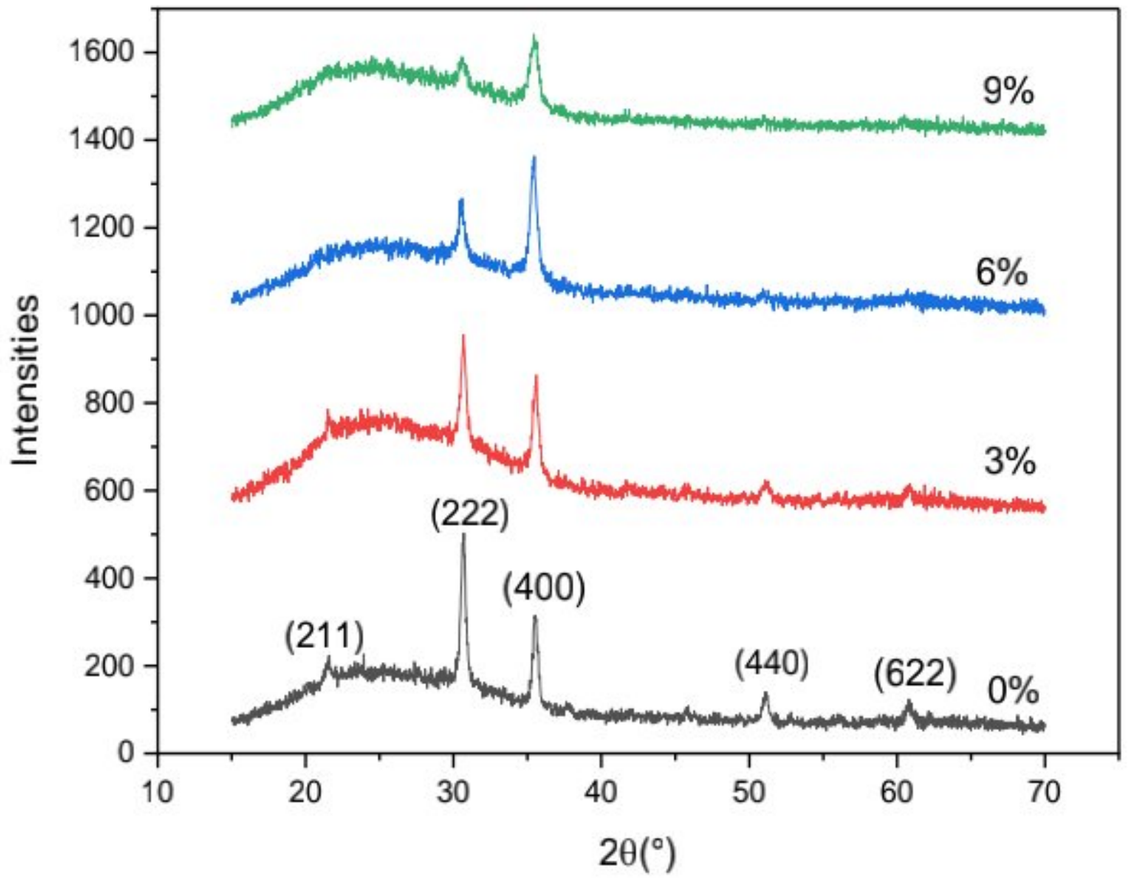

Fig 4.1: The XRD patterns of undoped and Sb-doped indium oxide thin films.

The lattice constant and stress were estimated using the equation (2.3) as shown in table 5.1; it can be seen the lattice constants are less than the bulk value (10.118A°) at increasing of molar concentration for Sb (3%, 6% and 9%). This reduction attributed to ionic radius of Sb^{+3} (0.76A°) is smaller than that of In^{+3} (0.8A°), the substitution of Sb on In sites in the In_2O_3 lattice can decrease the lattice constant, the stress has a negative values due to compressive in the lattice parameters.

Table 5.1: Structural parameters information of prepared Sb-doped In_2O_3thin films for different concentration of Sb.

Samples	***h k l* planes**	**2θ(degree)**	**Calculated parameters**		**Reference parameter (JCPDS card No 06-0416)**	**Stress (Gpa)**
			Lattice constant *a* (Å)	d-spacing (Å)		
0% Sb	(222)	30.69	10.093	2.9108		-0.0647
3% Sb	(222)	30.68	10.094	2.9141	a_0 = 10.118 Å	-0.0524
6% Sb	(400)	35.44	10.128	2.5328	d = 2.921 Å	0.022
9% Sb	(400)	35.49	10.116	2.5291	2θ = 30.58	-0.0044

Figure 5.2 presents the variation of crystallite size, strain and dislocation density of Sb-doped indium oxide thin films using the equations ((2.4), (2.5), (2.6)) respectively. However, it noted that the crystallite size reduces from 42.10nm to 13.23nm for increasing of Sb doping concentration; this reduction in crystallite size suggests decreased crystallinity with increased grain boundary. The reduction in crystallite size is attributed to the enhancement in the density of nucleation centers in the doped films. Since the ionic radius of the Sb^{3+} ion (0.76 Å) is smaller than that of the In^{3+} ion (0.8 Å), there is a creation of compressive stress in the films on Sb doping[179]. Ajili et al[180] reported that the decrease of crystallite size may be attributed to the increasing number of centers during incorporation of the doping into the host material . Also, the dislocation density and strain increase with increasing of Sb doping concentration indicate the formation of lower quality films with Sb doping concentration[181].

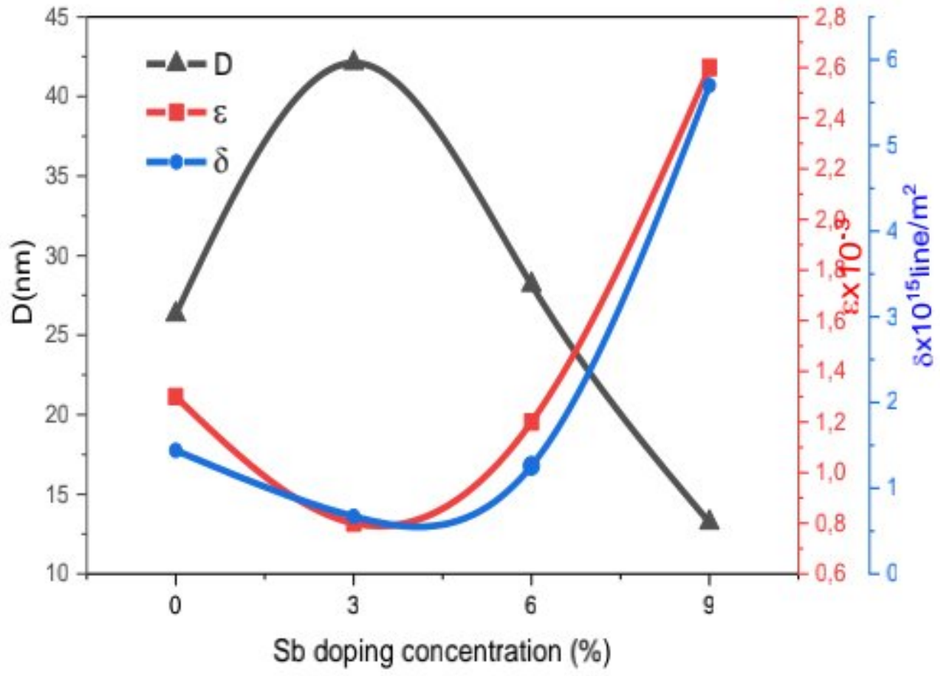

Fig 5.2: The variation of crystallite size D, strain ε and dislocation density with Sb doping concentration.

Figure 5.3 shows the different values of texture for the orientation (222) and (400) planes at Sb doped indium oxide thin films from XRD data to indicate the degree of preferred orientation of Sb-doped In_2O_3 thin films. As the results, it observed at undoped film the texture is higher at direction [111], it indicates the preferred orientation along (222) and a lack growth at [100] when Sb-doped film the texture has a higher value at the direction [100] which investigates the preferred orientation along (400) with a less growth at direction [111]. This proves that an increase in preferred orientation corresponds to an increase in the number of grains in that plane[182].

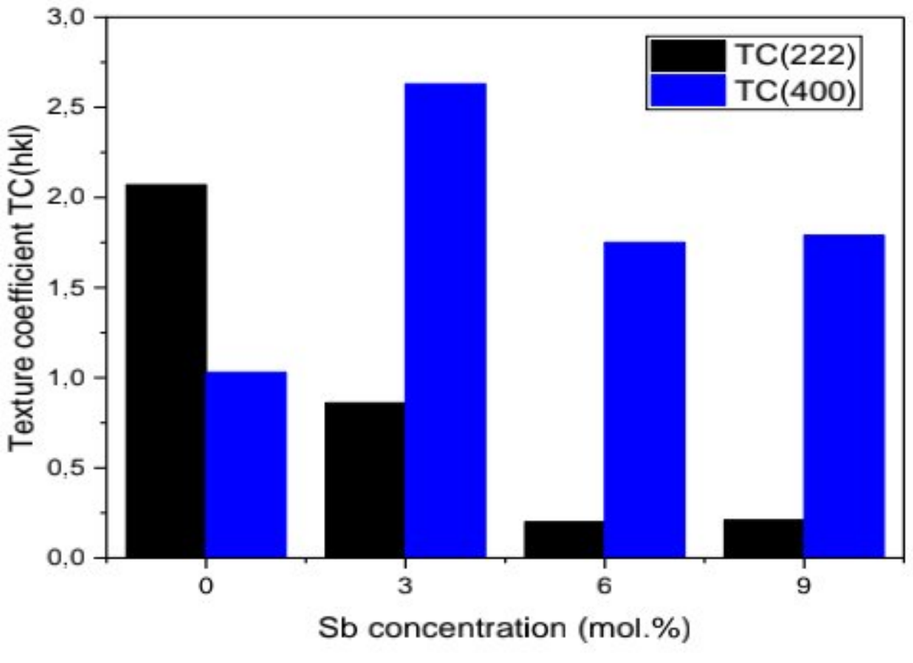

Fig 5.3: The texture coefficient TC(hkl) for Sb doped indium oxide thin films.

5.1.2 Morphological properties:

The SEM images of Sb-doping In_2O_3films are given in figure 5.4. It is clearly observed the non spherical, island growth consisting of continuous grainsof all the samples. It is also see the uniform and homogenous surface of Sb-doped In_2O_3thin films. Hence, it was found the grain size decreased with increasing of Sb concentration which was found to be in agreement with the decrease of crystallite size calculated from XRD profile of the samples using scherrer's formula. From the XRD and SEM results, it is concluded the doping Sb metal ion reduces the grain size.

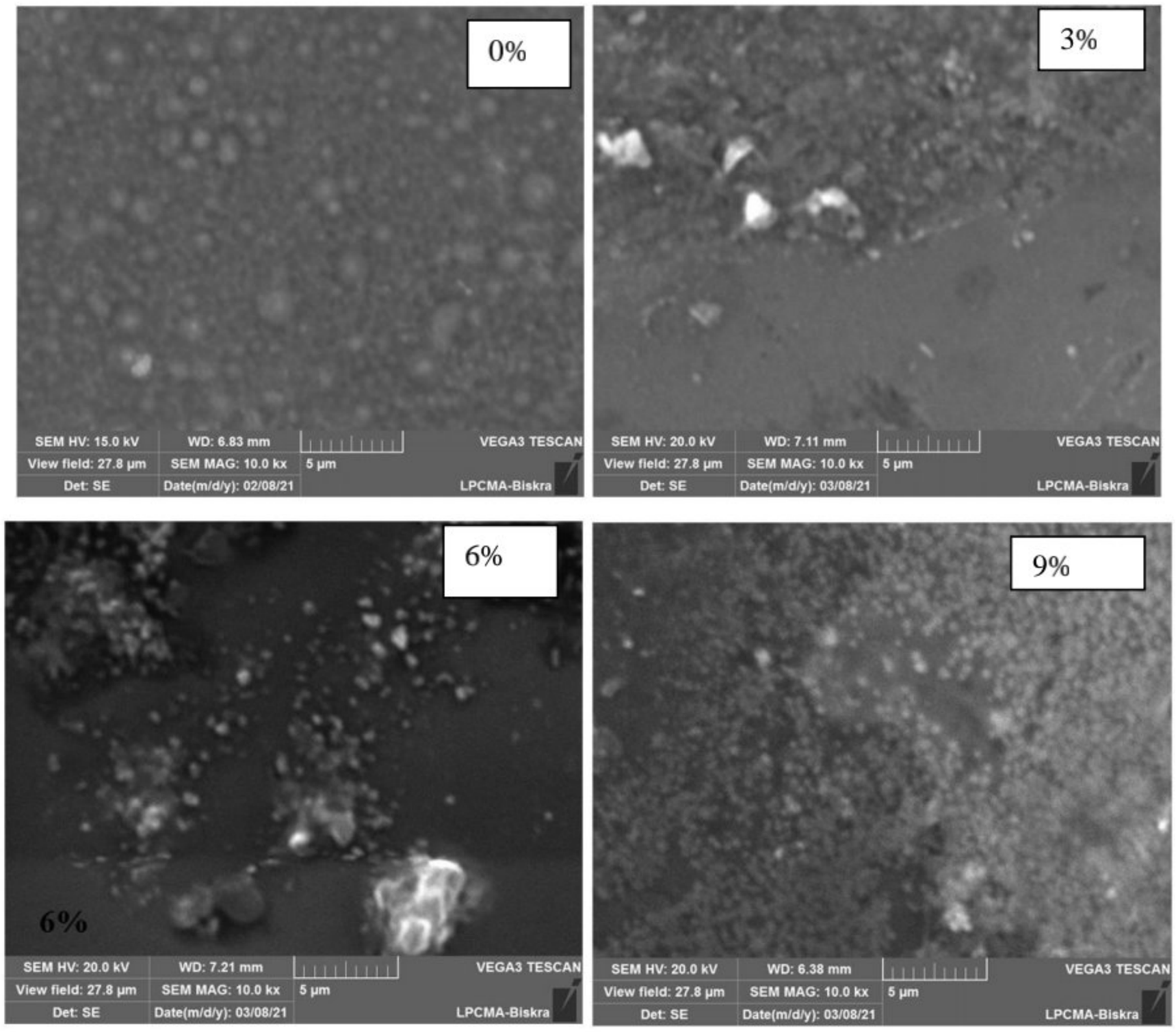

Fig 5.4: The SEM images of Sb-doped In_2O_3 films deposited at various Sb doping concentration.

5.1.3 Compositional properties:

The elemental analysis of undoped and Sb-doped In_2O_3 thin films was made by dispersive X-ray spectroscopy. The EDX spectra of In_2O_3: Sb films (figure 5.5) confirm the presence of Sb, O and In atoms in the films. The weight and atomic percentage compositions of In, Sb and O in the thin

films are presented in table 5.2. It noted that the amount of In element decreases with increasing Sb content, which very well supports the successful substitution of dopants in the In sites.

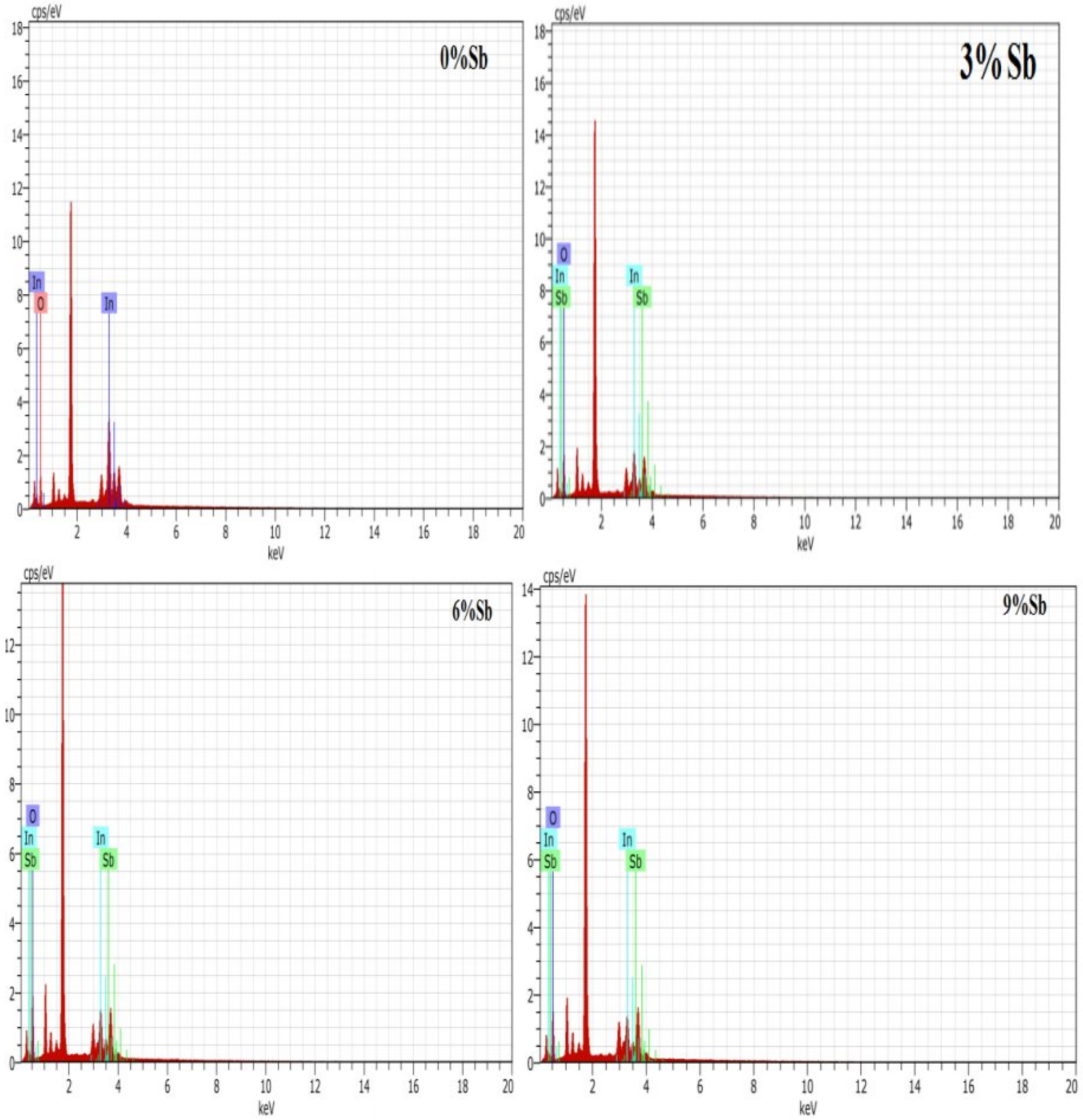

Fig 5.5: EDX spectra of undoped and Sb-doped In_2O_3 films.

Table 5.2: Results of quantitative elemental analysis of Sb-doped In_2O_3 thin films.

Samples	Elements					
	Wt%			at%		
	In	Sb	O	In	Sb	O
0%Sb	63.39	0	36.61	19.44	0	80.56
3%Sb	44.55	13.56	41.89	12.44	3.57	83.93
6%Sb	39.64	14.65	45.70	10.39	3.62	85.99
9%Sb	40.89	19.35	39.76	11.87	5.3	82.83

5.1.4 Optical properties:

Figure 5.6 presents the optical transmittance of prepared thin film samples with various Sb doping concentrations using UV-Vis spectrophotometer at wavelength range 200-1100nm. It is found that the undoped and Sb-doped indium oxide films exhibit a high transmittance in the range 84.69%-99% in the visible region with a sharp fundamental absorption edge. This sharp fall in transmission near the fundamental absorption edge is an identification of the good crystallinity of the films[183]. In contrast, the high transmittance with Sb doping concentration proves a lower scattering light and it may be ascribed to the improvement of stoichiometry[184]. The absorption edge in the region (λ<400nm) investigated the blue shifted with increasing of Sb doping concentration, this is observed in the first case as shown in figure 5.6 (inset); we can conclude that the direct transitions dominate in undoped and Sb doped indium oxide thin films.

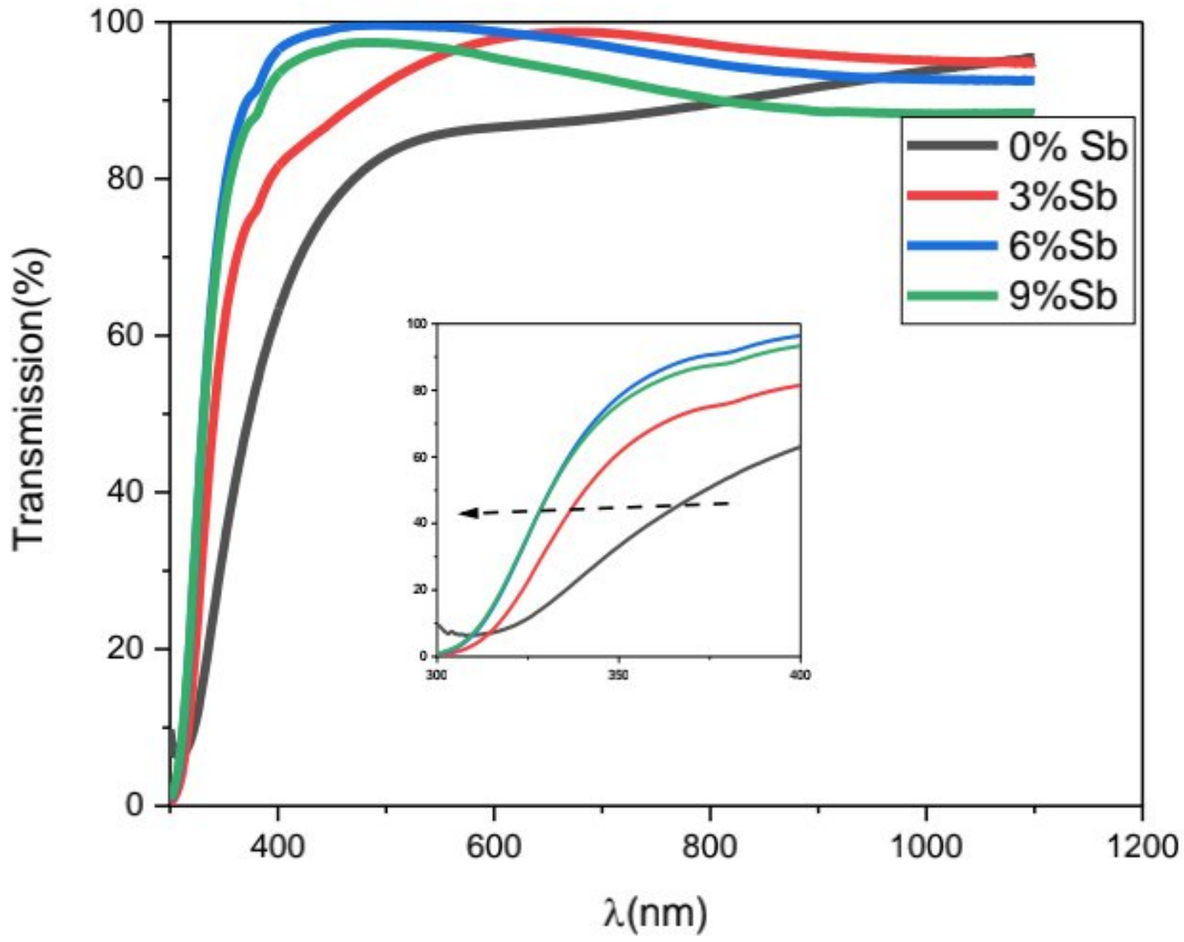

Fig 5.6: Optical transmittance spectra of Sb doped In_2O_3 thin films.

The band gap of In_2O_3films was estimated by extrapolation of the straight line of the plot of $(\alpha h\nu)^2$ versus photon energy ($h\nu$) for various Sb doping concentrations, as shown in figure 5.7. However, the variation of band gap energy for Sb-doping In_2O_3 thin films as function of Sb doping concentration is presented in figure 5.9. It is obviously observed that the values of optical band gap energy increases with increasing of Sb doping concentration from 3.18eV to 3.32 eV, this variation attributed to increase Sb concentration which creates free carriers in the host In_2O_3. The excess electrons occupy the lowest states in the conduction band and enhance the effective band gap. This behavior is called Burstein-Moss (BM) effect[185].

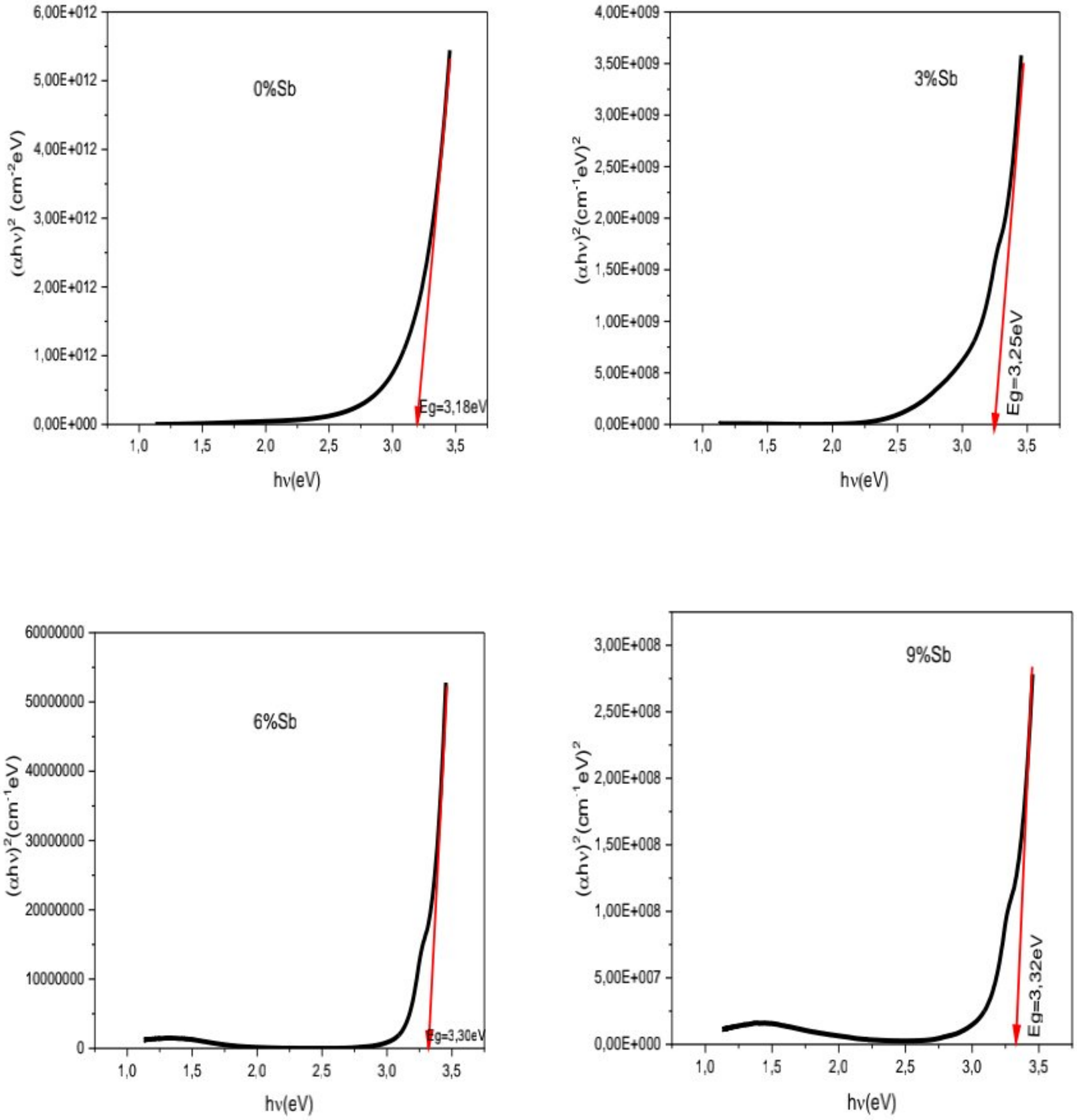

Fig 5.7: plot of $(\alpha h\nu)^2$ as function (hν) for different concentration of Sb doping In_2O_3thin films.

Urbach energy of Sb doped In_2O_3 thin films was estimated from the optical transmission by using the plot (lnα) as function (hν) and fitting the linear portion of the curve with a straight line. The reciprocal of the slope of this linear region yields the value of Eu as presented in figure 5.8. The Eu values were found to reduce from 0.487eV to 0.219eV with increasing of Sb doping concentration (see figure 5.9).

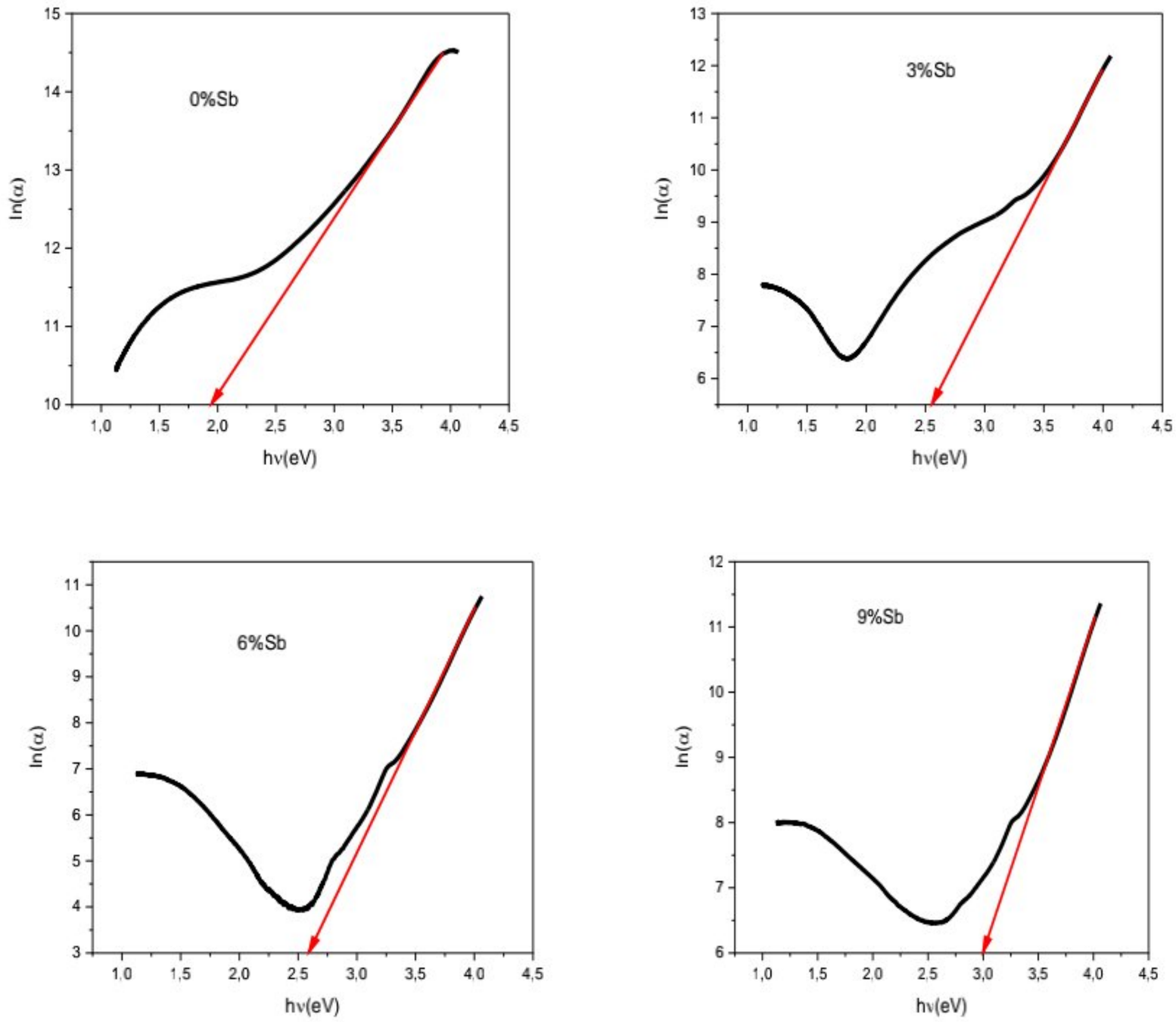

Fig 5.8: The plot of ln(α) as function hν for Sb-doping In_2O_3 thin films.

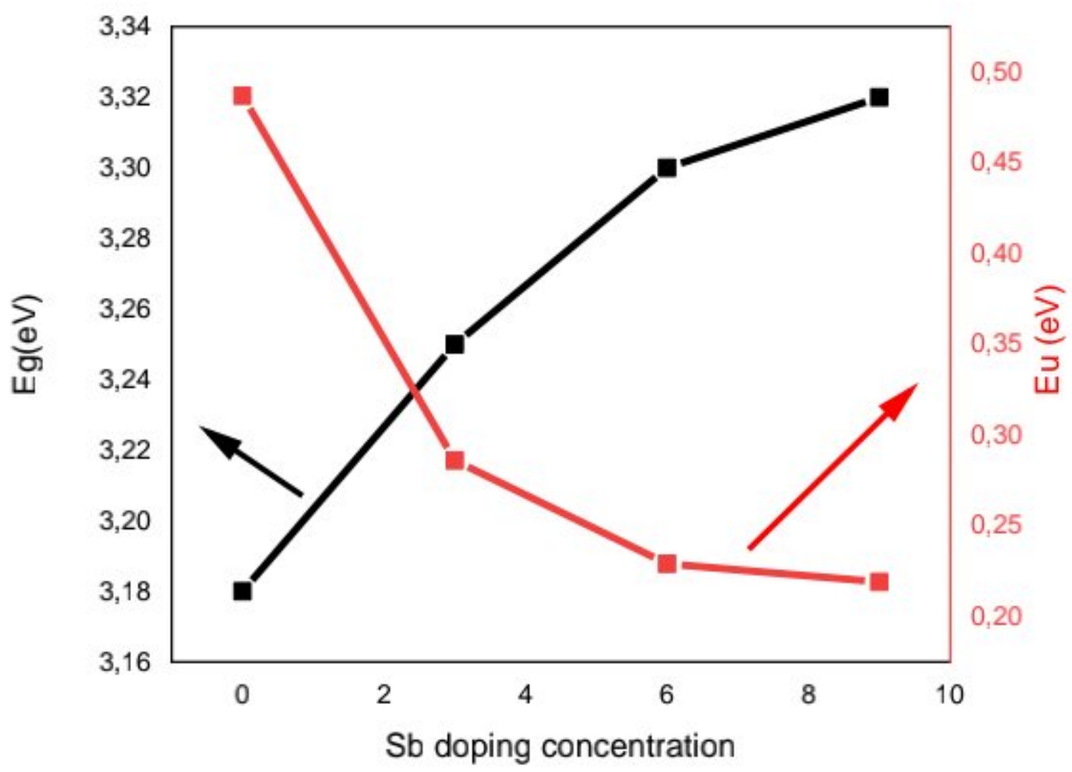

Fig 5.9: The variation of band gap energy Eg and Urbach energy Eu as function of Sb doping concentration for Sb-doping In_2O_3 thin films.

5.1.5 Electrical properties:

The variation of electrical measurement of Sb-doped In_2O_3 thin films as a function of Sb-doping concentration is given in table 5.3 (figure 5.10). The electrical resistivity increases from 0.00887 Ω.cm to 1.563Ω.cmand electrical conductivity reduces from $0.11\Omega^{-1}.cm^{-1}$ to $0.64\Omega^{-1}.cm^{-1}$with rising of Sb concentration, the undoped In_2O_3 thin films exhibit low resistivity due to the native defects of oxygen vacancies and indium interstitials[186]. As Sb doping, the electrical resistivity increase from 0.00887Ω.cm at 0wt % Sb to 3.99Ω.cm at 6wt% Sb concentration. It is known that Sb atoms are expected to be acceptors when substituting In atoms in In_2O_3. In the other side, the reduction of electrical conductivity attributed to the mobility of the electrons decreases and the impurities may precipitate, resulting in defect structures which would trap electrons to cause an increase in resistivity. Further, because the films are polycrystalline in nature, the high resistivity could be due to grain boundary effects[179]. At 6% Sb concentration, the electrical resistivity decreased while the conductivity increased from 0.25 to $0.421\Omega^{-1}.cm^{-1}$due to the reduction in lattice distortion.

Table 5.3: The variation of electrical measurement as function of Sb doping InO thin films.

Sb doping concentration	Resistivity (Ω.cm)	Conductivity($\Omega^{-1}.cm^{-1}$)	Sheet resistance Rsh (Ω/□)
0wt%	0.00887	112.73	658.13
3wt%	1.563	0.641	7.10×10^3
6wt%	3.994	0.25	5.05×10^3
9wt%	2.37	0.421	5.71×10^3

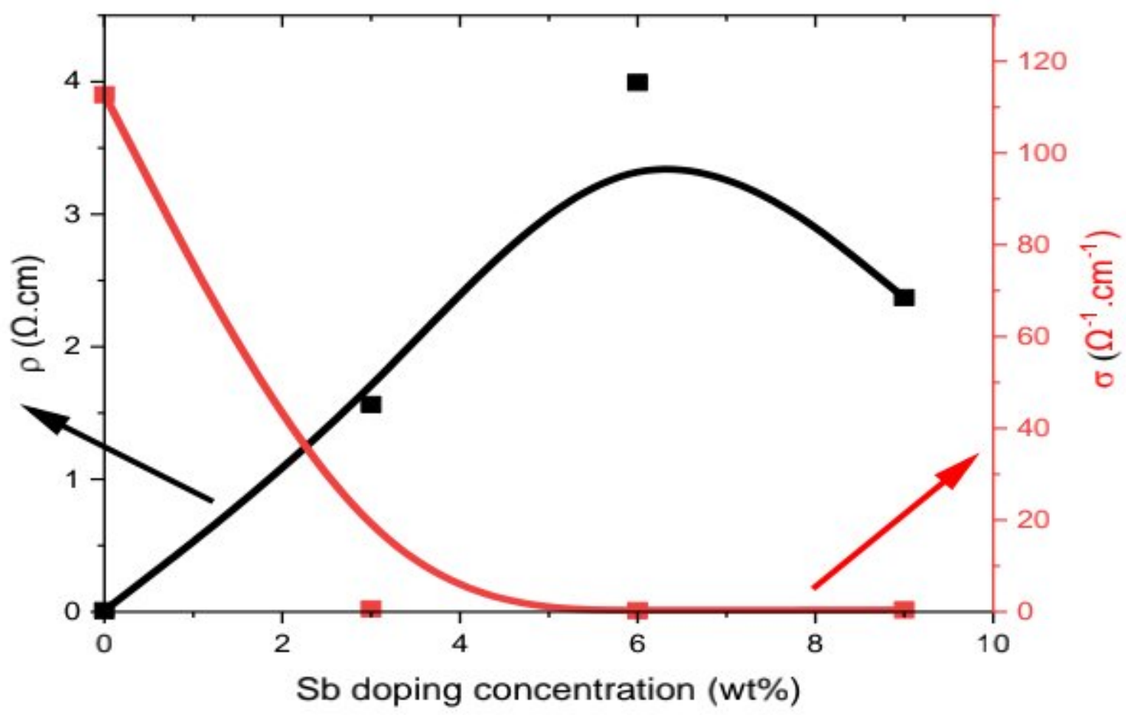

Fig 5.10: The variation of electrical resistivity and conductivity as function Sb doping concentration.

5.2 Influence of Ba-doped In_2O_3 thin films:

At last studies, we obtained the films doped with small ionic radius of Sb compared by In atom. Similarly, we prepared the films by bigger ionic radius such as Ba atom, Ba-doped In_2O_3 films were deposited using sol gel method (spin coating). The films obtained were characterized by XRD, UV-Vis, SEM and four point probe to achieved a high crystallinity, high transmittance, good surface morphology and high electrical conductivity for applied in optoelectronic and photovoltaic devices.

5.2.1 Structural properties:

Figure 5.11 presents the X-ray diffraction spectra for undoped and Ba-doped indium oxide thin films deposited on glass substrates by sol gel technique. The XRD results shows that all the films are polycrystalline in nature and crystallize in cubic structure according to JCPDS card (06-0416), it can be seen that no phases corresponding to barium have been detected in the XRD patterns. As the results, the undoped indium oxide thin films have a preferred and stronger orientation along (222) plane due to free energy surface of the formation of the main planes of the In_2O_3 bixbyite phase, the (111) texture is expected since the high atomic density (111) plane of the bixbyite presents a lower surface free energy plane, as it has been previously discussed[187]with weak peaks such as (211), (400), (440) and (622) correspond the angle 21.47°, 30.69°, 35.5°,51.12°and 60.80° respectively which due a strong crystalline. In the other hand , the films at different Ba doping concentration have a preferred orientation along (400)

plane which revealed that the growth of the films change the direction from [111] to direction [100], this phenomenon may be due a factor: that the increasing of growth along (400) lead to prevent the incorporation of oxygen in the structure, the growth along (222) indicates the films contains sufficient oxygen[188].Wang et al [156] reported that The incident indium species reach the substrate surface. Such In species will play a key role by acting as an auto surfactant that lowers the surface free energy difference between the(001) and (111) surface The same trend was observed in previously reported Ga doped ZnO [189] The weak peaks are disappeared at Ba-doped In_2O_3 films corresponding to lattice planes such as (211), (440) and (622), it revealed that the decrease of crystalline quality. This is attributed a newer nucleation centers reach saturation [190] and the difference of ionic radius between Ba^{2+}(1.42Å) and In^{3+}(0.80Å), when a large number of Ba^{2+}replace In^{3+}in lattice sites substitutionally, lattice distortion is intensified, resulting in larger strain in the films and consequently affecting the normal growth ofIn_2O_3crystal .

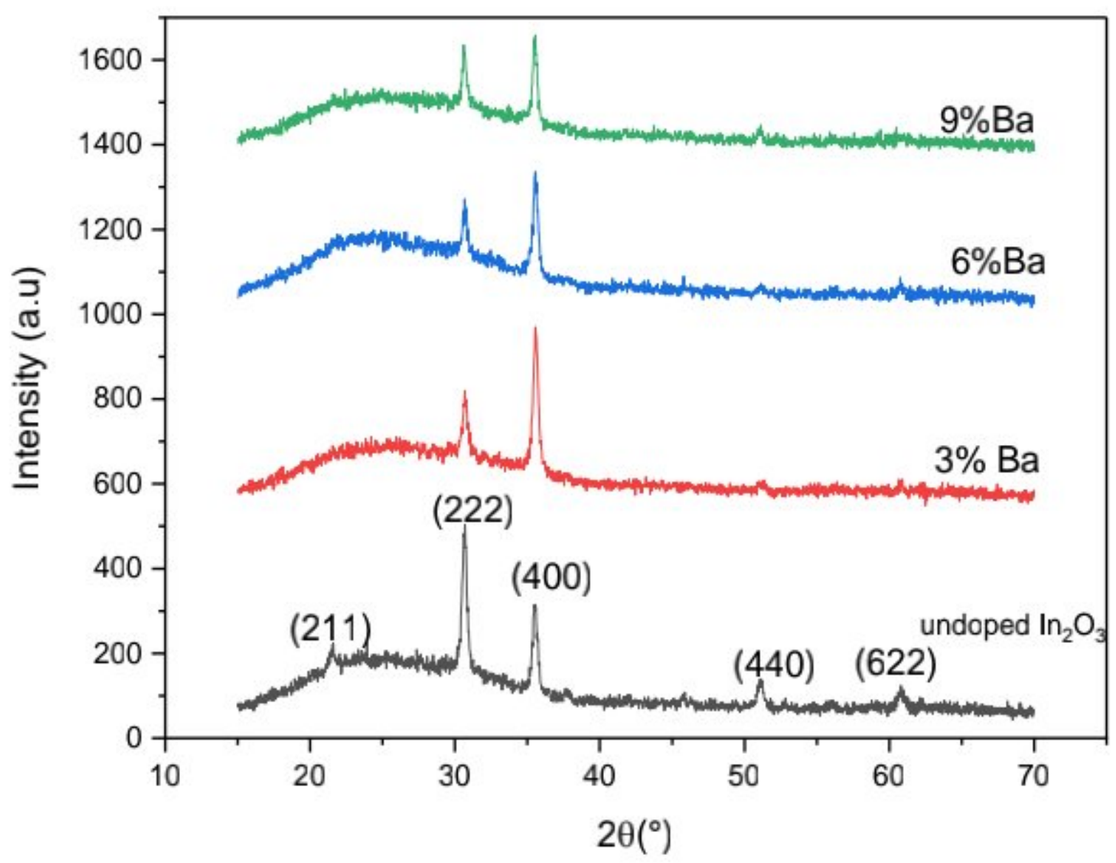

Fig 5.11: The XRD patterns of Ba-doped In_2O_3 thin films at different Ba concentration.

Table 5.4: The XRD parameters of Ba-doped In_2O_3 films.

Ba concentration %	*h k l* planes	2θ(degree)	Calculated parameters		Reference parameter (JCPDS card No 06-0416)
			Lattice constant *a* (Å)	d-spacing (Å)	
0	(222)	30.69	10.093	2.9108	a_0 = 10.118 Å
3	(400)	35.59	10.088	2.5220	*d* = 2.921 Å
6	(400)	35.52	10.107	2.5269	2θ = 30.58
9	(400)	35.49	10.116	2.5291	

The crystallite size, strain and dislocation density values were calculated from XRD patterns of In_2O_3 thin films at different Ba-doping concentration (0%, 3%, 6% and 9%); these values are presented in table 5.5. As can be seen, the lattice constant for undoped and 3, 6 and 9% Ba doped are less than the value of standard bulk In_2O_3 (10.118 Å) lead to contraction of lattice parameter due to interstitial doping (Ba^{2+}ions occupy interstitial sites).The variation of lattice confirmed by the values of stress which have a negative values attributed to compressive in the lattice structure. Montazeri et al[191] reported that Ba^{2+}(1.4 Å) has bigger ionic radius than In^{3+} (0.80Å), so this anomalously shifts occur only when Ba incorporated into In_2O_3 by interstitials. The crystallite size is decreased from 26.31nm (0%Ba) to a minimum 24.59 nm for the In_2O_3 thin film doped at 3 %. However, opposite tendency is observed for 6% Ba doping level; that is, the crystallite size is found to increase to reach value 30.26 nm. After that, the crystallite size decreased again 26.47 nm for the 9% Ba doped thin film, almost similar to undoped one. This behavior of the crystallite size may be explained by the improvement and deterioration of the crystalline state of the films. In addition, the obtained values of strain were varied from $1.47\times10^{-3}$to $1.14\times10^{-3}$and dislocation density were varied from 1.09×10^{15} line/m^2 to 1.44×10^{15} line/m^2 for undoped and Ba doped thin films. The minimum value of strain and dislocation density (1.14×10^{-3}, 1.09×10^{15} line/m^2) have been recorded for the films doped at 6% shows that this film is less strained which might be due to good crystallinity.

Table 5.5: The variation of calculated parameters from XRD patterns of undoped and Ba doped In_2O_3 film at different Ba concentration.

Ba concentration (%)	Crystallite size D (nm)	Strain ε × 10^{-3}	Dislocation density δ (line/m^2) ×10^{15}	Stress GPa
0	26.31	1.3	1.44	-0.0647
3	24.59	1.47	1.65	-0.066
6	30.26	1.14	1.09	-0.022
9	26.47	1.30	1.42	-0.0027

To describe the preferred orientation and the change direction of the films with doping Ba can be calculated the texture coefficient at the orientation plane (222) and (400). However, the figure 5.12 presents the variation of texture coefficient TC (hkl), as the increase of Ba concentration the value of TC (222) decreases and the value of TC(400) increases it is due to the change direction of growth the films along the increasing of Ba concentration. The higher value of TC (400) proves the preferred orientation at Ba-doped indium oxide and the highest growth at this direction.

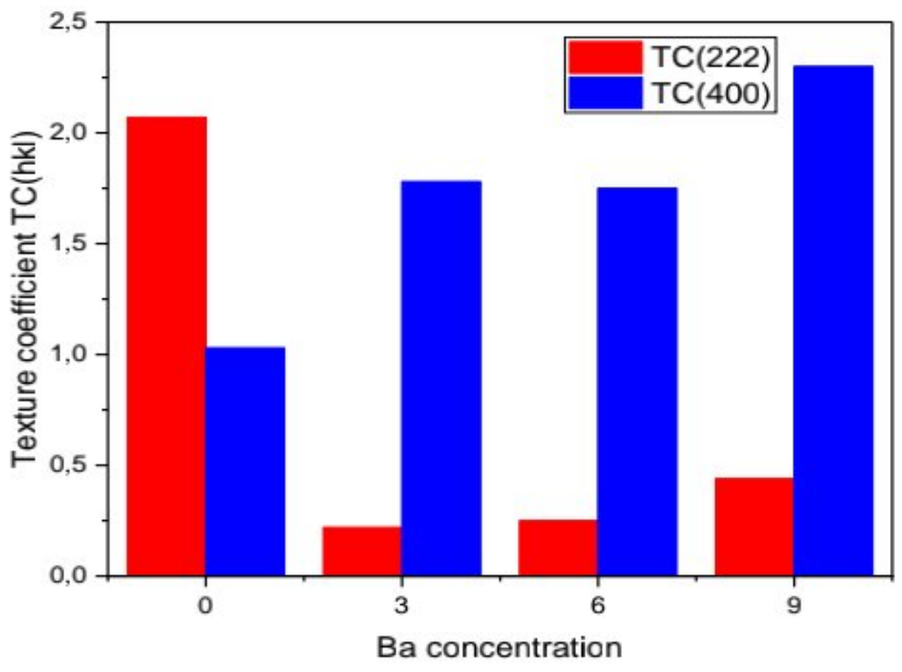

Fig 5.12: The texture coefficient TC(hkl) of Ba doped indium oxide thin films.

5.2.2 Morphological properties:

Figure 5.13 presents the SEM images of undoped and Ba doped In_2O_3 films fabricated by the sol gel spin coating technique with a different barium mol. % concentration. Surface morphology

analysis shows that undoped and 9mol. % Ba doped In_2O_3 thin films exhibit uniform, dense grains and smooth surface due to good crystal quality of the films. Obviously, the grains size reduced at higher Ba doping concentration (9mol. %) This confirmed the XRD results.

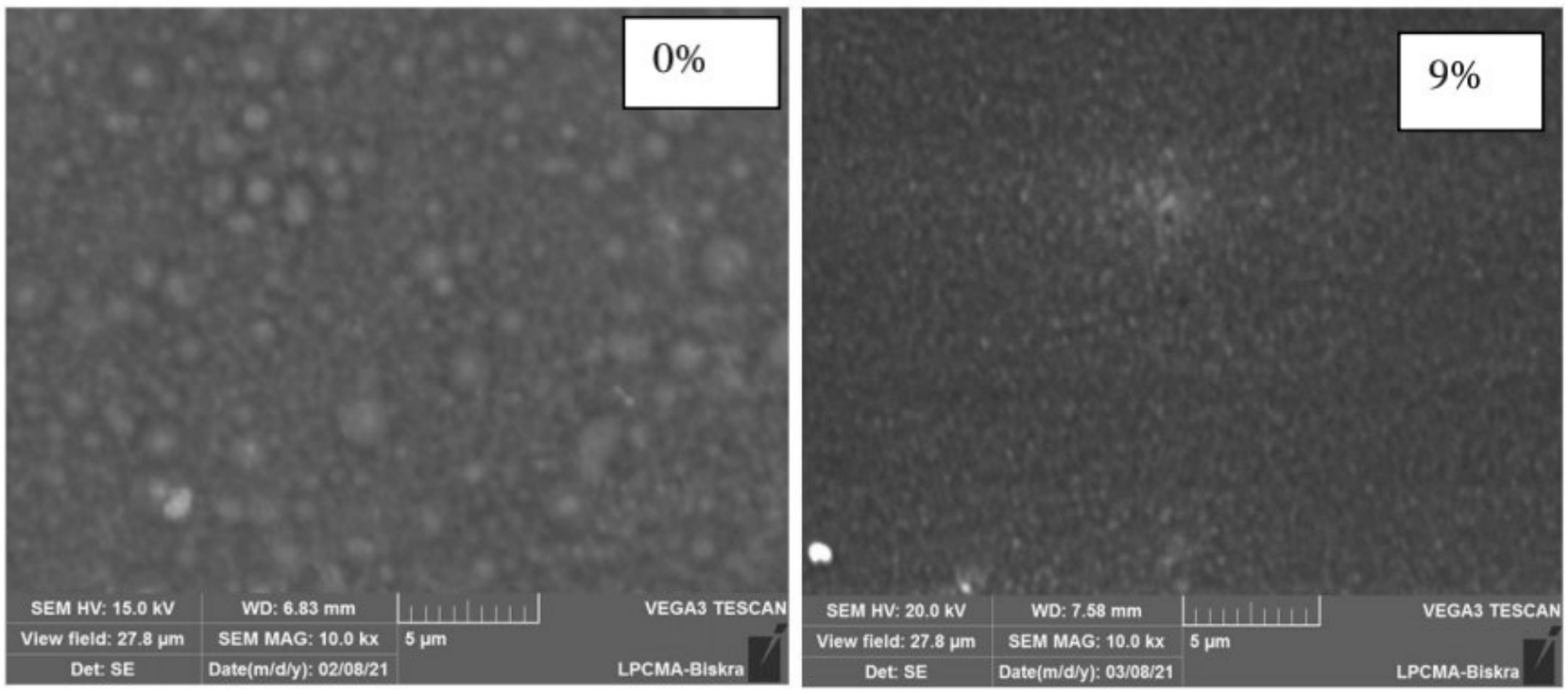

Fig 5.13: The SEM image of undoped and Ba doped In_2O_3 films at 9mol.%.

5.2.3 Compositional properties:

The EDX spectra of undoped and Ba doped In_2O_3 at 9mol. %are shown in figure 5.14. As the results, it confirms the presence In and O, the prominent peaks of Ba are also noted in the EDX patterns of doped sample. The weight and atomic percentage compositions ofIn, Ba and O in the thin films are presented in Table 4.6. It is clearly seen from the table thatthe amount of In element decreases with increasing Ba content. This result based on peak broadening and peak shifts in XRD patterns provide indirect evidence for successful incorporation of Ba into In_2O_3 lattice[191].

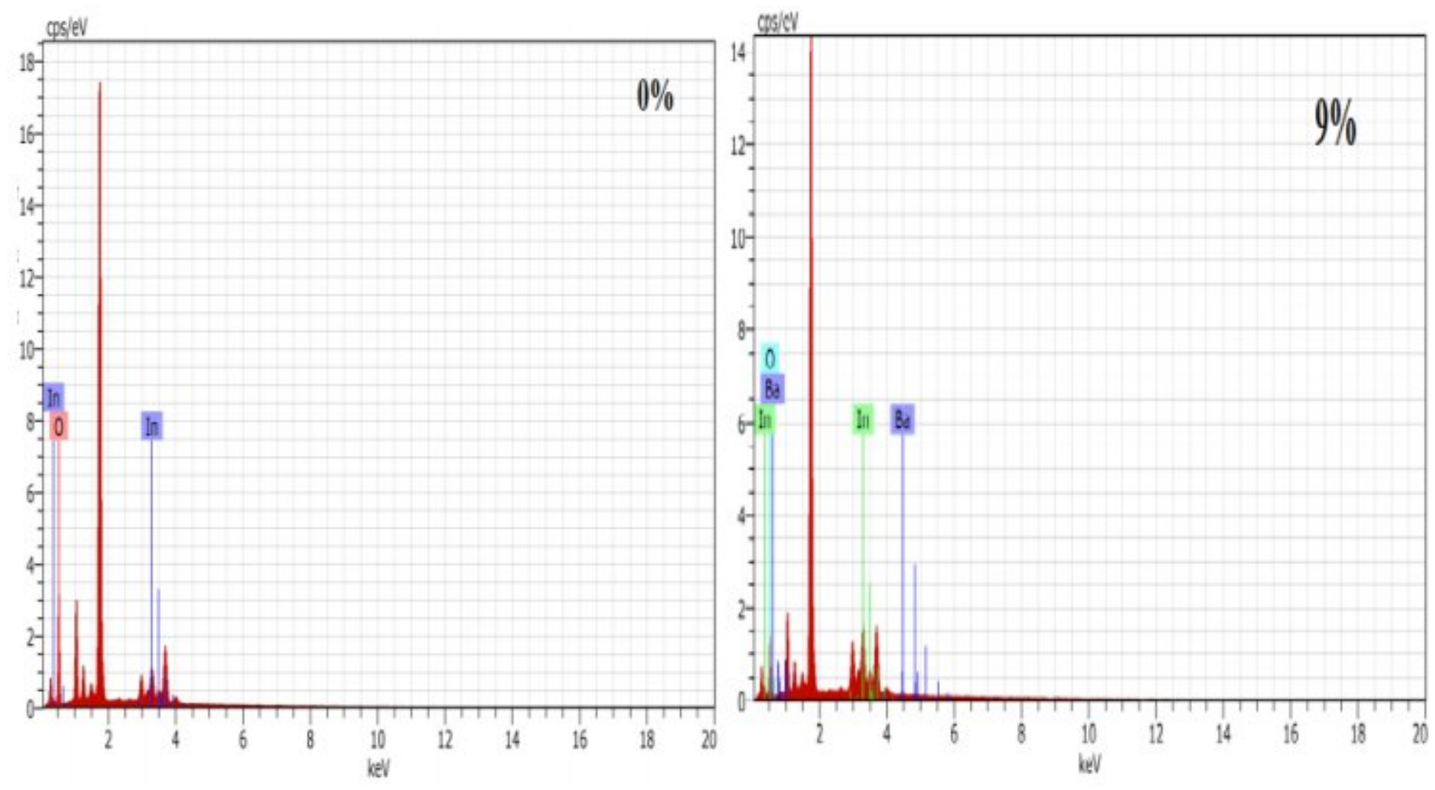

Fig 5.14: The EDX spectra of undoped and Ba doped In_2O_3 films at 9mol%.

Table 5.6: The weight and atomic percentage of element for undoped and Ba doped In_2O_3 films at 9mol%.

Samples	Elements					
	Wt%			at%		
	In	Ba	O	In	Ba	O
0%Ba	63.39	0	36.61	19.44	0	80.56
9%Ba	47.13	4.53	48.34	11.84	0.95	87.20

5.2.4 Optical properties:

The optical transmittance of deposited thin film samples at various Ba doping concentration is shown in figure 5.15. As the result, the transmittance of all the samples in the visible region (400-800nm) is higher (varied between 86.36%-96.68%) due to high crystallinity of the film, homogeneity and less scattering light. In contrast, the transmittance of the undoped indium oxide film is lower than the transmittance of Ba doped In_2O_3 film which is increased with increasing of Ba doping concentration. The high transmittance of Ba doped In_2O_3 film could be used as a window layer in solar cells. On the other side, the films have a good absorption in the ultra violet region (<400nm), while the absorption edge corresponds the transmission from the valence to the conduction band[192]; the absorption edge achieved a blue shifted of the optical band gap as shown in figure 5.15.

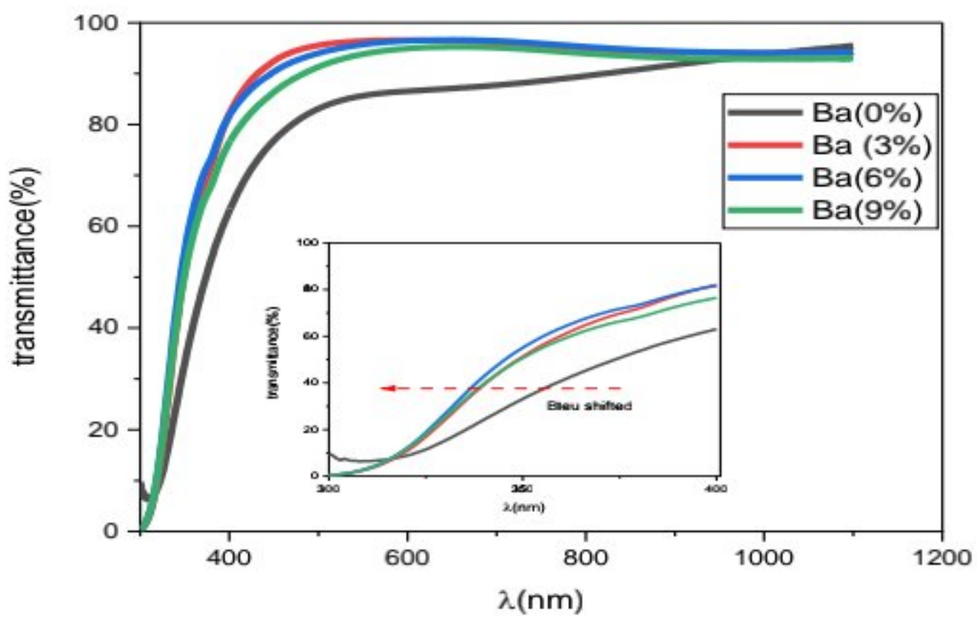

Fig 5.15: The transmittance of undoped and Ba doped In_2O_3 film at various Ba doping concentration.

The optical band gap (Eg) of Ba doped indium oxide thin films estimated by using the

extrapolation of the straight line of the plot $(\alpha h\nu)^2$ as a function $(h\nu)$ (see figure 5.16).In addition, the tail energy or Urbach energy Eu was estimated by taking the reciprocal slope of the straight line of plotting $Ln(\alpha)$ against the photon energy $(h\nu)$ (see figure5.17).

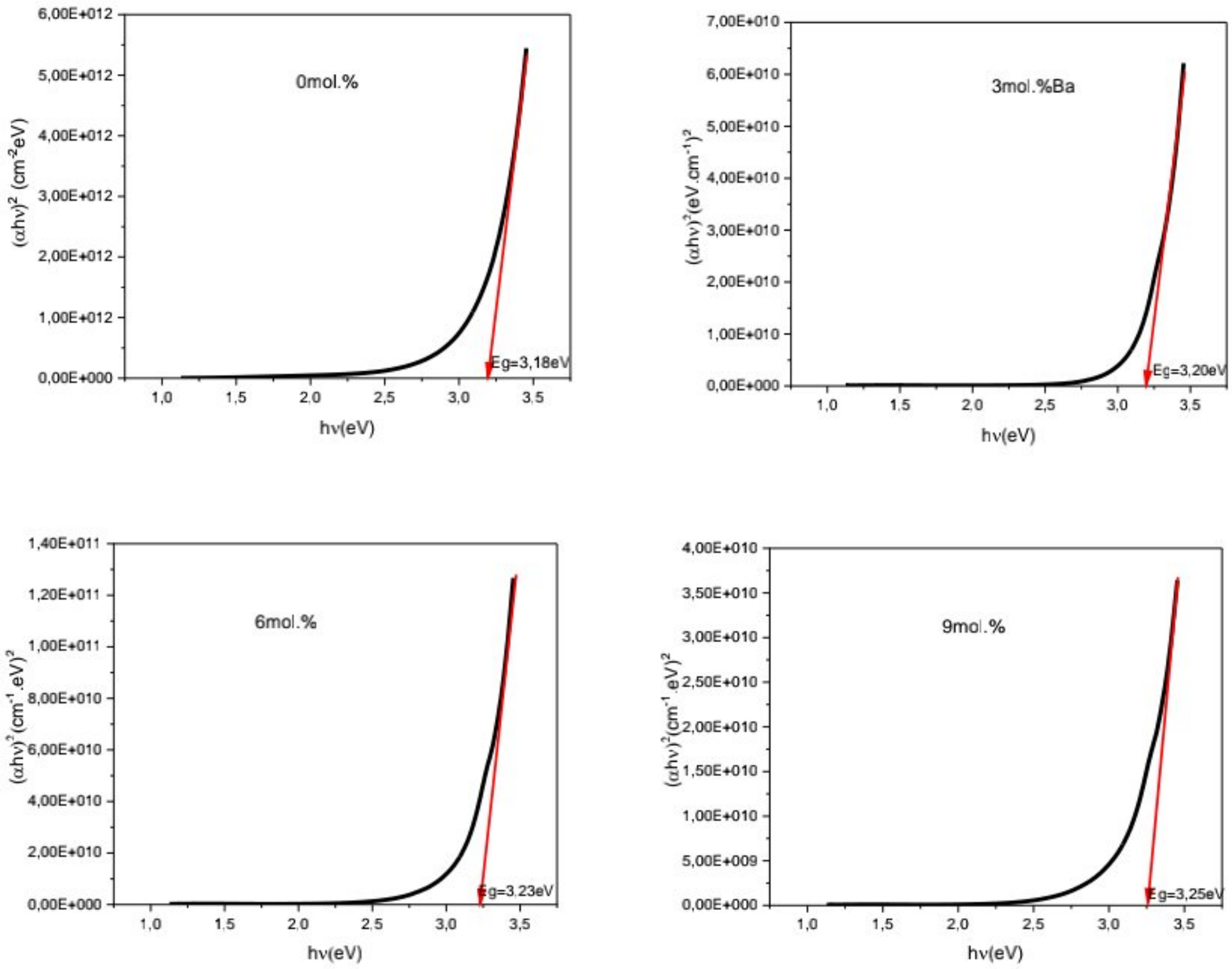

Fig 5.16: The plot $(\alpha h\nu)^2$ against the photon energy incident $(h\nu)$ of undoped and Ba doped In_2O_3 thin films.

The variation of band gap energy and Urbach energy presents in figure 5.18, it is clearly observed the band gap have inversely variation with Urbach energy. However, the band gap increases with increasing Ba doping concentration due to increase of Fermi level in conduction band attributed to Burstein Moss effect is responsible for the increase of energy band gap[193]. The Urbach energy reduces from 0.487 to0.273 eV with increasing of Ba doping concentration. This behavior proves that the degree of structural disorder decreases with the increase of Ba concentration and indicates the improvement of the films crystal quality.

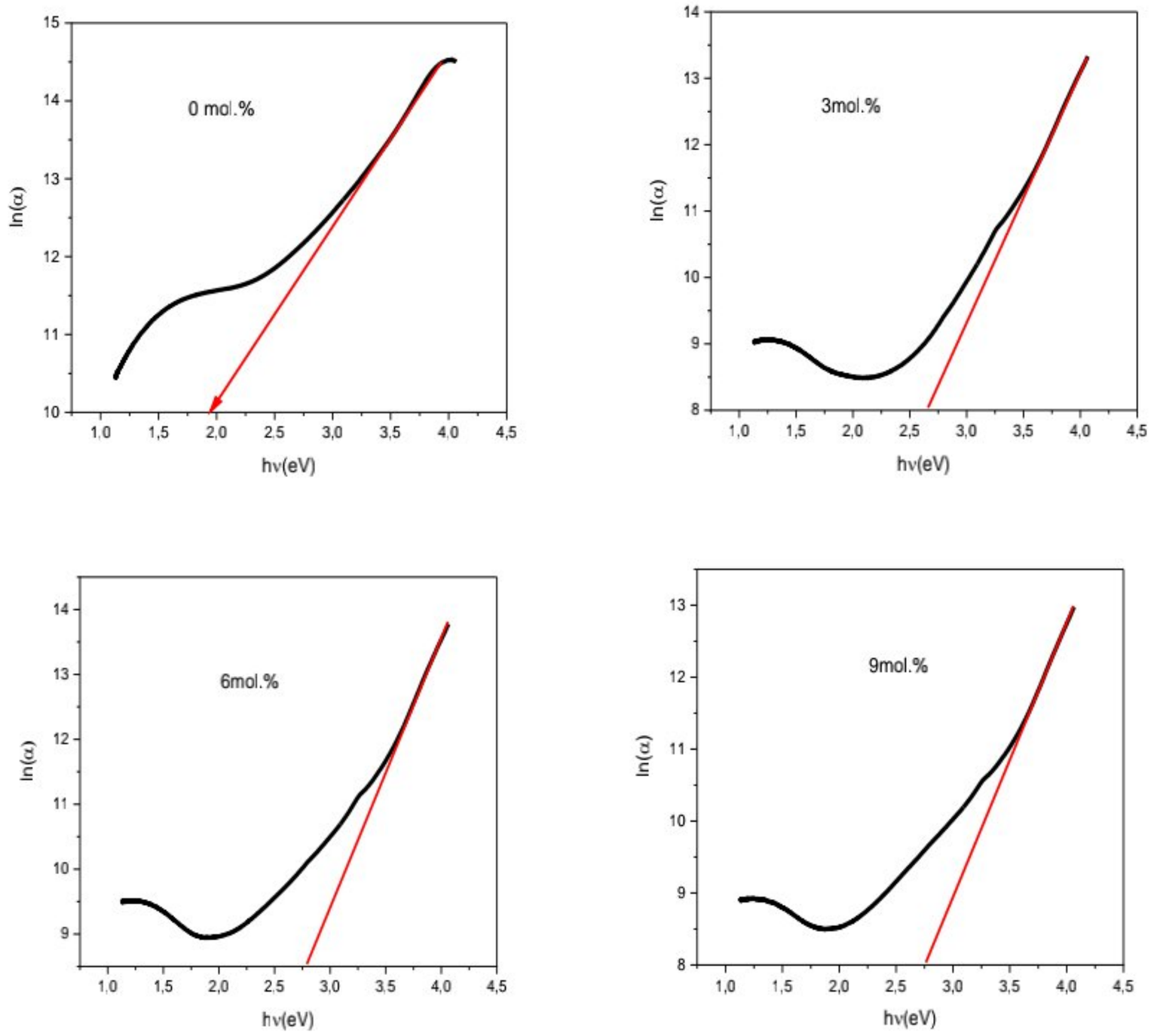

Fig 5.17: The plot Ln(α) as function photon energy incident (hν) for undoped and Ba doped indium oxide thin films.

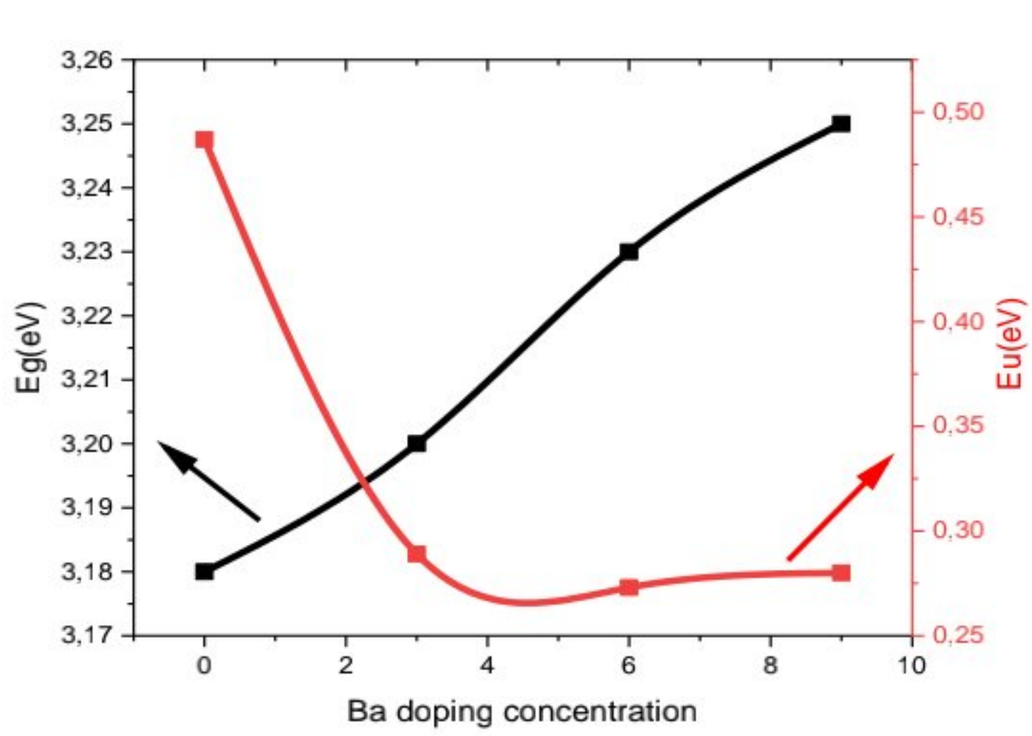

Fig 5.18: The variation of optical band gap energy Eg and Urbach energy Eu at various Ba doped concentration.

5.2.5 Electrical properties:

The electrical measurement of undoped and Ba doped indium oxide film is shown in figure 5.19. As the result, the electrical resistivity values are increased from 0.088 to 4.72×10^3 Ω.cm may be due to some Ba atoms became defects in the structure of the film when the Ba atoms occupy the interstitial sites, which acts as a carrier traps rather than electron donors. In contrast, the electrical conductivity reduces with increasing of Ba concentration as the reason of deterioration of crystallinity which related with XRD patterns.

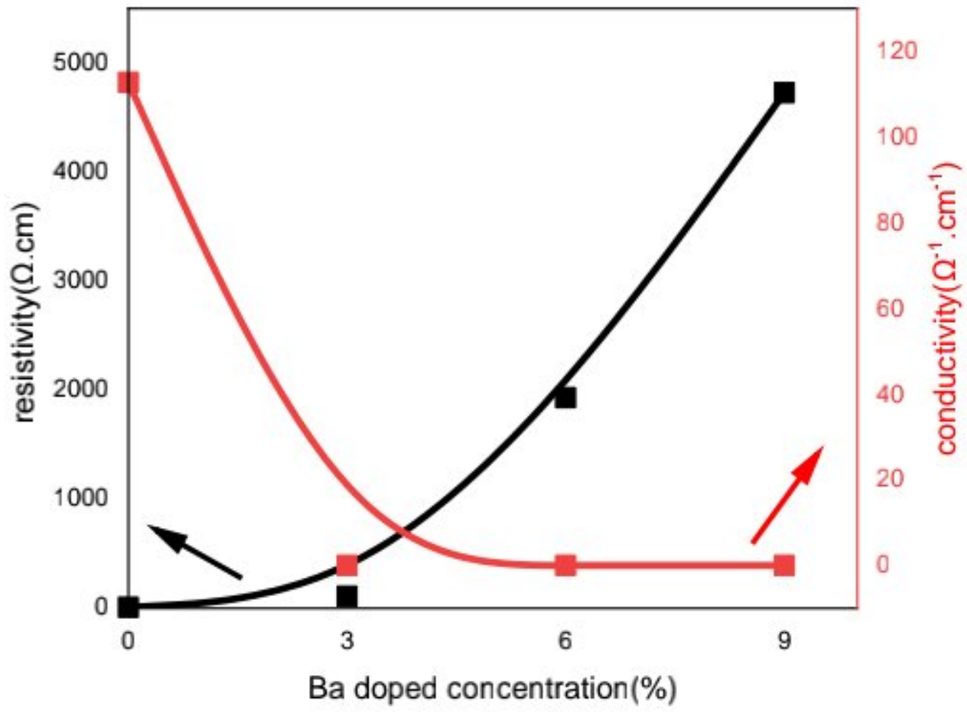

Fig 5.19: The variation of electrical resistivity and electrical conductivity of undoped and Ba doped indium oxide films.

Conclusion:

It can be concluded the doped indium oxide thin films is successfully with doped by Sb and Ba atoms by varied the molar concentration of this atoms using the spin coating sol gel method. The XRD patterns of Sb and Ba doped indium oxide films shows the change direction and the preferred orientation peak from (222) to (400). The transmittance of doped indium oxide is higher in the visible range (400-800nm). The band gap reduced from undoped film to doped film. The surface morphological of undoped and doped indium oxide thin films is smooth and uniform with the reduction of the grain size at higher Sb and Ba concentration. The electrical resistivity increases with the increasing of Sb and Ba concentration in the film. So, the Sb and Ba atoms revealed that no amelioration in the electrical resistivity while contributed in the rising of transmittance which can be applied in window solar cells.

GENERAL CONCLUSION AND PERSPECTIVES

1. General conclusion

From our studies, it can be concluded from the results of indium oxide prepared by sol gel spin coating method on glass substrate with influence film thickness, pH solution ,molar concentration precursor (Indium chloride In_2Cl_3, Indium acetate $C_6H_9InO_6$) and Sb ,Ba doped concentrations are investigated the properties of such as:

- **Film thickness:**

The influence of film thickness exhibits The X-ray diffraction analysis presented that the deposited thin films were polycrystalline with cubic crystal structure and a strongest preferred grain orientation along the (222) plane. In addition, the crystallite sizes enhancement with the thickness growth, it increases from 14 to 27 nm. Also, SEM images revealed the homogenous and uniform distribution without any voids or cracks. The EDX spectra confirmed the presence of In and O elements in the deposited films with nominal stoichiometry. Furthermore, the optical measurements of the films have a good transmittance in the visible region above 75% with blue shift in band gap energy from 3.37 to 3.7 eV owing to occurrence the Burstein–Moss effect. Finally, the physical properties are globally improves the quality of In_2O_3 thin film by films thickness, all these experimental results leads to conclude that prepared In_2O_3 thin films is a promising candidate can be used as TCO material in optoelectronic devices such as solar cell applications, due to its unique structural, optical and electrical properties.

- **pH precursor solution:**

The influence of pH solution achieved that the XRD patterns presented that the films have a polycrystalline structure with preferred orientation along (222) plane corresponding to In_2O_3 cubic structure. The preferential growth in the (222) plane for films reduces at higher pH solution. SEM images showed homogenous, smoothing surface and uniform distributed and reduction of grain size. EDX spectra achieved the presence of In and O elements in the prepared films and Na element start appeared at the adding NaOH solution with their atomic (at %) and weight (wt %) percentage. UV-Vis spectroscopy showed the high transmittance of the films reaches to 80.55% in the visible region. Furthermore, the optical band gap (Eg) increase from 3 to 3.15eV and Urbach energy vary between 0.15 -0.38eV. The electrical measurement showed that the electrical conductivity decreases with rising pH solution. From this result, we conclude that

the prepared In_2O_3 films can be used as a window in solar cells device.

- **Precursor solution:**

The effect of molar concentration precursor indium chloride investigated that the XRD patterns showed the films have a polycrystalline structure with a strong and preferred orientation (222) plane at 0.1M and 0.15M, the growth of the films change the direction at 0.2M and 0.25M from [111] to [100] plane with the increasing of crystallite size and decreasing of defects in the films. SEM images presented the homogenous and uniform distribution of grain in the films. EDX spectra showed the presence of In and O atoms in the films. The transmittance of indium oxide thin films is higher in the visible wave length range. The optical band gap reduced from 3.27 to 3.01 eV and Urbach energy increase from 0.2 to 0.71eV. The electrical resistivity decreases from 30.9 to 0.03 Ω.cm. The films thickness increases with increasing of In and O content in the films. On the other hand , the properties of the films deposited at molar concentration precursor indium acetate presented by X-ray diffraction analysis which achieved that the films have a crystalline structure with strong orientation a long (222) plane. The transmittance of the films is higher which reaches to 95.8% in the visible wavelength region. Optical band gap reduced from 3.12 to 2.97 eV while the Urbach energy increased from 0.23 to 0.30 eV. The film thickness increased with rising of molar concentration to be thicker for improvement the electrical conductivity by reduction of electrical resistivity. We conclude from the results that the films prepared at InCl3precursor are better than the films deposited at indium acetate precursor to continue the other effects. These films can be applied in photovoltaic and optoelectronic applications.

- **Sb and Ba doping In_2O_3 films:**

The effect of Sb and Ba doping concentration achieved that the structural properties of doped films revealed by XRD patterns which confirms the polycrystalline structure with a cubic byxbite structure. The growth of the films (Sb and Ba doped In_2O_3 thin films) change the direction from [111] to [100]. For the smallest ionic radius of Sb, the lattice parameters are less than the bulk value of indium oxide which proves the contraction in the structure lattice while the crystallite size decreased at rising of Sb concentration. Furthermore, the big ionic radius of Ba has occupied interstitial sites in the structure of the films which leads to reduce the crystalline quality, increase the defect in the structure of the films (grain boundaries) and the decrease of lattice constant. The SEM images of undoped and Sb doped indium oxide films showed the homogenous and the

reduction of grain size at rising of Sb concentration while the SEM images for undoped and Ba doped indium oxide films presented the smoothing surface and the increasing of grain boundaries in the films. The EDX spectra revealed the presence of In, O and Sb elements for undoped films Sb doped indium oxide films and In, O and Ba for Ba doped indium oxide thin films. The electrical resistivity for Ba and Sb doped In_2O_3 films increased (from 0.008 to 4.72× 10^3 Ω.cm) (from 0.008 to 3.99 Ω.cm) respectively with the decreasing of electrical conductivity according. We conclude that the doped indium oxide film can applied in optoelectronic applications.

2. Perspectives

As the results of this study, the following future research is indicated:

- Studying the effect of Sb and Ba codoped In_2O_3thin films in order to improve the structural, optical, and electrical properties of In_2O_3 thin films.
- Elaboration of In_2O_3 thin films by varying other parameters like speed coater, the substrates and solvent….etc.
- Additional characterizations, such as Raman spectroscopy, Hall effect measurements, and the investigation of current-voltage (I–V) properties as a function of temperature, are required.
- Investigating the use of deposited films in PN junctions, photocatalysts, and antibacterial applications, among others.
- Studying the magnetic properties of undoped and doped In_2O_3 thin films.

REFERENCES

References

[1] A. Kennedy, K. Viswanathan, and K. Pradeev raj, "*Study of the influence of substrate temperature on structural, optical, and electrical properties of Zn-doped MnIn2S4 thin films prepared by chemical spray pyrolysis*," Phys. Lett. Sect. *A* Gen. At. Solid State Phys., vol. 380, no. 36, pp. 2842–2848, 2016, doi: 10.1016/j.physleta.2016.06.043.

[2] A. Tiburcio-Silver, A. Sanchez-Juarez, and A. Avila-Garcia, "*Properties of gallium-doped ZnO deposited onto glass by spray pyrolysis,*" Sol. Energy Mater. Sol. Cells, vol. 55, no. 1–2, pp. 3–10, 1998, doi: 10.1016/S0927-0248(98)00040-3.

[3] A. B. Kashyout, M. Soliman, and M. Fathy, "*Effect of preparation parameters on the properties of TiO2 nanoparticles for dye sensitized solar cells*," Renew. Energy, vol. 35, no. 12, pp. 2914–2920, 2010, doi: 10.1016/j.renene.2010.04.035.

[4] G. D. Yüzüak and Ö. D. Coşkun, "*The effect of annealing on the structural, electrical, optical and electrochromic properties of indium-tin-oxide films deposited by RF magnetron sputtering technique*," Optik (Stuttg)., vol. 142, pp. 320–326, 2017, doi: 10.1016/j.ijleo.2017.06.016.

[5] A. Sudha, S. L. Sharma, and A. N. Gupta, "*Achieving sensitive and stable indium oxide thin films for gamma radiation monitoring*" Sensors Actuators A. Phys, 2018, doi: 10.1016/j.sna.2018.10.015.

[6] C. J. Huang, Y. K. Su, and S. L. Wu, "*The effect of solvent on the etching of ITO electrode*," Mater. Chem. Phys., vol. 84, no. 1, pp. 146–150, 2004, doi: 10.1016/j.matchemphys.2003.11.021.

[7] H. Cho and Y. Yun, "*Characterization of indium tin oxide (ITO) thin films prepared by a sol – gel spin coating process,*" Ceram. Int., vol. 37, no. 2, pp. 615–619, 2011, doi: 10.1016/j.ceramint.2010.09.033.

[8] M. A. Flores-Mendoza, R. Castanedo-Perez, G. Torres-Delgado, J. Márquez Marín, and O. Zelaya-Angel, "*Influence of the annealing temperature on the properties of undoped indium oxide thin films obtained by the sol-gel method,*" Thin Solid Films, vol. 517, no. 2, pp. 681–685, 2008, doi: 10.1016/j.tsf.2008.07.036.

[9] Z. Ding, C.An, Q.Li, Z.Hou, J.Wang, H.Qi and F.Qi "*Preparation of ITO nanoparticles by liquid phase coprecipitation method,*" J. Nanomater., vol. 2010, 2010, doi: 10.1155/2010/543601.

[10] M. Girtan, H. Cachet, and G. I. Rusu, "*On the physical properties of indium oxide thin films deposited by pyrosol in comparison with films deposited by pneumatic spray pyrolysis,*" Thin Solid Films, vol. 427, no. 1–2, pp. 406–410, 2003, doi: 10.1016/S0040-6090(02)01185-9.

[11] G. Korotcenkov, V.Brinzari, A.Cerneavschi , M.Ivanov , V.Golovanov , A.Cornet J.Morante and A.Cabot , "*The influence of film structure on In_2O_3 gas response*," Thin Solid Films, vol. 460, no. 1–2, pp. 315–323, 2004, doi: 10.1016/j.tsf.2004.02.018.

[12] N. Fellahi, M. Addou, A. Kachouane, M. El Jouad, and Z. Sofiani, "*Optical properties of undoped and tin-doped nanostructured In2O3 thin films deposited by spray pyrolysis,*" EPJ Appl. Phys., vol. 74, no. 2, 2016, doi: 10.1051/epjap/2015150383.

[13] D. Sariket, S. Shyamala, P. Hajraa, H.Mandala, A. Beraa, A. Maityb,S. Kundud and C. Bhattacharya "*Temperature controlled fabrication of chemically synthesized cubic In2O3 crystallites for improved photoelectrochemical water*

oxidation," Mater. Chem. Phys., vol. 201, pp. 7–17, 2017, doi: 10.1016/j.matchemphys.2017.08.010.

[14] H. Y. Yeom, N. Popovich, E. Chason, and D. C. Paine, "*A study of the effect of process oxygen on stress evolution in d.c. magnetron-deposited tin-doped indium oxide*," Thin Solid Films, vol. 411, no. 1, pp. 17–22, 2002, doi: 10.1016/S0040-6090(02)00166-9.

[15] K. Daoudi, B. Canut, M. G. Blanchin, C. S. Sandu, V. S. Teodorescu, and J. A. Roger, "*Tin-doped indium oxide thin films deposited by sol – gel dip-coating technique*," Materials Science and Engineering C, vol. 21, pp. 313–317, 2002.

[16] C. P. Chu, T. S. Ko, Y. C. Chang, T. C. Lu, H. C. Kuo, and S. C. Wang, "*Thermally evaporated In2O3 nanoloquats with oxygen flow-dependent optical emissions*," Mater. Sci. Eng. B Solid-State Mater. Adv. Technol., vol. 147, no. 2–3, pp. 276–279, 2008, doi: 10.1016/j.mseb.2007.08.024.

[17] N. Kumari, S. R. Patel, and J. V. Gohel, "*Optical and structural properties of ZnO thin films prepared by spray pyrolysis for enhanced efficiency perovskite solar cell application*," Opt. Quantum Electron., vol. 50, no. 4, pp. 1–22, 2018, doi: 10.1007/s11082-018-1376-5.

[18] J. Charlesbabu, K. Gopalakrishnan, M. Elango, and K. Vasudevan, "*Preparation and characterization of Cd-doped ZnO thin films by spin coating method*," Inorg. Nano-Metal Chem., vol. 47, no. 9, pp. 1298–1303, 2017, doi: 10.1080/24701556.2016.1242627.

[19] S. Mohammadi, H. Abdizadeh, and M. Reza, "*Opto-electronic properties of molybdenum doped indium tin oxide nanostructured thin films prepared via sol – gel spin coating,*" Ceram.Int., pp. 1–9, 2013, doi: 10.1016/j.ceramint.2013.02.032.

[20] A. A. Al-ghamdi, W. E. Mahmoud, S. J. Yaghmour, and F. M. Al-marzouki, "*Structure and optical properties of nanocrystalline NiO thin film synthesized by sol – gel spin-coating method,*" Alloy. Compd., vol. 486, pp. 9–13, 2009, doi: 10.1016/j.jallcom.2009.06.139.

[21] H. Baqiah, N. B. Ibrahim, S. A. Halim, S. K. Chen, K. P. Lim, and M. M. A. Kechik, "*Physical properties of Fe doped In2O3 magnetic semiconductor annealed in hydrogen at different temperature*," J. Magn. Magn. Mater., vol. 401, pp. 102–107, 2016, doi: 10.1016/j.jmmm.2015.10.013.

[22] T. Coutts, T. O. Mason, J. . Perkins, and D. . Ginley, "*Transparent Conducting Oxides: Status and Opportunities in Basic Research*," 1999.

[23] B. G. Lewis and D. C. Paine, "*Applications and processing of transparent conducting oxides*," MRS Bull., vol. 25, no. 8, pp. 22–27, 2000, doi: 10.1557/mrs2000.147.

[24] G. Gökçeli and N. Karatepe, "*Improving the properties of indium tin oxide thin films by the incorporation of carbon nanotubes with solution-based techniques,*" Thin Solid Films, vol. 697, no. February, p. 137844, 2020, doi: 10.1016/j.tsf.2020.137844.

[25] F. K. Shan, G. X. Liu, W. J. Lee, B. C. Shin, and Y. C. Kim, "*Structural, optical and electrical properties of transparent conductive In2O3-doped ZnO thin films grown by pulsed laser deposition,*" J. Korean Phys. Soc., vol. 50, no. 3, pp. 626–631, 2007, doi: 10.3938/jkps.50.626.

[26] Z. Yao, W.Duan, P.Steuter "*In fl uence of Oxygen on Sputtered Titanium-Doped Indium Oxide Thin Films and Their Application in Silicon Heterojunction Solar Cells*,"Advanced science news, vol. 2000501, no. January, 2021, doi: 10.1002/solr.202000501.

[27] N. Hamani,A.Attaf "*ANNEALING EFFECT ON THE PROPERTIES OF INDIUM TIN OXIDES (IN2O3 :SN) THIN FILMS PREPARED BY ULTRASONIC SPRAY TECHNIC*," Fundam. Appl. Sci. ISSN, 2018.

[28] B. Yilbas, A. Al-Sharafi, and H. Ali, "*Surfaces for Self-Cleaning*," in Self-Cleaning of Surfaces and Water Droplet Mobility, 2019, pp. 45–98.

[29] A. Mishra, N. Bhatt, and A. K. Bajpai, *Chapter 12. Nanostructured superhydrophobic coatings for solar panel applications*. Elsevier Inc., 2019.

[30] A. Palomares-Sanchez, B. Wattsa, D.Klimmb, A. Baraldic, A. Parisinic, S.Vantaggioc, R. Fornaria"*Sol-gel growth and characterization of In2O3 thin films*," Thin Solid Films, vol. 645, no. October 2017, pp. 383–390, 2018, doi: 10.1016/j.tsf.2017.10.049.

[31] P. K. Shihabudeen and A. R. Chaudhuri, "*Improving ethanol sensing characteristics of indium oxide thin films by nitrogen incorporation*" Sensors Actuators B. Chem., p. 127523, 2019, doi: 10.1016/j.snb.2019.127523.

[32] S. A. Kuznetsova and L. P. Borilo, "*Obtaining Sol-Gel By Means of Indium Oxide Thin Films*," Glas. Ceram., vol. 70, pp. 429–433, 2014.

[33] C. Falcony, M. A. Aguilar-frutis, and M. Garc, "*Spray Pyrolysis Technique ; High- K Dielectric Films and Luminescent Materials* "Micromachines pp. 1–33, 2018, doi: 10.3390/mi9080414.

[34] D. Sumanth Kumar, B. Jai Kumar, and H. M. Mahesh, "*Quantum Nanostructures (QDs)*" in Synthesis of Inorganic Nanomaterials, Elsevier Ltd., 2018, pp. 59–88.

[35] T. V. Gavrilović, D. J. Jovanović, and M. D. Dramićanin, "*Synthesis of multifunctional inorganic materials: From micrometer to nanometer dimensions*," Nanomater. Green Energy, pp. 55–81, 2018, doi: 10.1016/B978-0-12-813731-4.00002-3.

[36] U. P. M. Ashik, S. Kudo, and J. Hayashi, "*An Overview of Metal Oxide Nanostructures,*" in Synthesis of Inorganic Nanomaterials, Elsevier Ltd., 2018, pp. 19–57.

[37] L. F. Gorup,L.Amorin, E.Camargo "*Methods for design and fabrication of nanosensors: the case of ZnO-based nanosensor,*" *Nanosensors for Smart Cities*, pp. 9–30, 2020, doi: 10.1016/b978-0-12-819870-4.00002-5.

[38] P. Prathap, G. G. Devi, Y. P. V Subbaiah, and K. T. R. Reddy, "*Growth and characterization of indium oxide films*," Current applied ohysics, vol. 8, pp. 120–127, 2008, doi: 10.1016/j.cap.2007.06.001.

[39] M. Jothibas, C. Manoharan, S. Ramalingam, S. Dhanapandian, S. Johnson Jeyakumar, and M. Bououdina, "*Preparation, characterization, spectroscopic (FT-IR, FT-Raman, UV and visible) studies, optical properties and Kubo gap analysis of In $_2O_3$ thin films,*" J. Mol. Struct., vol. 1049, pp. 239–249, 2013, doi: 10.1016/j.molstruc.2013.06.047.

[40] C. Manoharan, M. Jothibas, S. Dhanapandian, G. Kiruthigaa, and S. J. Jeyakumar, "*Role of titanium doping on indium oxide thin films using spray pyrolysis techniques,*" Proc. Int. Conf. "Advanced Nanomater. Emerg. Eng. Technol. ICANMEET 2013, pp. 335–339, 2013, doi: 10.1109/ICANMEET.2013.6609310.

[41] A. Bashir, T. I. Awan, A. Tehseen, M. B. Tahir, and M. Ijaz, "*Interfaces and surfaces*," in Chemistry of Nanomaterials, INC, 2020, pp. 51–87.

[42] C. Grèzes-Besset and G. Chauveau, "Optical coatings for large facilities," in *Optical Thin Films and Coatings: From Materials to Applications*, Woodhead Publishing Limited, 2013, pp. 695–717.

[43] K. Wasa, M. Kitabatake, and H. Adachi, "*CHAPTER 2 Thin Film Materials Technology,*" Thin Film Mater. Technol., pp. 17–69, 2004, [Online]. Available:

http://www.sciencedirect.com/science/article/pii/B9780815514831500034.

[44] M. Girtan, G. I. Rusu, G. G. Rusu, and S. Gurlui, "*Influence of oxidation conditions on the properties of indium oxide thin films*," Appl. Surf. Sci., vol. 162, pp. 492–498, 2000, doi: 10.1016/S0169-4332(00)00238-5.

[45] K. K. Makhija, A. Ray, R. M. Patel, U. B. Trivedi, and H. N. Kapse, "*Indium oxide thin film based ammonia gas and ethanol vapour sensor,*" Bull. Mater. Sci., vol. 28, no. 1, pp. 9–17, 2005, doi: 10.1007/BF02711165.

[46] J. Lawrence, J. Pou, F. Lusquiños, R. Comesaña, and M. Boutinguiza, "*Production of Biomaterial Coatings by Laser-Assisted Processes*," Second Edi. Elsevier Ltd., 2018.

[47] A. Matei, R.Berjega, A.Vlad "*LDH-interlayered nanostructures for biomedical and environmental applications*". Elsevier Inc., 2019.

[48] F. Ii, C. Universitario, and S. Angelo, "*6 - Plume characterization in pulsed laser deposition of metal oxide thin films*". Elsevier Inc., 2018.

[49] K. V. Madhuri, "*Thermal protection coatings of metal oxide powders*". INC, 2020.

[50] N. Tripathi, S. Rath, V. Ganesan, and R. J. Choudhary, "*Growth dynamics of pulsed laser deposited indium oxide thin films: A substrate dependent study*," Appl. Surf. Sci., vol. 256, no. 23, pp. 7091–7095, 2010, doi: 10.1016/j.apsusc.2010.05.033.

[51] T. Kerdcharoen and C. Wongchoosuk, "*Carbon nanotube and metal oxide hybrid materials for gas sensing*". Woodhead Publishing Limited, 2013.

[52] M. Souli, L. Ajili, B. Alhalaili, A. Khadaraoui, R. Vidu, and N. Kamoun-Turki, "*Enhancement in structural, optical and morphological properties of sprayed In_2O_3 thin films induced by low energy electron beam irradiation,*" Mater. Sci. Semicond. Process., vol. 124, no. November 2020, p. 105595, 2021, doi: 10.1016/j.mssp.2020.105595.

[53] F. Ghamari, D. Raoufi, and J. Arjomandi, "*Characteristic Evaluations of Tin-Doped Indium Oxide Nanostructure Films: A Case Study of the Influences of Thickness Growth on Crystallographic, Optoelectronic, Stereometric and Electrochemical Properties Fatemeh*," Mater. Chem. Phys., p. 124051, 2020, doi: 10.1016/j.matchemphys.2020.124051.

[54] A. Renken and L. Kiwi-minsker, "*2 - Microstructured Catalytic reactors*", 1st ed., vol. 53, no. 10. Elsevier Inc., 2010.

[55] T. English, "*Physical Sputtering and Sputter*". 2010.

[56] A. O. Adeyeye and G. Shimon, *Growth and Characterization of Magnetic Thin Film and Nanostructures*, 1st ed., vol. 5. Elsevier B.V., 2016.

[57] M. S. Zafar, I. Farooq, M. Awais, S. Najeeb, Z. Khurshid, and S. Zohaib, *Bioactive surface coatings for enhancing osseointegration of dental implants*. Elsevier Ltd., 2018.

[58] A. H. Ali, Z. Hassan, and A. Shuhaimi, "Enhancement of Optical Transmittance and Electrical Resistivity of Post-Annealed ITO Thin Films RF Sputtered on Si," *Appl. Surf. Sci.*, 2018, doi: 10.1016/j.apsusc.2018.03.024.

[59] S. Cho, "Structural, optical, and electrical properties of RF-sputtered indium oxide thin films," *J. Korean Phys. Soc.*, vol. 60, no. 12, pp. 2058–2062, 2012, doi: 10.3938/jkps.60.2058.

[60] X. Li, W. Miao, Q. Zhang, L. Huang, Z. Zhang, and Z. Hua, "Preparation of molybdenum-doped indium oxide thin films using reactive direct-current magnetron sputtering," *J. Mater. Res.*, vol. 20, no. 6, pp. 1404–1408, 2005, doi: 10.1557/JMR.2005.0184.

[61] O. Bierwagen, "Indium oxide - A transparent, wide-band gap semiconductor for (opto)electronic applications," *Semicond. Sci. Technol.*, vol. 30, no. 2, p. 24001, 2015, doi: 10.1088/0268-1242/30/2/024001.

[62] W. A. P. and C. J. A. J R Bellingham, "Electrical and optical properties of amorphous indium oxide," *J. Phys. Condens. Matter 2*, vol. 6207–6221, 1990.

[63] Y. Tak, K. Kim, H. Park, K. Lee, and J. Lee, "Criteria for ITO (indium – tin-oxide) thin film as the bottom electrode of an organic light emitting diode," *Thin Solid Film. 411*, vol. 411, pp. 12–16, 2002.

[64] M. MIZUNO and T. MIYAMOTO, "Properties of Germanium-Doped Indium Oxide Thin Films Prepared by DC Magnetron Sputtering Properties of Germanium-Doped Indium Oxide Thin Films Prepared by DC Magnetron Sputtering," *Japan Soc. Appl. Phys.*, vol. 39, pp. 1849–1854, 2000.

[65] X. Li, Q. Zhang, W. Miao, L. Huang, and Z. Zhang, "Transparent conductive oxide thin films of tungsten-doped indium oxide," *Thin Solid Films*, vol. 515, no. 4, pp. 2471–2474, 2006, doi: 10.1016/j.tsf.2006.07.014.

[66] C. Nefzi, M. Souli, N. Beji, A. Mejri, and N. Kamoun-Turki, "*Improvement of structural, optical and electrical properties of iron doped indium oxide thin films by high gamma radiations for photocatalysis applications*," *Mater. Sci. Semicond. Process.*, vol. 90, no. March 2018, pp. 32–40, 2019, doi: 10.1016/j.mssp.2018.09.022.

[67] S. SEMMARI, "*L ' effet de la molarité et de la température du substrat sur les propriétés des couches minces d ' Oxyde d ' Etain (SnO 2) déposées par spray Ultrasonique*". Université Mohamed Khider-Biskra N°, 2012.

[68] A. .Chennoufi, "*L'effet de la molarité et de la température du substrat sur les propriétés des couches minces d'Oxyde d'Indium déposées par spray Ultrasonique, mémoire de magister*," Université de Biskra, 2012.

[69] T. Moriga, D. Edwards, and T. Mason "*Phase relationships and physical properties of homologous compounds in the zinc oxide-indium oxide system*," J. Am. Ceram. Soc., vol. 81, no. 5, pp. 1310–1316, 1998, doi: 10.1111/j.1151-2916.1998.tb02483.x.

[70] G. Golan, A. Axelevitch, B. Gorenstein, and A. Peled, "*Novel type of indium oxide thin films sputtering for opto-electronic applications*," Appl. Surf. Sci., vol. 253, no. 15, pp. 6608–6611, 2007, doi: 10.1016/j.apsusc.2007.01.030.

[71] J. E. Medvedeva and D. B. Buchholz, "*Scholars ' Mine Origin of High Carrier Concentration in Amorphous Wide-Bandgap Oxides : Role of Disorder in Defect Formation and Electron Localization in In $_2$ O $_{3-x}$ Origin of high carrier concentration in amorphous wide-bandgap oxides : Role of disorder*," vol. 127, no. 17, pp. 0–24, 2020, doi: 10.1063/1.5144219.

[72] V. Das, S. Kirupavathy, L. Damodare, and N. Lakshminarayan, "*Optical and electrical investigations of indium oxide thin films prepared by thermal oxidation of indium thin films,*" J. Appl. Phys., vol. 79, no. 11, pp. 8521–8530, 1996, doi: 10.1063/1.362477.

[73] J. Zemann, "*Iineralog.-Kristallographisches lnstitut*",vol. 18, no. 1. 1965.

[74] A. Bouhdjer, "*Study of Thin Layers of Indium Oxide (In 2 O 3) Elaborated by Chemical Means*," Med Khider University of Biskra Faculty, 2016.

[75] R. AZIZI, "*The effect of doping on the properties of thin films of Indium oxide (In2O3) deposited by ultrasonic spray for optoelectronic application*". University Med KhiderBiskra, 2020.

[76] A. Attaf, A. Bouhdjer, H. Saidi, M. S. Aida, N. Attaf, and H. Ezzaouia, "*On tuning the preferential crystalline orientation of spray pyrolysis deposited indium*

oxide thin films," Thin Solid Films, vol. 625, pp. 177–179, 2017, doi: 10.1016/j.tsf.2017.01.055.

[77] W. Seiler, M Nistor, J Perrière, C. Heber "*Epitaxial undoped indium oxide thin films : Structural and physical properties*" Solar Energy Materials and Solar Cells, vol. 116, no. 10, p. pp.34-42, 2014, doi: 10.1016/j.solmat.2013.04.002ff.

[78] L. N. Lau, N. B. Ibrahim, and H. Baqiah, "*Influence of precursor concentration on the structural, optical and electrical properties of indium oxide thin film prepared by a sol-gel method*," Appl. Surf. Sci., pp. 1–20, 2015, doi: 10.1016/j.apsusc.2015.03.129.

[79] V. Senthilkumar and P. Vickraman, "*Annealing temperature dependent on structural, optical and electrical properties of indium oxide thin films deposited by electron beam evaporation method*," Curr. Appl. Phys., vol. 10, no. 3, pp. 880–885, 2010, doi: 10.1016/j.cap.2009.10.014.

[80] A. P. Rambu, D. Sirbu, M. Dobromir, and G. G. Rusu, "*Electronic transport and optical properties of indium oxide thin films prepared by thermal oxidation,*" Solid State Sci., vol. 14, no. 10, pp. 1543–1549, 2012, doi: 10.1016/j.solidstatesciences.2012.08.030.

[81] M.Veeraswamy, y, Vijayakumr.y, "*Structural and Optical Characterization of Indium Oxide Thin Films by Vacuum Thermal Evaporation*," Proc. International Conf. Adv. Nanomater. Emerg. Eng. Technol., pp. 502–505, 2013.

[82] K. Dey, A. G. Aberle, S. van Eek, and S. Venkataraj, "*Superior optoelectrical properties of magnetron sputter-deposited cerium-doped indium oxide thin films for solar cell applications,*" Ceram. Int., vol. 47, no. 2, pp. 1798–1806, 2021, doi: 10.1016/j.ceramint.2020.09.006.

[83] C. Nefzi, M. Souli, N. Beji, A. Mejri, and N. Kamoun-turki, "*Enhancement by high gamma radiations of optical and electrical properties of indium oxide thin films for solar devices*," J. Mater. Sci., vol. 52, no. 1, pp. 336–345, 2016, doi: 10.1007/s10853-016-0334-5.

[84] H. Kim, J. S. Horwitz, G. P. Kushto, S. B. Qadri, Z. H. Kafafi, and D. B. Chrisey, "*Transparent conducting Zr-doped In2O3 thin films for organic light-emitting diodes*," Appl. Phys. Lett., vol. 78, no. 8, pp. 1050–1052, 2001, doi: 10.1063/1.1350595.

[85] J. A. N. and D. McMorrow, "*Element of modern X-ray physics*," WILY Ed. Second Ed., 2011.

[86] M. Omidi, A. Fatehinya, M. Farahani, Z. Akbari, S.Shahmoradi, F. Yazdian, M. Tahriri, K. Moharamzadeh, L.Tayebi and D. Vashaee "Characterization of biomaterials," Biomater. Oral Dent. Tissue Eng., pp. 97–115, 2017, doi: 10.1016/B978-0-08-100961-1.00007-4.

[87] K. D. Vernon-Parry, "*Microscopy : An introduction*," III-Vs Rev., vol. 13, no. 4, pp. 40–44, 2000.

[88] A. Pinto, V. B. Oliveira, and D. S. Falcão, "*Experimental methods of characterization*". 2018.

[89] J. Telegdi, A. Shaban, and G. Vastag, "*Biocorrosion-steel*". Elsevier Inc., 2018.

[90] M. Nasrollahzadeh, M. Atarod, M. Sajjadi, S. M. Sajadi, and Z. Issaabadi, "*Plant-Mediated Green Synthesis of Nanostructures: Mechanisms, Characterization, and Applications*", 1st ed., vol. 28. Elsevier Ltd., 2019.

[91] C.Colpan,Y. Nalbant, and M. Ercelik, "*Fundamentals of Fuel Cell Technologies*," Compr. Energy Syst., vol. 4–5, pp. 1107–1130, 2018, doi: 10.1016/B978-0-12-809597-3.00446-6.

[92] V. Vishwakarma and S. Uthaman, "*9 - Environmental impact of sustainable*

green concrete". Elsevier Inc., 2020.

[93] K. Stern, "*Metallurgical and Ceramic Protective Coatings*," Springer Sci. Bus. Media, 2012.

[94] A. Pandey, S. Dalal, S. Dutta, and A. Dixit, "*Structural characterization of polycrystalline thin films by X-ray diffraction techniques*," J. Mater. Sci. Mater. Electron., vol. 32, no. 2, pp. 1341–1368, 2021, doi: 10.1007/s10854-020-04998-w.

[95] Yahia Anouar, "*Optimization of indium oxide thin films properties prepared by sol gel spin coating process for optoelectronic applications*".University Med Khider of Biskra 2020.

[96] B. Youcef, "*Elaboration and characterization of thin layers of zinc oxide (ZnO) deposited by ultrasonic spray for photovoltaic and optoelectronic applications*," University Med Khider of Biskra 2019.

[97] O. Belahssen, M. Ghougali, and A. Chala, "*Effect of iron doping on physical properties of NiO thin films*," J. Nano- Electron. Phys., vol. 10, no. 2, 2018, doi: 10.21272/jnep.10(2).02039.

[98] M. Mekhnache, A. Drici , L. Saad Hamideche , H. Benzarouk , A. Amara , L. Cattin , J.C. Bernède , M. Guerioune "*Properties of ZnO thin films deposited on (glass, ITO and ZnO:Al) substrates*," Superlattices Microstruct., vol. 49, no. 5, pp. 510–518, 2011, doi: 10.1016/j.spmi.2011.02.002.

[99] H. Benamra, H. Saidi, A. Attaf, M. S. Aida, A. Derbali, and N. Attaf, "*Physical properties of Al-doped ZnS thin films prepared by ultrasonic spray technique*," Surfaces and Interfaces, vol. 21, no. August, p. 100645, 2020, doi: 10.1016/j.surfin.2020.100645.

[100] J. Bartolomé, P. Hidalgo, D. Maestre, A. Cremades, and J. Piqueras, "*In-situ scanning electron microscopy and atomic force microscopy Young's modulus determination of indium oxide microrods for micromechanical resonator applications*," Appl. Phys. Lett., vol. 104, no. 16, 2014, doi: 10.1063/1.4872461.

[101] K. Zhang, A. Regoutz, R. Palgrave, D. Payne, and R. Egdell "*Determination of the Poisson ratio of (001) and (111) oriented thin films of In 2O 3 by synchrotron-based x-ray diffraction*," Phys. Rev. B - Condens. Matter Mater. *Phys.*, vol. 84, no. 23, pp. 1–4, 2011, doi: 10.1103/PhysRevB.84.233301.

[102] E. Muchuweni, T. S. Sathiaraj, and H. Nyakotyo, "*Synthesis and characterization of zinc oxide thin films for optoelectronic applications*," Heliyon, vol. 3, no. 4, p. e00285, 2017, doi: 10.1016/j.heliyon.2017.e00285.

[103] M. Caglar, S. Ilican, Y. Caglar, and F. Yakuphanoglu, "*Electrical conductivity and optical properties of ZnO nanostructured thin film*," Appl. Surf. Sci., vol. 255, no. 8, pp. 4491–4496, 2009, doi: 10.1016/j.apsusc.2008.11.055.

[104] N. NicDaéid "*Systematic drug identification,*" *Encycl. Anal. Sci.*, no. June, pp. 75–80, 2019, doi: 10.1016/B978-0-12-409547-2.14457-9.

[105] M. Maâche, "*Dépôt et Caractérisation de Couches Minces de ZnO par Spray Pyrolyse* "Université de Biskra, 2005.

[106] M. Radhia, "*Elaboration and characterization of undoped and doped titanium dioxide thin layers by sol gel (spin coating) for photocatalytic applications.,*" University Med Khider of Biskra, 2021.

[107] D. Bao, X. Wu, L. Zhang, and X. Yao, "*Preparation , electrical and optical properties of (Pb , Ca) TiO_3 thin lms using a modied sol-gel technique*," Thin Solid Films, vol. 350, pp. 30–37, 1999.

[108] N. Tripathi and S. Rath, "*Effect of Thermal Annealing and Swift Heavy Ion Irradiation on the Optical Properties of Indium Oxide Thin Films*," ECS J. Solid

State Sci. Technol., vol. 3, no. 3, pp. P21–P25, 2014, doi: 10.1149/2.002403jss.

[109] K. Senthil, D. Mangalaraj, S. K. Narayandass, and S. Adachi, "*Optical constants of vacuum-evaporated cadmium sulphide thin films measured by spectroscopic ellipsometry,*" Materials Science and Engineering B78 , elsevier ,vol. 78, pp. 53–58, 2000.

[110] A. Y. Oral, Z. B. Bahs, and M. H. Aslan, "*Microstructure and optical properties of nanocrystalline ZnO and ZnO :(Li or Al) thin films*," Applied Surface Science, elsevier, vol. 253, pp. 4593–4598, 2007, doi: 10.1016/j.apsusc.2006.10.015.

[111] M. F. Faznny, M. K. Halimah, A. A. Latif, F. D. Muhammad, and L. Hasnimulyati, "*Optical properties of la3+ nps/ag+ co-doped zinc borotellurite glass*," Solid State Phenom, vol. 290 SSP, pp. 3–8, 2019, doi: 10.4028/www.scientific.net/SSP.290.3.

[112] N. Abdelmalek and H. Farh, "*Influence of Fe and Al dopants on the optical properties of zinc oxide thin films obtained by spray pyrolysis*," Int. J. Eng. Res. Africa, vol. 29, pp. 21–27, 2017, doi: 10.4028/www.scientific.net/JERA.29.21.

[113] K. Daoudi, "*ELABORATION ET CARACTERISATION DE FILMS MINCESD ' OXYDE D ' INDIUM DOPE A L ' ETAIN OBTENUS PAR VOIE SOL-GEL*" l'UNIVERSITE CLAUDE BERNARD – LYON 1, 2006.

[114] H. Cao, P. Xing, D. Yao, and P. Wu, "*Annealing temperature dependent non-monotonic d0 ferromagnetism in pristine In2O3 nanoparticles*," J. Magn. Magn. *Mater.*, vol. 429, no. December 2016, pp. 69–73, 2017, doi: 10.1016/j.jmmm.2017.01.015.

[115] R. Riveros, E. Romero, and G. Gordillo, "*Synthesis and characterization of highly transparent and conductive SnO2:F and in2O3:Sn thin films deposited by spray pyrolysis*," *Brazilian J. Phys.*, vol. 36, no. 3 B, pp. 1042–1045, 2006, doi: 10.1590/S0103-97332006000600065.

[116] E. Gagaoudakis, M. Bender, E. Douloufakis, N. Katsarakis, E. Natsakou, V. Cimalla and G. Kiriakidis "*The influence of deposition parameters on room temperature ozone sensing properties of InOx films,*" Sensors Actuators, B Chem., vol. 80, no. 2, pp. 155–161, 2001, doi: 10.1016/S0925-4005(01)00908-X.

[117] M. Girtan, "*The influence of post-annealing treatment on the electrical properties of In2O3 thin films prepared by an ultrasonic spray CVD process*," Surf. Coatings Technol., vol. 184, no. 2–3, pp. 219–224, 2004, doi: 10.1016/j.surfcoat.2003.10.136.

[118] M. Khan, W. Khan, M. Ahamed, and M. Alhoshan, "*Structural and optical properties of In_2O_3 nanostructured thin film*," Mater. Lett., vol. 79, no. November, pp. 119–121, 2012, doi: 10.1016/j.matlet.2012.03.110.

[119] A. Bouhdjer, A. Attaf, H. Saidia, Y. Benkhettaa, M.S. Aidab, I. Bouhafa and A. Rhil "*Optik Influence of annealing temperature on In_2O_3 properties grown by an ultrasonic spray CVD process*," *Opt. - Int. J. Light Electron Opt.*, vol. 127, no. 16, pp. 6329–6333, 2016, doi: 10.1016/j.ijleo.2016.04.100.

[120] S. Koh, Y. Han, J. Lee, U.Yeo, and J. S. Cho, "*Material properties and growth control of undoped and Sn-doped In_2O_3 thin films prepared by using ion beam technologies,*" Thin Solid Films, vol. 496, no. 1, pp. 81–88, 2006, doi: 10.1016/j.tsf.2005.08.251.

[121] K. Zhang, A. Walsh, C. Catlow, V. Lazarov, and R. Egdell, "*Surface energies control the self-organization of oriented In 2O3 nanostructures on cubic zirconia,*" Nano Lett., vol. 10, no. 9, pp. 3740–3746, 2010, doi: 10.1021/nl102403t.

[122] A. Kashyout, M. Fathy, and M. B. Soliman, "*Studying the properties of RF-*

sputtered nanocrystalline tin-doped indium oxide," Int. J. Photoenergy, vol. 2011, 2011, doi: 10.1155/2011/139374.

[123] S. Goswami and A. Sharma, "*Investigation of the optical behavior of indium oxide thin films with the aid of spectroscopic ellipsometry technique,*" Appl. Surf. Sci., vol. 495, no. May, p. 143609, 2019, doi: 10.1016/j.apsusc.2019.143609.

[124] A. Yahia, A. Attaf , H. Saidi , M. Dahnoun , C. Khelifi , A. Bouhdjer , A. Saadi , H. Ezzaouia"*Structural, optical, morphological and electrical properties of indium oxide thin films prepared by sol gel spin coating process*," Surfaces and Interfaces, 2018, doi: 10.1016/j.surfin.2018.12.012.

[125] Z. Yuan, X. Zhu, X. Wang, X. Cai, B. Zhang, D. Qiu, H. Wu "*Annealing effects of In2O3 thin films on electrical properties and application in thin film transistors,*" Thin Solid Films, vol. 519, no. 10, pp. 3254–3258, 2011, doi: 10.1016/j.tsf.2010.12.022.

[126] E. Nishimura, T. SASABAYASHI, N. ITO, Y.SATO, K. UTSUMI, K. YANO, A. KAIJO, Kazuyoshi INOUE4, and Yuzo SHIGESATO1? "*Structure and internal stress of tin-doped indium oxide and indium-zinc oxide films deposited by DC magnetron sputtering*," Appl. Phys., vol. 46, no. 12, pp. 7806–7811, 2007, doi: 10.1143/JJAP.46.7806.

[127] A. K. and A. M. Swann, S. Song, Y. Shigesato, K.Utsumi, "*INTERNAL STRESS OF ITO, IZO AND GZO FILMS DEPOSITED BY RF AND DC MAGNETRON SPUTTERING*," Phys. Technol., vol. 19, no. 2, pp. 67–75, 1988, doi: 10.1088/0305-4624/19/2/304.

[128] H. Ennaceri, M. Boujnah, D. Erfurt, J. Rappich, X. Lifei, A. Khaldoun, A. Benyoussef, A. Ennaoui, A.Taleb "*Influence of stress on the photocatalytic properties of sprayed ZnO thin films*," Sol. Energy Mater. Sol. Cells, vol. 201, 2019, doi: 10.1016/j.solmat.2019.110058.

[129] M. Gulen, G. Yildirim, S. Bal, A. Varilci, I. Belenli, and M. Oz, "*Role of annealing temperature on microstructural and electro-optical properties of ITO films produced by sputtering*," J. Mater. Sci. Mater. Electron., vol. 24, no. 2, pp. 467–474, 2013, doi: 10.1007/s10854-012-0768-8.

[130] A. R. Hegazy, B. Salameh, and A. M. Alsmadi, "*Optical transitions and photoluminescence of fluorine-doped zinc tin oxide thin films prepared by ultrasonic spray pyrolysis*," Ceram. Int., vol. 45, no. 15, pp. 19473–19480, 2019, doi: 10.1016/j.ceramint.2019.06.204.

[131] N. Beji, M. Souli, S. Azzaza, S. Alleg, and N. Kamoun Turki, "*Study on the zinc doping and annealing effects of sprayed In2O3 thin films*," J. Mater. Sci. Mater. Electron., vol. 27, no. 5, pp. 4849–4860, 2016, doi: 10.1007/s10854-016-4367-y.

[132] F. H. Wang and C. L. Chang, "*Effect of substrate temperature on transparent conducting Al and F co-doped ZnO thin films prepared by rf magnetron sputtering*," Appl. Surf. Sci., vol. 370, pp. 83–91, 2016, doi: 10.1016/j.apsusc.2016.02.161.

[133] I. Ben Miled, M. Jlass, I. Sta, M. Dhaouadi, M. Hajji, G. Mousdis, M. Kompitsas,H. Ezzaouia"*Influence of In-doping on microstructure, optical and electrical properties of sol–gel derived CdO thin films*," J. Mater. Sci. Mater. Electron., vol. 29, no. 13, pp. 11286–11295, 2018, doi: 10.1007/s10854-018-9216-8.

[134] J. George and C. S. U. Menon, "*Electrical and optical properties of electron beam evaporated ITO thin films*," Surf. Coatings Technol., vol. 132, pp. 45–48, 2000.

[135] V. Malathy, S. Sivaranjani, V. S. Vidhya, T. Balasubramanian, J. Joseph Prince

,C. Sanjeeviraja , M. Jayachandran "*Role of substrate temperature on the structural , optoelectronic and morphological properties of (400) oriented indium tin oxide thin films deposited using RF sputtering technique*," *Mater Sci Mater Electron*, pp. 1299–1307, 2010, doi: 10.1007/s10854-010-0066-2.

[136] Z. W. Chen, J. K. L. Lai, and C. H. Shek, "*Insights into microstructural evolution from nanocrystalline SnO 2 thin films prepared by pulsed laser deposition*," Phys. Rev. B - Condens. Matter Mater. Phys., vol. 70, no. 16, pp. 1–7, 2004, doi: 10.1103/PhysRevB.70.165314.

[137] T. Obulapathi, A. GuruSampath Kumar, T. Sofi Sarmash, D. Jhansi Rani G.V.V. Bhaskara Rao, "*Effect of film thickness on physical properties of CuCrO 2 thin films*," Aust. Ceram. Soc. Vol., vol. 52, pp. 102 – 105, 2016.

[138] D. Tsai, Z. Chang, B. Kuo, Y. Wang, E. Chen, and F. Shieu, "*Thickness dependence of the structural , electrical , and optical properties of amorphous indium zinc oxide thin films*," J. Alloys Compd., vol. 743, pp. 603–609, 2018, doi: 10.1016/j.jallcom.2017.12.062.

[139] H. Han, J. W. Mayer, T. L. Alford, H. Han, and J. W. Mayer, "*Band gap shift in the indium-tin-oxide films on polyethylene napthalate after thermal annealing in air Band gap shift in the indium-tin-oxide films on polyethylene napthalate*," Appl. Phys., vol. 083715, no. 2006, 2007, doi: 10.1063/1.2357647.

[140] P. K. Biswas, A. De, K. Ortner, and S. Korder, "*Study of sol-gel-derived high tin content indium tin oxide (ITO) films on silica-coated soda lime silica glass*," Mater.Lett,vol. 58, no. 10, pp. 1540–1545, 2004, doi: 10.1016/j.matlet.2003.10.023.

[141] L. Voisin, M. Ohtsuka, S. Petrovska, R. Sergiienko, and T. Nakamura, "*Structural, optical and electrical properties of DC sputtered indium saving indium-tin oxide (ITO) thin films*," Optik (Stuttg)., vol. 156, no. 2010, pp. 728–737, 2018, doi: 10.1016/j.ijleo.2017.12.021.

[142] H. E. a Jlassi, MI. Staa, M. Hajjia, b, "*Effect of nickel doping on physical properties of zinc oxide thin films prepared by the spray pyrolysis method*," Appl. Surf. Sci, vol. 301, pp. 216–224, 2014.

[143] A. Solieman, "*Effect of sintering temperature on the structural , optical and electrical properties of sol – gel derived indium oxide thin films,*" Sol-Gel Sci Technol, vol. 60, pp. 48–57, 2011, doi: 10.1007/s10971-011-2549-x.

[144] T. Tomita , K.Yamashita, Y.Hayafuji, and H. Adachi "*The origin of n -type conductivity in undoped In 2 O 3 The origin of n -type conductivity in undoped In_2O_3*," *Appl. Phys. Lett.*, vol. 051911, pp. 5–8, 2005, doi: 10.1063/1.2001741.

[145] S. K, S. Arulkumar, K. Jenifer, and S. Parthiban, "*Effect of vacuum annealing on the optical and electrical properties of sputtered silicon doped indium oxide thin films*," Opt. Mater. (Amst)., vol. 122, no. PB, p. 111751, 2021, doi:10.1016/j.optmat.2021.111751.

[146] S. Z. Werta, O. K. Echendu, and F. B. Dejene, "*Simplified two-electrode electrochemical growth and characterization of Cd1−xZnxS thin films: Influence of electrolytic bath pH*," Phys. B Condens. Matter, vol. 580, p. 411939, 2020, doi: 10.1016/j.physb.2019.411939.

[147] R. Karmakar, S. K. Neogi, A. Banerjee, and S. Bandyopadhyay, "*Structural , Morphological , Optical and Magnetic Property of Mn doped Ferromagnetic ZnO thin film*," Appl. Surf. Sci., vol. 263, pp. 671–677, 2012.

[148] A. Ahmed Ali, N. Ahmeda, S.Mohammad, F.Sabaha, E. Kabaaa, A.Alsadigc, A. Sulieman "*Effect of gamma irradiation dose on the structure and pH sensitivity of ITO thin films in extended gate field effect transistor*," Results Phys, vol. 12, no.

November 2018, pp. 615–622, 2019, doi: 10.1016/j.rinp.2018.10.066.

[149] F. Ghamari, D. Raoufi, and J. Arjomandi, "*Influence of thickness on crystallographic, stereometric, optoelectronic, and electrochemical characteristics of electron-beam deposited indium tin oxide thin films*," Mater. Chem. Phys., vol. 260, no. January 2020, p. 124051, 2021, doi: 10.1016/j.matchemphys.2020.124051.

[150] M. Narasimha Murthy, C.Sreelatha, G. Ravinder, and S. Anusha, "*The effect of solution pH on the structural, surface morphological, and optical characteristics of ZnO thin films synthesized by the chemical bath deposition technique*," Mater. Today Proc, 2021, doi: 10.1016/j.matpr.2021.10.093.

[151] J. Som , J. Choi , H. Zhang , N. Reddy Mucha , S. Fialkova , K. Mensah-Darkwa , J. Suntivich, R.Gupta , D. Kumar "*Materials Science & Engineering B Effect of substrate-induced lattice strain on the electrochemical properties of pulsed laser deposited nickel oxide thin film,*" Mater. Sci. Eng. B, vol. 280, no. March, p. 115711, 2022, doi: 10.1016/j.mseb.2022.115711.

[152] S. Devasia, P. V. Athma, R. Raphael, and E. I. Anila, "*Effect of source-substrate distance on the transparent electrode properties of spray pyrolysed aluminium doped zinc oxide thin films*," Mater. Today Pro, 2021, doi: 10.1016/j.matpr.2021.10.203.

[153] N. Manjula, M. Pugalenthi, V. S. Nagarethinam, K. Usharani, and A. R. Balu, "*Effect of doping concentration on the structural, morphological, optical and electrical properties of Mn-doped CdO thin films,*" Mater. Sci. Pol., vol. 33, no. 4, pp. 774–781, 2015, doi: 10.1515/msp-2015-0115.

[154] C. Aparna, M. G. Mahesha, and P. Kumara Shetty, "*Structural and optical properties of indium oxide thin films synthesized at different deposition parameters by spray pyrolysis*," Mater. Today Proc, vol. 55, pp. 141–147, 2022, doi: 10.1016/j.matpr.2022.01.048.

[155] Y. H. Yan, Y. C. Liu, L. Fang, Z. C. Lu, Z. B. Li, and S. X. Zhou, "*Growth of CuI buffer layer prepared by spraying method*," Trans. Nonferrous Met. Soc. China, vol. 21, no. 2, pp. 359–363, 2011, doi: 10.1016/S1003-6326(11)60722-X.

[156] G. H. Wang, C. Y. Shi, L. Zhao, H. W. Diao, and W. J. Wang, "*Applied Surface Science Transparent conductive Hf-doped In 2 O 3 thin films by RF sputtering technique at low temperature annealing*," Appl. Surf. Sci., vol. 399, pp. 716–720, 2017, doi: 10.1016/j.apsusc.2016.11.239.

[157] A.Isiyaku, A.Ali , S. Abdu , M.Tahan , N. Raship, A.Bakri , N. Nayan "*Improvement of transparent conductive indium tin oxide based multilayer films on p-silicon through the inclusion of thin copper-aluminium metals interlayer*," Thin Solid Films, vol. 738, no. October, p. 138959, 2021, doi: 10.1016/j.tsf.2021.138959.

[158] C. Ruan, Q. Sun, D. Xiao, H. Li, G. Xia, and S. Wang, "*Lightwave irradiation-assisted low-temperature solution synthesis of indium-tin-oxide transparent conductive films*," Ceram. Int., vol. 48, no. 9, pp. 12317–12323, 2022, doi: 10.1016/j.ceramint.2022.01.094.

[159] D. Beena, K. Lethy , R. Vinodkumar , V.Mahadevan, V. Ganesan , D. Phase , S. Sudheer "*Effect of substrate temperature on structural, optical and electrical properties of pulsed laser ablated nanostructured indium oxide films*," Appl. Surf. Sci., vol. 255, no. 20, pp. 8334–8342, 2009, doi: 10.1016/j.apsusc.2009.05.057.

[160] P. Prathap, Y. P. V. Subbaiah, M. Devika, and K. T. R. Reddy, "*Optical properties of In2O3 films prepared by spray pyrolysis*," Mater. Chem. Phys., vol. 100, no. 2–3, pp. 375–379, 2006, doi: 10.1016/j.matchemphys.2006.01.016.

[161] A. C. M. Ghougali1, O. Belahssen, "*Structural, Optical and Electrical Properties of NiO Nanostructure Thin Film*," J. NANO- Electron. Phys., vol. 8, no. 4, pp. 4–7, 2016, doi: 10.21272/jnep.8(4(2)).04059.

[162] J. R. Mohamed and L. Amalraj, "*Effect of precursor concentration on physical properties of nebulized spray deposited In_2S_3 thin films*," Integr. Med. Res., vol. 4, no. 3, pp. 357–366, 2018, doi: 10.1016/j.jascer.2016.07.002.

[163] V. A. Dao, H. Choi, J. Heo , H. Park , K. Yoon , Y. Lee ,Y. Kim , N. Lakshminarayan , J.Yi "*Rf-Magnetron sputtered ITO thin films for improved heterojunction solar cell applications*," Curr. Appl. Phys., vol. 10, no. SUPPL. 3, pp. 2–5, 2010, doi: 10.1016/j.cap.2010.02.019.

[164] R. Sandoval-Paz, R. Ramírez-Bon "*Indium tin oxide fi lms deposited on polyethylene naphthalate substrates by radio frequency magnetron sputtering*," Thin Solid Films, vol. 517, no. 8, pp. 2596–2601, 2009, doi: 10.1016/j.tsf.2008.10.016.

[165] Y. WANG, Y. Zhu "*Effect of post-annealing on the structure and optical properties of ZnO films deposited on Si substrates Effect of post-annealing on the structure and optical properties of ZnO films deposited on Si substrates*," 2018, doi: 10.1088/1757-899X/382/2/022054.

[166] N. M. Ahmed, F. A. Sabah, H. I. Abdulgafour, A. Alsadig, A. Sulieman, and M. Alkhoaryef, "*The eff ect of post annealing temperature on grain size of indium-tin-oxide for optical and electrical properties improvement*," Results Phys., vol. 13, no. December 2018, p. 102159, 2019, doi: 10.1016/j.rinp.2019.102159.

[167] Y. Chen, W. Yu, and Y. Liu, "*Effects of annealing on structural, optical and electrical properties of Al-doped ZnO thin films*," Sci. China, Ser. G Phys. Astron., vol. 47, no. 5, pp. 588–596, 2004, doi: 10.1360/03yw0198.

[168] S. H. Sabeeh and R. H. Jassam, "*The effect of annealing temperature and Al dopant on characterization of ZnO thin films prepared by sol-gel method*," Results Phys., vol. 10, no. March, pp. 212–216, 2018, doi: 10.1016/j.rinp.2018.05.033.

[169] M. Sarma and G. Wary, "*Effect of Molarity on Structural and Optical Properties of Chemically Deposited Nanocrystalline PbS Thin Film*," Int. Lett. Chem. Phys. Astron., vol. 74, pp. 22–35, 2017, doi: 10.18052/www.scipress.com/ilcpa.74.22.

[170] A. Ibraheem and A. Ali, "*Molarities effect on structural and optical properties of ZnO prepared by spray pyrolysis*," Sci. Eng. Res., vol. 5, no. 1, pp. 2250–2256, 2014.

[171] M. Manickam, V. Ponnuswamy, C. Sankar, and R. Suresh, "*Optik Cobalt oxide thin films prepared by NSP technique : Impact of molar concentration on the structural , optical , morphological and electrical properties*," Opt. - Int. J. Light Electron Opt., vol. 127, no. 13, pp. 5278–5284, 2016, doi: 10.1016/j.ijleo.2016.03.008.

[172] S. Ravishankar, A. R. Balu, M. Anbarasi, and V. S. Nagarethinam, "*Optik Influence of precursor molar concentration on the structural , morphological , optical and electrical properties of PbS thin films deposited by spray pyrolysis technique using perfume atomizer*," Optik (Stuttg)., vol. 126, pp. 2550–2555, 2015.

[173] I. B. Kherchachi,A.Attaf, H.Saidi "*Structural, optical and electrical properties of SnxSy thin films grown by spray ultrasonic*," J. Semicond., vol. 37, no. 3, pp. 21–26, 2016, doi: 10.1088/1674-4926/37/3/032001.

[174] M. A. Flores, R. Castanedo, G. Torres, and O. Zelaya, "*Optical , electrical and structural properties of indium-doped cadmium oxide films obtained by the sol –*

gel technique," Sol. Energy Mater. Sol. Cells, vol. 93, pp. 28–32, 2009, doi: 10.1016/j.solmat.2008.02.006.

[175] N. B. Ibrahim, A. Z. Arsad, N. Yusop, and H. Baqiah, "*The physical properties of nickel doped indium oxide thin fi lm prepared by the sol-gel method and its potential as a humidity sensor*," Mater. Sci. Semicond. Process., vol. 53, pp. 72–78, 2016, doi: 10.1016/j.mssp.2016.05.020.

[176] H. Pan, M. Shiao, C. Su, and C. Hsiao "*Influence of sputtering parameter on the optical and electrical properties of zinc-doped indium oxide thin films Influence of sputtering parameter on the optical and electrical properties of zinc-doped indium oxide thin films*," Vac. Sci. Technol. A, vol. 1187, no. 2005, 2014, doi: 10.1116/1.1924473.

[177] P. Pujar, R. V. Vardhan, D. Gupta, and S. Mandal, "*A balancing between super transparency and conductivity of solution combustion derived titanium doped indium oxide: Effect of charge carrier density and mobility*," Thin Solid Films, vol. 660, no. September 2017, pp. 267–275, 2018, doi: 10.1016/j.tsf.2018.06.031.

[178] P. S. Devi, M. Chatterjee, and D. Ganguli, "*Indium tin oxide nano-particles through an emulsion technique*," Mater. Lett., vol. 55, no. August, pp. 205–210, 2002.

[179] N. G. Pramod and S. N. Pandey, "*Influence of Sb doping on the structural, optical, electrical and acetone sensing properties of In2O3 thin films*," Ceram. Int., vol. 40, no. 2, pp. 3461–3468, 2014, doi: 10.1016/j.ceramint.2013.09.084.

[180] M. Ajili, N. Jebbari, N. K. Turki, and M. Castagné, "*Effect of Al-doped on physical properties of ZnO Thin films grown by spray pyrolysis on SnO2: F/glass*," in EPJ Web of Conferences, 2012, vol. 29, doi: 10.1051/epjconf/20122900002.

[181] N. Jabena Begum and K. Ravichandran, "*Effect of source material on the transparent conducting properties of sprayed ZnO:Al thin films for solar cell applications*," J. Phys. Chem. Solids, vol. 74, no. 6, pp. 841–848, 2013, doi: 10.1016/j.jpcs.2013.01.029.

[182] T. P. Rao and M. C. Santhoshkumar, "*Highly oriented (1 0 0) ZnO thin films by spray pyrolysis*," Appl. Surf. Sci. J., vol. 255, pp. 7212–7215, 2009, doi: 10.1016/j.apsusc.2009.03.065.

[183] V. Senthamilselvi, K. Saravanakumar,N. Jabena Begum, R. Anandhi, A. T. Ravichandran, B. Sakthivel,K. Ravichandran "*Photovoltaic properties of nanocrystalline CdS films deposited by SILAR and CBD techniques-a comparative study*," J. Mater. Sci. Mater. Electron., vol. 23, no. 1, pp. 302–308, 2012, doi: 10.1007/s10854-011-0409-7.

[184] M. S. Alqahtani, N. M. A. Hadia, and S. H. Mohamed, "*Effects of V doping on magnetic and optical properties of oxygen-deficient In2O3 thin films*," Optik (Stuttg)., vol. 145, no. April, pp. 377–386, 2017, doi: 10.1016/j.ijleo.2017.07.059.

[185] K. J. Kim and Y. R. Park, "*Large and abrupt optical band gap variation in In-doped ZnO,*" Appl. Phys. Lett., vol. 78, no. 4, pp. 475–477, 2001, doi: 10.1063/1.1342042.

[186] K. Usharani, N. Raja, N. Manjula, V. S. Nagarethinam, and A. R. Balu, "*Characteristic Analysis on the Suitability of CdO Thin Films Towards Optical Device Applications – Substrate Temperature Effect*," Int. J. Thin. Fil. Sci. Tec. Int. J. Thin Film. Sci. Technol., vol. 4, no. 89, pp. 89–96, 2015. doi: http://dx.doi.org/10.12785/ijtfst/040205.

[187] A. Bouhdjer, A. Attaf, H. Saidi, H. Bendjedidi, Y. Benkhetta, and I. Bouhaf, "*Correlation between the structural , morphological , optical , and electrical*

properties of In 2 O 3 thin films obtained by an ultrasonic spray CVD process," vol. 36, no. 8, pp. 1–6, 2015, doi: 10.1088/1674-4926/36/8/082002.

[188] A. Bouhdjer, H. Saidi, A. Attaf, M. S. Aida, M. Jlassi, and I. Bouhaf, "*Optik Structural , morphological , optical , and electrical properties of In 2 O 3 nanostructured thin films*," Opt. - Int. J. Light Electron Opt., vol. 127, no. 18, pp. 7319–7325, 2016, doi: 10.1016/j.ijleo.2016.05.035.

[189] S. D. Ponja, S. Sathasivam, I. P. Parkin, and C. J. Carmalt, "*Highly conductive and transparent gallium doped zinc oxide thin films via chemical vapor deposition*," Sci. Rep., vol. 10, no. 1, pp. 1–7, 2020, doi: 10.1038/s41598-020-57532-7.

[190] L. Xu and X. Li, "*Influence of Fe-doping on the structural and optical properties of ZnO thin films prepared by sol-gel method*," J. Cryst. Growth, vol. 312, no. 6, pp. 851–855, 2010, doi: 10.1016/j.jcrysgro.2009.12.062.

[191] A. Montazeri and F. Jamali-Sheini, "*Enhanced ethanol gas-sensing performance of Pb-doped In2O3 nanostructures prepared by sonochemical method*," Sensors Actuators, B Chem., vol. 242, pp. 778–791, 2017, doi: 10.1016/j.snb.2016.09.181.

[192] R. K. Mishra and P. P. Sahay, "*Zn-doped and undoped SnO2 nanoparticles : A comparative structural , optical and LPG sensing properties study*," Mater. Res. Bull., vol. 47, no. 12, pp. 4112–4118, 2012, doi: 10.1016/j.materresbull.2012.08.051.

[193] P. Banerjee, W. Lee, K. Bae, S.Lee, and G. Rubloff "*Structural , electrical , and optical properties of atomic layer deposition Al- doped ZnO films Structural , electrical , and optical properties of atomic layer deposition Al-doped ZnO films*," J. Appl. Phys , vol. 043504, 2010, doi: 10.1063/1.3466987.

LIST OF PUBLICATIONS AND CONFERENCES

Publication

Nouadji, R., Attaf, A., Derbali, A., Bouhdjer, A., Saidi, H., Aida, M. S., ... & Attaf, N. (2021). Film thickness effect on structural, optical and electrical properties of indium oxide (In_2O_3) thin films grown via sol-gel method. *Main Group Chemistry*, (Preprint), 1-15.

Conferences

- R.Nouadji, A.Attaf, A.Bouhdjer et al " Effect of number layers on the properties of indium oxide thin films deposited by spin coating process",1st International Symposium on Materials, Energy and Environment January 20-21st; 2020, El-Oued, Algeria.
- R. Nouadji, A.Attaf et al " Effect of annealing time on the properties of indium oxide thin films deposited by spin coating technique", Fifth International Conference on Energy, Materials, Applied Energetics and Pollution.ICEMAEP2019, October22-24, 2019, Constantine, Algeria.
- R.Nouadji, A.Attaf et al "The structural and morphological properties of undoped In_2O_3 thin films deposited by spin coating" 1st International Conference on Sustainable Energy and Advanced Materials IC-SEAM'21 April 21-22 2021, Ouargla, Algeria.